Title
Synthesis and Characterization of Novel Conjugated Polymers and Small Molecules for Photovoltaic Applications

Author
Thompson, Robert James

Publication Date
2017

Peer reviewed|Thesis/dissertation

UNIVERSITY OF CALIFORNIA

Los Angeles

Synthesis and Characterization of Novel Conjugated Polymers and Small Molecules for Photovoltaic Applications

A dissertation submitted

in partial satisfaction of the requirements for the degree

Doctor of Philosophy in Chemistry

by

Robert James Thompson

2017

ABSTRACT OF THE DISSERTATION

Synthesis and Characterization of Novel Conjugated Polymers and Small Molecules for Photovoltaic Applications

by

Robert James Thompson

Doctor of Philosophy in Chemistry

University of California, Los Angeles, 2017

Professor Yves F. Rubin, Chair

This dissertation describes the synthesis and characterization of several novel conjugated polymers and small molecules for use in research on organic photovoltaics (i.e. polymer solar cells/organic solar cells).

Chapter 1 is an introductory chapter that briefly introduces semiconducting polymers and gives a brief overview of their use in polymer solar cells.

Chapter 2 describes the synthesis and characterization of the conjugated polyelectrolyte, poly{(4,4-bis(3'-(*N*-ethyl-*N*,*N*-dimethylammonio)propyl)cyclopenta[2,1-b:3,4-b']dithiophene)-2,6-diyl-alt-(thiophene-2,5-diyl)} bromide (PCT).

Chapter 3 describes the synthesis and characterization of a series of conjugated polymers containing substituted dithieno[3,2-a:2',3'-c]phenazine monomer units, and also describes the fabrication and analysis of solar cells devices made from these materials.

Chapter 4 describes the synthesis and characterization of a series of conjugated polymers and small molecules based on the condensation of various aromatic *o*-diamines with *o*-diketones to produce novel N-heteroacenes.

Chapter 5 gives a brief review of the work reported in this dissertation and provides suggestions for future work that can be built on those findings.

The dissertation of Robert James Thompson is approved.

Jeffrey I. Zink

Andrea M. Kasko

Sarah H. Tolbert

Yves F. Rubin, Committee Chair

University of California, Los Angeles

2017

Table of Contents

List of Figures

List of Tables

Acknowledgements

I would like to thank my parents. This wouldn't have been possible without all your love and support throughout the years. I feel lucky and blessed to be your son.

I would also like to thank my P.I.s Yves Rubin and Sarah Tolbert. I learned so much from both of you over the last 7 years. You both have changed the way I see the physical world. When I walk through the park I think of chlorophyll molecules and photosystem II. When I cook my dinner, I'm thinking of the curcumin in my turmeric, the piperine in my pepper, and the eugenol and citral in my basil. I am glad you helped enrich my everyday experience of my world. I am also grateful that you both understood that my happiness and growth as a person was important, and I'm glad you helped foster that.

I would like to thank all of my collaborators through the years. This dissertation is just as much a product of their work as it is my own. I'd like to specifically thank the following people: Nick Knutson, Robert Jordan, Krastina Petrova, Daniel Kilbride, Amy Ferreira, Rachel Huber, Christopher Day, Jordan Aguirre, Steve Hawks, Andrew Herzing, Yolanda Li, Terri Lin, KJ Winchell, Patrick Yee, Mathew Fontana, Matthew Voss, Benjamin Schwartz, David Patrick, Betsy Melenbrink, and Barry Thompson.

I would also like to thank all of my friends and bandmates over the last 7 years. I might have become a great chemist if y'all weren't constantly distracting me. Thanks a lot, ya bunch of jerks.

Vita

2009-2010	Undergraduate Laboratory Researcher Western Washington University
2010	B.S. Chemistry Western Washington University
2010-2017	Teaching Assistant University of California Los Angeles
2013	Research Internship National Institute of Standards and Technology (NIST)

Published Work

[1] Thompson, R.; Lund, C.; Hickman, S.A.; Krohn, E. & Patrick, D.L. Stamping Oriented Molecular Monolayers Using Liquid Crystal Inks *Chem. Commun*. 47, (2011): 7668-7670

[2] Hawks, S. A.; Aguirre, J. C.; Schelhas, L. T.; Thompson, R. T.; Huber, R. C.; Ferreira, A. S.; Zhang, G.; Herzing, A. A.; Tolbert, S. H.; and Schwartz, B. J. Matched Polymer: Fullerene Solar Cells Made by Solution-Sequential Processing and Traditional Blend Casting: Nanoscale Structure and Device Performance *J. Phys. Chem. C* 118, (2014): 12413–12425

[3] Huber, R. C.; Ferreira, A. S.; Thompson, R.; Kilbride, D.; Knutson, N. S.; Sudha Devi, L.; Toso, D. B.; Zhou, Z. H.; Rubin, Y.*; Schwartz, B. J.*; Tolbert, S. H.* "Long-Lived Photoinduced Polaron Formation in Conjugated Polyelectrolyte/Fullerene Assemblies", *Science* (2015), 348, 1340-1343.

Chapter 1 : Introduction

Semiconducting polymers

Semiconducting polymers are a class of organic polymer composed of aromatic or olefinic units linked by covalent bonds.[1] These materials are perhaps the most dazzling member of the family of materials we call plastics. They can possess vibrant and often fluorescent colors that range across the whole visible spectrum, from violet to deep red. Some semiconducting polymers, such as polyacetylene, even possess a metallic luster that is reminiscent of films of silver or gold; but their resemblance to metals and semimetals doesn't just stop at their appearance: the semiconducting electronic properties of these materials allows them to function as diodes,[2] transistors,[3] chemical sensors,[4,5] and conductors.[6,7] However, these chimeric carbon based polymers are also flexible, stretchable, lightweight, and moldable like most common plastics such as nylon and polystyrene. Semiconducting polymers may indeed represent the next generation of plastics: enabling clothes to conduct electricity and sense the physical condition of its wearer,[8,9,10] allowing furniture and other common objects to electroluminescence in a wide range of colors,[11] and they could even possibly revolutionize the way the world produces[12] and stores[13] energy.

These revolutionary materials aren't new by any means. Although the chemical identity of semiconducting polymers could not be appreciated at the time of their initial discovery, Semiconducting polymeric materials have been known for over 180 years. Polyaniline was first discovered in 1834 by Ferdinand Runge, who found that mixing aniline with a number of chemical oxidants led to the formation of insoluble emerald green films.[14] But as one might

surmise, the formation of an insoluble green film with no practical application would and should have remained an unexplored area of chemical interest in an era that would not even have a correct model of the atomic nucleus for some seventy years. Indeed, polyaniline would remain a chemical curiosity for over one-hundred years, and it would take many important scientific discoveries before that material and other polymeric semiconductors could be fully understood.

The next momentous event in the story of semiconducting polymers came In 1920, when Staudinger proposed that natural rubber was composed of molecules with very high molecular weights that were result of reactions which linked together a large number of small molecules.[15] He dubbed these relatively large molecules "macromolecules", and, like many theories that later turn out to be correct, Staudinger's concept of the macromolecule faced strong resistance from his contemporaries, who believed dogmatically in hypotheses that would later prove to be false. Staudinger's macromolecular theory would eventually gain widespread acceptance during the 1930s largely due to the discovery of many new synthetic condensation polymers by Wallace Carothers at Dupont.[16]

Even after polymer theory had become well established, the unique electronic properties of semiconducting polymers remained overlooked and unexplored until the 1960s. Polyphenylenes were first synthesized by Kovacic and Kyriakis in the 1960s using the Wurtz reaction between various benzene derivatives, but the authors did not explore the physical properties of these materials.[17] Later in that same decade, Weiss and co-workers explored the synthesis of various polypyrrole derivatives produced via the thermal decomposition of

tetraiodopyrrole. These authors realized that they had created a unique new material, and they had the bright idea of testing the electronic properties of the polymers they had synthesized. To their surprise they found that the black powders they produced had low resistivities ranging from 10 to 200 Ω cm^{-1}.[18,19] Weiss *et al*. were the first to realize that polymeric materials consisting of chemically unsaturated units could conduct electricity. At the same time the scientists Buvet and Jozefowicz were studying the synthesis and electrical characterization of polyaniline in France, and they discovered that these materials could display exceptionally high conductivities when treated with certain chemical dopants. Furthermore, these scientists correctly surmised that the conductivity of these materials was electronic in nature and not ionic.[18] Buvet and Josefowicz were unknowingly only a few steps away from breaking open the nutshell of the underlying chemical—physical properties that explained their observations in polyaniline. They were the first to realize that polymeric materials consisting of unsaturated or aromatic units connected by covalent bonds could conduct electricity, but they failed to notice the important seed in that revelation: they failed to make the further hypothesis that *any* polymer consisting of repeating aromatic or unsaturated units could conduct electricity.

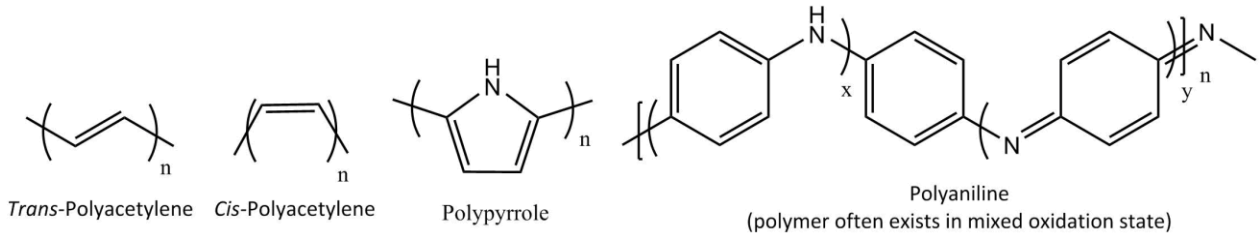

Trans-Polyacetylene *Cis*-Polyacetylene Polypyrrole Polyaniline
(polymer often exists in mixed oxidation state)

Figure 1.1. Chemical structures of *trans* and *cis* polyacetylene, polypyrrole, and polyaniline

It would take several more years, but in 1967, a simple mistranslation would result in the discovery of a shiny new semiconducting polymer that would provide the theoretical understanding that would plant the seed that led to the explosive growth of new semiconducting polymers. Ideka Shirakawa and Hyung Pyun were studying the Ziegler-Natta polymerization of acetylene in Japan. Dr. Pyun was a visiting researcher from Korea working under Dr. Shirakawa, and the latter researcher mistakenly used one thousand times the desired catalyst loading after mistranslating mmol to mol in his protocol for the Ziegler-Natta polymerization of acetylene. These conditions produced silvery polymeric films; and the researchers were naturally curious as to what caused the almost metallic-like appearance of these plastic materials. Conductivity measurements revealed that although these materials appeared to resemble metals, they certainly did not conduct electricity with much proclivity (measured conductivities were 10^{-4} S cm^{-1}).[20]

This new plastic with a notably metallic luster would remain a laboratory curiosity for nearly a decade until Alan MacDiarmid was shown this material by Shirakawa in 1975. MacDiarmid had been working with Alan Heeger on an isoelectronic polymer polythiazyl, $(SN)_x$, which was a golden, highly conductive material (1200 Ω cm^{-1}). MacDiarmid worked on polyacetylene with Shirakawa during the following year and showed that the conductivity of these films could be drastically increased to 500 S cm^{-1} after doping them with iodine vapor, just as was seen in materials such as polyaniline and polythiazyl. These findings eventually led to the final revelation that was needed to understand semiconducting polymers: electrons were delocalized in the π orbitals of the covalently linked sp^2 hybridized atoms which are present in polyacetylene and polyaniline and every other semiconducting polymer. These delocalized

electrons are able to move along the backbone of such polymers through the π orbitals of the polymer, leading to electronic conductivity.[21] The exact nature of these processes will be outlined in more detail later in the next section of this chapter, but the author will end the chapter by noting it was this key insight that lead to Shirakawa, Heeger, and MacDiarmid to receive the 2000 Nobel Prize in chemistry.

Electronic properties of semiconducting polymers

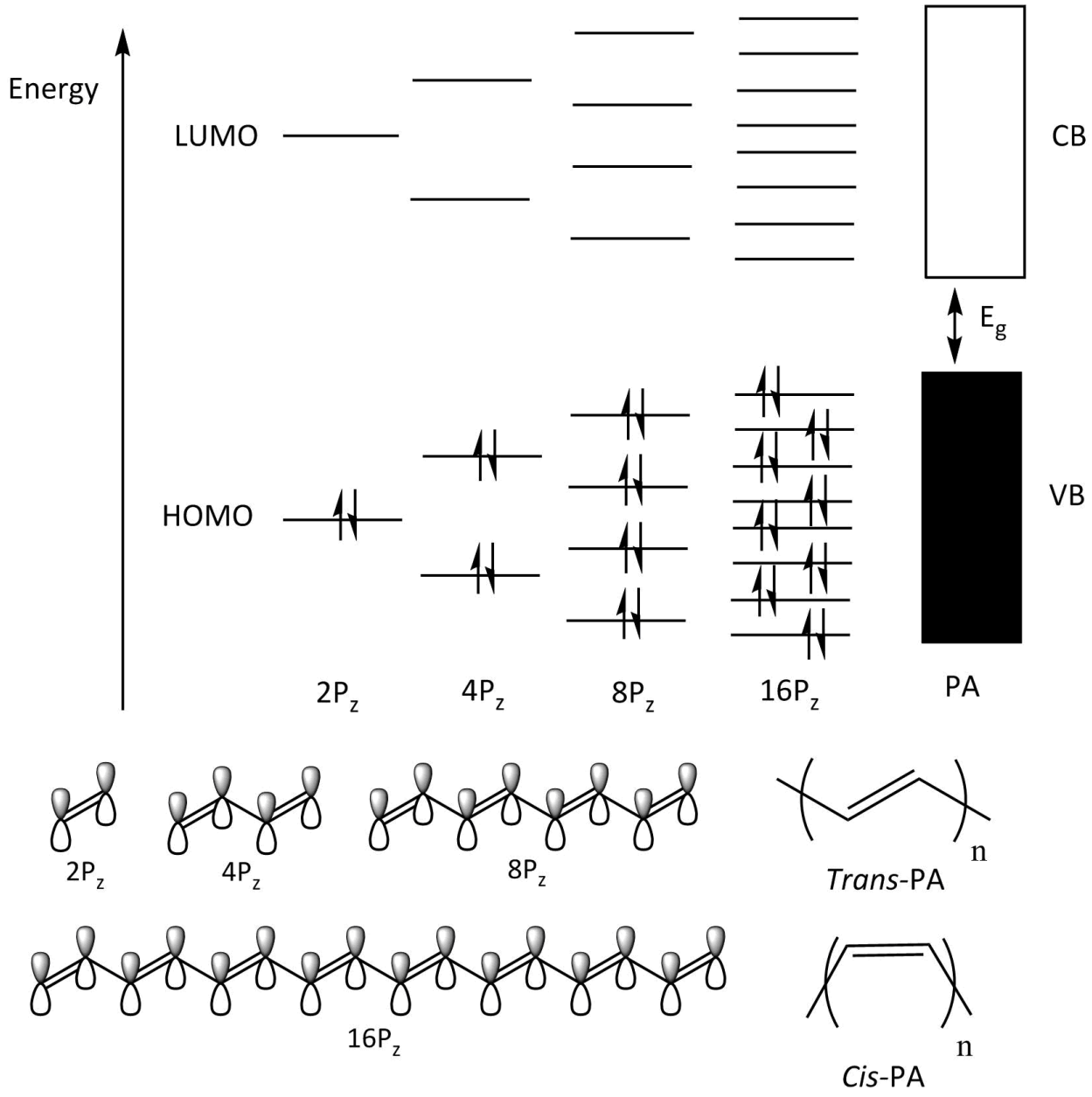

Figure 1.2. Schematic showing the combination of double bonds leading to the formation of the band structure in polyacetylene

One cannot understand any of the applications of semiconducting polymers without first understanding their electronic band structure, and, being as such, it would be useful to describe the band structure of the simplest semiconducting polymer, polyacetylene, before further discussing more complex systems. Polyacetylene actually exists as two separate regioisomeric polymers: *cis* and *trans*-polyacetylene. *Trans*-polyacetylene has a simpler, more symmetric chemical structure compared to *cis*-polyacetylene because the resonance structures for both forms of *trans*-polyacetylene are identical (i.e. *trans*-polyacetylene has a degenerate ground state) while the two resonance forms of *cis*-polyacetylene are inequivalent (i.e. non-degenerate). For the sake of simplicity, the properties of *trans*-polyacetylene will be discussed in this section of the introduction. The frontier molecular orbitals of *trans*-polyacetylene consist of a linear combination of π orbitals along the polymer chain (see Figure 1.2). Electrons in these orbitals are delocalized, (they are not localized on a single atom, and the wavefunction of the electron is delocalized through the P_z orbitals of many carbon atoms along the polymer chain). Molecular orbital theory and tight binding theory would predict that as more and more P_z orbitals are combined, the band gap would shrink leading to the formation of a one-dimensional metal. However, 1-D metals are unstable and they undergo a so-called Peierls transition which effectively breaks the symmetry of a one-dimensional lattice introducing a band gap into the one-dimensional material. In *trans*-polyacetylene this distortion manifests itself as alternating single and double bonds along the polymer backbone.[22]

The Peierls distortion in *trans*-polyacetylene leads to the formation of a valence band filled with electrons and an unoccupied conduction band separated by a band gap of 1.8 eV.[1] Electrons are delocalized along the length of the polymer chain leading to essentially one

dimensional charge transport, with weak interchain hopping between polymer chains. As discussed earlier, undoped polyacetylene has a relatively low conductivity (10^{-4} S $cm^{-}1$), but the conductivity can be greatly enhanced upon doping the polymer. Polyacetylene can be doped using oxidizing or reducing agents which generate radical cationic species in the valence band or radical anion species in the conduction band, introducing free carriers into the polymer backbone which can produce a current.[22,23] This general model developed for polyacetylene laid the groundwork for the understanding of more complex semiconducting conjugated polymers, all of which are essentially linear combinations of double bonds.

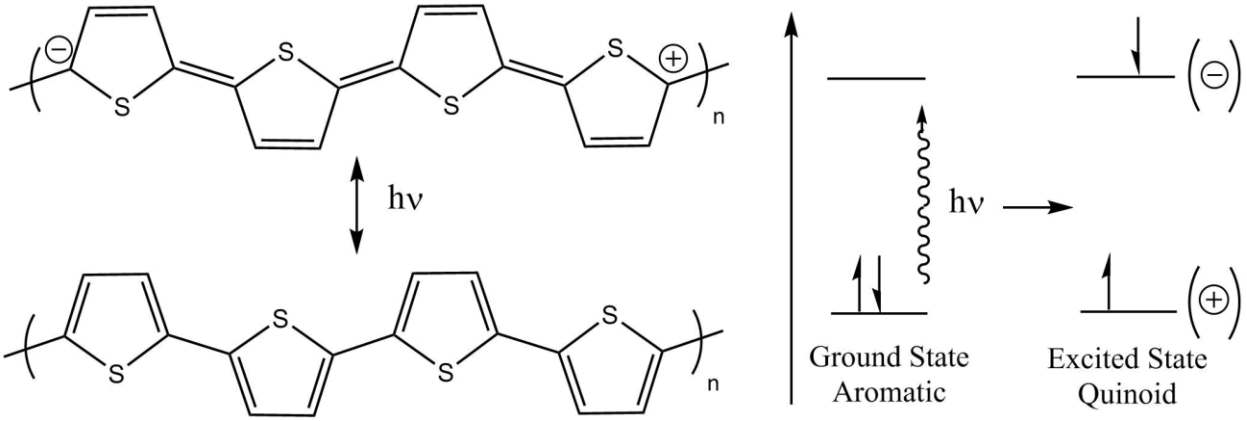

Figure 1.3. Model of polaron formation in polythiophene upon optical excitation

The band gap is perhaps the most important property of a semiconducting polymer because it determines the absorptive and emissive properties of polymeric materials. For semiconducting polymers, the bond length alternation along the polymer backbone largely determines the band gap of the conjugated polymer.[24] Most semiconducting polymers consist of aromatic units connected by covalent bonds, unlike polyacetylene which consists of

covalently linked olefin units. One example of a semiconducting polymer consisting of covalently linked aromatic units is polythiophene. Polythiophene can be drawn as two separate non-degenerate resonance structures. The aromatic resonance structure of polythiophene is stabilized relative to the quinoidal state because the aromatic rings have a formal sextet of electrons in the aromatic state while in the quinoidal form they do not. The band gap in polythiophene is therefore a reflection of the loss of the resonance stabilization energy in the transition between the lower energy aromatic resonance structure (the HOMO) and the higher energy quinoidal resonance structure (the LUMO). The quinoidal state of polythiophene can also be thought of as a more accurate model of the excitonic excited state of polythiophene, while the aromatic resonance structure can be thought of as a more accurate model of the ground state (Figure 1.3).[25] The excitonic excited state of conjugated polymers will be discussed in detail later in the introduction, but for now it will be mentioned that an exciton is a state consisting of a Coulombically bound electron—hole pair.

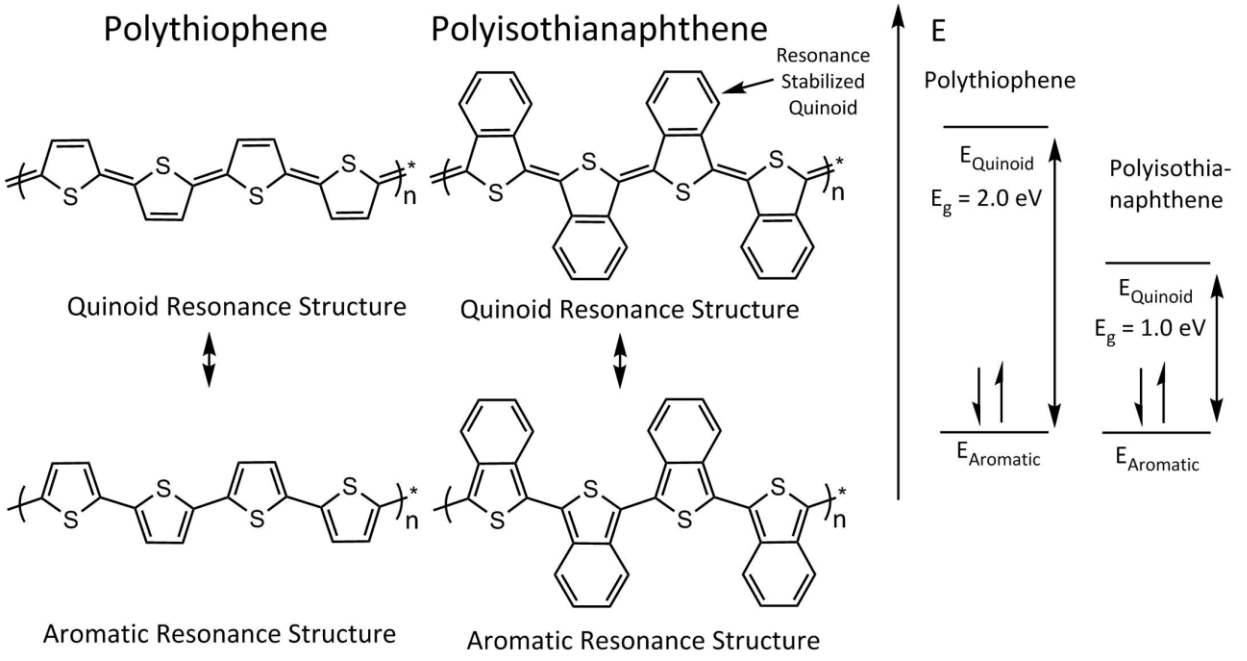

Figure 1.4. Schematic showing the aromatic and quinoidal resonance structures of polythiophene and polyisothianaphthene

This aromatic *vs*. quinoidal model is useful in providing coarse design rules that can allow for the tuning of the band gap of a particular polymer. For instance, this model provides a simple explanation for the dramatic reduction in the band gap of polyisothianaphthene, (E_g = 1.1 eV) in comparison to the band gap of polythiophene (E_g = 2.0 eV).[26] Upon comparing the two structures (Figure 1.4) it can be seen that the transition from the aromatic to the quinoidal resonance structure in polythiophene leads to a loss of a formal aromatic sextet of electrons in the thiophene rings. The same is true in polyisothianaphthene: the transition from an aromatic resonance structure to a quinoidal resonance structure still leads to the loss of a formal aromatic sextet of electrons in the thiophene rings, but this same transition also creates a formal aromatic sextet of electrons in the benzene ring fused to the thiophene rings at the 3

and 4 positions of the thiophene rings. The formation of formally aromatic benzene rings in the quinoidal form of the polymer stabilizes the quinoidal resonance structure of the polymer, thus leading to a reduction in the energy gap between the aromatic *vs*. quinoidal resonance structures.

Another useful method of engineering the band gap of a semiconducting polymer is by synthesizing a copolymer consisting of an electron donating unit and an electron accepting unit to create a so called πD-πA alternating copolymer. From a linear combination of molecular orbitals perspective the HOMO and LUMO levels of the resulting copolymer are a linear combination of the HOMO and LUMO levels of the pure donor and acceptor polymeric materials. The resulting band gap of the resulting polymer ends up being decreased because the HOMO and LUMO orbitals of the resulting polymer are close in energy to the HOMO and LUMO units of the donor and acceptor units of the copolymer.[27] An example of a donor-acceptor polymer with such properties is the polymer poly(bis-ethylenedioxythiophene)-cyanovinylene (PBEDOT-CNV) which is composed of a polycyanovinylene acceptor moiety and a polyethylenedioxythiophene donor moiety (Figure 1.5). Intramolecular charge transfer between donor and acceptor units in this polymer lead to hybridization of the HOMO and LUMO orbitals, forming a narrow band gap material.[28]

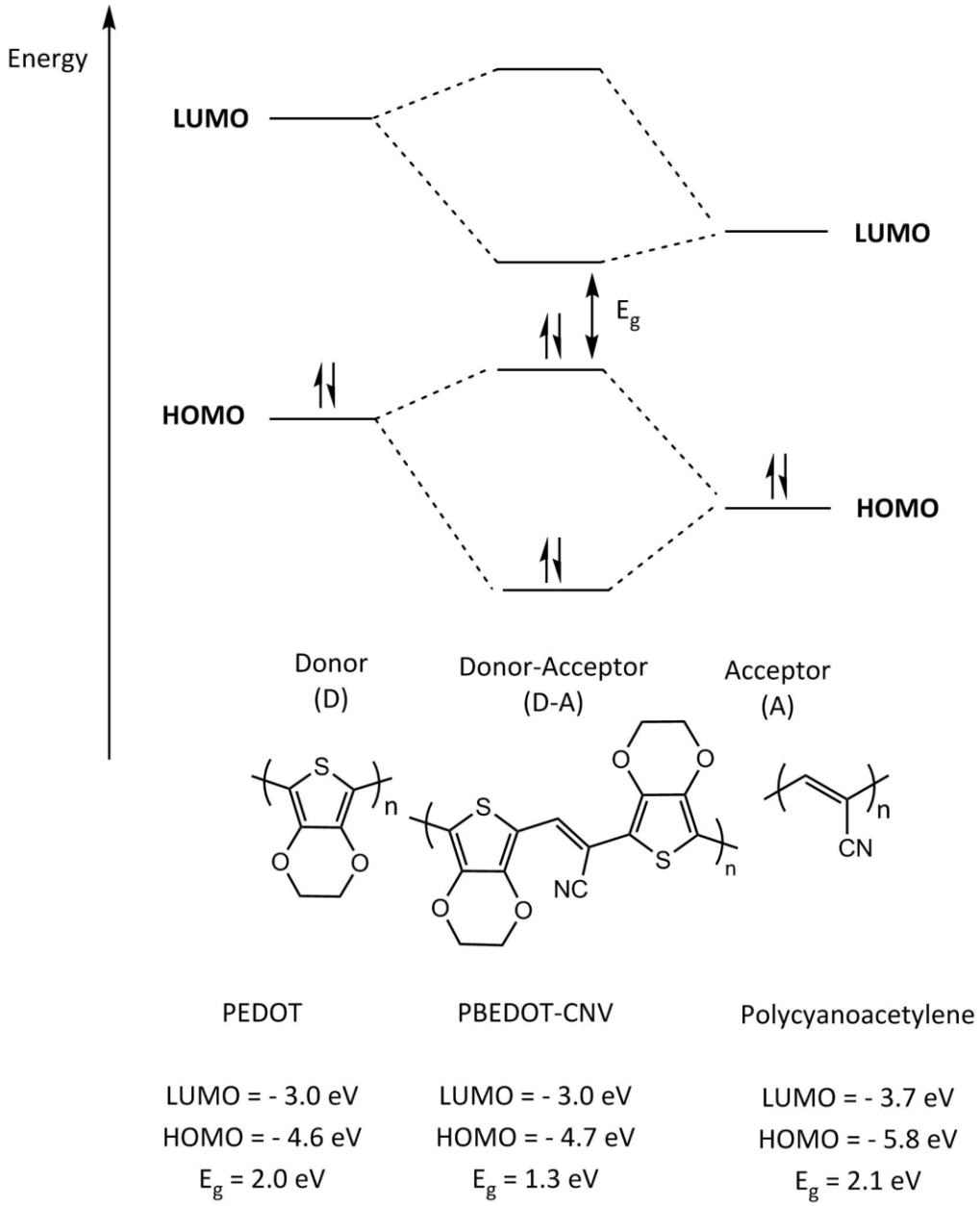

Figure 1.5. Schematic showing the hybridization of molecular orbitals leading to the formation of a narrow band gap donor acceptor polymer. Adapted from Thompson, B. C.; **Variable band gap poly(3,4-alkylenedioxythiophene)-based polymers for photovoltaic and electrochromic applications**.[28]

Synthesis of π-conjugated semiconducting polymers

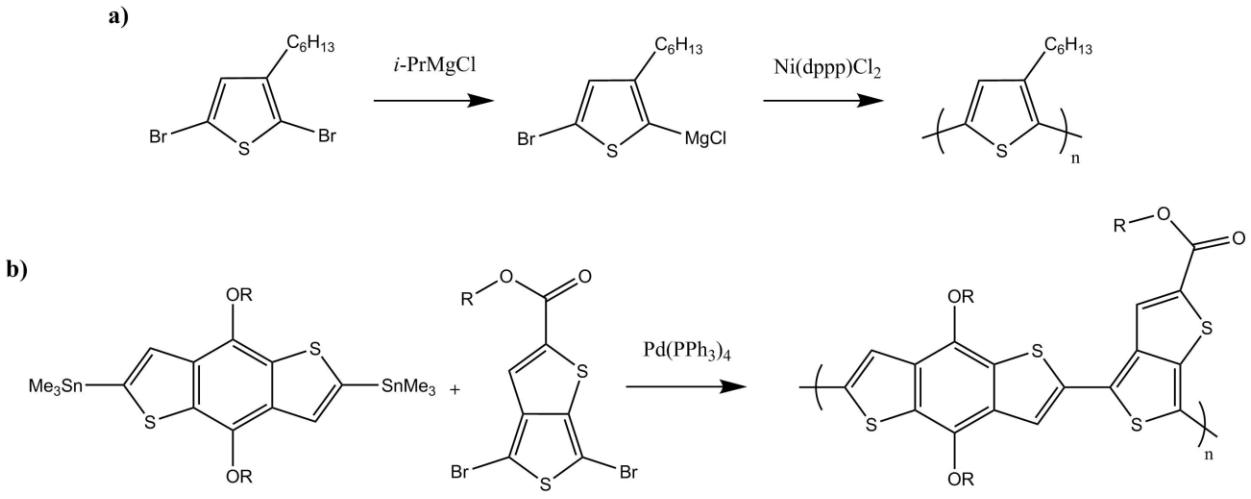

Figure 1.6. Examples of the synthesis of π-conjugated semiconducting polymers using a) nickel catalyzed Kumada cross-coupling reactions and b) palladium catalyzed Stille cross-coupling reactions

A number of synthetic approaches have been developed for the synthesis of π-conjugated semiconducting polymers, but nickel and palladium catalyzed cross coupling reactions are most often employed for the synthesis of π-conjugated semiconducting polymers. Many regioregular polymers such as poly-3-hexylthiophene are synthesized using a Kumada type cross coupling of monomer units using Grignard reagents and Ni(II) catalysts,[29] while many copolymers consisting of electron deficient and electron rich aromatic units are synthesized using palladium catalyzed Stille cross-coupling reactions,[30] and to a lesser extent, palladium catalyzed Suzuki and Negishi cross-coupling reactions as well as other more exotic cross-coupling reactions (Figure 1.6).[31] Recently direct (hetero)arylation polymerization reactions have been developed by several groups, which allows cross-coupling reactions to occur without the use of reducing metals or without the use of the extremely toxic aryl stannane reagents

used in Stille cross-coupling reactions.[32,33] This procedure is of tremendous synthetic use for polymer chemists because it allows cross coupling reactions to occur simply by using aryl halides and unsubstituted aromatic units using a palladium catalyst.

Polymer solar cells

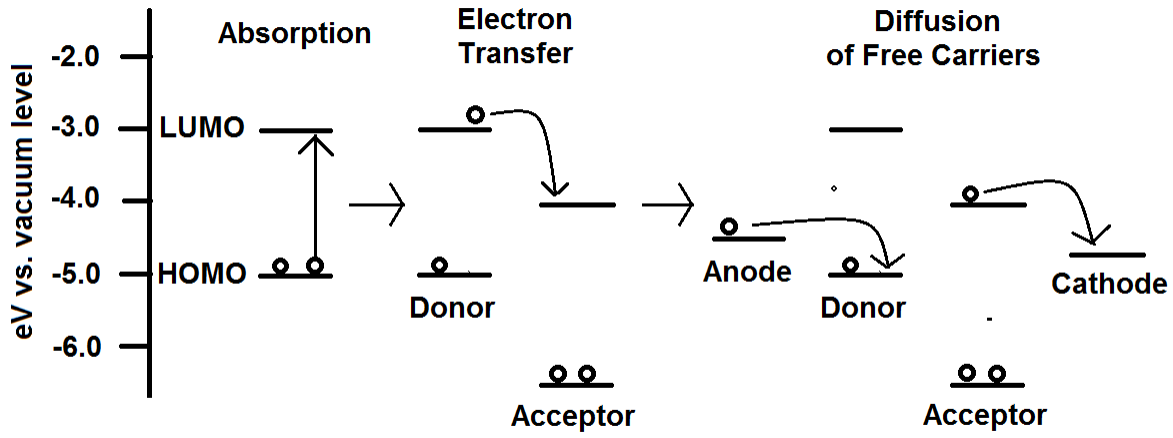

Figure 1.7. Physical processes which occur to generate photocurrent in solar cells. Open circles represent electrons.

Polymer solar cells are a class of photovoltaic device utilizing π-conjugated semiconducting polymers in the active layer of the device. Absorption of a photon in organic semiconducting materials leads to the creation of an exciton, *i.*e. the creation of an electron and hole pair bound by a Coulomb force.[34] Normally excitation leads to photorelaxation via radiative or non-radiative processes after a short time (typically picoseconds to nanoseconds). However, if this exciton encounters an electron accepting material with a low lying LUMO before relaxation, then a thermodynamically favorable electron transfer from the polymer to the electron acceptor can occur. This electron transfer process creates a hole localized on the

polymer and an electron localized on the fullerene acceptor. These free carriers are then free to diffuse to their respective electrodes under the guidance of an electric field, to create a photovoltaic current (see Figure 1.8).[35]

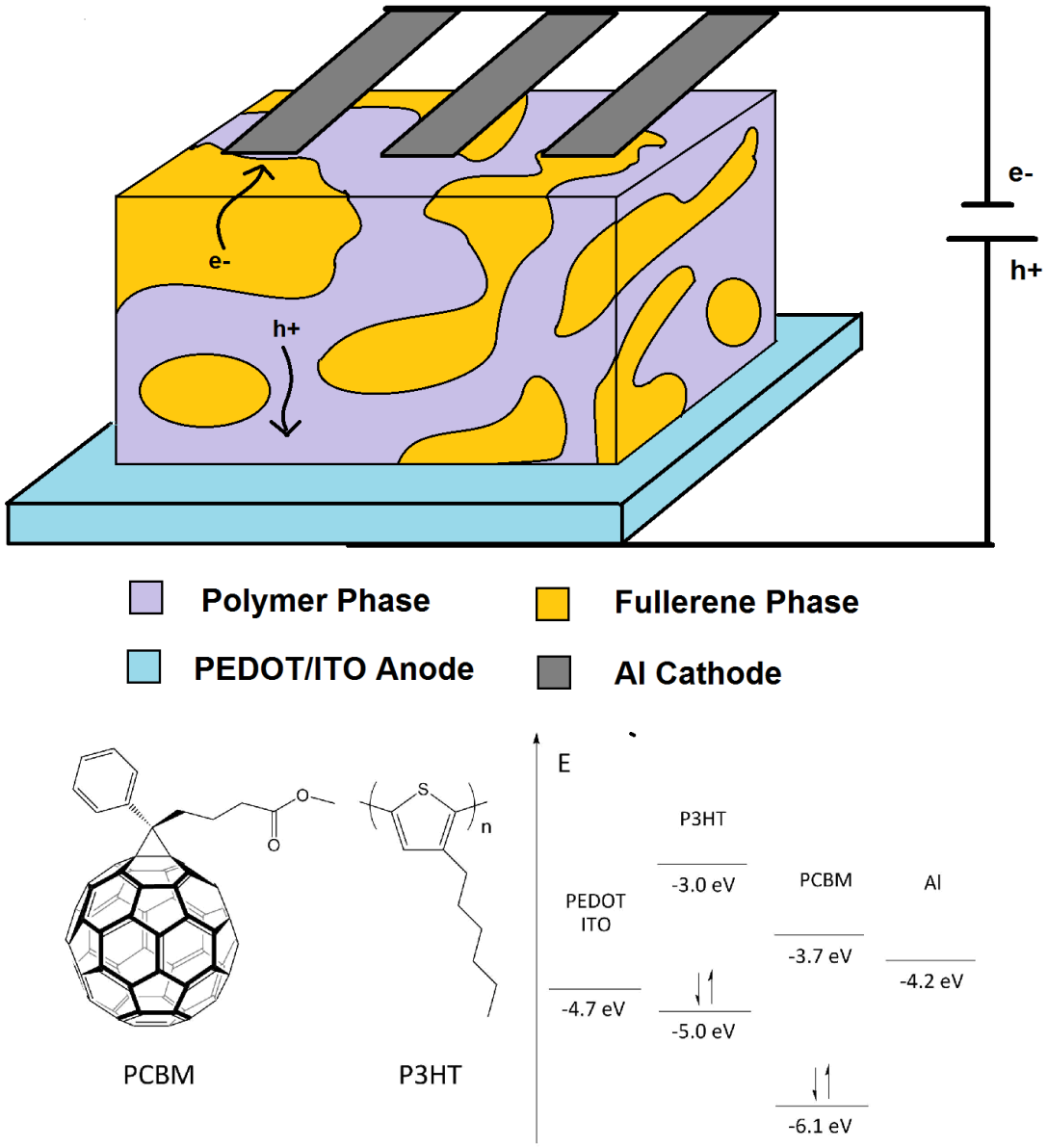

Figure 1.8. Schematic representation of a P3HT/PCBM solar cell, with molecular structures and a band diagram to show the relative energy levels of P3HT/PCBM and the PEDOT/ITO anode and Al cathode.

The most well studied example of a polymer solar cell utilizes poly-3-hexylthiophene (P3HT) and phenyl-C_{61}-butyric acid methyl ester (PCBM). Photoexcitation of P3HT leads to the promotion of an electron from the highest occupied molecular orbital (HOMO) to the lowest unoccupied molecular orbital (LUMO) of P3HT. The LUMO of P3HT (—3.0 V *vs* vacuum level) is high enough to allow for a thermodynamically favorable charge transfer to the LUMO of PCBM (—3.8 V *vs*. vacuum level) to occur.[36] There is, however, one major caveat to this electron transfer process: the exciton diffusion length in P3HT and PCBM is quite short (10 nm).[37] The exciton diffusion length is effectively a measure of how far the exciton can diffuse before the electron in the excited state relaxes back to the ground state through either radiative or non-radiative processes, and the extremely short exciton diffusion lengths of most organic semiconducting polymers pose a significant challenge: P3HT and PCBM must be finely intermixed so that excitons can efficiently diffuse to the P3HT/PCBM interface to facilitate charge transfer. Therefore the processing conditions used to create these solar cells must be finely tuned in order to create an active layer with a finely mixed morphology.[38]

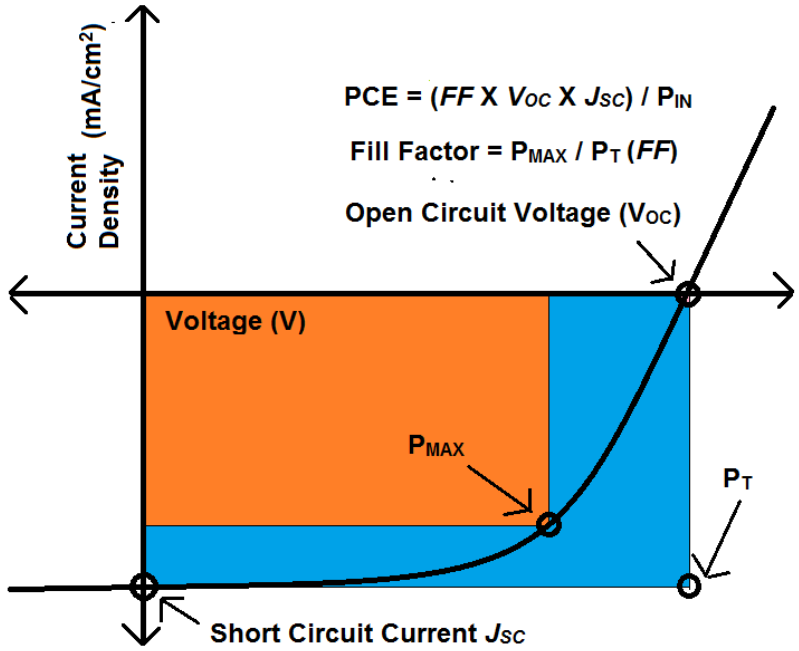

Figure 1.9. An example of *J-V* curve for a solar cell showing the meaning of the key parameters of a solar cell.

The most common method of evaluating the performance of a solar cell is testing the current-voltage characteristics of the solar cell under illumination. The resulting curve displaying the current under different bias voltages is referred to as the current-voltage or *J-V* curve, and it contains key information about the performance of the solar cell (Figure 1.9). The current density (mA/cm^2) is the unit of the y-axis in these curves and bias voltage (V) is the unit of the x-axis. The x intercept of these curves is known as the open circuit voltage (V_{OC}) , and this parameter is equal to the voltage at which the applied bias is equal to the generated photovoltage. The V_{OC} in excitonic solar cells is roughly equal to the difference in the absolute potential of the HOMO of the donor component and the LUMO of the acceptor component.[39] The open circuit voltage is often several hundred millivolts lower than this value because of

energy losses during the electron transfer process and because of resistive losses within the solar cell itself.[40] The y-intercept of these graphs is referred to as the short-circuit current (J_{SC}) and this value is equal to the amount of free carriers reaching the electrodes of the solar cell. The amount of free carriers that are generated is highly dependent on film morphology because the domain sizes of the donor and acceptor components need to be on the same length scale of the exciton diffusion length for efficient charge separation. Other parameters such as film thickness, optical density, and free carrier mobilities also play a key role in the value of the short-circuit current.

The final key parameter that can be gleaned from a *J-V* curve is the fill factor. Under ideal conditions the theoretical maximum power (P_T) that can be attained from a solar cell would be equal to J_{SC} X V_{OC} = P_T. However, solar cells do not operate under idealized conditions and the maximum power attained from a solar cell is normally only a fraction of the theoretical maximum power. This is due to the fact that free carriers feel a smaller effective electric field as bias voltage increases, which in turn leads to a build-up of free carriers within the solar cell. This increase in the density of free carriers causes higher levels of recombination between electrons and holes.[41] Few solar cells have fill factors near 100%, and the fill factor represents the ratio between the actual maximum power attained in the solar cell (P_{MAX}) and the theoretical maximum power attained (P_T) $FF = P_{MAX}/P_T$. The power conversion efficiency (*PCE*, η) of the solar cell can then be calculated using these parameters obtained from the *J-V* curve via the equation: $\eta = (J_{SC} \text{ X } V_{OC} \text{ X } FF)/ P_{IN}$ where P_{IN} represents the incident power illuminating the solar cell. It will be noted that the numerator of the previous equation calculates the power output

(P_{OUT}) of the solar cell so the equation simplifies to $\eta = P_{OUT} / P_{IN}$ when this is taken in to account.

After the exciton is effectively split into free carriers via electron transfer, the free carriers must diffuse to their respective electrodes. This process as it turns, out is not as simple as it first sounds. The free carriers can recombine through several processes and these recombination events lead to losses in the efficiency of solar cells. Recombination losses can occur through a geminate recombination process where the nascent free carriers recombine soon after exciton dissociation,[42,43] or through non-geminate processes. Non-geminate recombination losses occur in two main forms in polymer solar cells: Langevin recombination and Shockley-Read-Hall recombination. Langevin recombination describes the process wherein free carriers recombine when electrons and holes encounter one another within their Coulomb radius. Langevin type recombination typically assumes that the recombination rate increases as the carrier mobilities increase because carriers will be able to encounter each other more easily if the carriers are able to move more easily. Shockley-Read-Hall recombination results from trap states within the valence and conduction bands of the organic semiconductors. When charges are localized on deep trap states, they can effectively act as recombination centers which continually cause recombination between holes and electrons. Unlike Langevin recombination, Shockley-Read-Hall recombination does not necessarily increase in proportion to the carrier mobility, but is more dependent upon the density of trap states within a material.[44]

Shockley-Read-Hall otherwise known as trap-assisted recombination is the dominate mode of recombination within most high performing solar cells.[45,46,47] Although the nature of

these trap states is still far from clear and is due in part to extrinsic factors such as morphology, there is some evidence that these states result from the conformational disorder resulting from kinks and bends within the polymer backbone.[48,49,50] For instance, P3HT/PCBM show drastically enhanced hole mobilities when confined to one-dimensional pores made of titania and alumina and it has been posited that the enhanced mobility results from straightening of polymer chains.[51,52] It has also been shown that polymers can be engineered to have higher mobilities by straightening the polymer backbone using interactions between sulfur and nitrogen,[53,54,55] or through hydrogen bond interactions.[56,57]

Using self-assembly to reduce recombination and optimize morphology within solar cells

One possible way of optimizing the morphology of polymer solar cells and reducing the number of trap states is by using self-organization to direct the assembly of polymers into micellular structures which will facilitate efficient exciton harvesting and that will increase carrier mobilities. Several groups have synthesized copolymers with the aim of using self-assembly to drive formation of donor-acceptor domains on the length scales of the exciton diffusion length.[58,59,60] Other groups have used chain-end functionalization to cause polymers like P3HT to adopt orientations which are more favorable for charge extraction.[61] Yet another strategy, which will be explored in depth in this dissertation, uses amphiphilic polymers. An amphiphilic polymer consists of a hydrophobic moiety and a hydrophilic moiety. When introduced into an aqueous environment, these polymers self-assemble into micellular structures in order to minimize the interaction of the hydrophobic moieties with the aqueous solvent. Several examples of such polymers exist in the literature.[62,63,64]

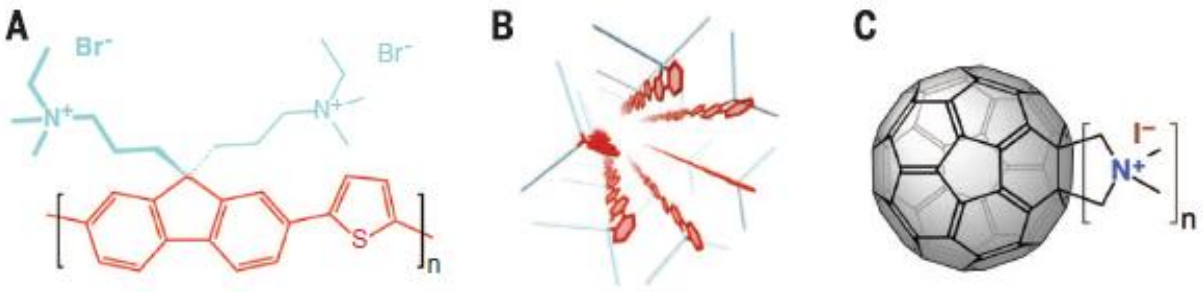

Figure 1.10. (a) Chemical structure of PFT showing hydrophobic aromatic backbone (red) and amphiphilic side-chains (blue). (b) representation of the worm-like micelles that PFT forms in aqueous solution. (c) chemical structure of fulleropyrrolidinium iodide amphiphiles where n represents the number of pyrrolidinium substituents. Figure reprinted with permissions from Huber, R. C. *et al.* "**Long-Lived Photoinduced Polaron Formation in Conjugated Polyelectrolyte-Fullerene Assemblies**" *Science* (2015) *348*, 1340–1343.

In 2013 Clark *et al.* reported the synthesis of an amphiphilic semiconducting polymer, poly{(9,9-bis(3'-(*N*-ethyl-*N*,*N*-dimethylammonio)propyl)fluorene)-2,7-diyl-*alt*-(thiophene-2,5-diyl)} bromide (**PFT**), which spontaneously form into micellular structures (see Figure 1.10).[65] **PFT** was shown to form worm-like micelles in aqueous solution, and **PFT** thin films cast from assembled micelles were shown to exhibit increased hole mobilities compared to films cast of the unquaternized precursor polymer which is identical to **PFT** in terms of the electronic structure of its conjugated backbone. The enhanced conductivity of **PFT** compared to its parent polymer is presumably due to the straightening of the polymer chains in the micellular structures of **PFT**. **PFT** also formed hydrogels in aqueous solution due to the formation of a three-dimensional network of worm-like micelles.[66]

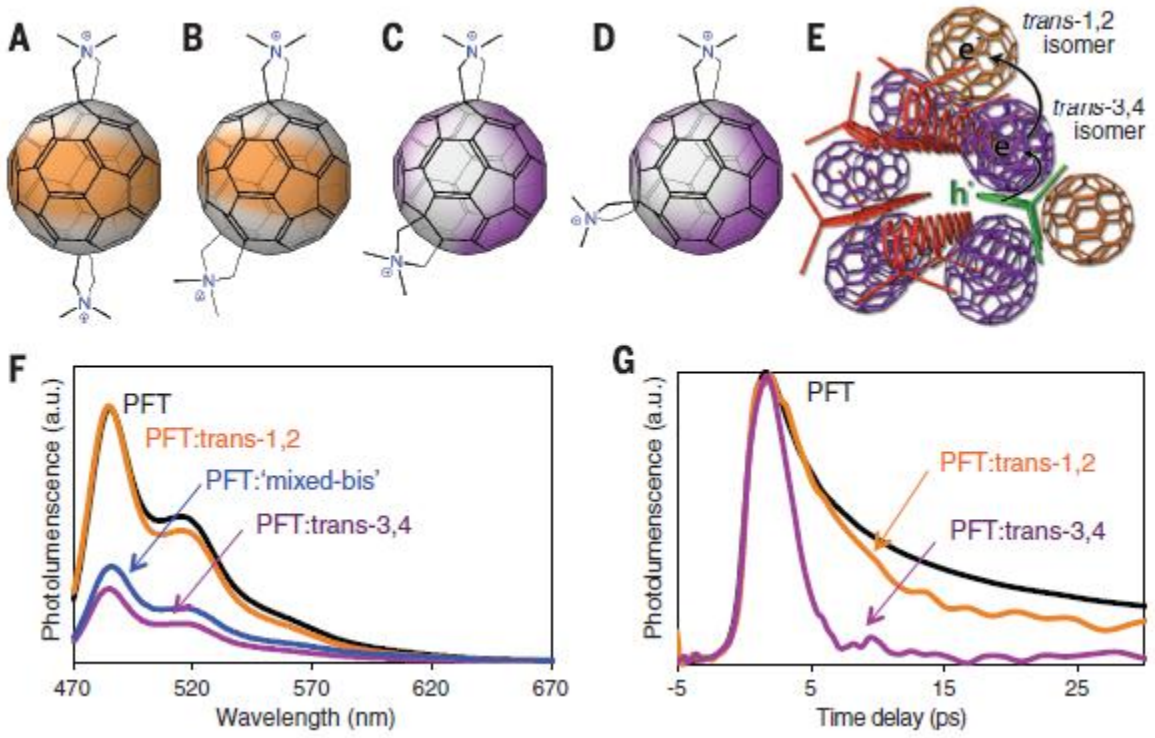

Figure 1.11. Schematic showing chemical structures of (a) *trans*-1 (b) *trans*-2 (c) *trans*-3 (d) *trans*-4 bisfulleropyrrolidinium iodide species with coloring indicating the hydrophobic regions of the fullerene amphiphiles. Photoexcitation of **PFT** leads to an electron transfer cascade from **PFT** to the intercalated and unintercalated fullerene species (E). Photoluminescence (PL) shows that the unintercalated *trans* 1 and 2 species show poor PL quenching while the intercalated *trans* 3 and 4 species show strong PL quenching (F). Time resolved photoluminescence shows that the unintercalated species show the formation of long lived polarons while the intercalated species show fast geminate recombination holes and electrons generated from electron transfer between **PFT** and the *trans* 3 and 4 species. Figure reprinted with permissions from Huber, R. C. *et al.* "**Long-Lived Photoinduced Polaron Formation in Conjugated Polyelectrolyte-Fullerene Assemblies**" *Science* (2015) *348*, 1340–1343.

In 2015 Huber *et al.* reported that these polymer micelles could be combined with amphiphilic fullerene derivatives in order to create an intermixed phase of fullerenes and polymers.[67] The amphiphilic fullerene derivatives consisted of mixtures of bis tris and tetrakis adducts of pyrrolidinium iodide salts. Higher adducts are bulky and cannot effectively

intercalate into the polymer micelles, while fullerene derivatives with fewer substituents, namely some bis adducts, could effectively insert into the polymer micelles. Upon photoexcitation, **PFT** could transfer an electron to the LUMO orbitals of the bisfulleropyrrolidinium iodide salts which had intercalated into the fullerene micelle, and these fullerenes could subsequently transfer this same electron into the LUMO orbitals of higher adducts of fulleropyrrolidinium iodide salts which sat on the outside of the fullerene micelle.

Although the molecular structure of these polymer/fullerene assemblies was explored by a number of characterization techniques such as cryo-TEM and solution SAXS measurements, perhaps the most convincing proof of these assemblies came from exploring the electron transfer properties of **PFT** co assembled with mixtures of several fullerene bispyrrolidinium iodide regioisomers. There are 8 possible regioisomers for bis substituted fullerene derivatives. Huber *et al*. showed that mixtures of the *trans* 3 and 4 bisfulleropyrrolidinium iodide species co-assembled closely with **PFT** micelles, allowing for efficient electron transfer from **PFT** to the *trans* 3 and 4 bisfulleropyrrolidinium iodide species (see Figure 1.11). These assemblies showed fast geminate recombination after the initial electron transfer process. Mixtures of the *trans* 1 and 2 bisfulleropyrrolidinium species with **PFT** had very different behavior compared to the *trans* 3 and 4 species, however. The steric demands of the *trans* 1 and 2 bisfulleropyrrolidinium regioisomers are much different than the *trans* 3 and 4 regioisomers, because the charged bisfulleropyrrolidinium species are located on opposite sides of the fullerene cage in the *trans* 1 and 2 species. This particular geometry prevents the efficient intercalation of the *trans* 1 and 2 regioisomers into the **PFT** micelle. The angle between the pyrrolidinium moieties is more acute for the *trans* 3 and 4 species on the

other hand, and this arrangement of the hydrophilic moieties allows the hydrophobic portion of the fullerene cage to more effectively intercalate into the **PFT** micelle.

Because the *trans* 1 and 2 regioisomers are not intimately intercalated into the **PFT** micelles, mixtures of the *trans* 1 and 2 regioisomers and **PFT** have relatively slow rates of electron transfer from the **PFT** micelles to the fullerene derivatives; most importantly, however, the rate of geminate recombination is very slow, and long lived polaron species can be created from these assemblies. When mixtures of the *trans* 1-4 regioisomers are used an idealized assembly for electron transfer is created. Efficient electron transfer occurs between **PFT** and the *trans* 3 and 4 fullerene derivatives, and these *trans* 3 and 4 derivatives can then transfer an electron to the *trans* 1 and 2 derivatives sitting on the outside of the micelle, thereby efficiently facilitating electron transfer and creating long lived polaron species.

Formation of long lived polaron species is exceedingly rare: most intermixed phases of polymer and fullerene have extremely fast geminate recombination, but the reports of Huber *et al.* showed that by using an electron transfer cascade to physically separate the donor polymer and the fullerene acceptor, geminate recombination of the hole and the electron could be essentially eliminated. Furthermore, this study showed that an assembly of an amphiphilic polymer and fullerene derivatives could form an idealized interface which leads to efficient exciton harvesting. Such assemblies of amphiphilic polymers and fullerenes may improve polymer solar cells by decreasing the amount of trap states in the polymer backbone and by providing ideal architectures that facilitate efficient charge transfer between polymers and solar cells while limiting the amount of geminate recombination. Chapter 2 outlines the

synthesis of a new semiconducting polyelectrolyte that is structurally analogous to **PFT**. We wished to explore the self-assembly and electron transfer properties of this new polymer in order to see if changes in the conjugated backbone of the polymer would lead to more mechanically stable assemblies which could be processed into photovoltaic devices.

Optimizing donor-acceptor π-conjugated semiconducting copolymers for solar cell applications

Part of optimizing polymer solar cells involves carefully engineering the electronic properties of polymers to maximize J_{SC}, V_{OC}, and *FF*. Polymers must have broad absorption across the visible spectrum in order to produce the maximum amount of free carriers, and the band gaps of these polymers must be engineered to maximize the open circuit voltage. Although multiple combinations of donor polymers and acceptor materials can lead to high efficiency devices, a general rule of thumb for a high efficiency device is to have a band gap near 1.5 eV and a LUMO of –3.5 eV *vs*. vacuum when using PCBM as an acceptor molecule.[68] Polymers must also be designed to possess high carrier mobilities to reduce trap-assisted recombination and maximize fill factors. One strategy that allows for the fine tuning of these properties is by creating co-polymers consisting of electron rich and electron deficient monomer units.

Intramolecular charge transfer between electron rich and electron poor units of the polymer facilitate delocalization of electrons in the polymer backbone. The interaction between these units leads to the hybridization of the HOMO and LUMO orbitals of the electron rich and electron poor monomeric units, resulting in polymers with narrow band gaps.[69] The absolute

potentials of the HOMO and LUMO orbitals as well as the band gaps of D-A copolymers can be tuned by carefully selecting monomer units with appropriate HOMO and LUMO levels. The ideal polymer for solar cells cannot simply be designed by selecting polymers which possess monomer units with the appropriate HOMO and LUMO levels, however. Carrier mobility, molecular packing, and solubility all have important repercussions on the performance of solar cells, and these parameters must also be taken into account when designing new polymeric materials.

_N_-Heteroacenes as electron deficient units in D-A semiconducting polymers

There has been a significant amount of research over the last 20 years into applications of acenes and heteroacene derivatives for use organic electronic devices such as organic field effect transistors (OFETs), organic light emitting diodes (OLEDs), and organic photovoltaic devices (OPVs).[70,71,72] The explosive growth of this field was due in no small part to the effort of many groups to synthesize new acene and heteroacene derivatives with the aim of advancing the state of the art in all the aforementioned fields. *N*-heteroacenes have been attracting a significant amount of attention in the field of organic electronics as of late, although they are by no means a new arrival to the field of chemical research: *N*-heteroacenes characterized and studied for well over one-hundred years. [73]

N-Heteroacenes resemble their analogous hydrocarbon acene compounds in many respects: they have similar band gaps and absorptive properties, but substitution of electronegative nitrogen atoms into the aromatic rings of an acene has a net stabilizing effect on the HOMO and LUMO orbitals of a given acene.[74] For instance, the HOMO and LUMO levels

of 6,13-Bis(triisopropylsilylethynyl)pentacene (TIPS pentacene) are -3.1 and -4.9 eV *vs*. vacuum level[75] while the HOMO and LUMO levels of 6,13-Bis(triisopropylsilylethynyl)-5,7,12,14-tetraazapentacene (TIPS tetraazapentacene) are -3.7 and -5.3 eV *vs*. vacuum level,[76] which shows that the LUMO of pentacene can be drastically lowered by substituting nitrogen atoms for carbon atoms (see Figure 1.12). The electronic properties also drastically change between TIPS pentacene and TIPS tetaazapentacene: The band gap is reduced by 0.2 eV in the latter molecule and TIPS tetraazapentacene displays ambipolar charge transport with field effect mobilities measured as μ_h = 0.05 cm^2 V^{-1} s^{-1} and μ_e = 3.3 cm^2 V^{-1} s^{-1}.[76,77,] In contrast, TIPS pentacene is mainly a hole transporting material with field effect mobilities measured as μ_h = 1.2 cm^2 V^{-1} s^{-1} and μ_e = 5 X 10^{-5} cm^2 V^{-1} s^{-1}.[78,79]

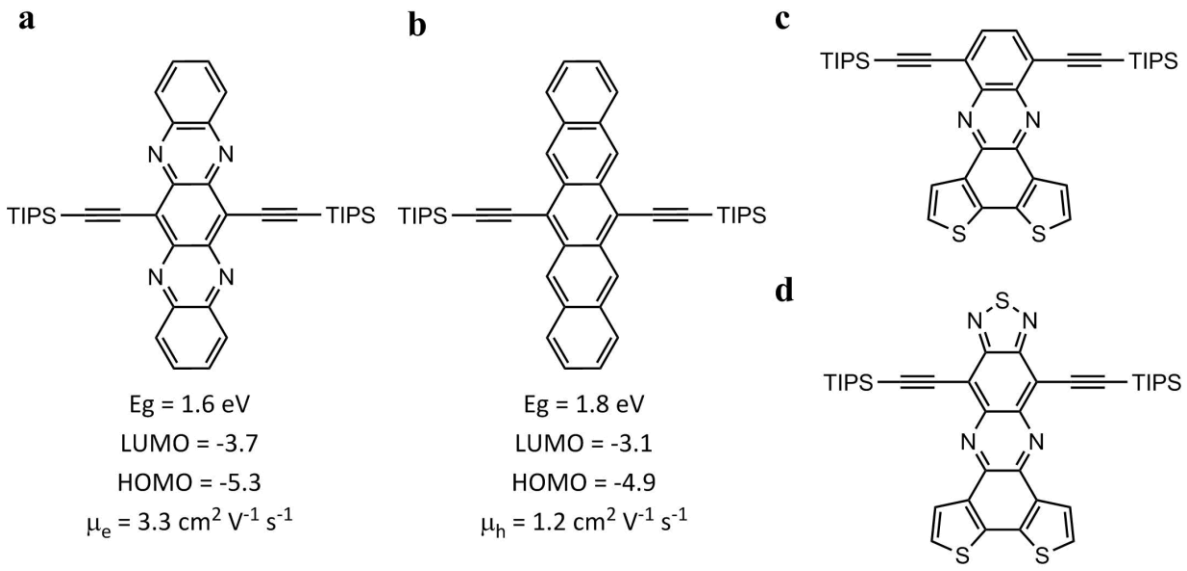

Figure 1.12. Comparison of the electronic properties of TIPS tetraazapentacene (a) and TIPS pentacene (b). *N*-heteroacenes **c** and **d** will be explored at length later in this dissertation.

In addition to having lower HOMO and LUMO levels *N*-heteroacenes have other attractive properties: they are more resistant to oxidation compared to their carbon-based analogs due to lower absolute reduction potentials of their LUMO orbitals. Many of the larger *N*-Heteroacenes also display ambipolar charge transport, high carrier mobilities, and have also been shown to undergo singlet fission.[80] Due to these attractive properties, it would seem that pairing *N*-heteroacenes with electron rich aromatic units in D-A copolymers would lead to polymers with low lying LUMO orbitals and small band gaps, which are all requisites for high efficiency polymer solar cells as discussed in the previous section.

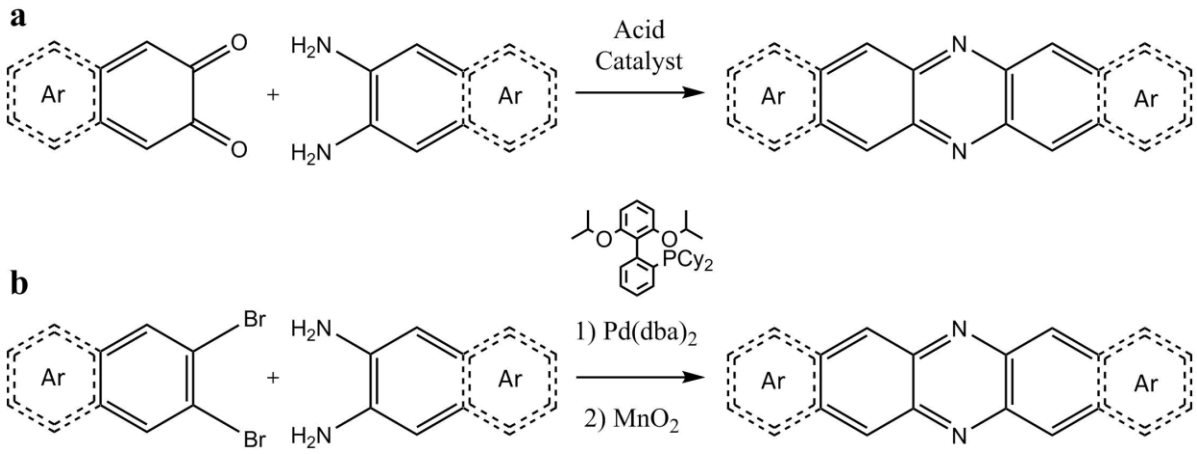

Figure 1.13. Synthetic approaches to the larger *N*-heteroacenes: (a) using the condensation of aryl-*o*-diones and aryl-*o*-diamines (b) using palladium catalyzed couplings of aryl halides and aniline derivatives followed by oxidation.

There are a number of synthetic approaches to producing *N*-Heteroacenes. One method of producing *N*-Heteroacenes involves the condensation of *o*-aryldiamines with *o*-aryldiketones to produce pyrazine derivatives (see Figure 1.13). Another method involves the palladium catalyzed cross-couplings of primary aniline derivatives with aryl halides using palladium

catalyzed cross-coupling reactions followed by oxidation of the resulting *N*-hydroacenes to the fully aromatic species. These methodologies have allowed for the synthesis of a large number of *N*-heteroacene derivatives from relatively simple starting materials. Heteroacenes containing four to seven consecutive aryl rings can be accessed in several steps from commercially available starting materials under mild conditions.[80]

Considering the excellent materials properties of *N*-Heteroacenes and the ease with which they can be accessed, we decided to explore these materials for their use as electron deficient units in D-A copolymers for solar cell applications. Considering the low lying HOMO and LUMO orbitals of these materials should lead to higher V_{OC} values in solar cells, and the decreased band gap and high absorption coefficients should lead to high J_{SC}. Furthermore, the strong intermolecular interactions seen in single crystals of many *N*-Heteroacenes should lead to high interchain conductivity and high carrier mobilities when they are incorporated into a semiconducting polymer. There has been limited use of extended *N*-Heteroacenes in polymer solar cells,[81,82,83] but we set out to synthesize a number of novel polymers consisting of *N*-Heteroacenes fused with electron rich thiophene units in order to create systems with strong interchain electronic coupling, low lying HOMO and LUMO orbitals, and broad absorption across the visible spectrum. Chapters 2 and 3 of this dissertation will focus on donor-acceptor polymers containing monomer units **c** and **d** from Figure 1.12, and will discuss the photophysical properties of the derived polymers.

References

(1) Heeger, A. J. Semiconducting polymers: the Third Generation. *Chem. Soc. Rev.* **2010**, *39*, 2354. DOI: 10.1039/b914956m.

(2) Zheng, H.; Zheng, Y.; Liu, N.; Ai, N.; Wang, Q.; Wu, S.; Zhou, J.; Hu, D.; Yu, S.; Han, S.; et al. All-solution processed polymer light-emitting diode displays. *Nat. Commun.* **2013**, *4*, 1–7. DOI: 10.1038/ncomms2971.

(3) Sirringhaus, H. 25th anniversary article: Organic field-effect transistors: The path beyond amorphous silicon. *Advanced Materials*. **2014**, *26*, 1319–1335.

(4) Janata, J.; Josowicz, M. Conducting polymers in electronic chemical sensors. *Nat. Mater.* **2003**, *2*, 19–24. DOI: 10.1038/nmat768.

(5) Swager, T. M.; Wosnick, J. H. Self-amplifying semiconducting polymers for chemical sensors. *Mrs Bull.* **2002**, *27*, 446–450. DOI: 10.1557/mrs2002.143.

(6) Lee, K.; Cho, S.; Sung, H. P.; Heeger, A. J.; Lee, C. W.; Lee, S. H. Metallic transport in polyaniline. *Nature* **2006**, *441*, 65–68. DOI: 10.1038/nature04705.

(7) Cao, Y.; Treacy, G. M.; Smith, P.; Heeger, A. J. Solution-cast films of polyaniline: Optical-quality transparent electrodes. *Appl. Phys. Lett.* **1992**, *60*, 2711–2713. DOI: 10.1063/1.106852.

(8) Cherenack, K.; Zysset, C.; Kinkeldei, T.; Münzenrieder, N.; Tröster, G. Woven electronic fibers with sensing and display functions for smart textiles. *Adv. Mater.* **2010**, *22*, 5178–5182. DOI: 10.1002/adma.201002159.

(9) Hamedi, M.; Forchheimer, R.; Inganäs, O. Towards woven logic from organic electronic fibres. *Nat. Mater.* **2007**, *6*, 357–362. DOI: 10.1038/nmat1884.

(10) White, M. S.; Kaltenbrunner, M.; Głowacki, E. D.; Gutnichenko, K.; Kettlgruber, G.; Graz, I.; Aazou, S.; Ulbricht, C.; Egbe, D. A. M.; Miron, M. C.; et al. Ultrathin, highly flexible and stretchable PLEDs. *Nat. Photonics* **2013**, *7*, 811–816. DOI: 10.1038/nphoton.2013.188.

(11) Friend, R. H.; Gymer, R. W.; Holmes, A. B.; Burroughes, J. H.; Marks, R. N.; Taliani, C.; Bradley, D. D. C.; Dos Santos, D. A.; Brédas, J. L.; Lögdlund, M.; et al. Electroluminescence in conjugated polymers. *Nature* **1999**, *397*, 121–128. DOI: 10.1038/16393.

(12) Li, G.; Zhu, R.; Yang, Y. Polymer solar cells. *Nat. Photonics* **2012**, *6*, 153–161. DOI: 10.1038/nphoton.2012.11.

(13) Liang, Y.; Chen, Z.; Jing, Y.; Rong, Y.; Facchetti, A.; Yao, Y. Heavily n-dopable π-conjugated redox polymers with ultrafast energy storage capability. *J. Am. Chem. Soc.* **2015**, *137*, 4956–4959. DOI: 10.1021/jacs.5b02290.

(14) Rasmussen, S. C. The Early History of Polyaniline : Discovery and Origins The Early History of Polyaniline : Discovery and Origins. *Substantia* **2017**, *1* DOI: 10.13128/substantia-30.

(15) Staudinger, H. Uber Polymerisation. *Berichte Der Dtsch. Chem. Gesellschafl* **1920**, *53*, 1073–1085. DOI: 10.1017/CBO9781107415324.004.

(16) Oster, G. Herman Francis Mark. *J. Chem. Educ.* **1952**, *29*, 544. DOI: 10.1021/ed029p544.

(17) Hammer, B. A. G.; Müllen, K. Dimensional evolution of polyphenylenes: Expanding in all

directions. *Chem. Rev.* **2016**, *116*, 2103–21040. DOI: 10.1021/acs.chemrev.5b00515.

(18) Rasmussen, S. C. Electrically Conducting Plastics : Revising the. *ACS Symp. Ser.* **2011**, *1080*, 147–163.

(19) Bolto, B. A.; McNeill, R.; Weiss, D. E. Electronic Conduction in Polymers III. Electronic Properties of Polypyrrole. *Aust. J. Chem.* **1963**, *16*, 1090–1103. DOI: https://doi.org/10.1071/CH9631090.

(20) Foundation, T. N. Nobel Prize in Chemistry 2000 Electrically Conductive Plastic The Discovery of Polyacetylene Film : The Dawning of an Era. *Angew. Chem. Int. Ed.* **2001**, *40*, 2574–2580. DOI: 10.1002/1521-3773(20010716)40:14<2574::AID-ANIE2574>3.0.CO;2-N.

(21) MacDiarmid, a. G. "Synthetic Metals": A Novel Role for Organic Polymers (Nobel Lecture). *Angew. Chemie Int. Ed.* **2001**, *40*, 2581–2590. DOI: 10.1002/1521-3773(20010716)40:14<2581::AID-ANIE2581>3.0.CO;2-2.

(22) Heeger, A. J. Semiconducting and Metallic Polymers: The Fourth Generation of Polymeric Materials (Nobel Lecture) Copyright(c) The Nobel Foundation 2001. We thank the Nobel Foundation, Stockholm, for permission to print this lecture. *Angew. Chem. Int. Ed. Engl.* **2001**, *40*, 2591–2611. DOI: 10.1002/1521-3773(20010716)40:14<2591::AID-ANIE2591>3.0.CO.

(23) Brédas, J. L.; Thémans, B.; Fripiat, J. G.; André, J. M.; Chance, R. R. Highly conducting polyparaphenylene, polypyrrole, and polythiophene chains: An ab initio study of the geometry and electronic-structure modifications upon doping. *Phys. Rev. B* **1984**, *29*,

6761–6773. DOI: 10.1103/PhysRevB.29.6761.

(24) Brédas, J. L. Relationship between band gap and bond length alternation in organic conjugated polymers. *J. Chem. Phys.* **1985**, *82*, 3808–3811. DOI: 10.1063/1.448868.

(25) Bredas, J.; Street, G. Polarons, Bipolarons, and Solitons in Conducting Polymers. *Acc. Chem. Res.* **1985**, *1305*, 309–315.

(26) Kwon, O.; McKee, M. L. Calculations of Band Gaps in Polyaniline from Theoretical Studies of Oligomers. *J. Phys. Chem. B* **2000**, *104*, 1686–1694. DOI: 10.1021/jp9910946.

(27) Van Mullekom, H. A. M.; Vekemans, J. A. J. M.; Havinga, E. E.; Meijer, E. W. *Developments in the chemistry and band gap engineering of donor-acceptor substituted conjugated polymers*. *Materials Science and Engineering R: Reports* **2001,** *32, 1-40*.

(28) Thompson, B. C. VARIABLE BAND GAP POLY(3,4-ALKYLENEDIOXYTHIOPHENE)-BASED POLYMERS FOR PHOTOVOLTAIC AND ELECTROCHROMIC APPLICATIONS, **2005**.

(29) McCullough, R. D.; Spectus, C. O. N.; Osaka, I.; McCullough, R. D. Advances in Molecular Design and Synthesis of Regioregular Polythiophenes. *Acc. Chem. Res.* **2008**, *41*, 1202–1214. DOI: 10.1021/ar800130s.

(30) Bao, Z.; Chan, W. K.; Yu, L. Exploration of the Stille Coupling Reaction for the Syntheses of Functional Polymers. *J. Am. Chem. Soc.* **1995**, *117*, 12426–12435. DOI: 10.1021/ja00155a007.

(31) Xu, S.; Kim, E. H.; Wei, A.; Negishi, E. Pd- and Ni-catalyzed cross-coupling reactions in the

synthesis of organic electronic materials. *Sci. Technol. Adv. Mater.* **2014**, *15*, 44201. DOI: 10.1088/1468-6996/15/4/044201.

(32) Bura, T.; Blaskovits, J. T.; Leclerc, M. Direct (Hetero)arylation Polymerization: Trends and Perspectives. *J. Am. Chem. Soc.* **2016**, *138*, 10056–10071. DOI: 10.1021/jacs.6b06237.

(33) Pouliot, J. R.; Grenier, F.; Blaskovits, J. T.; Beaupré, S.; Leclerc, M. Direct (Hetero)arylation Polymerization: Simplicity for Conjugated Polymer Synthesis. *Chem. Rev.* **2016**, *116*, 14225–14274. DOI: 10.1021/acs.chemrev.6b00498.

(34) Gregg, B. A. Excitonic Solar Cells. *J. Phys. Chem. B* **2003**, *107*, 4688–4698. DOI: 10.1021/jp022507x.

(35) Brabec, C. J.; Sariciftci, N. S.; Hummelen, J. C. Plastic solar cells. *Adv. Funct. Mater.* **2001**, *11*, 15–26. DOI: 10.1002/1616-3028(200102)11.

(36) Li, G.; Zhu, R.; Yang, Y. Polymer solar cells. *Nat. Photonics* **2012**, *6*, 153–161. DOI: 10.1038/nphoton.2012.11.

(37) Shaw, P. E.; Ruseckas, A.; Samuel, I. D. W. Exciton Diffusion Measurements in Poly(3-hexylthiophene). *Adv. Mater.* **2008**, *20*, 3516–3520. DOI: 10.1002/adma.200800982.

(38) Vanlaeke, P.; Swinnen, A.; Haeldermans, I.; Vanhoyland, G.; Aernouts, T.; Cheyns, D.; Deibel, C.; D'Haen, J.; Heremans, P.; Poortmans, J.; et al. P3HT/PCBM bulk heterojunction solar cells: Relation between morphology and electro-optical characteristics. *Sol. Energy Mater. Sol. Cells* **2006**, *90*, 2150–2158. DOI: 10.1016/j.solmat.2006.02.010.

(39) Brabec, C. J.; Cravino, A.; Meissner, D.; Sariciftci, N. S.; Fromherz, T.; Rispens, M. T.; Sanchez, L.; Hummelen, J. C. Origin of the open circuit voltage of plastic solar cells. *Adv. Func. Mat* **2001**, *11*, 374–380.

(40) Ma, W.; Yang, C.; Gong, X.; Lee, K.; Heeger, A. J. Thermally stable, efficient polymer solar cells with nanoscale control of the interpenetrating network morphology. *Adv. Funct. Mater.* **2005**, *15*, 1617–1622. DOI: 10.1002/adfm.200500211.

(41) Guo, X.; Zhou, N.; Lou, S. J.; Smith, J.; Tice, D. B.; Hennek, J. W.; Ortiz, R. P.; Navarrete, J. T. L.; Li, S.; Strzalka, J.; et al. Polymer solar cells with enhanced fill factors. *Nat. Photonics* **2013**, *7*, 825–833. DOI: 10.1038/nphoton.2013.207.

(42) Müller, J. G.; Lupton, J. M.; Feldmann, J.; Lemmer, U.; Scharber, M. C.; Sariciftci, N. S.; Brabec, C. J.; Scherf, U. Ultrafast dynamics of charge carrier photogeneration and geminate recombination in conjugated polymer:fullerene solar cells. *Phys. Rev. B - Condens. Matter Mater. Phys.* **2005**, *72*, 1–10. DOI: 10.1103/PhysRevB.72.195208.

(43) Cowan, S. R.; Roy, A.; Heeger, A. J. Recombination in polymer-fullerene bulk heterojunction solar cells. *Phys. Rev. B* **2010**, *82*, 245207. DOI: 10.1103/PhysRevB.82.245207.

(44) Wetzelaer, G. A. H.; Kuik, M.; Nicolai, H. T.; Blom, P. W. M. Trap-assisted and Langevin-type recombination in organic light-emitting diodes. *Phys. Rev. B - Condens. Matter Mater. Phys.* **2011**, *83*, 1–5. DOI: 10.1103/PhysRevB.83.165204.

(45) Tzabari, L.; Tessler, N. Shockley–Read–Hall recombination in P3HT:PCBM solar cells as

observed under ultralow light intensities. *J. Appl. Phys.* **2011**, *109*, 64501. DOI: 10.1063/1.3549820.

(46) Mandoc, M. M.; Kooistra, F. B.; Hummelen, J. C.; de Boer, B.; Blom, P. W. M. Effect of traps on the performance of bulk heterojunction organic solar cells. *Appl. Phys. Lett.* **2007**, *91*, 263505–3.

(47) Cowan, S. R.; Roy, A.; Heeger, A. J. Recombination in polymer-fullerene bulk heterojunction solar cells. *Phys. Rev. B* **2010**, *82*, 245207. DOI: 10.1103/PhysRevB.82.245207.

(48) Rossi, G.; Chance, R. R.; Silbey, R. Conformational disorder in conjugated polymers. *J. Chem. Phys.* **1989**, *90*, 7594. DOI: 10.1063/1.456193.

(49) Westenhoff, S.; Beenken, W. J. D.; Yartsev, A.; Greenham, N. C. Conformational disorder of conjugated polymers. *J. Chem. Phys.* **2006**, *125* DOI: 10.1063/1.2358682.

(50) Grozema, F. C.; Van Duijnen, P. T.; Berlin, Y. A.; Ratner, M. A.; Siebbeles, L. D. A. Intramolecular charge transport along isolated chains of conjugated polymers: Effect of torsional disorder and polymerization defects. *J. Phys. Chem. B* **2002**, *106*, 7791–7795. DOI: 10.1021/jp021114v.

(51) Allen, J. E.; Yager, K. G.; Hlaing, H.; Nam, C.-Y.; Ocko, B. M.; Black, C. T. Enhanced charge collection in confined bulk heterojunction organic solar cells. *Appl. Phys. Lett.* **2011**, *99*, 163301. DOI: 10.1063/1.3651509.

(52) Coakley, K. M.; McGehee, M. D. Photovoltaic cells made from conjugated polymers

infiltrated into mesoporous titania. *Appl. Phys. Lett.* **2003**, *83*, 3380–3382. DOI: 10.1063/1.1616197.

(53) Zhang, X.; Bronstein, H.; Kronemeijer, A. J.; Smith, J.; Kim, Y.; Kline, R. J.; Richter, L. J.; Anthopoulos, T. D.; Sirringhaus, H.; Song, K.; et al. Molecular origin of high field-effect mobility in an indacenodithiophene-benzothiadiazole copolymer. *Nat. Commun.* **2013**, *4*, 2238. DOI: 10.1038/ncomms3238.

(54) Tseng, H. R.; Phan, H.; Luo, C.; Wang, M.; Perez, L. A.; Patel, S. N.; Ying, L.; Kramer, E. J.; Nguyen, T. Q.; Bazan, G. C.; et al. High-mobility field-effect transistors fabricated with macroscopic aligned semiconducting polymers. *Adv. Mater.* **2014**, *26*, 2993–2998. DOI: 10.1002/adma.201305084.

(55) Zhang, W.; Smith, J.; Watkins, S. E.; Gysel, R.; McGehee, M.; Salleo, A.; Kirkpatrick, J.; Ashraf, S.; Anthopoulos, T.; Heeney, M.; et al. Indacenodithiophene semiconducting polymers for high-performance, air-stable transistors. *J. Am. Chem. Soc.* **2010**, *132*, 11437–11439. DOI: 10.1021/ja1049324.

(56) Lei, T.; Dou, J. H.; Cao, X. Y.; Wang, J. Y.; Pei, J. Electron-Deficient Poly(p-phenylene vinylene) Provides Electron Mobility over 1 cm2 V-1 s-1 under Ambient Conditions. *J. Am. Chem. Soc.* **2013**, *135*, 12168–12171. DOI: 10.1021/ja403624a.

(57) Lei, T.; Xia, X.; Wang, J. Y.; Liu, C. J.; Pei, J. “conformation Locked” Strong Electron-Deficient Poly(p -Phenylene Vinylene) Derivatives for Ambient-Stable n-Type Field-Effect Transistors: Synthesis, Properties, and Effects of Fluorine Substitution Position. *J. Am.*

Chem. Soc. **2014**, *136*, 2135–2141. DOI: 10.1021/ja412533d.

(58) Yang, C.; Lee, J. K.; Heeger, A. J.; Wudl, F. Well-defined donor–acceptor rod–coil diblock copolymers based on P3HT containing C60: the morphology and role as a surfactant in bulk-heterojunction solar cells. *J. Mater. Chem.* **2009**, *19*, 5416. DOI: 10.1039/b901732a.

(59) De Boer, B.; Stalmach, U.; Van Hutten, P. F.; Melzer, C.; Krasnikov, V. V.; Hadziioannou, G. Supramolecular self-assembly and opto-electronic properties of semiconducting block copolymers. *Polymer (Guildf).* **2001**, *42*, 9097–9109. DOI: 10.1016/S0032-3861(01)00388-3.

(60) Segalman, R. A.; McCulloch, B.; Kirmayer, S.; Urban, J. J. Block copolymers for organic optoelectronics. *Macromolecules* **2009**, *42*, 9205–9216. DOI: 10.1021/ma901350w.

(61) Ma, J.; Hashimoto, K.; Koganezawa, T.; Tajima, K. End-on orientation of semiconducting polymers in thin films induced by surface segregation of fluoroalkyl chains. *J. Am. Chem. Soc.* **2013**, *135*, 9644–9647. DOI: 10.1021/ja4051179.

(62) Duarte, A.; Pu, K. Y.; Liu, B.; Bazan, G. C. Recent advances in conjugated polyelectrolytes for emerging optoelectronic applications. *Chem. Mater.* **2011**, *23*, 501–515. DOI: 10.1021/cm102196t.

(63) Tuncel, D.; Demir, H. V. Conjugated polymer nanoparticles. *Nanoscale* **2010**, *2*, 484. DOI: 10.1039/b9nr00374f.

(64) Prescher, S.; Ghasimi, S.; H??hne, P.; Grygiel, K.; Landfester, K.; Zhang, K. A. I.; Yuan, J. Polyfluorene polyelectrolyte nanoparticles: Synthesis of innovative stabilizers for

heterophase polymerization. *Macromol. Rapid Commun.* **2014**, *35*, 1925–1930. DOI: 10.1002/marc.201400440.

(65) Clark, A. P.; Shi, C.; Ng, B. C.; Wilking, J. N.; Ayzner, A. L.; Stieg, A. Z.; Schwartz, B. J.; Mason, T. G.; Rubin, Y.; Tolbert, S. H.; et al. Self-Assembling Semiconducting Electronic Materials. **2013**, No. 2, 962–977.

(66) Huber, R. C.; Ferreira, A. S.; Aguirre, J. C.; Kilbride, D.; Toso, D. B.; Mayoral, K.; Zhou, Z. H.; Kopidakis, N.; Rubin, Y.; Schwartz, B. J.; et al. Structure and Conductivity of Semiconducting Polymer Hydrogels. *J. Phys. Chem. B* **2016**, *120*, 6215–6224. DOI: 10.1021/acs.jpcb.6b02202.

(67) Huber, R. C.; Ferreira, A. S.; Thompson, R.; Kilbride, D.; Knutson, N. S.; Devi, L. S.; Toso, D. B.; Challa, J. R.; Zhou, Z. H.; Rubin, Y.; et al. Long-lived photoinduced polaron formation in conjugated polyelectrolyte-fullerene assemblies. *Science (80-.).* **2015**, *348*, 1340–1343. DOI: 10.1126/science.aaa6850.

(68) Scharber, M. C.; Mühlbacher, D.; Koppe, M.; Denk, P.; Waldauf, C.; Heeger, A. J.; Brabec, C. J. Design rules for donors in bulk-heterojunction solar cells - Towards 10 % energy-conversion efficiency. *Adv. Mater.* **2006**, *18*, 789–794. DOI: 10.1002/adma.200501717.

(69) Beaujuge, P. M.; Amb, C. M.; Reynolds, J. R. Spectral Engineering in π -Conjugated Polymers Interactions. *Acc. Chem. Res.* **2010**, *43*, 1396–1407. DOI: 10.1021/ar100043u.

(70) Anthony, J. E. The larger acenes: Versatile organic semiconductors. *Angew. Chemie - Int. Ed.* **2008**, *47*, 452–483. DOI: 10.1002/anie.200604045.

(71) Facchetti, A. Semiconductors for organic transistors. *Mater. Today* **2007**, *10*, 28–37. DOI: 10.1016/S1369-7021(07)70017-2.

(72) Anthony, J. E. Functionalized acenes and heteroacenes for organic electronics. *Chem. Rev.* **2006**, *106*, 5028–5048. DOI: 10.1021/cr050966z.

(73) Bunz, U. H. F.; Engelhart, J. U.; Lindner, B. D.; Schaffroth, M. Large N-heteroacenes: New tricks for very old dogs? *Angew. Chemie - Int. Ed.* **2013**, *52*, 3810–3821. DOI: 10.1002/anie.201209479.

(74) Bunz, U. H. F. N-heteroacenes. *Chemistry* **2009**, *15*, 6780–6789. DOI: 10.1002/chem.200900990.

(75) Yang, L.; Tabachnyk, M.; Bayliss, S. L.; Böhm, M. L.; Broch, K.; Greenham, N. C.; Friend, R. H.; Ehrler, B. Solution-processable singlet fission photovoltaic devices. *Nano Lett.* **2015**, *15*, 354–358. DOI: 10.1021/nl503650a.

(76) Miao, Q. Ten years of N-heteropentacenes as semiconductors for organic thin-film transistors. *Adv. Mater.* **2014**, *26*, 5541–5549. DOI: 10.1002/adma.201305497.

(77) Liang, Z.; Tang, Q.; Xu, J.; Miao, Q. Soluble and stable N-heteropentacenes with high field-effect mobility. *Adv. Mater.* **2011**, *23*, 1535–1539. DOI: 10.1002/adma.201004325.

(78) Park, S. K.; Jackson, T. N.; Anthony, J. E.; Mourey, D. A. High mobility solution processed 6,13-bis(triisopropyl-silylethynyl) pentacene organic thin film transistors. *Appl. Phys. Lett.* **2007**, *91*, 6–9. DOI: 10.1063/1.2768934.

(79) Nicolas, Y.; Castet, F.; Devynck, M.; Tardy, P.; Hirsch, L.; Labrugère, C.; Allouchi, H.; Toupance, T. TIPS-triphenodioxazine versus TIPS-pentacene: Enhanced electron mobility for n-type organic field-effect transistors. *Org. Electron. physics, Mater. Appl.* **2012**, *13*, 1392–1400. DOI: 10.1016/j.orgel.2012.04.010.

(80) Bunz, U. H. F. The Larger Linear N-Heteroacenes. *Acc. Chem. Res.* **2015**, *48*, 1676–1686. DOI: 10.1021/acs.accounts.5b00118.

(81) Planells, M.; Nikolka, M.; Hurhangee, M.; Tuladhar, P. S.; White, A. J. P.; Durrant, J. R.; Sirringhaus, H.; McCulloch, I. The effect of thiadiazole out-backbone displacement in indacenodithiophene semiconductor polymers. *J. Mater. Chem. C* **2014**, *2*, 8789–8795. DOI: 10.1039/C4TC01500B.

(82) Mondal, R.; Becerril, H. a.; Verploegen, E.; Kim, D.; Norton, J. E.; Ko, S.; Miyaki, N.; Lee, S.; Toney, M. F.; Brédas, J.-L.; et al. Thiophene-rich fused-aromatic thienopyrazine acceptor for donor–acceptor low band-gap polymers for OTFT and polymer solar cell applications. *J. Mater. Chem.* **2010**, *20*, 5823. DOI: 10.1039/c0jm00903b.

(83) Zhang, Y.; Zou, J.; Yip, H.-L.; Chen, K.-S.; Zeigler, D. F.; Sun, Y.; Jen, A. K.-Y. Indacenodithiophene and Quinoxaline-Based Conjugated Polymers for Highly Efficient Polymer Solar Cells. *Chem. Mater.* **2011**, *23*, 2289–2291. DOI: doi: 10.1021/cm200316s.

Chapter 2 : Synthesis and electrochemical characterization of Poly{(4,4-bis(3'-(*N*-ethyl-*N,N*-dimethylammonio)propyl)cyclopenta[2,1-b:3,4-b']dithiophene)-2,6-diyl-alt-(thiophene-2,5-diyl)} bromide (PCT)

Introduction

Conjugated polyelectrolytes (CPEs) are a class of polymer consisting of polymeric conjugated π-systems, usually bearing aromatic rings, and substituted with side chains containing ionic functionalities such as ammonium, alkylphosphonium, or carboxylate ions.[1] The combination of a hydrophilic ionic side chain with a hydrophobic neutral π-conjugated polymer core can lead to solution phase self-organization into micellar structures, due to preferential solvation of the ionic functionalities in aqueous solution. Self-organization of CPEs into micelles can lead to a number of changes in the photochemical[2] and conductive[3] properties of CPEs when compared to the fully solvated (unassembled) species. CPEs have therefore been utilized in OPVs,[4,5] sensors,[6,7,8] and biomedical applications,[9,10,11] because their tendency toward self-assembly in aqueous solution allows for greater control over a wide range of electrochemical and photochemical properties.

This chapter concerns a particular class of CPE consisting of fluorene or cyclopenta[2,1-b:3,4-b']dithiophene units covalently linked to thiophene rings (see Figure 2.1). The main goal of this work was to utilize the unique structural features of these monomer units to form polymers which self-assemble into micellar structures. Fluorene and cyclopenta[2,1-b:3,4-b']dithiophene monomer units are somewhat unique compared to other planar conjugated monomers in that the 9-position of fluorene and the 4-position of cyclopenta[2,1-b:3,4-

b']dithiophene are sp^3 hybridized and conformationally locked, due to the fact that these atoms form a “bridge” between two coplanar aromatic rings fused together by a cyclopentadiene unit. When the 9-position of the fluorene or the 4-position of the cyclopenta[2,1-b:3,4-b']dithiophene is disubstituted with alkyl ammonium side chains, the ionic functionalities are geometrically constrained to sit above and below the plane of the flat aromatic backbone, forming an almost wedge like shape (see Figure 2.1).

CPEs containing either 9,9-bisalkylammonium substituted fluorene monomers or 4,4-bisalkylammonium substituted cyclopenta[2,1-b:3,4-b']dithiophene units have been shown to form nanoscale micellar structures in aqueous solution consisting of several polymer chains.[12,13,14,15] The polymer chains are organized within the micelle in such a way as to allow the hydrophilic alkylammonium to be solvated on the outside of the micelle while the hydrophobic aromatic backbone is on the inside of the micelle (see Figure 2.1). These polymers tend to form worm-like micelles with the long axis of the conjugated polymer backbone defining the long axis of the micelle.

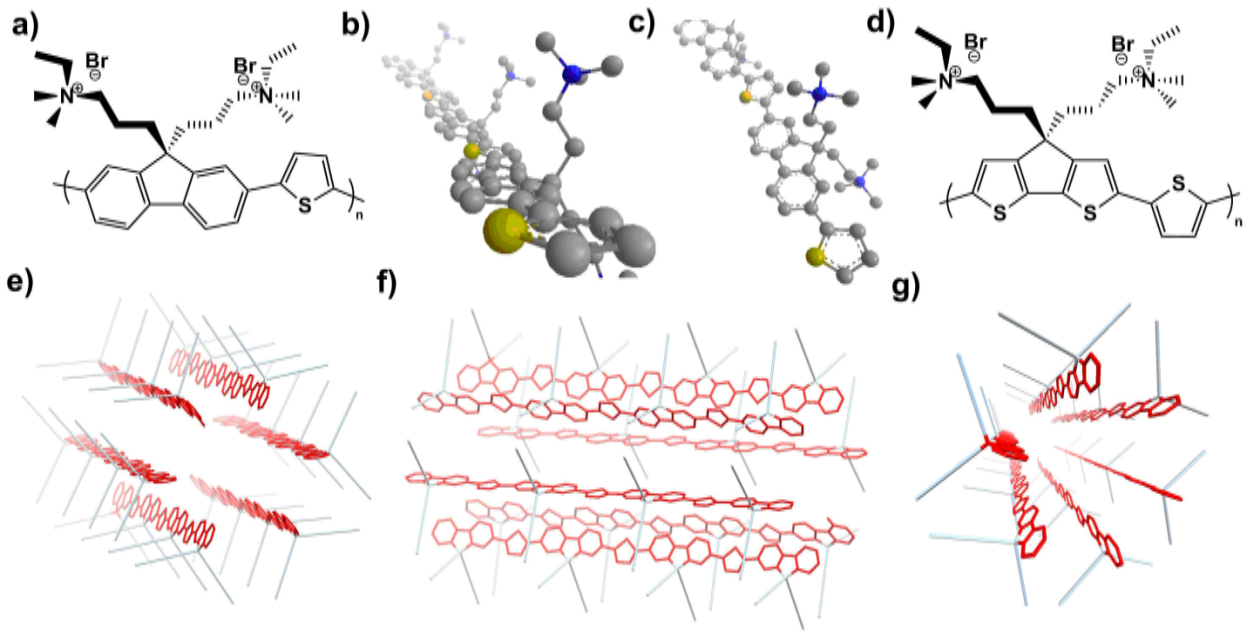

Figure 2.1. a) Molecular structure of the CPE **PFT**. b) Side view of a ball-and-stick model of a **PFT** polymer chain. c) Top-down view of a **PFT** polymer chain. d) Molecular structure of the CPE **PCT**. e-g) Models of the molecular structure of the worm like micelles formed by the hydrophilic interaction between alkylammonium side chains (blue) and an aqueous environment and the hydrophobic interaction with the aromatic backbone (red) with an aqueous environment.

The self-organization of fluorene or cyclopenta[2,1-b:3,4-b']dithiophene-based polymers into worm-like micelles in aqueous solution helps to planarize the conjugated polymer backbone. This is because deplanarization of the polymer backbone would disrupt the structure of the worm-like micelle, thereby increasing the amount of unfavorable interactions between water molecules and the hydrophobic aromatic backbone of the polymer. The forced planarization of the polymer backbone has been shown to improve the mobility of free carriers along the polymer backbone.[3] In relation to this, there is a good amount of theoretical and experimental evidence that suggests that increased planarity of the polymer backbone should be highly favorable in terms of its potential photophysical applications as a result of a decrease

in the density of trap states along the polymer backbone, and higher mobilities of free carriers.[16,17,18]

CPEs have been utilized in the active layers of OPVs with the express aim of using their self-assembly properties to control the active layer morphology of OPVs.[19,20] The Rubin, Schwartz, and Tolbert groups have shown that solution phase self-assembly of the CPE poly{(9,9-bis(3'-(*N*-ethyl-*N*,*N*-dimethylammonio)propyl)fluorene)-2,7-diyl-*alt*-(thiophene-2,5-diyl)} bromide (**PFT**) (Figure 2.1) into worm-like micelles in water leads to formation of hydrogels.[13] **PFT** hydrogels show increased conductivity when compared to the solvated polymer.[3] It has also been shown that mixtures of **PFT** hydrogels and polycationic fullerene species self-organize into micellar structures thereby facilitating the formation of long lived polaron species created via photoinduced charge transfer from **PFT** to the polycationic fullerene species.[21]

Our group therefore set out to synthesize an analogous CPE based on the substitution of the fluorenyl unit of **PFT** by incorporating a cyclopenta[2,1-b:3,4-b']dithiophene unit. We hypothesized that the new polymer would share many similar materials properties to **PFT** due to the structural similarities of the two polymers, but substitution of the fluorene unit of **PFT** with a cyclopenta[2,1-b:3,4-b']dithiophene unit would be expected to enhance the conductive, electrochemical, and photochemical properties of the new polymer compared to **PFT**. We were particularly interested to see how the new polymer would also form self-assembled structures and produce long lived polarons when it was mixed with polycationic fullerene species. This chapter describes the synthesis and characterization of this new polymer: Poly{(4,4-bis(3'-(*N*-

ethyl-*N*,*N*-dimethylammonio)propyl)cyclopenta[2,1-b:3,4-b']dithiophene)-2,6-diyl-alt-(thiophene-2,5-diyl)} bromide (**PCT**).

Synthesis of PCT

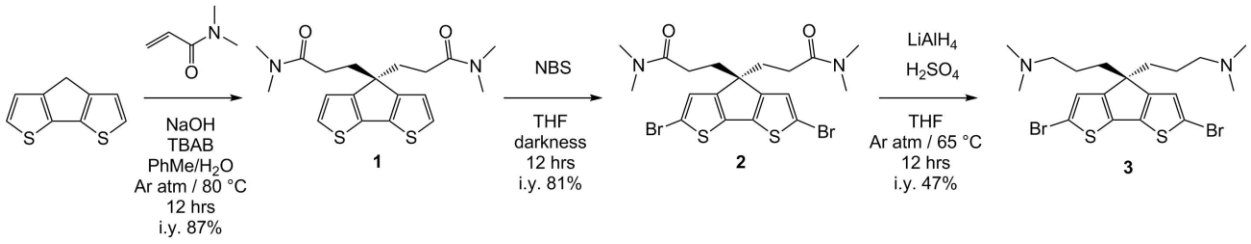

Figure 2.2. Synthesis of monomer **3.**

The monomer used in the synthesis of **PCT** was itself synthesized using the scheme outlined in Figure 2.2. Briefly, intermediate **1** was obtained via the Michael addition of the cyclopentadithiophene anion onto excess *N*,*N*-dimethylacrylamide to generate the bis-amide species. Intermediate **1** was then brominated using *N*-bromosuccinimide to yield dibromide **2**. Compound **2** was then reduced to the corresponding bisamine species using alane generated *in-situ* via the addition of anhydrous sulfuric acid to lithium aluminum hydride, to yield **3**.

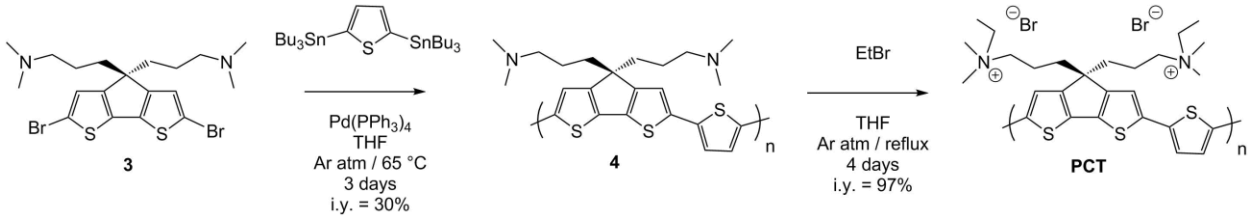

Figure 2.3. Synthesis of **PCT.**

PCT was then synthesized from dibromide **3** using the reactions outlined in Figure 2.3. Polymer **4** was synthesized via a palladium catalyzed Stille cross—coupling reaction between

dibromide **3** and 2,5-bis(tributylstannyl)thiophene. The amine groups of the resulting polymer were then quaternized to the ammonium salt using excess ethyl bromide at reflux to yield **PCT**. Attempts to characterize the molecular weight and polydispersity index of both amine polymer **4** and **PCT** via GPC were unsuccessful in a number of solvents. However, light scattering measurements of **4** in dilute solutions of chloroform were successful in establishing the M_n and M_w of **4** and the results are summarized in Table 2.1. The light scattering data was fit using Zimm's formalism of the Raleigh-Debye-Grans light scattering model for dilute polymer solutions[22,23] using the ASTRA 8.0 software to calculate the number average molecular weight (9,760 Da) and polydispersity (2.13) of **4.** The M_n and dispersity derived from light scattering were extremely close to the previously reported M_n and dispersity for unfractionated samples of unquaternized samples of **PFT**.[3]

Table 2.1. Summary of properties of **4** derived from light scattering analysis.

Polymer	M_n	Dispersity	DP_n
4	9,760	2.13	22.7

Photophysical characterization of PCT

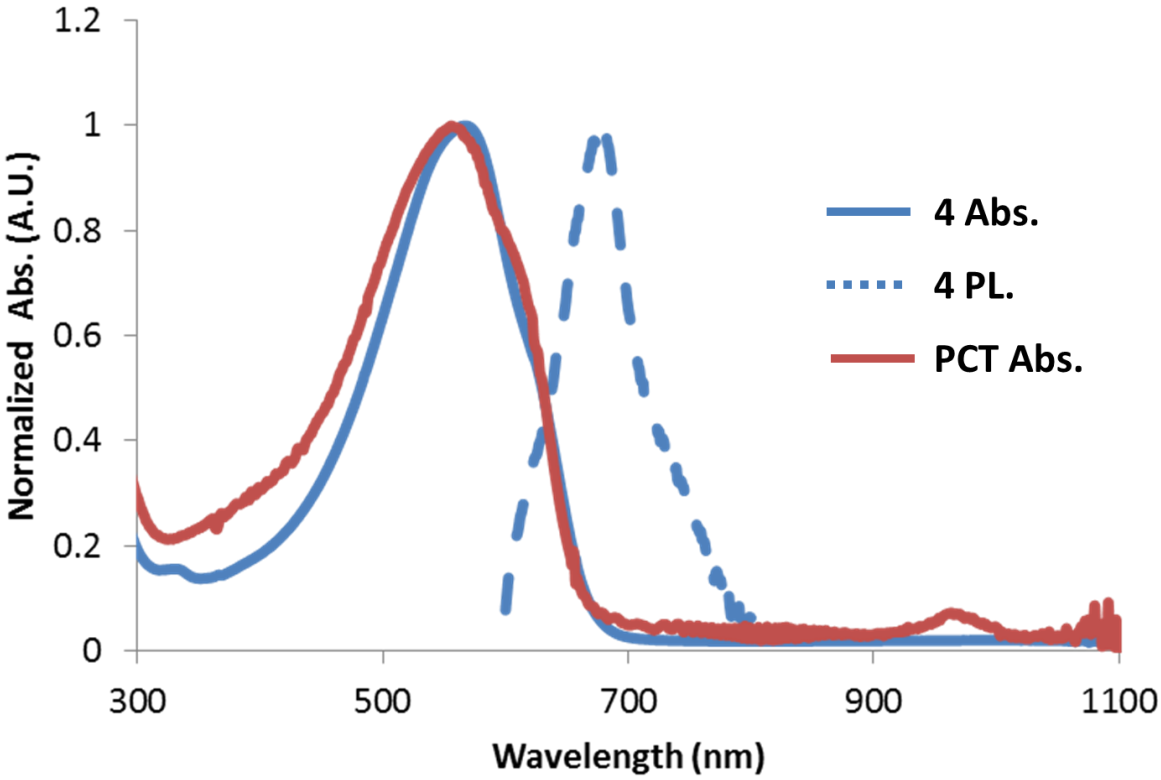

Figure 2.4. Normalized absorbance (blue solid) and normalized fluorescence (blue dashed, excitation 580 nm) of **4** in $CHCl_3$, and the normalized absorbance spectrum of **PCT** in H_2O (red).

Bisamine polymer **4** gives a fluorescent indigo solution in chloroform and exhibits an optical band gap of 690 nm (1.8 eV) and broad absorption from 410 nm to 690 nm as can be seen in Figure 2.4. When excited at the max absorbance of 580 nm, **4** displays an emission with a maximum at 670 nm. Upon quaternization, there is a slight broadening of the absorbance of **PCT** when measured in dilute solutions in water (≈ 0.001 mg/mL), but the absorption spectra of **PCT** and **4** are otherwise identical. There is a significant decrease in the optical band gap of **PCT** (690 nm), compared to the optical band gap of **PFT** (500 nm).[3] This drastic decrease in the

optical band gap confirms the anticipated smaller HOMO-LUMO gap resulting from the lower degree of aromaticity of a thiophene ring compared to a phenyl ring.

Electrochemical Characterization of PCT

Table 2.2. Electrochemical properties of **PCT** measured by cyclic voltammetry.

Polymer	I.P. vs. Li/Li+	HOMO vs. vacuum level	Optical E_g	LUMO calc[a]
PCT	4.1 V	–5.4 V	1.8 eV	–3.4 eV

[a] LUMO calculated from the optical band gap.

The electrochemical properties of **PCT** were measured via cyclic voltammetry (Figure 2.5) and are summarized in Table 2.2. CVs were obtained on films drop-cast on ITO glass and CVs were measured in propylene carbonate with Li/Li^+ as the reference electrode and the ITO glass as the working electrode using a sweep rate of 0.5 mV/s. **PCT** exhibits two irreversible oxidation peaks at 4.1 and 4.5 V *vs*. Li/Li+. The reduction peak could not be measured possibly due to the degradation of the polymer during oxidation. Absolute ionization potentials were calculated using –4.3 V as the absolute electrode potential for the standard hydrogen electrode[24] and –3.0 V as the standard reduction potential of Li/Li^+ vs. the standard hydrogen electrode.[25] It should be noted that the HOMO and LUMO values of **PCT** are 200 mV lower than the HOMO of poly-3-hexylthiophene (P3HT) which has a HOMO level of –5.2 eV vs. vacuum level.[26] The LUMO of **PCT** (–3.4 eV vs. vacuum level) is still sufficiently high enough to allow a thermodynamically favorable electron transfer to polysubstituted fullerene derivatives as acceptors (LUMOs of di- or trisubstituted fullerenes are ≤ –3.8 eV vs. vacuum level).[27]

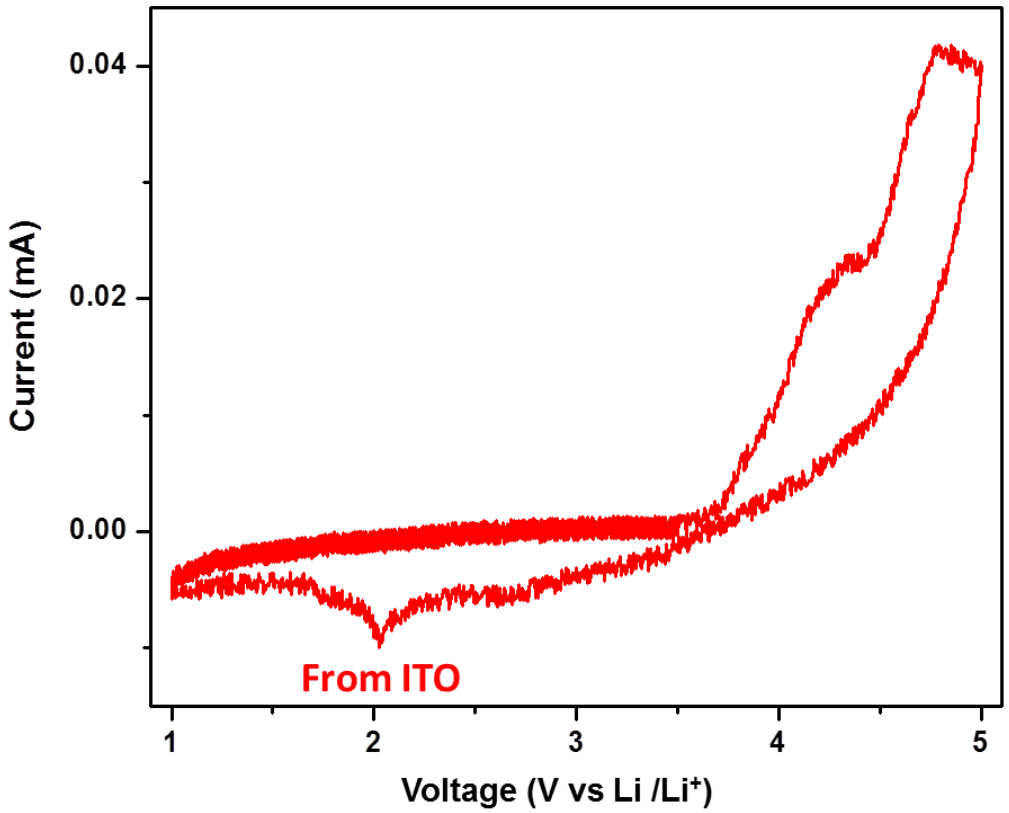

Figure 2.5. Cyclic voltammogram of **PCT.**

Conclusion

We have herein reported the synthesis and characterization of some of the photochemical and electrochemical properties a new CPE, poly{(4,4-bis(3'-(*N*-ethyl-*N*,*N*-dimethylammonio)propyl)cyclopenta[2,1-b:3,4-b']dithiophene)-2,6-diyl-alt-(thiophene-2,5-diyl)} bromide (PCT). We have found this polymer to possess broad absorption across the visible spectrum with a relatively small band gap (1.8 eV). The polymer possesses a low-lying HOMO (–5.4 eV vs. vacuum level) but still has a high enough LUMO level for favorable electron transfer to fullerene derivatives. Future studies will explore its self-assembly behavior in aqueous

solution as well as its photochemical behavior when mixed with polycationic fullerene or polycationic perylene diimide species.

Experimental

Unless otherwise noted, all reagents and solvents were purchased and used as received from commercial sources. All NMR spectra were collected on a Varian AV500 spectrometer with a 5 mm dual cryoprobe and a Bruker DRX500 spectrometer with a 5 mm broadband probe.

Light scattering analysis was collected using a Wyatt DAWN HELEOS-II MALS detector and an Opitlab T-rEX dRI detector,and analyzed using the ASTRA 8.0 software. Light scattering data was fit using Zimm's formalism of the Raleigh-Debye-Grans light scattering model for dilute polymer solutions.[22,23] The Rayleigh ratio (dn/dc) of **4** was measured using the *dn/dc from peak* function of the ASTRA 8.0 program.

ESI mass spectra were acquired on an *Agilent 6890-5975* GC- MS and MALDI-TOF spectra were acquired on a Bruker Ultraflex MALDI-TOF-TOF instrument using a 9-nitroanthracene matrix.

3,3'-(4H-Cyclopenta[2,1-b:3,4-b']dithiophene-4,4-diyl)bis(*N*,*N*-dimethylpropanamide) (1)

To a 100 mL round bottom flask was added 3.00 g of cyclopenta[2,1-b:3,4-b]dithiophene (16.8 mmol, 1.0 eq), 500 mg of tetrabutylammonium bromide, and 6.66 g of *N*,*N*-dimethylacrylamide (67.2 mmol, 4.0 eq) and a magnetic stirring bar. These reagents were then dissolved in 30 mL of toluene. The mixture was then sparged with a stream of argon for 15 min under vigorous stirring. Then, 15 mL of an air-free 50% w/v aqueous sodium hydroxide solution was added to the flask, upon which the organic layer immediately changed to a deep green color. The biphasic mixture was then stirred for 12 hours at 65 °C under an argon atmosphere. The organic

layer was then separated from the aqueous layer and washed with 30 mL of 1 M NaOH and 30 mL of brine, then dried over anhydrous sodium sulfate, filtered through a coarse fritted filter, evaporated under reduced pressure on a Rotavap, and dried under high vacuum overnight. The brown solid was then washed with pentanes and filtered through a coarse fritted filter to yield 5.52 g of a tan crystalline solid (87%). ^{1}H NMR (500 MHz, $CDCl_3$) δ (ppm) 7.14 (d, *J* = 4.7 Hz, 2H) 6.9 (d, *J* = 4.7 Hz, 2H), 2.74 (s, 6H), 2.60 (s, 6H), 2.32 (t, *J* = 7.8 Hz, 4H), 1.70 (t, *J* = 7.8 Hz, 4H). ^{13}C NMR (125 MHz, $CDCl_3$) δ (ppm) 172.4, 155.8, 137.2, 125.3, 121.6, 52.3, 37.0, 35.2, 33.2, 27.7. DART-MS: *m/z* found 377.1337; calculated for $C_{19}H_{24}N_2O_2S_2$ 377.1352.

3,3'-(2,6-Dibromo-4H-cyclopenta[2,1-b:3,4-b']dithiophene-4,4-diyl)bis(*N*,*N*-dimethylpropan-amide) (2)

To a 250 mL round-bottom flask charged with a magnetic stirring bar was added 4.00 g of **1** (11.5 mmol, 1.0 eq), followed by 100 mL of THF and 4.29 g of *N*-bromosuccinimide (24.1 mmol, 2.1 eq). The mixture was covered with aluminum foil and stirred for 12 h at room temperature. The mixture was then diluted with 50 mL of diethyl ether and extracted with 50 mL of 10% aqueous sodium thiosulfate solution, 50 mL of 1 M sodium hydroxide and, 50 mL of brine. The organic layer was then dried ($MgSO_4$), filtered, and evaporated on a Rotavap to yield a tan solid. Trace impurities were removed by running the product through a silica gel plug using a hexanes/CH_2Cl_2/MeOH (1:1:0.1) mixture as eluent to yield 4.98 g (81%) of a cream colored solid. ^{1}H NMR (500 MHz, $CDCl_3$) δ (ppm) 6.95 (s, 2H), 2.80 (s, 6H), 2.68 (s, 6H), 2.32 (t, *J* = 7.4 Hz, 4H), 1.73 (t, *J* = 7.4 Hz, 4H). ^{13}C NMR (125 MHz, $CDCl_3$) δ (ppm) 171.7, 153.8, 136.9, 124.6,

111.8, 54.0, 36.9, 35.3, 32.8, 27.3. ESI-MS: *m/z* (rel intensity) found 532.9928 MH^+ (48); calculated $C_{19}H_{23}Br_2N_2O_2S_2$ 532.9568.

2,6-Dibromo-4,4-bis(3'-(*N*,*N*-dimethylamino)propyl) cyclopenta[2,1-b:3,4-b']dithiophene) (3)

Compound **3** was synthesized using the following procedure: Lithium aluminum hydride, 0.512 g, (13.48 mmol, 3.0 eq) was added to a flame dried 100 mL round bottom flask charged with a magnetic stirring bar under an argon atmosphere followed by 35 mL of dry, air-free tetrahydrofuran. The suspension was then cooled to 0 °C and then 0.660 g of 100% sulfuric acid (6.74 mmol, 6.0 eq) was then added drop wise via a glass syringe under stirring. The mixture was allowed to stir for 5 min, and then 1.20 g (2.24 mmol, 1.0 eq) of **2** dissolved 20 mL of tetrahydrofuran. The mixture was heated to reflux and kept under argon atmosphere for 12 hours. The mixture was then cooled to 0 °C and quenched with 16 mL of 1 M HCl, and then basified with 20 mL of 1 M NaOH. The mixture was then filtered with a coarse fritted filter and the filter cake was washed with two 30 mL portions of tetrahydrofuran. The organic layer was then separated and the organic layer was washed with brine, dried with sodium sulfate, and filtered. The organic layer was rotary evaporated under reduced pressure and dried under high vacuum to yield a low melting tan solid. The crude product was purified via SiO_2 chromatography using 5% methanol in dichloromethane as eluent to yield 0.534 g of a low melting white solid, **3**. (1.06 mmol, 47%) ^{1}H NMR (500 MHz, $CDCl_3$) δ (ppm) 6.94 (s, 2H), 2.2-2.1 (m, 16H), 1.83 (quintet, 4H), 1.07 (t, 4H). ^{13}C NMR (125 MHz, $CDCl_3$) δ (ppm) 155.3, 136.6, 124.4, 111.5, 59.6, 54.6, 45.4, 35.2, 22.6. ESI-MS: *m/z* (rel intensity) found 504.9826 MH+ (49) calculated $C_{19}H_{27}Br_2N_2S_2$ 504.9982.

Poly{(4,4-bis(3'-(*N*,*N*-dimethylamino)propyl) cyclopenta[2,1-b:3,4-b']dithiophene)-2,6-diyl-alt-(thiophene-2,5-diyl)} (4)

Compound **4** (356 mg, 0.70 mmol, 1.0 eq) was added to 50 mL flask charged with a magnetic stirring bar and dissolved in 20 mL THF and several drops of methanol. Bis-2,5-(tri-*n*-butylstannyl)thiophene (466 mg, 0.70 mmol, 1 eq) was then added to the flask and the solution was sparged with argon for 15 minutes. Tetrakis(triphenylphosphine)palladium(0) (40 mg) was then added to the flask and the round-bottom flask was connected to a reflux condenser, and sparged with argon for another 10 minutes. The reaction was then heated to a gentle reflux for 4 days under argon. The reaction mixture was then precipitated by pouring into 100 mL of hexanes and the solids collected by centrifugation at 4000 rpms for 2 minutes. The solid pellet was washed with hexanes and centrifuged two more times to remove oligomers until the supernatant was only light purple. The pelletized polymer was then dried under high vacuum overnight to yield a dark blue powder (168 mg, ~30%). ^{1}H NMR (500 MHz, $CDCl_3$) δ (ppm) 7.9-6.0 (br s, 4H), 2.4-1.5 (m, 20H), 1.5-1.0 (br s, 4H). LS Analysis: Mn 9,760, PDI 2.193.

Poly{(4,4-bis(3'-(*N*-ethyl-*N*,*N*-dimethylammonio)propyl)cyclopenta[2,1-b:3,4-b']dithiophene)-2,6-diyl-alt-(thiophene-2,5-diyl)} bromide. (PCT)

Polymer **4** (100 mg) was added to a 100 mL round bottom flask charged with a magnetic stirring bar and the powder was dissolved in 30 mL of THF. Ethyl bromide (15 mL) was added to the solution, and the round-bottom flask was connected to a reflux condenser. The mixture was sparged with argon for 15 minutes and the reaction was heated to reflux for 5 days. The

reaction mixture was then cooled and evaporated under reduced pressure on a Rotavap to give a purple-blue powder (146 mg, 97%). ^{1}H NMR (500 MHz, DMSO-d_6) δ (ppm) 7.8-7.2 (m, 4H), 3.0-2.7 (m, 10H), 2.47 (br s, 4H), 2.0-1.7 (br s, 4H), 1.7-1.4 (br s, 4H), 1.3-1.0 (m, 10H).

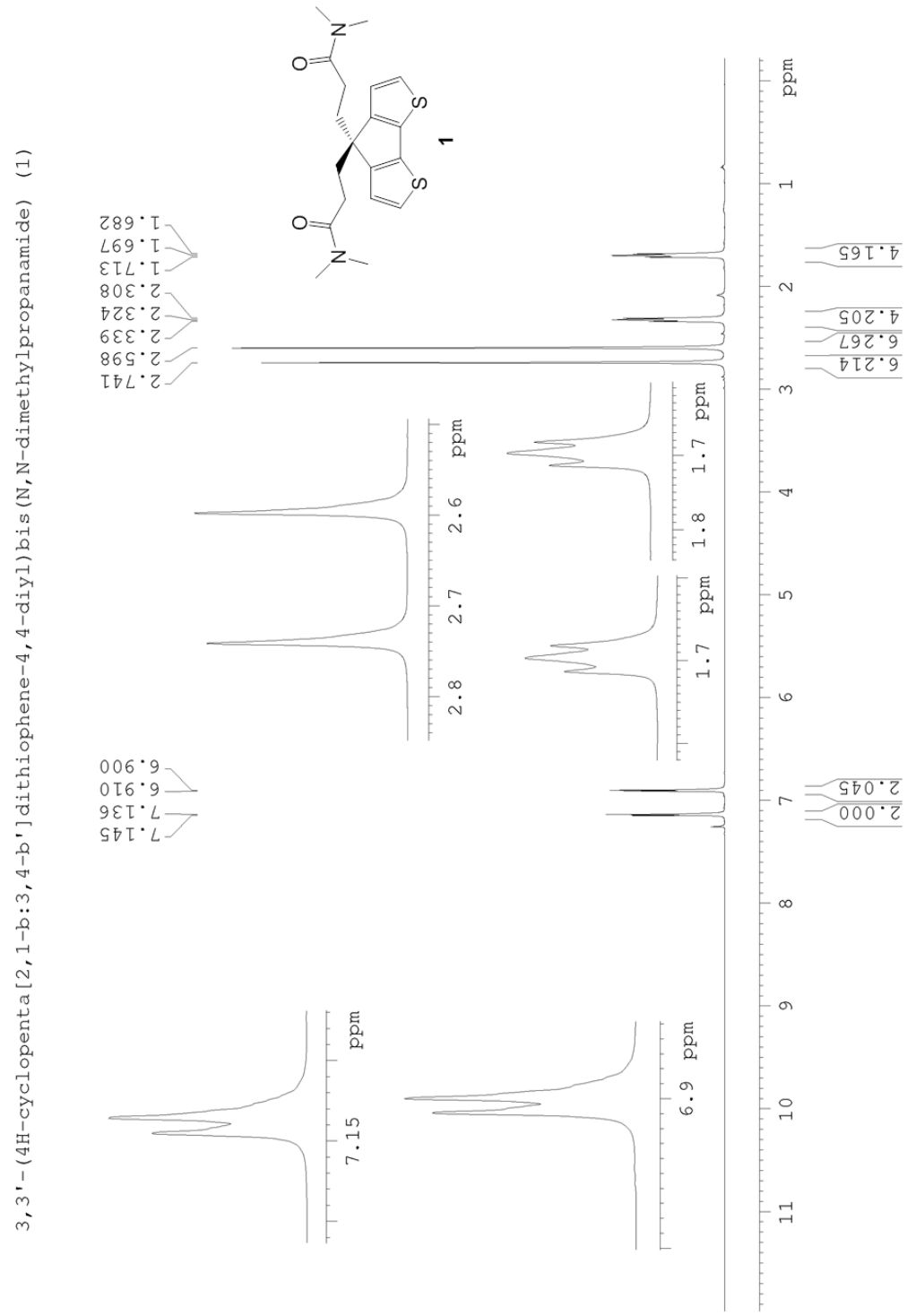

Figure 2.6. ^{1}H NMR spectrum of **1.**

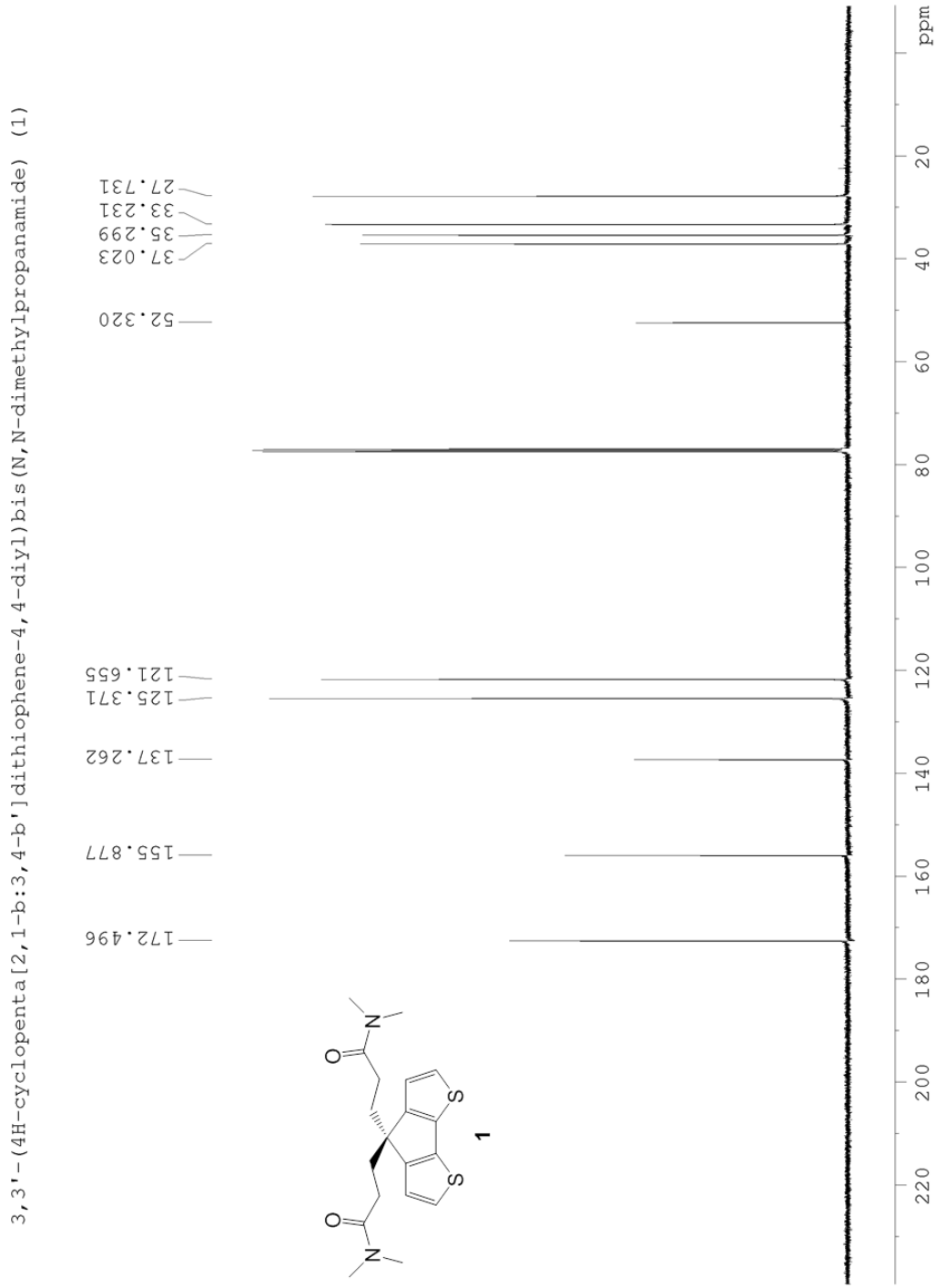

Figure 2.7. ^{13}C NMR spectrum of **1.**

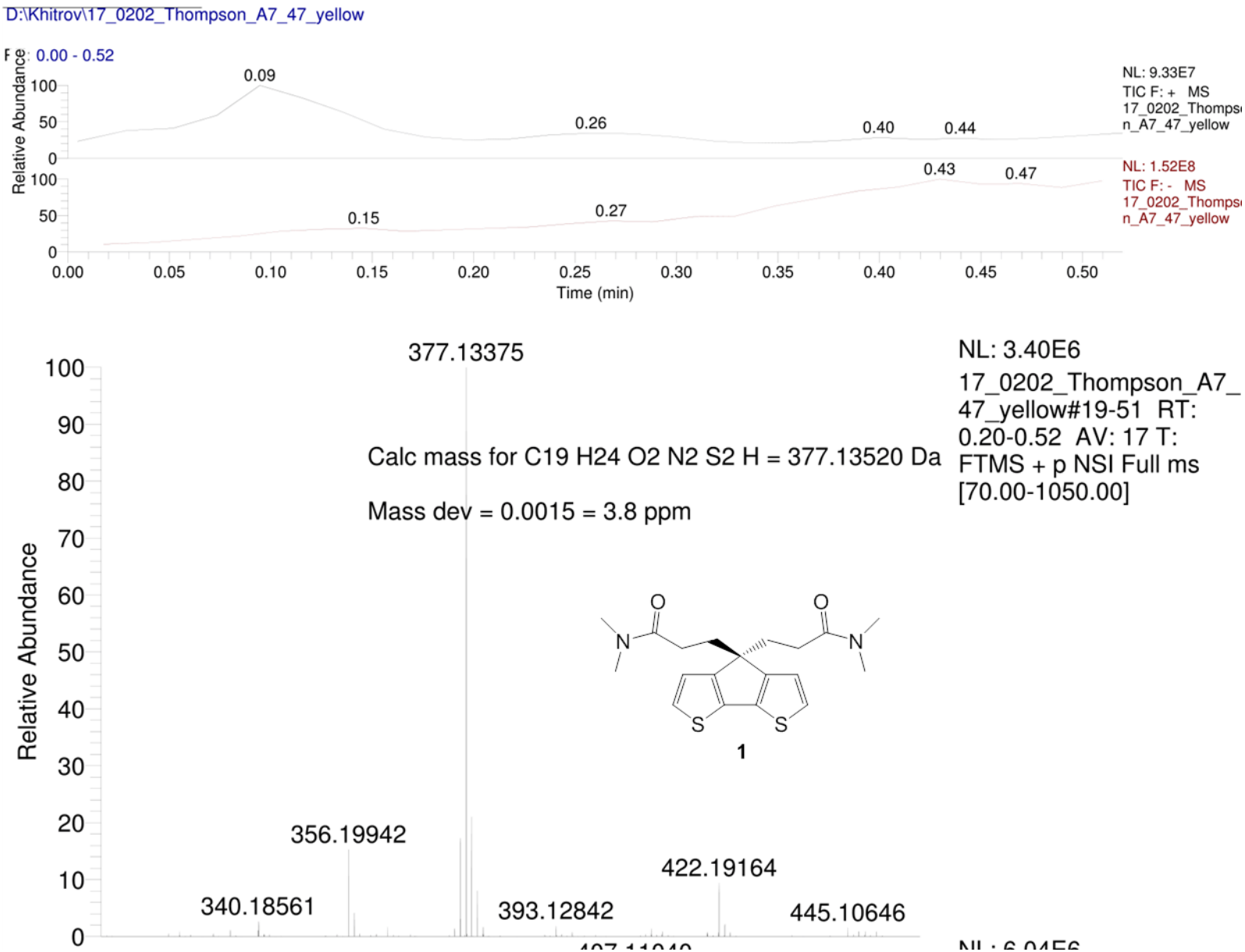

Figure 2.8. DART-MS of **1**.

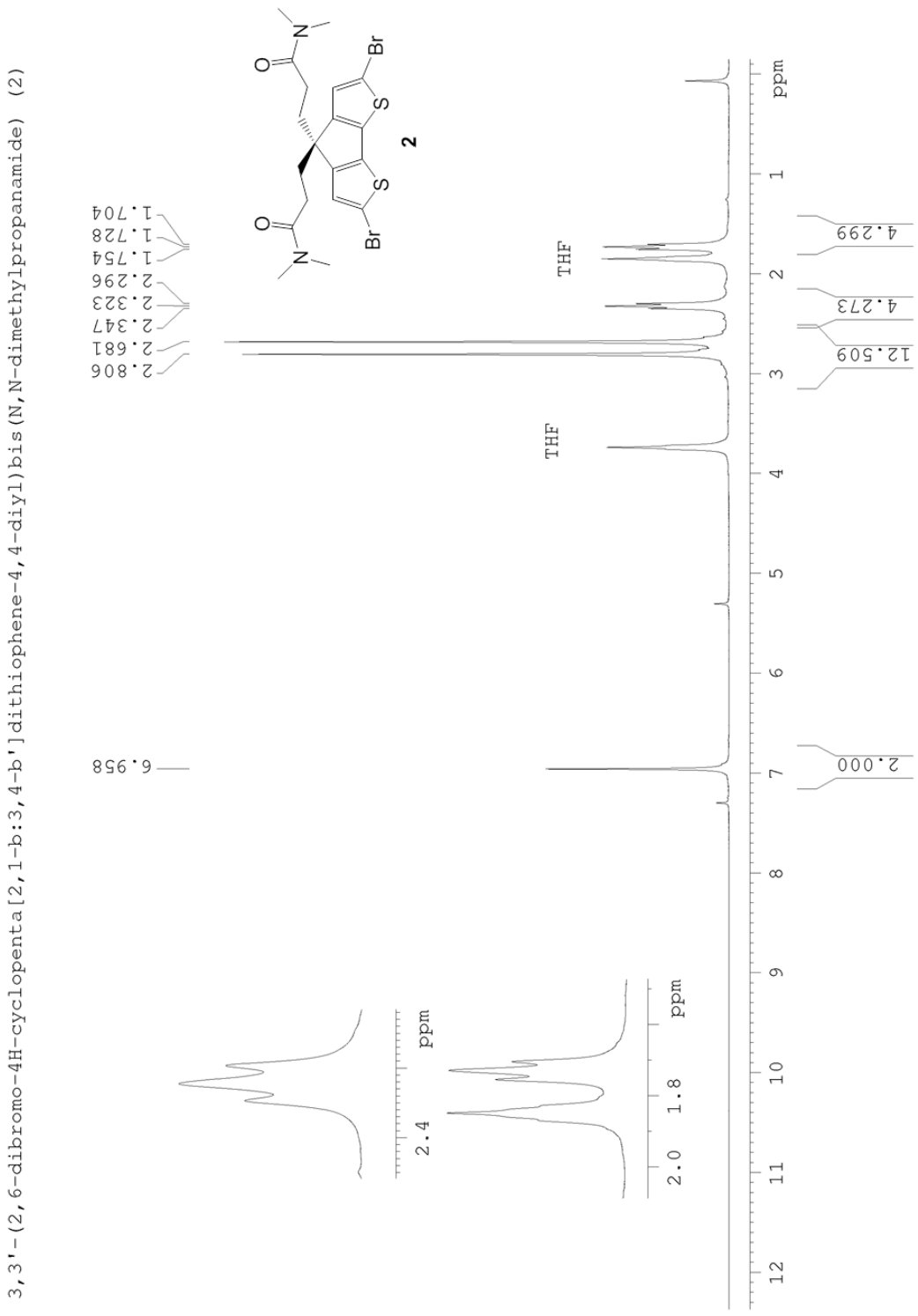

Figure 2.9. ^{1}H NMR spectrum of **2.**

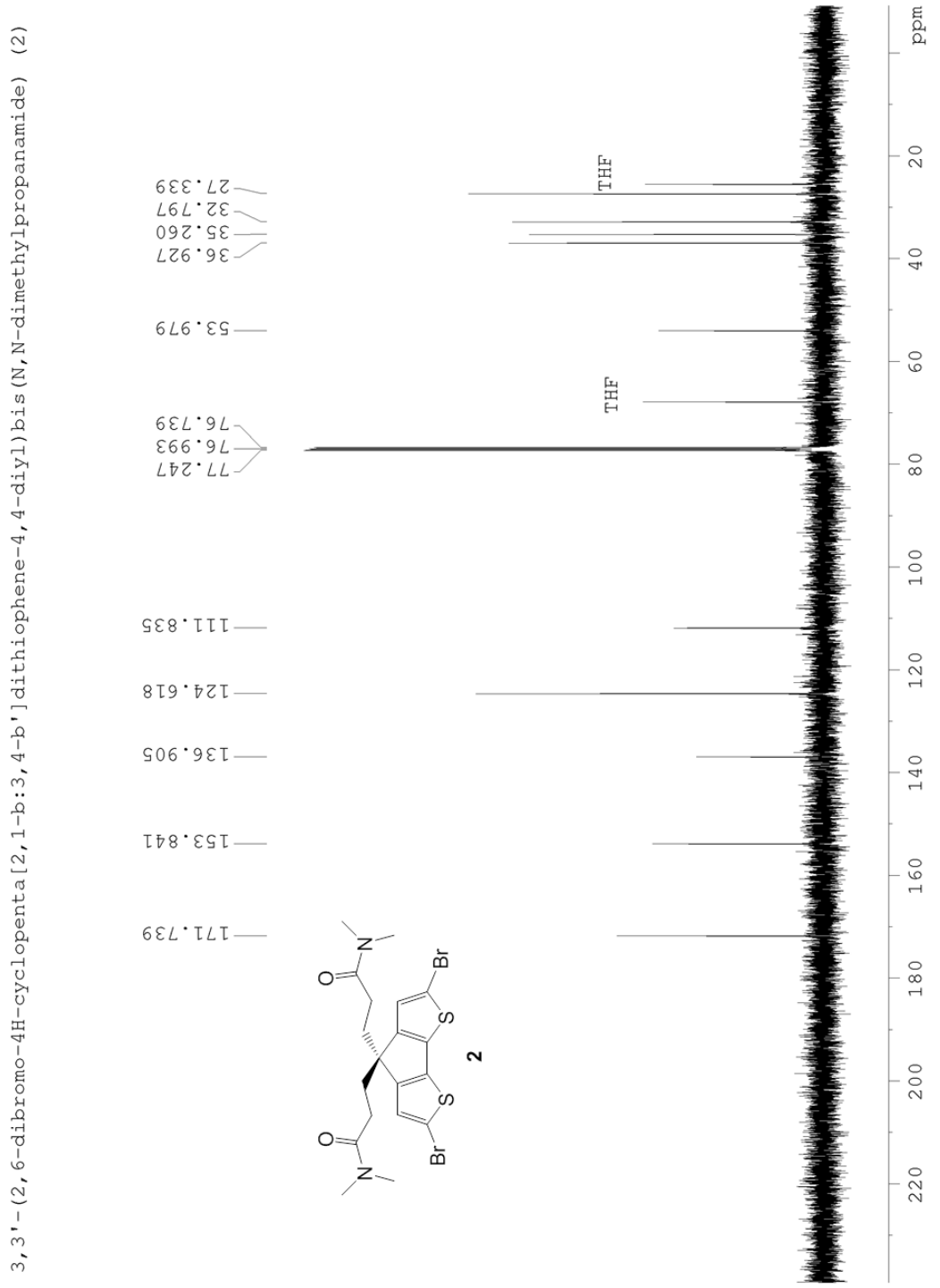

Figure 2.10. ^{13}C NMR spectrum of **2.**

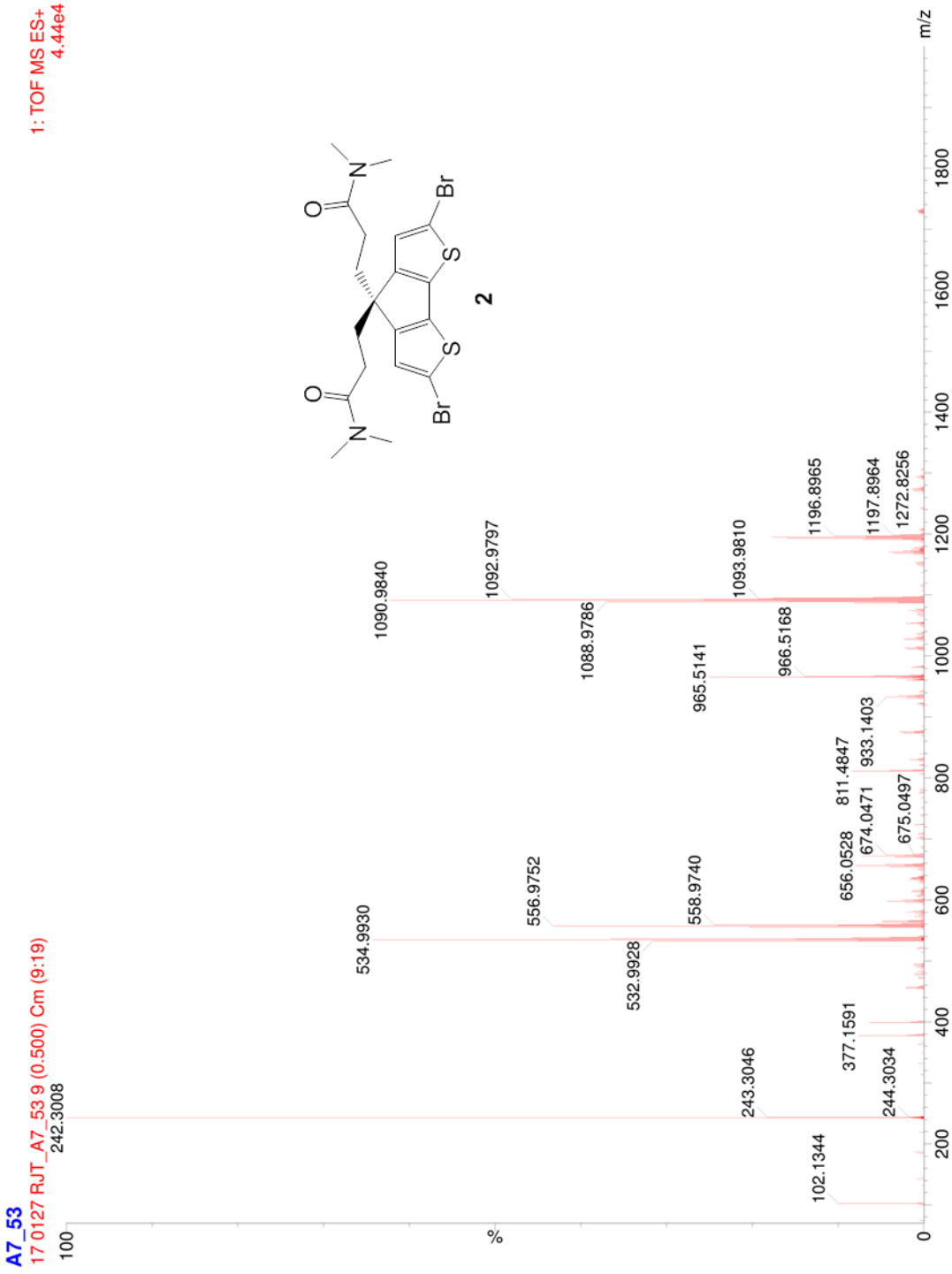

Figure 2.11. ESI-MS of **2**.

Figure 2.12. ESI-MS of **2** parent ion.

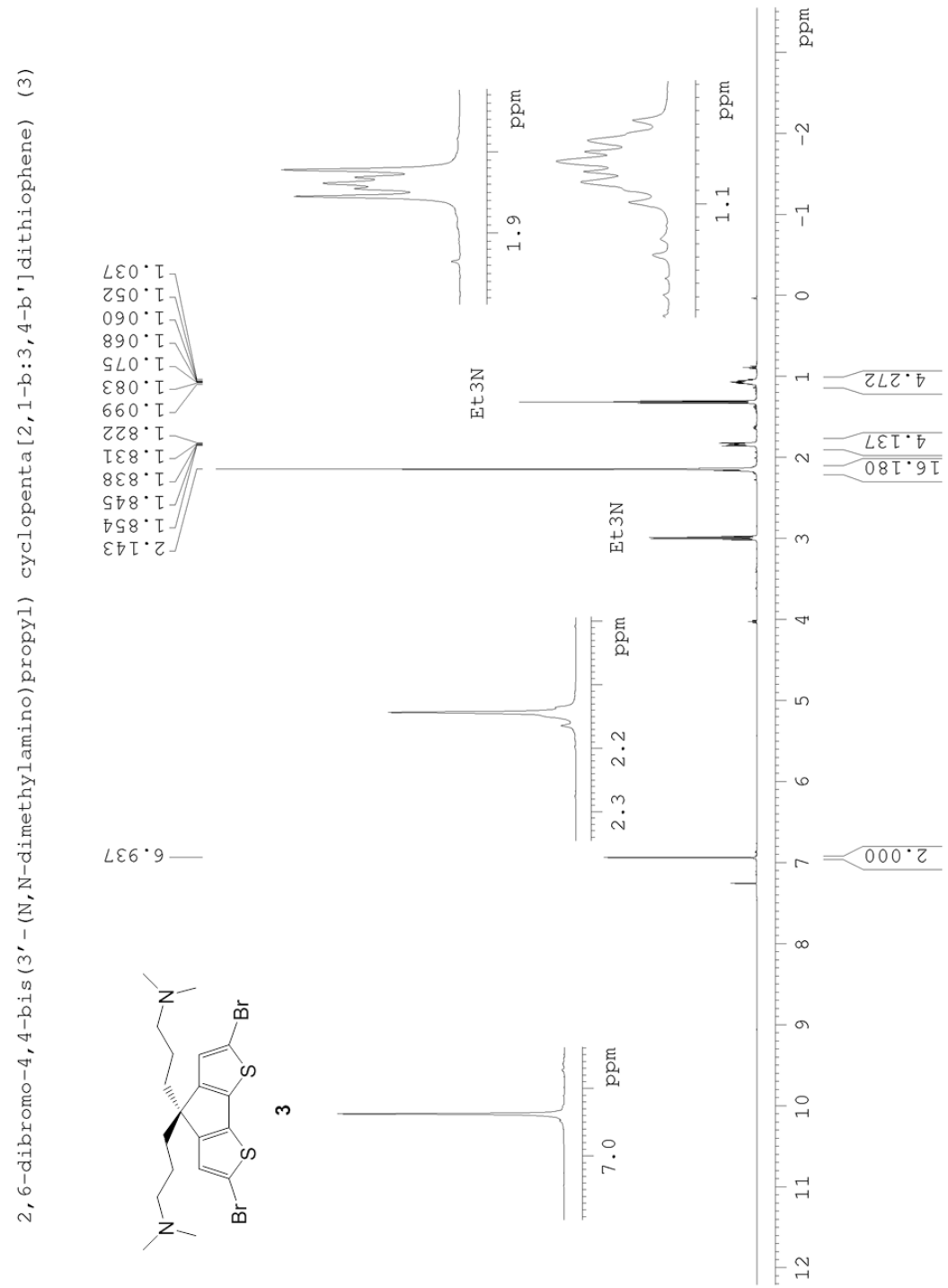

Figure 2.13. ^{1}H NMR of **3.**

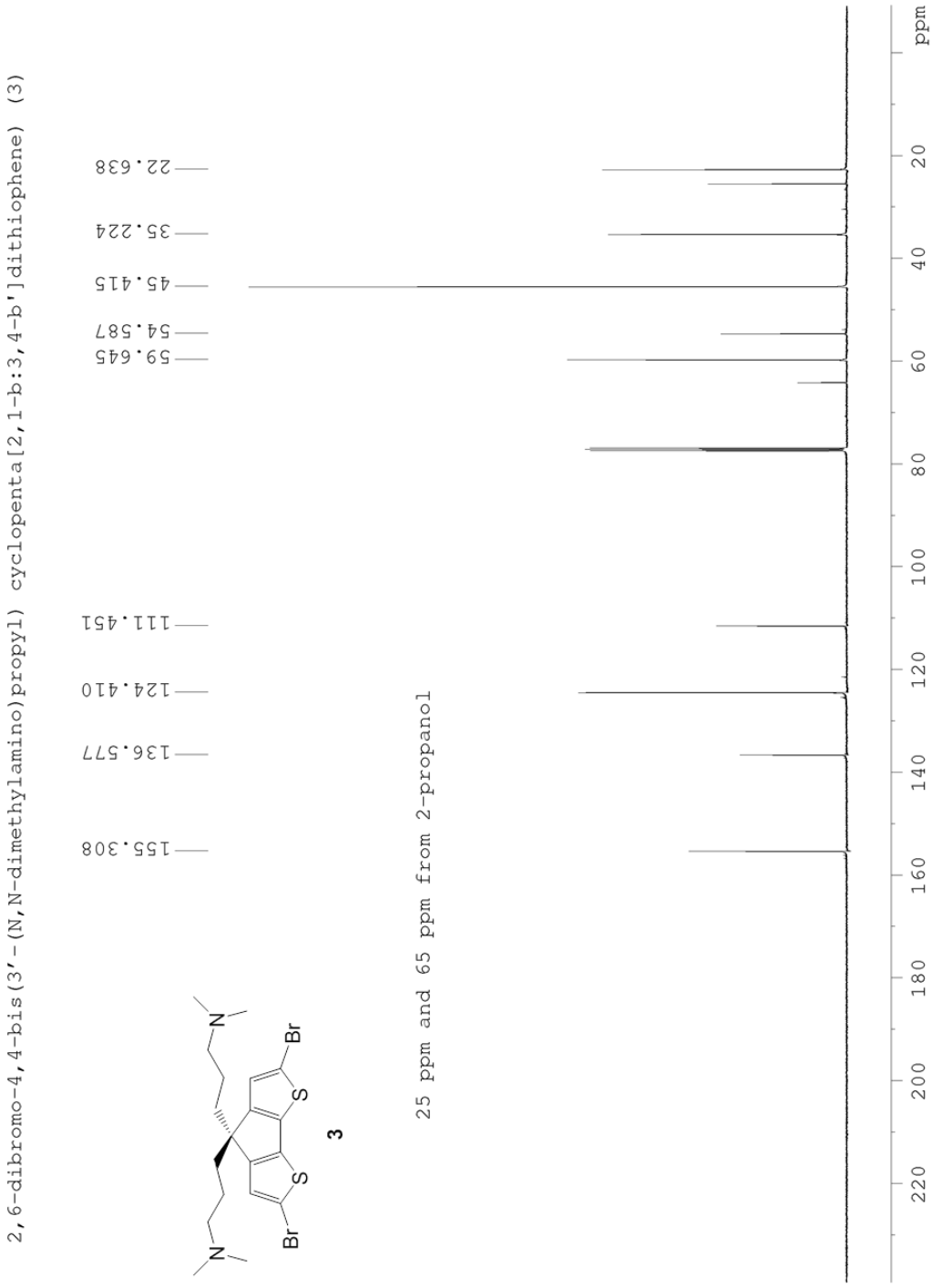

Figure 2.14. ^{13}C NMR of **3.**

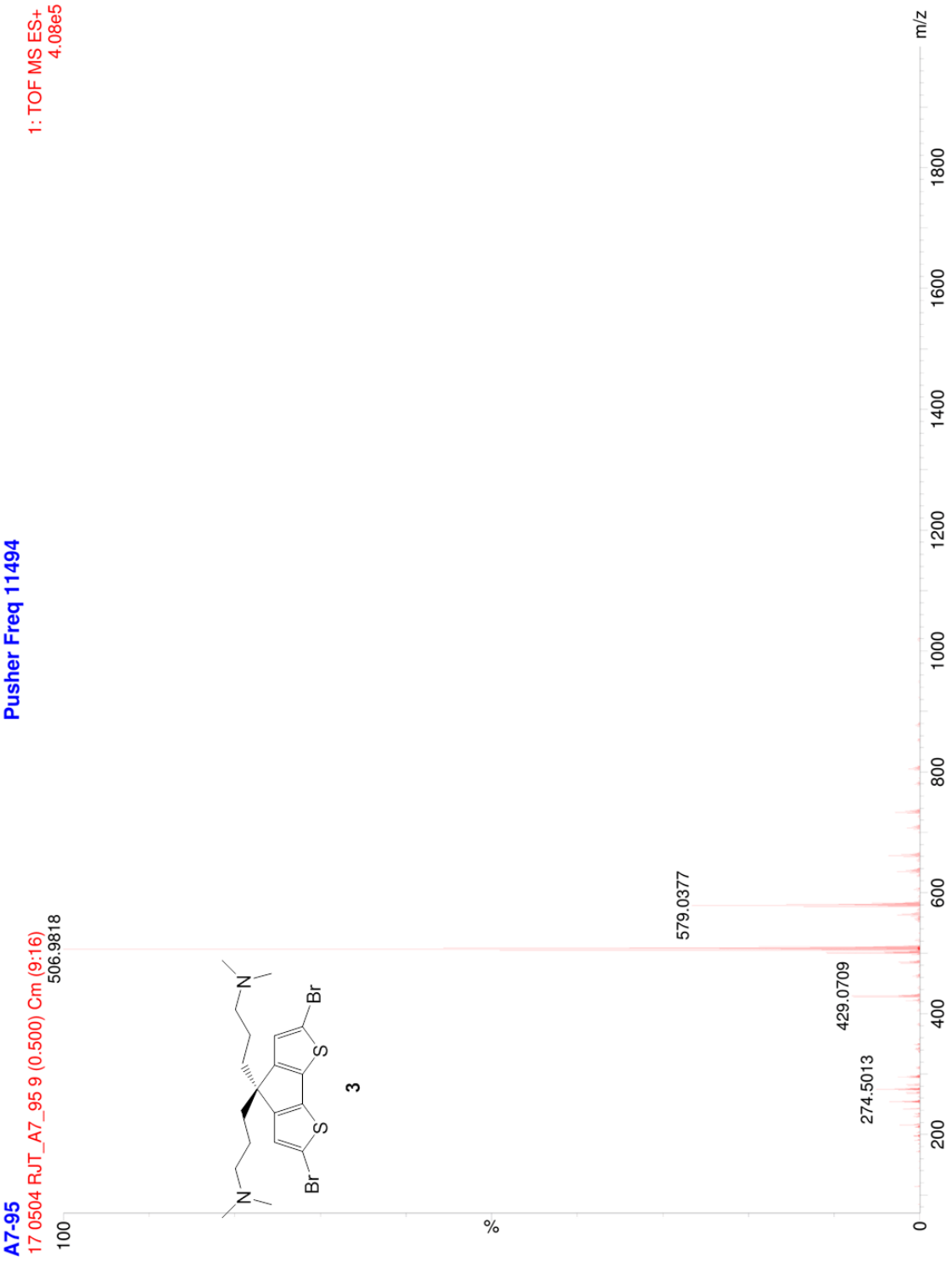

Figure 2.15. ESI-MS of **3.**

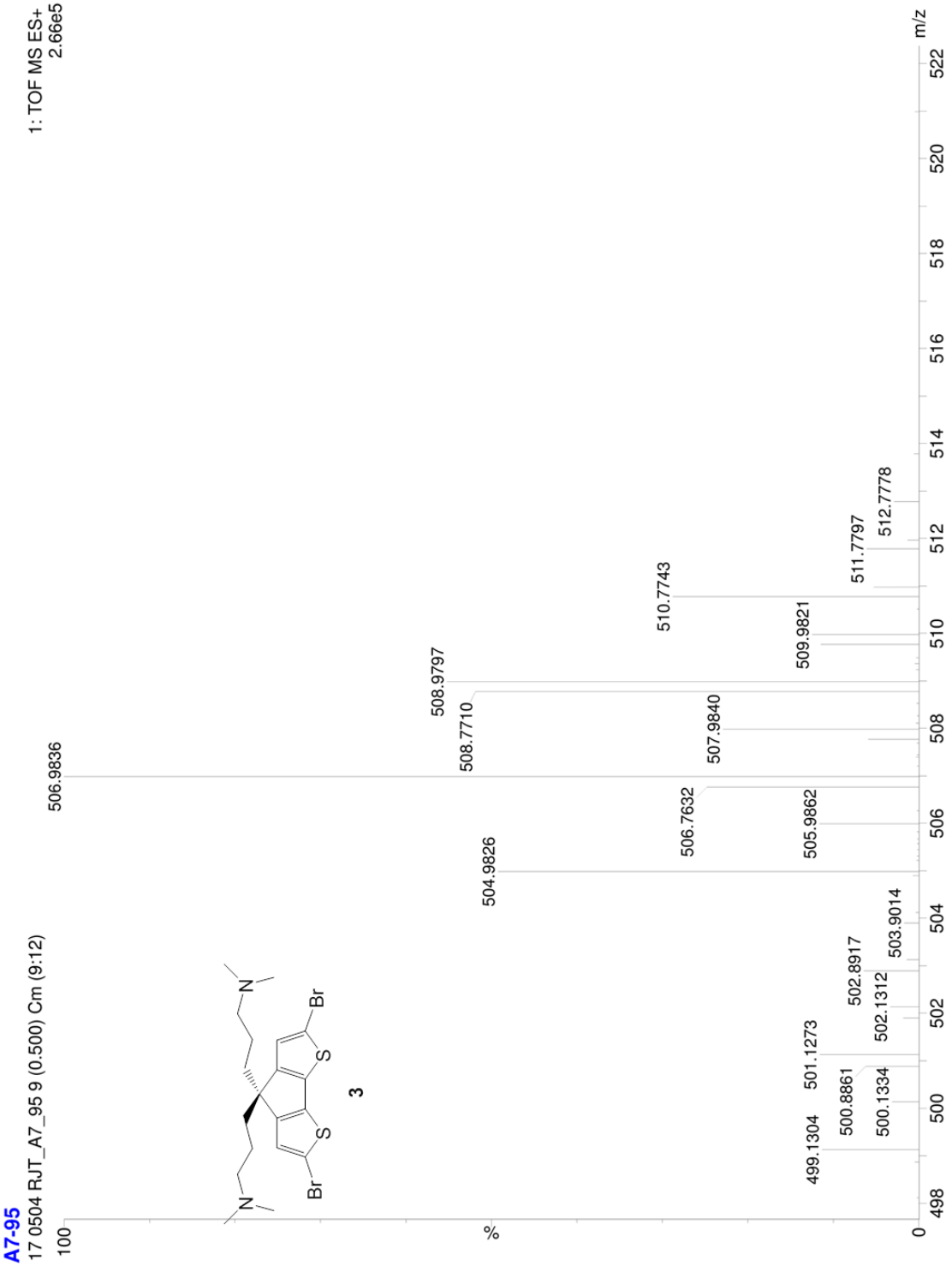

Figure 2.16. ESI-MS of **3** parent ion.

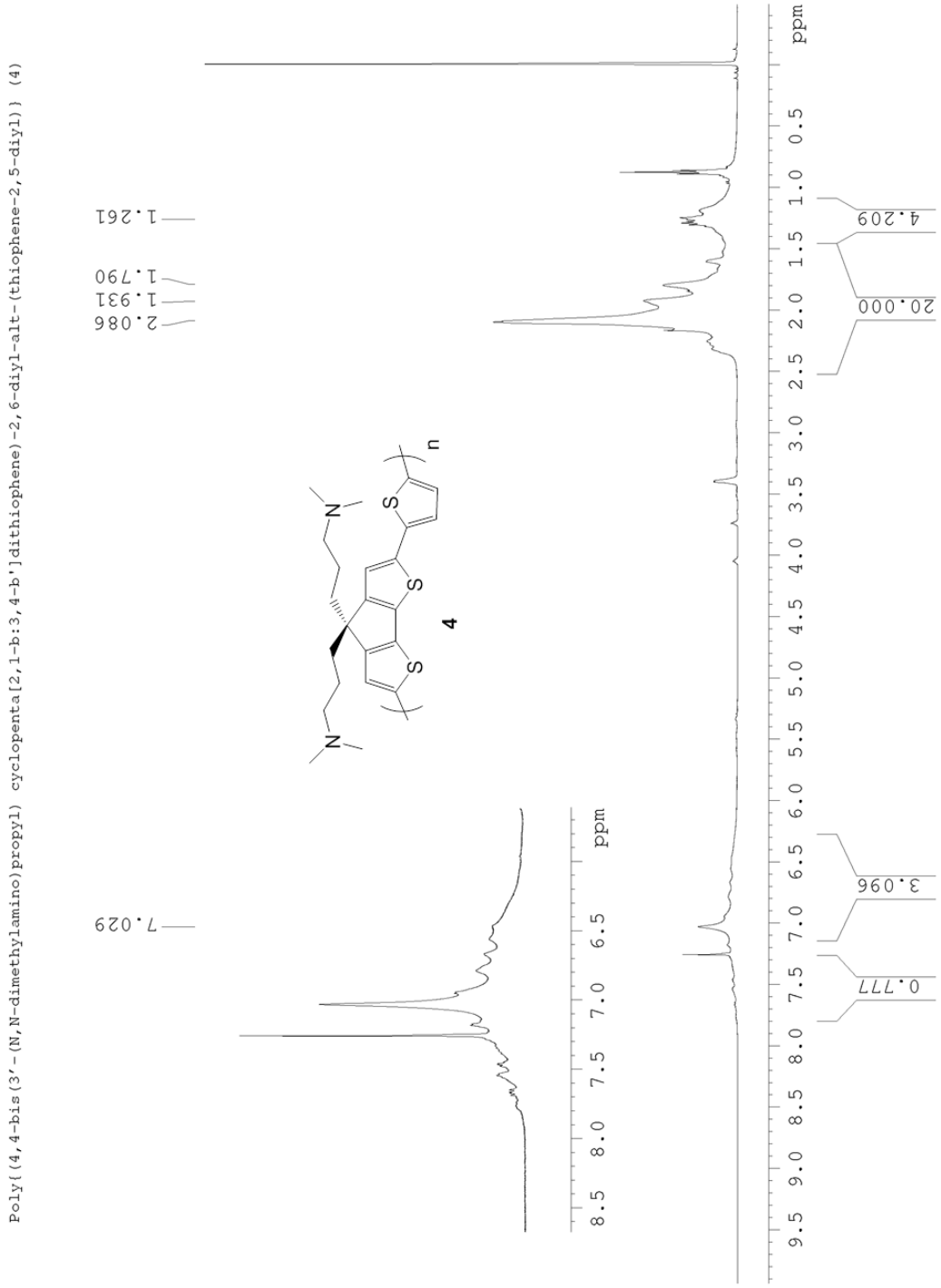

Figure 2.17. ^{1}H NMR of **4.**

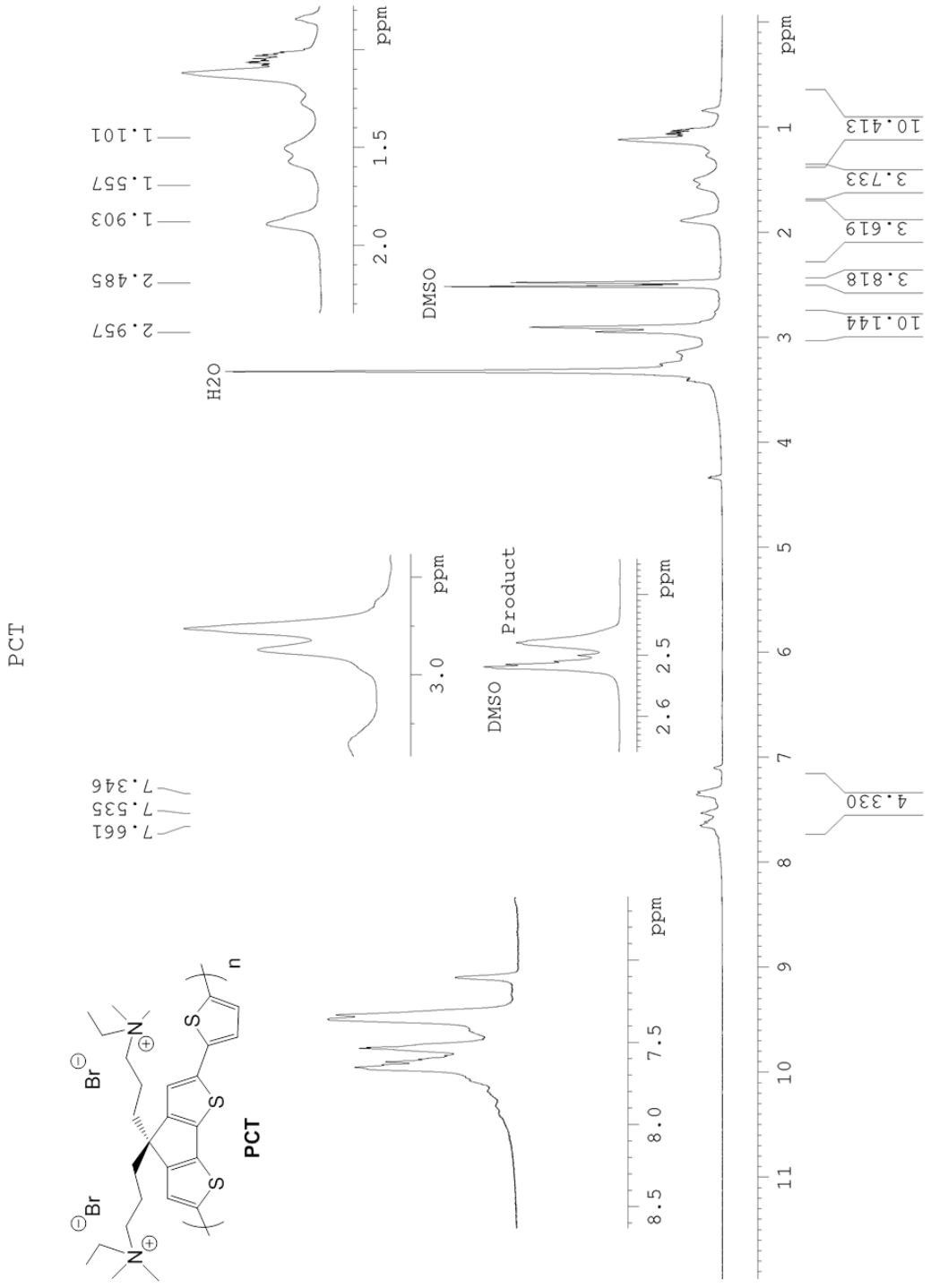

Figure 2.18. ^{1}H NMR spectrum of **PCT.**

References

(1) Jiang, H.; Taranekar, P.; Reynolds, J. R.; Schanze, K. S. Conjugated polyelectrolytes: Synthesis, photophysics, and applications. *Angew. Chemie - Int. Ed.* **2009**, *48*, 4300–4316. DOI: 10.1002/anie.200805456.

(2) Nguyen, T.-Q.; Martini, I. B.; Liu, J.; Schwartz, B. J. Controlling Interchain Interactions in Conjugated Polymers: The Effects of Chain Morphology on Exciton−Exciton Annihilation and Aggregation in MEH−PPV Films. *J. Phys. Chem. B* **2000**, *104*, 237–255. DOI: 10.1021/jp993190c.

(3) Clark, A. P.-Z.; Shi, C.; Ng, B. C.; Wilking, J. N.; Ayzner, A. L.; Stieg, A. Z.; Schwartz, B. J.; Mason, T. G.; Rubin, Y.; Tolbert, S. H. Self-Assembling Semiconducting Polymers-Rods and Gels from Electronic Materials. *ACS Nano* **2013**, *7*, 962–977.

(4) He, Z.; Zhong, C.; Su, S.; Xu, M.; Wu, H.; Cao, Y. Enhanced power-conversion efficiency in polymer solar cells using an inverted device structure. **2012**, *6*, 591–595. DOI: 10.1038/NPHOTON.2012.190.

(5) Seo, J. H.; Gutacker, A.; Sun, Y.; Wu, H.; Huang, F.; Cao, Y.; Scherf, U.; Heeger, A. J.; Bazan, G. C. Improved high-efficiency organic solar cells via incorporation of a conjugated polyelectrolyte interlayer. *J. Am. Chem. Soc.* **2011**, *133*, 8416–8419. DOI: 10.1021/ja2037673.

(6) Thomas, S. W.; Joly, G. D.; Swager, T. M. Chemical sensors based on amplifying fluorescent conjugated polymers. *Chem. Rev.* **2007**, *107*, 1339–1386. DOI: 10.1021/cr0501339.

(7) Wang, D.; Gong, X.; Heeger, P. S.; Rininsland, F.; Bazan, G. C.; Heeger, A. J. Biosensors from conjugated polyelectrolyte complexes. *Proc. Natl. Acad. Sci.* **2002**, *99*, 49–53. DOI: 10.1073/pnas.012581399.

(8) Ho, H. A.; Najari, A.; Leclerc, M. Optical detection of DNA and proteins moth cationic polythiophenes. *Acc. Chem. Res.* **2008**, *41*, 168–178. DOI: Doi 10.1021/Ar700115t.

(9) Shu, S.; Zhang, X.; Wu, Z.; Wang, Z.; Li, C. Gradient cross-linked biodegradable polyelectrolyte nanocapsules for intracellular protein drug delivery. *Biomaterials* **2010**, *31*, 6039–6049. DOI: 10.1016/j.biomaterials.2010.04.016.

(10) Lee, J. H.; Kim, D. G.; Kwon, N. Y.; Jang, G. S.; Son, J. H.; Lee, M.; Cho, H. J.; Kweon, H. S.; Lee, T. S. Protein-induced aggregation of fluorescent conjugated polyelectrolytes with sulfonate groups: Synthesis and its sensing application. *J. Polym. Sci. Part A Polym. Chem.* **2011**, *49*, 138–146. DOI: 10.1002/pola.24428.

(11) Zhu, X.; Guo, W.; Li, H.; Zhang, G.; Pei, M.; Wang, L.; Feng, J. Synthesis of a novel water-soluble conjugated polyelectrolyte based on polycyclopentadithiophene backbone and its application for heparin detection. *Des. Monomers Polym.* **2014**, *17*, 624–628. DOI: 10.1080/15685551.2014.907616.

(12) Tuncel, D.; Demir, H. V. Conjugated polymer nanoparticles. *Nanoscale* **2010**, *2*, 484. DOI: 10.1039/b9nr00374f.

(13) Huber, R. C.; Ferreira, A. S.; Aguirre, J. C.; Kilbride, D.; Toso, D. B.; Mayoral, K.; Zhou, Z. H.; Kopidakis, N.; Rubin, Y.; Schwartz, B. J.; et al. Structure and Conductivity of Semiconducting Polymer Hydrogels. *J. Phys. Chem. B* **2016**, *120*, 6215–6224. DOI:

10.1021/acs.jpcb.6b02202.

(14) Prescher, S.; Ghasimi, S.; Hőhne, P.; Grygiel, K.; Landfester, K.; Zhang, K. A. I.; Yuan, J. Polyfluorene polyelectrolyte nanoparticles: Synthesis of innovative stabilizers for heterophase polymerization. *Macromol. Rapid Commun.* **2014**, *35*, 1925–1930. DOI: 10.1002/marc.201400440.

(15) Duarte, A.; Pu, K. Y.; Liu, B.; Bazan, G. C. Recent advances in conjugated polyelectrolytes for emerging optoelectronic applications. *Chem. Mater.* **2011**, *23*, 501–515. DOI: 10.1021/cm102196t.

(16) Rossi, G.; Chance, R. R.; Silbey, R. Conformational disorder in conjugated polymers. *J. Chem. Phys.* **1989**, *90*, 7594. DOI: 10.1063/1.456193.

(17) Westenhoff, S.; Beenken, W. J. D.; Yartsev, A.; Greenham, N. C. Conformational disorder of conjugated polymers. *J. Chem. Phys.* **2006**, *125* DOI: 10.1063/1.2358682.

(18) Grozema, F. C.; Van Duijnen, P. T.; Berlin, Y. A.; Ratner, M. A.; Siebbeles, L. D. A. Intramolecular charge transport along isolated chains of conjugated polymers: Effect of torsional disorder and polymerization defects. *J. Phys. Chem. B* **2002**, *106*, 7791–7795. DOI: 10.1021/jp021114v.

(19) Mwaura, J. K.; Pinto, M. R.; Witker, D.; Ananthakrishnan, N.; Schanze, K. S.; Reynolds, J. R. Photovoltaic cells based on sequentially adsorbed multilayers of conjugated poly(p-phenylene ethynylene)s and a water-soluble fullerene derivative. *Langmuir* **2005**, *21*, 10119–10126. DOI: 10.1021/la050599m.

(20) Durstock, M. F.; Taylor, B.; Spry, R. J.; Chiang, L.; Reulbach, S.; Heitfeld, K.; Baur, J. W. Electrostatic self-assembly as a means to create organic photovoltaic devices. *Synth. Met.* **2001**, *116*, 373–377. DOI: 10.1016/S0379-6779(00)00440-9.

(21) Huber, R. C.; Ferreira, A. S.; Thompson, R.; Kilbride, D.; Knutson, N. S.; Devi, L. S.; Toso, D. B.; Challa, J. R.; Zhou, Z. H.; Rubin, Y.; et al. Long-lived photoinduced polaron formation in conjugated polyelectrolyte-fullerene assemblies. *Science (80-.).* **2015**, *348*, 1340–1343. DOI: 10.1126/science.aaa6850.

(22) Zimm, B. H. The Scattering of Light and the Radial Distribution Function of High Polymer Solutions. *J. Chem. Phys.* **1948**, *16*, 1093–1099. DOI: 10.1063/1.1746738.

(23) Folta-Stogniew, E.; Williams, K. R. Determination of molecular masses of proteins in solution: Implementation of an HPLC size exclusion chromatography and laser light scattering service in a core laboratory. *J. Biomol. Tech.* **1999**, *10*, 51–63.

(24) Isse, A. A.; Gennaro, A. Absolute Potential of the Standard Hydrogen Electrode and the Problem of Interconversion of Potentials in Different Solvents. *J. Phys. Chem. B* **2010**, *114*, 7894–7899. DOI: 10.1021/jp100402x.

(25) Haynes W. M. *CRC Handbook of Chemistry and Physics, 97th Edition*; 2017.

(26) Acevedo-Peña, P.; Baray-Calderón, A.; Hu, H.; González, I.; Ugalde-Saldivar, V. M. Measurements of HOMO-LUMO levels of poly(3-hexylthiophene) thin films by a simple electrochemical method. *J. Solid State Electrochem.* **2017**, *21*, 2407–2414. DOI: 10.1007/s10008-017-3587-2.

(27) Boudon, C.; Cisselbrecht, J.; Cross, M.; Chimie, F. De; Pasteur, U. L.; Pascal, B.; Cedex, F.-S.; Isaacs, L.; Anderson, H. L.; Faust, R.; et al. Electrochemistry of Mono- through Hexakis-adducts of C60. *Helv. Chim. Acta* **1995**, *78*, 1334–1344. DOI: 10.1002/hlca.19950780523.

Acknowledgements

Cyclic Voltammetry for this chapter was collected by Terri Lin, florescence data was collected by Mathew Voss, and the visible spectrum **PCT** was collected by Katherine Winchell.

Chapter 3 : Synthesis and characterization of polymers containing substituted dithieno[3,2-a:2',3'-c]phenazines

Low band gap semiconductors based on π-donor/π-acceptor interactions

Low band gap π-conjugated polymer semiconductors based on alternating π-donor (πD) and π-acceptor (πA) units have gained prominence in the fields of organic light emitting diodes,[1] organic field effect transistors,[2,3,4] and organic photovoltaic materials.[5,6,7] One attractive aspect of low bandgap D-A polymers is that their band gap, as well as their HOMO and LUMO levels and other materials properties such as photoemission behavior,[8,9] crystallinity,[10,11,12] and conductivity,[13,14,15] can be tuned by engineering the properties of these πD and πA units on the molecular scale. New πD and πA monomer units are constantly being explored and modified to create new low bandgap πD—πA copolymers with exciting materials properties. Accordingly, low bandgap πD—πA polymers have markedly improved the performance of OPVs, with many reviews outlining their use in OPV devices.[16,17,18,19,20]

Fused π-donor π-acceptor molecules

One way of engineering new monomer units for polymer solar cells is by chemically fusing two πD—πA moieties to create an extended π system with enforced planarity and a low band gap resulting from the mixing of the HOMO and LUMO orbitals of the πD and the πA moieties. There are numerous advantages for creating fused πD—πA polymers: the electron transport properties of polymers synthesized from these unit often show ambipolar charge transport,[21,22,23] broad absorption across the visible spectrum,[24,25] and often have high mobilities resulting from strong interchain π—π interactions.[26,27] Due to their tunable nature,

polymers containing fused πD—πA monomer units have been utilized in organic photovoltaic cells to yield devices with high power conversion efficiencies[26,28,29]

Dithieno[3,2-a:2',3'-c]phenazines as electron deficient monomer units

Dithieno[3,2-a:2',3'-c]phenazines (DTPs) belong to a class of fused πD—πA molecules consisting of an electron-rich benzo[2,1-b:3,4-b']dithiophene unit fused at the 4 and 5 positions with a quinoxaline ring. DTPs have been explored as electron deficient π-acceptor materials recently in scientific literature, but the first reported synthesis of a DTP derivative was reported by Tigler *et al.* in 1975.[30] More recently, a facile synthesis of DTP was developed using condensations of substituted derivatives of *ortho*-phenylene diamine with benzo[2,1-b:3,4-b']dithiophene-4,5-dione. DTP units fused at the 9 and 10 positions with an electron rich tetrathiafulvalene unit were reported by Guegano *et al.*; and were found to have broad absorption from 520 nm to 1240 nm. These compounds were found to undergo a reversible two-electron oxidation at 0.38 V *vs.* Fc/Fc^{+} and a two electron reduction at –0.14 V *vs.* Fc/Fc^{+}.[31]

Meyer .*et al*. synthesized D-A-D small molecule semiconductors based on 2,5-disubstituted DTPs. The molecules were characterized for their absorbance and fluorescence properties, and self-assembled monolayers of these molecules were characterized by STM.[32] Chen *et al*. also reported the synthesis of a regioisomeric series of dithieno[2,3-a:3',2'-c]phenazine derivatives substituted at various positions with electron donating *N*,*N*-di-*n*-hexylaniline groups. These molecules were characterized for their photochemical and photophysical properties and were found to possess a strong intramolecular charge transfer band resulting from electron donation from the aniline nitrogen lone pairs to the DTP units. The HOMO levels of these regioisomeric aniline substituted DTP derivatives ranged from –4.92 to –

4.65 eV *vs*. vacuum level and the LUMO levels ranged from –2.85 to –2.66 eV *vs.* vacuum level.[33]

DTPs have also been employed as monomeric units in D-A polymers used in OPV devices. DTP based monomers were co-polymerized using a palladium-catalyzed Stille cross-coupling reaction with indenodithiophene to create polymers linked at the 8 and 11 positions of the DTPs. These polymers attained a PCE of 6.1% when used in OPVs containing $PC_{71}BM$ as the electron accepting component of the active layer.[29] The relatively high efficiency of these polymers is due in part to the large open circuits (0.83 V) due to the low lying HOMO orbitals of these polymers, high fill factors resulting from the high field—effect mobilities of these polymers (5.6 X 10^{-2} cm^2 V^{-1} s^{-1}, and high short circuit currents 11.6 mA cm^{-2} resulting from broad absorption across the visible spectrum.

Based on the above mentioned results of Zhang *et al*,[29] we hypothesized that we could improve on the performance of DTP-based polymers by synthesizing polymers that are covalently linked to πD units at the 2 and 5 postions of the DTP unit. The conjugated backbone of the resulting polymer would possess a higher thiophene character (less aromaticity than phenyl) and would be expected to have a lower band gap due to the fact that thiophene units have a larger quinoidal character than phenyl rings. The DTP monomer units were also substituted with TIPS alkynyl and alkoxy chains to improve the solubility of the resulting polymers. We hypothesized that the resulting polymers would possess low lying HOMOs, high free carrier mobilities, and broad absorption across the visible spectrum.

Synthesis of substituted dithieno[3,2-a:2',3'-c]phenazines

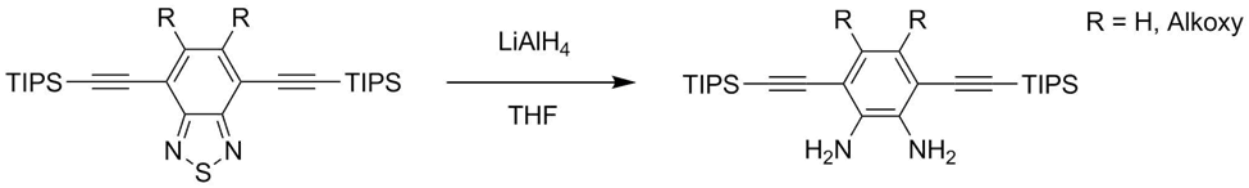

Figure 3.1. General synthetic strategy for conversion of substituted benzo[c][1,2,5]thiadiazoles into substituted phenylene diamines.

The general synthetic strategy employed for the synthesis of DTP monomers involves the condensation of substituted *o*-aryl diamines with the *o*-diketone 2,7-dibromobenzo[2,1-b:3,4-b']dithiophene-4,5-dione (**1,** Figure 3.2). The benzo[c][1,2,5]thiadiazole system had to be employed as a protecting group for *o*-aryldiamines because these units are very sensitive to oxidation, while benzo[c][1,2,5]thiadiazoles are stable under a wide variety of conditions, thus allowing for chemical modification of the unsubstituted positions of benzo[c][1,2,5]thiadiazoles. After installing substituents onto the benzo[c][1,2,5]thiadiazole scaffold, the thiadiazole unit could be easily reduced to an *o*-aryldiamine using the strategy outlined in Figure 3.1. The resulting 2,3,4,5-substituted *o*-aryl diamines oxidized almost immediately when exposed to air, therefore these reagents were generally used immediately after they were generated, and the condensation reactions were conducted under inert atmosphere.

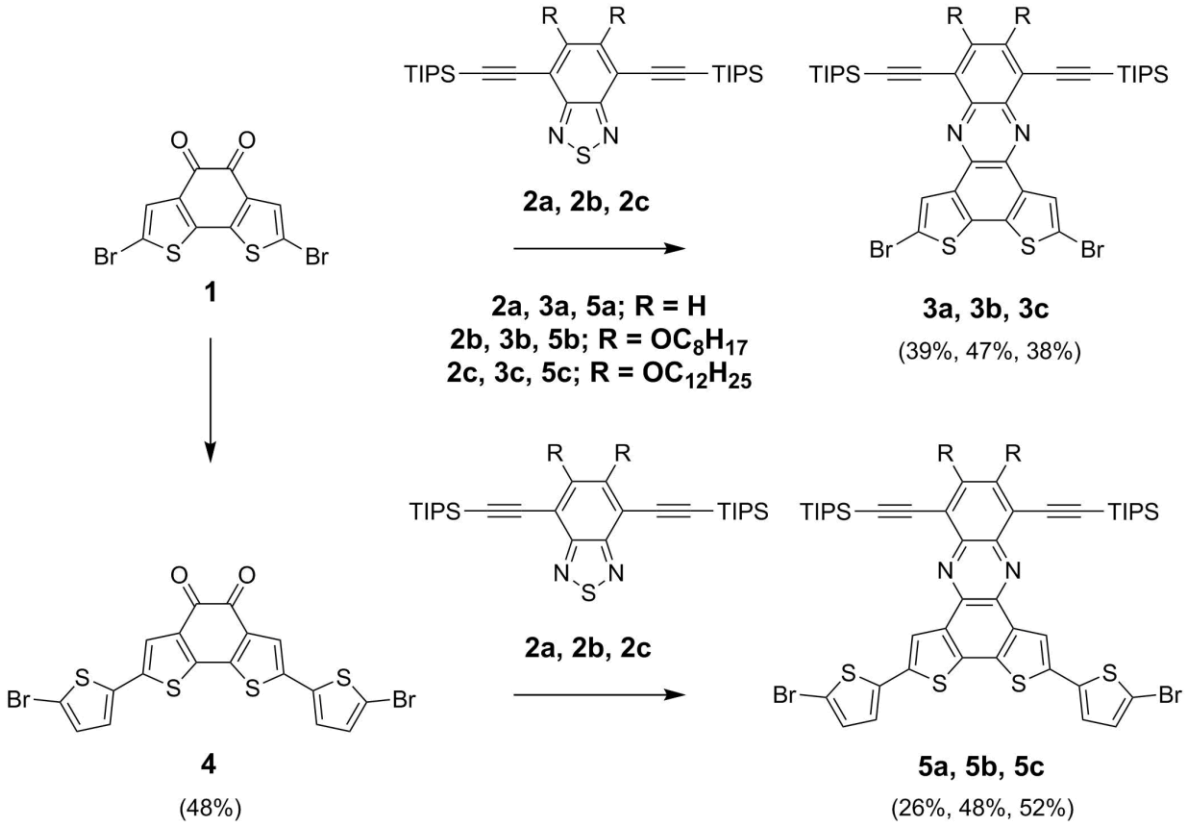

Figure 3.2. General synthetic strategy employed for the synthesis of **3** and **5**.

Substituted thiadiazoles **2a-c** were synthesized via published procedures[34,35] and were reduced using the procedure outlined in Figure 3.1. The resulting o-aryl diamines were then condensed onto diketone **1** to yield DTPs **3a-c** in moderate yields (Figure 3.2). Similarly, thiadiazoles **2a**-**c** could be reduced and condensed onto diketone **4** in moderate yield to produce 5-bromo-2-thienyl substituted DTPs **5a**-**c**.

Synthesis of π-donor π-acceptor polymers containing substituted dithieno[3,2-a:2',3'-c]phenazines

A homologous series of polymers was created by copolymerizing monomers **3b**-**c** and

5b-**c** with 2,5-bis(tributylstannyl)thiophene or 5,5'-bis(tributylstannyl)thiophene using a palladium-catalyzed Stille cross-coupling reaction (Figure 3.3). Polymers were generated from **3a** and **5a** using the same methodology but it was found that these polymers were too insoluble for full characterization or use in photovoltaic devices. Polymerizations were conducted using stoichiometric amounts of reagents to limit polycondensation reactions, and a 5% molar ratio of tetrakis(triphenylphosphine) palladium (0) was used as the catalyst for this polymerization. The polymerization reactions were sluggish for two reasons: firstly, the relatively slowly reacting tributylstannyl Stille coupling reagents were used instead of the more toxic trimethylstannyl reagents and, secondly, the polymers became increasingly less soluble as their molecular weight rose. D-A polymers **P1**-**P8** possessed similar band gaps but the solubility of the polymers decreased drastically as the number of unsubstituted thiophene spacers was increased. We will also note that higher molecular weight polymers of **P2**-**P4** and **P6**-**P7** were synthesized using higher catalyst loadings and longer reaction times, but the polymers obtained under these conditions were too insoluble for proper characterization or use in solar cells. Obtained polymers had similar UV-vis absorption but possessed considerable scattering.

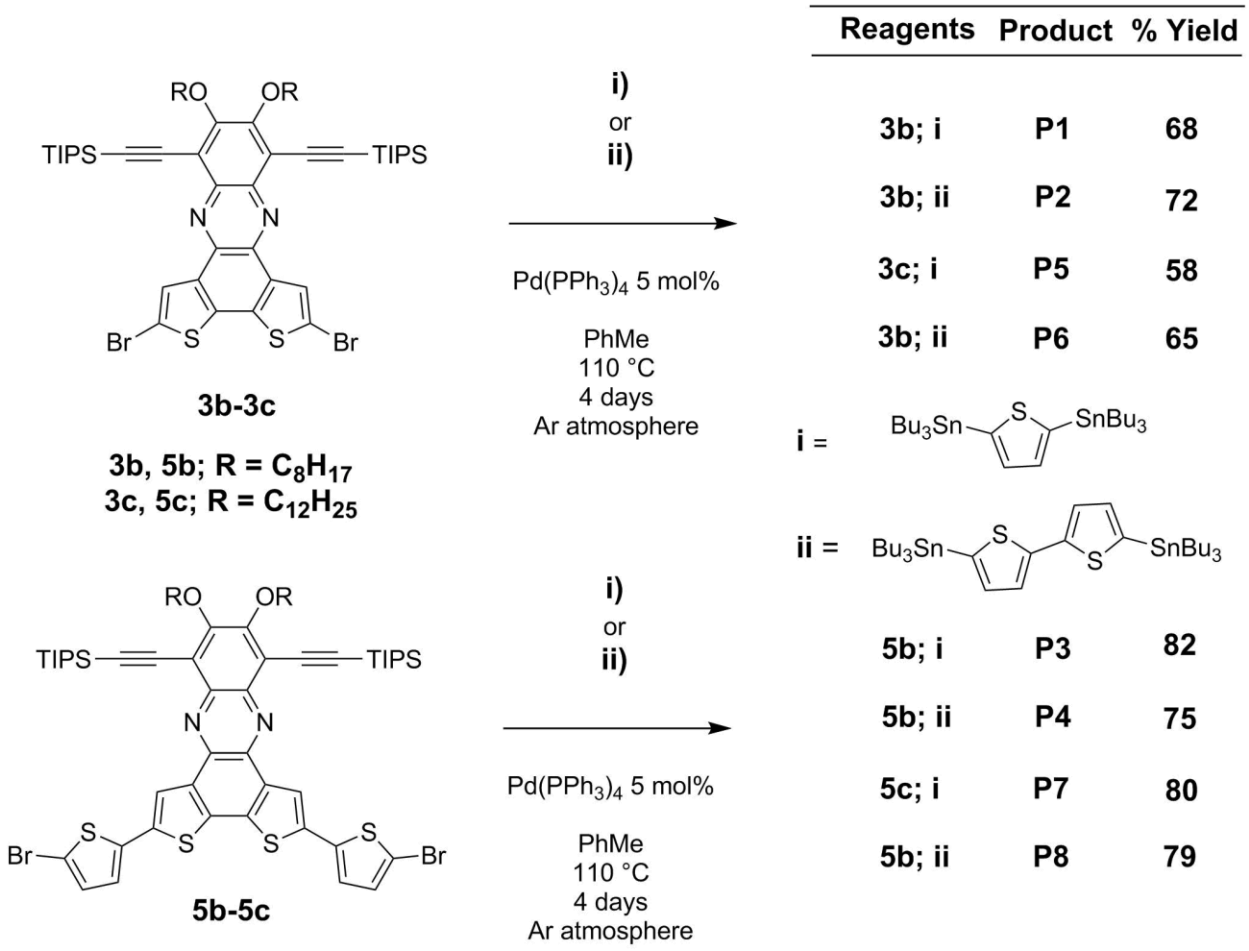

Figure 3.3. Scheme for the synthesis of D-A polymers **P1 – P8**.

DTP derivative **7** was synthesized in order to explore the effect of aryl substitution at the 8 and 11 positions, and what it would impose on the materials properties of resulting DTP molecules (Figure 3.4). Due to its more electron-rich nature, reduction of **6** required harsher reaction conditions than were required for **2a—2c**. Condensation of the diamine resulting from reduction of thiadiazole **6** onto **1** proceeded with a moderate yields to produce DTP **7**. This monomer unit was then polymerized using the same reaction conditions employed for **P1—P8** to produce **P9**.

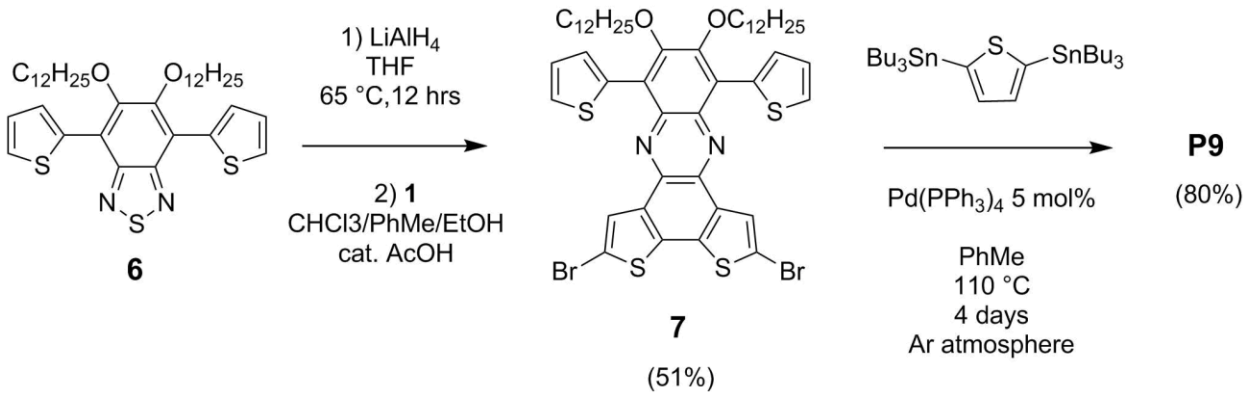

Figure 3.4. Synthesis of DTP **7** and polymer **P9**.

Monomers **3c**, **5c**, and **7** were also copolymerized with the electron-rich Stille coupling reagent 2,6-bis(tributylstannyl)-4,4-bis(2'-ethylhexyl)-4H-cyclopenta[2,1-b:3,4-b']dithiophene[36] in order to produce polymers with reduced band gaps and greater solubility (Figure 3.5). The reaction conditions employed for the synthesis of **P10**—**P12** were similar to the conditions employed for **P1**—**P9**, but the resulting polymers displayed a marked increase in solubility and a decrease in their band gaps (see below).

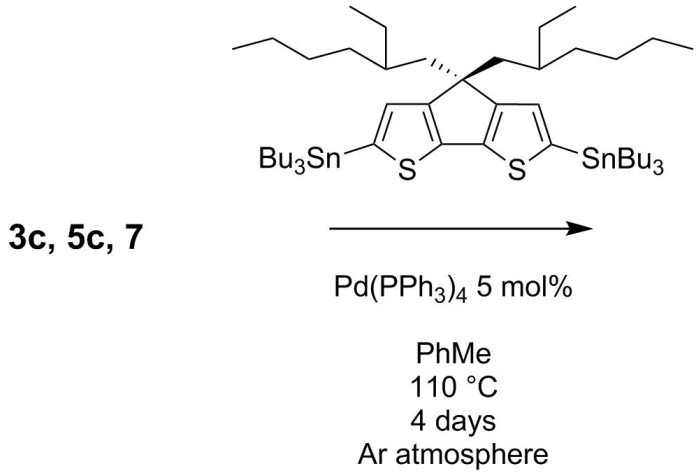

Reagent	Product	Yield
3c	**P10**	**49%**
5c	**P11**	**60%**
7	**P12**	**64%**

Figure 3.5. Synthesis of polymers **P10**, **P11**, **P12**.

The GPC results for **P1—P12** are summarized in Table 3.1. Solution phase aggregation of these polymers led to artificially high molecular weights when GPC measurements were attempted in THF and $CHCl_3$ because aggregation was significant in these solvents even at concentrations as low as ~0.1 mg/mL. This is a notable observation because these solvents are often used for GPC measurements of conjugated polymers with a strong tendency towards solution-phase aggregation, which may lead to artificially high reported molecular weights. Accurate GPC measurements were obtained by running samples in 1,2-dichloro-benzene as eluent at dilute concentrations (0.1—0.5 mg/mL). Average molecular weights were low for these samples due to the insolubility of the resulting polymers. As can be seen in Table 3.1, the most soluble polymers of the **P1—P8** series, **P1** and **P5** have higher degrees of polymerization. Somewhat surprisingly, **P12** achieved a high molecular weight and had an unexpectedly high solubility compared to **P9**, even though these two polymers were synthesized from the same monomer unit, **7**.

Table 3.1. Summary of GPC data for polymers **P1—P12** using 1,2-dichlorobenzene as eluent.

Polymer	M_n	Dispersity	DP_n
P1	11,089	1.57	22.4
P2	4,317	1.33	8.0
P3	5,886	3.50	10.0
P4	3,849	1.84	6.2
P5	6,232	1.25	10.2
P6	3,849	1.57	6.4
P7	6,242	2.05	9.8
P8	4,871	1.93	7.2
P9	3,630	3.64	8.0
P10	4,652	1.87	6.6
P11	4,480	1.16	7.4
P12	10,700	1.38	13.4

Photophysical characterization of substituted dithieno[3,2-a:2',3'-c]phenazines

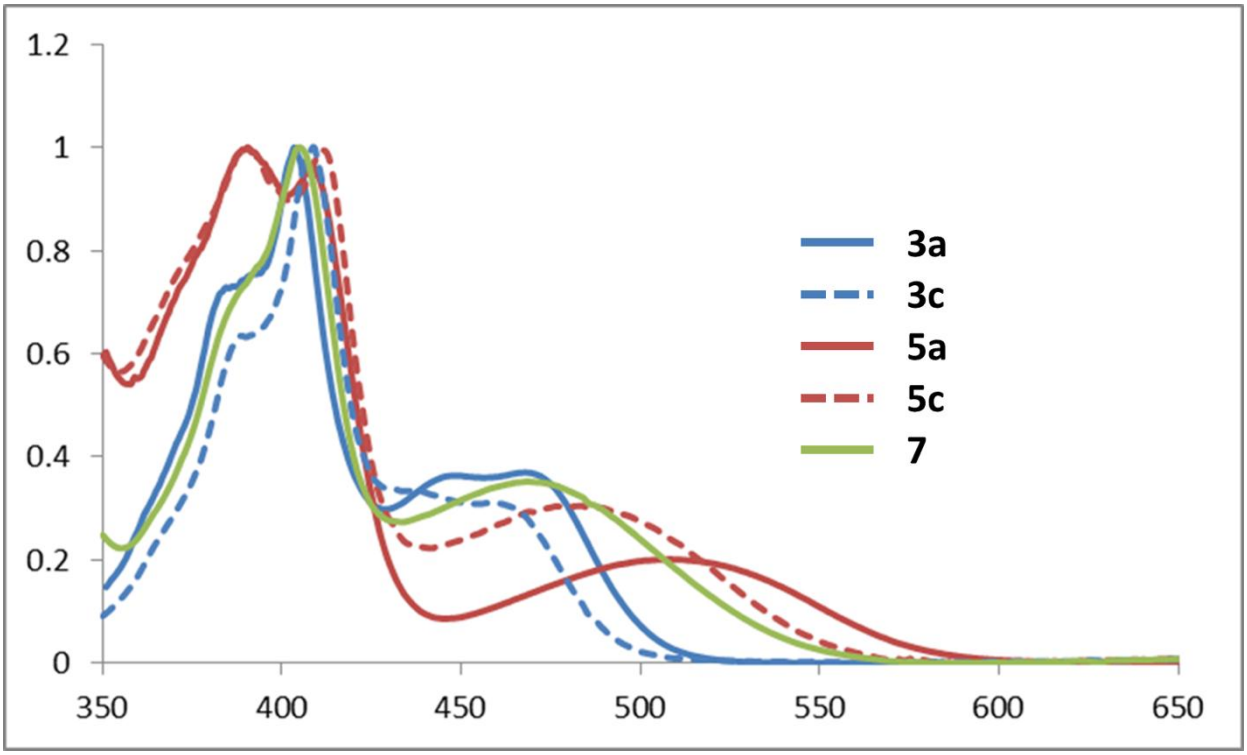

Figure 3.6. Normalized absorbance of monomers **3a** (solid blue), **3c** (dashed blue), **5a** (solid red), **5c** (dashed red) and **7** (green) in chloroform solution.

The normalized absorption of monomers **3a**, **3c**, **5a**, **5c**, and **7** can be seen in Figure 3.6. There is an obvious hypsochromic shift when comparing the absorption edge of **3c** to the absorption edge of **3a**. This blue shift of the band edge of **3c** most likely results from the introduction of the alkoxy substituents at the 9 and 10 positions of the DTP monomer unit. Alkoxy substituents are electron donating and the aromatic ring containing the alkynyl substituents would therefore be electron-rich overall in the case of monomer **3c** compared to **3a**. Therefore it is not surprising that the band gap of **3c** would be smaller if the π acceptor moiety became more electron-rich upon introduction of alkoxy substituents. The bathochromic

shift in the absorption of **3a** compared **3c** may also be explained by J-type aggregation behavior.[37] This hypothesis is supported by evidence of the strong aggregation behavior of **3a** observed via peak broadening of the aromatic protons in its ^{1}H NMR spectrum. Based on this evidence it is apparent that alkoxy substituents are needed in addition to TIPS alkynyl substituents in order to reduce solution phase aggregation and produce soluble conjugated polymers

A blue shift in the band edge is also seen when comparing the normalized absorption of **5a** and **5c**. Again we hypothesize that both the more electron-rich nature of **5c** and the decreased tendency towards solution phase aggregation causes this blue shift. Interestingly **5a** displayed redder absorption compared to the 2,5-thienyl substituted DTP units synthesized by Meyer *et al*.[32] This observation is significant because it suggests that the TIPS alkynyl substituents at the 8 and 11 positions might make the DTP units more electron deficient, thereby reducing the band gap of **5a** compared to its unsubstituted analog. Substitution of the alkynyl groups at the 8 and 11 positions with electron-rich thiophenes causes a red shift in the band edge as can be seen upon comparison of the absorption spectrum of **3a** and **7**. This shift is most likely due to the increased conjugation of **7** compared to **3c**. The broader absorption of monomer **7** compared to **3c** translated into broader absorption in its resulting polymers (**P9** and **P12**) resulting in higher short—circuit currents in solar cells, but the more electron—rich nature of these units also may result in higher HOMO levels which would decrease the open—circuit voltage in solar cells. It is difficult to judge which of these factors would dominate in the performance of the solar cells incorporating **P9** or **P12**.

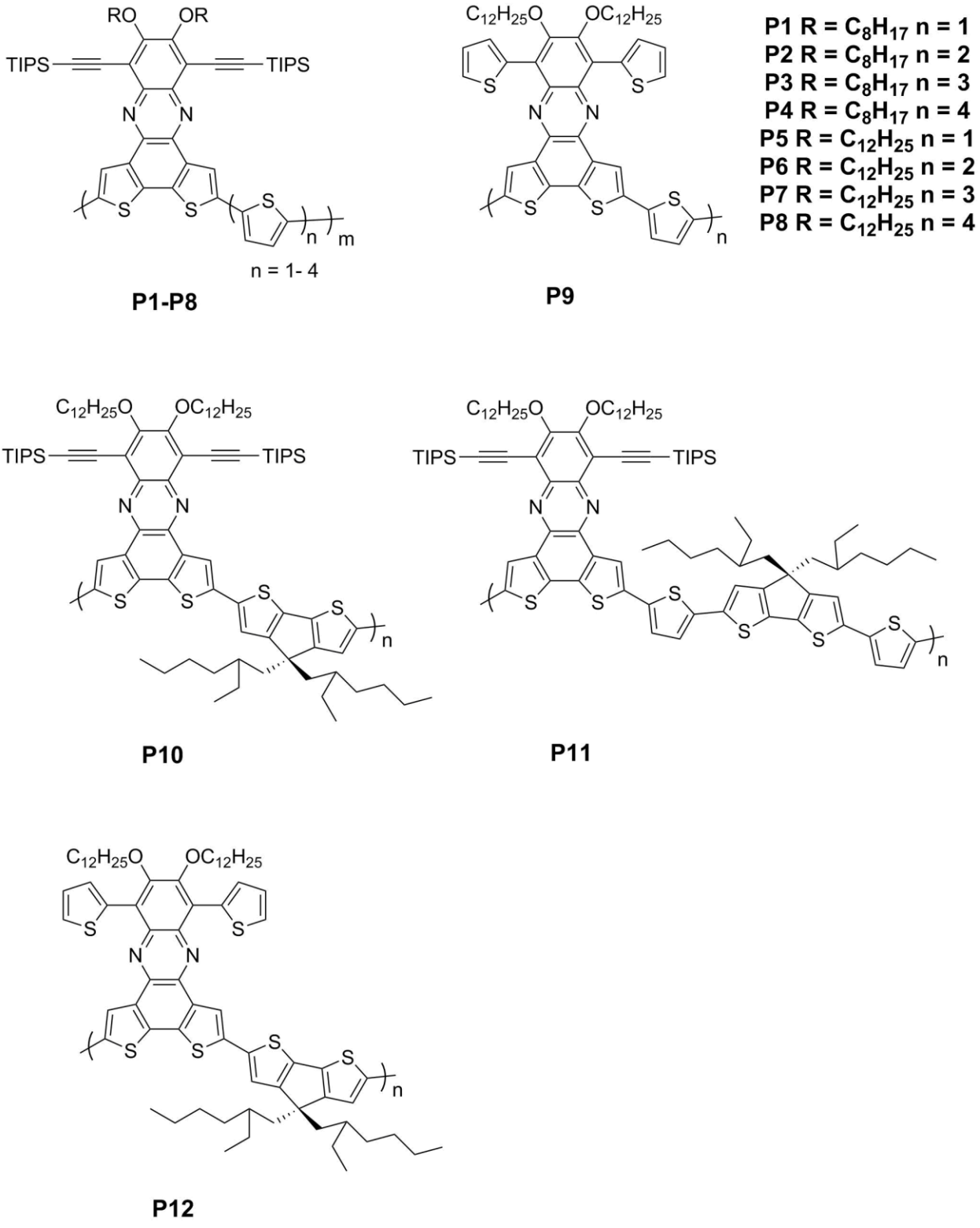

Figure 3.7. Structures of the polymers synthesized in this study.

The structures of polymers **P1**—**P12** can be seen in Figure 3.7, and the absorption spectra of **P1**—**P4** can be seen in Figure 3.8, while the normalized absorbance of **P5**—**P8** can be seen in Figure 3.9. In both homologous series of polymers it can be seen that there is a strong absorbance near 400 nm that bears strong resemblance to the peak near 400 nm in the DTP monomers **3a** and **3c**. Due to the similarity in appearance and the similarity in the wavelength of the absorbance we have putatively assigned this absorption to an excitation localized primarily on the DTP monomer unit. **P1** and **P5** also possess an absorption band centered at 550 nm that is similar in appearance to the band seen in **5a** and **5c**. We hypothesize that this absorption is most likely due to excitations that are localized on the polymer backbone incorporating the benzo[3,2-a:2',3'-c]dithiophene moiety of the DTP unit and the thiophene linkages. This hypothesis is supported by the observation that this band grows in relative intensity to the putative DTP excitation at 400 nm as the number of thiophene groups comprising the polymer backbone increases. Generally the optical band gap is seen to decrease slightly as the number of thiophene spacers increases. The band gaps of polymers possessing the same electronic structure also tend to closely match between the two series as well, with the notable exception of **P8** which exhibits a 20 nm red shift in its optical band gap compared to the other polymers in the series.

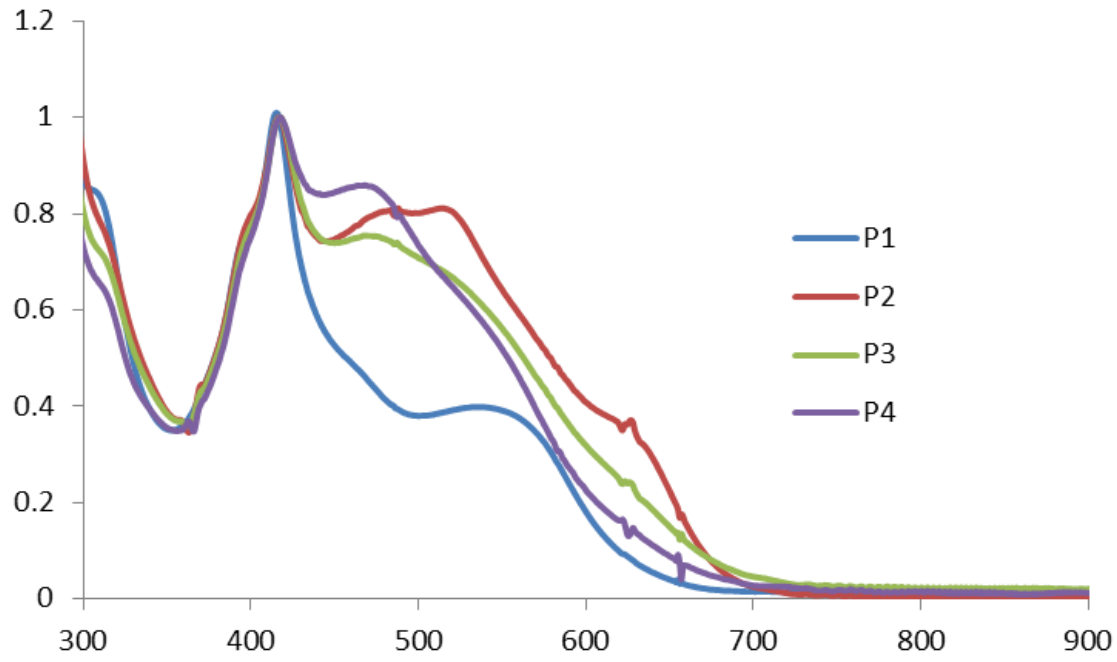

Figure 3.8. Normalized absorbance spectra of **P1** (blue), **P2** (red), **P3** (green), and **P4** (purple) in chloroform solution.

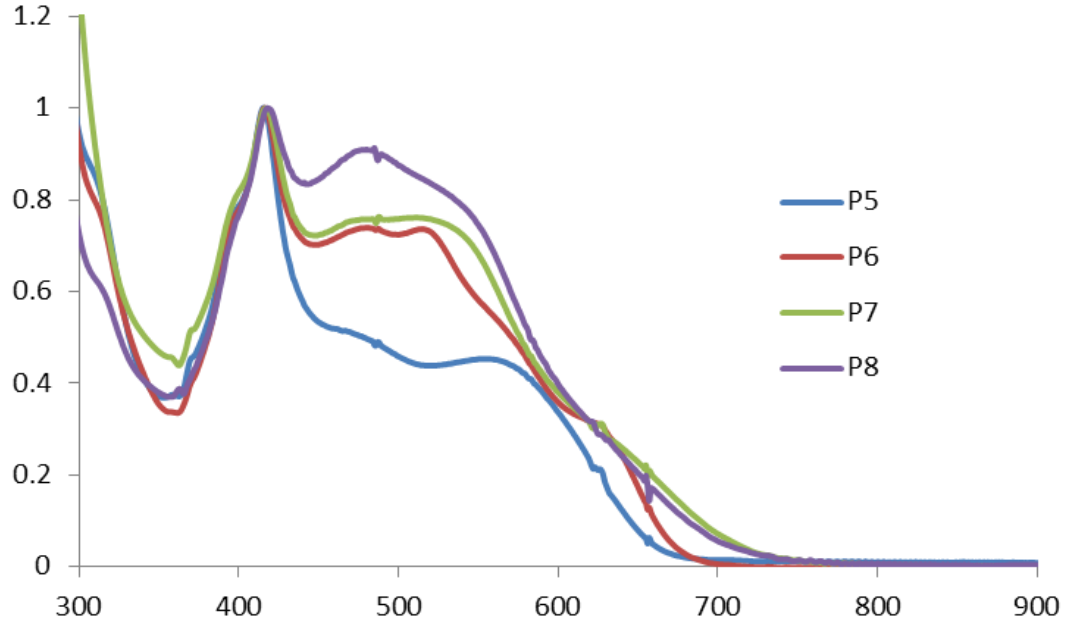

Figure 3.9. Normalized absorbance spectra of **P5** (blue), **P6** (red), **P7** (green) and **P8** (purple) in chloroform solution.

The normalized absorbance spectra of **P9—P12** can be seen in Figure 3.10. It can be readily seen that the optical band gap of **P9** is red shifted in comparison to **P1** and **P5** which is to be expected considering that the monomer **7** exhibits a red shift compared to monomer **3c** due to the extended conjugation possessed by monomer **7**. Polymer **P10** appears as a purple-red solution and shares similar features to **P1**; however, the band edge of **P10** is red shifted by 30 nm and the peak centered near 500 nm is broader and has a larger cross section in comparison to the peak at 400 nm compared to **P1**. The red shift seen in **P10** is most likely due to a higher lying HOMO orbital resulting from the use of the relatively more elctron rich 4,4-bis(2'-ethylhexyl)-4H-cyclopenta[2,1-b:3,4-b']dithiophene unit. **P11** has a similar appearance to **P10** but the single peak at 500 nm has resolved into two separate excitations most likely due to separate π to π* excitations resulting from πD—πA interactions between thiophenes and the DTP units and cyclopenta[2,1-b:3,4-b']dithiophene units and the DTP units. The band edge of **P11** is also slightly red shifted by 10 nm in comparison to **P10** most likely due to the extended conjugation of **P11**. Polymer **P12** appears as a black solution, which is notable in that it is the only polymer reported in this series that does not appear reddish purple in solution. The visible absorption of **P12** consists of three peaks centered at 410, 500, and 630 nm. The peaks at 500 and 630 nm most likely result from the same excitations that result in similar peaks for **P11**. The band edge of **P12** is also red shifted in comparison to **P9—P11.** Polymers **P1—P12** have larger band gaps than the DPT based polymer reported by Zhang *et al*, which has an optical band gap of 760 nm.[34] We attribute the difference in the band gap to their use of the relatively more electron rich indenodithiophene copolymerization unit. This hypothesis is supported by the fact that the HOMO levels measured for **P1—P8** and **P10—P11** were 200-300 mV lower than the

DTP based polymer reported by Zhang *et al*.

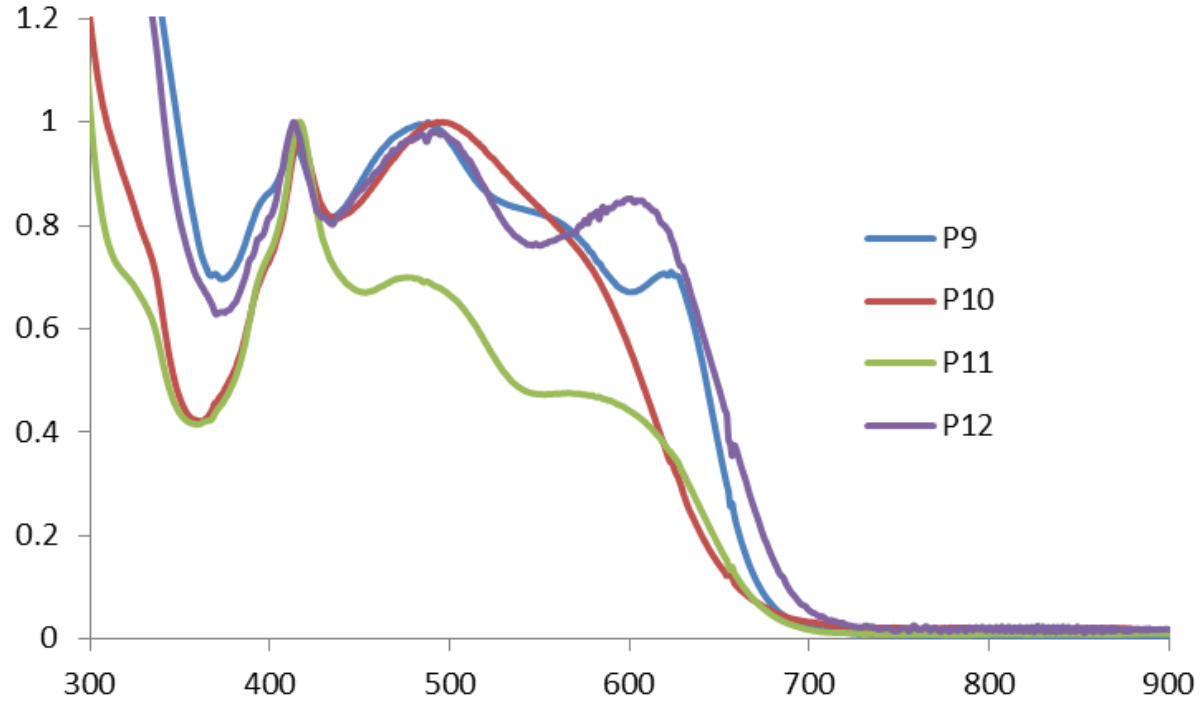

Figure 3.10. Normalized absorbance spectra of **P9** (blue), **P10** (red), **P11** (green), and **P12** (purple) in chloroform solution.

Crystal structures and crystallinity trends of dithieno[3,2-a:2',3'-c]phenazines and selected polymers

The crystal structure of monomer **5a** can be seen in Figure 3.11. Monomer **5a** was crystallized out of a mixture of chloroform and ethanol to form fine red needles. Single crystal diffraction of the crystals was performed and the unit cell of the crystal was found to have triclinic symmetry belonging to the space group *P*-1. The unit cell of **5a** was found to have the following dimensions: the a, b, and c axes were found to have lengths of 9.71, 14.9, and 18.4 Å respectively and α, β, γ were found to be 66.4, 81.6, and 79.1 ° respectively. The bis(5-bromo-2-

thienyl)benzo[3,2-a:2',3'-c]dithiophene moieties of **5a** had strong π-π interactions with the carbon carbon distances ranging between 3.4-3.7 Å and carbon sulfur distances ranging between 3.5 and 3.8 Å. **5a** forms extended columns of π-stacked molecules roughly along the a—axis of the unit cell. Single crystals of **5a** may therefore display high field effect mobilities along the a-axis of the crystallographic unit cell.

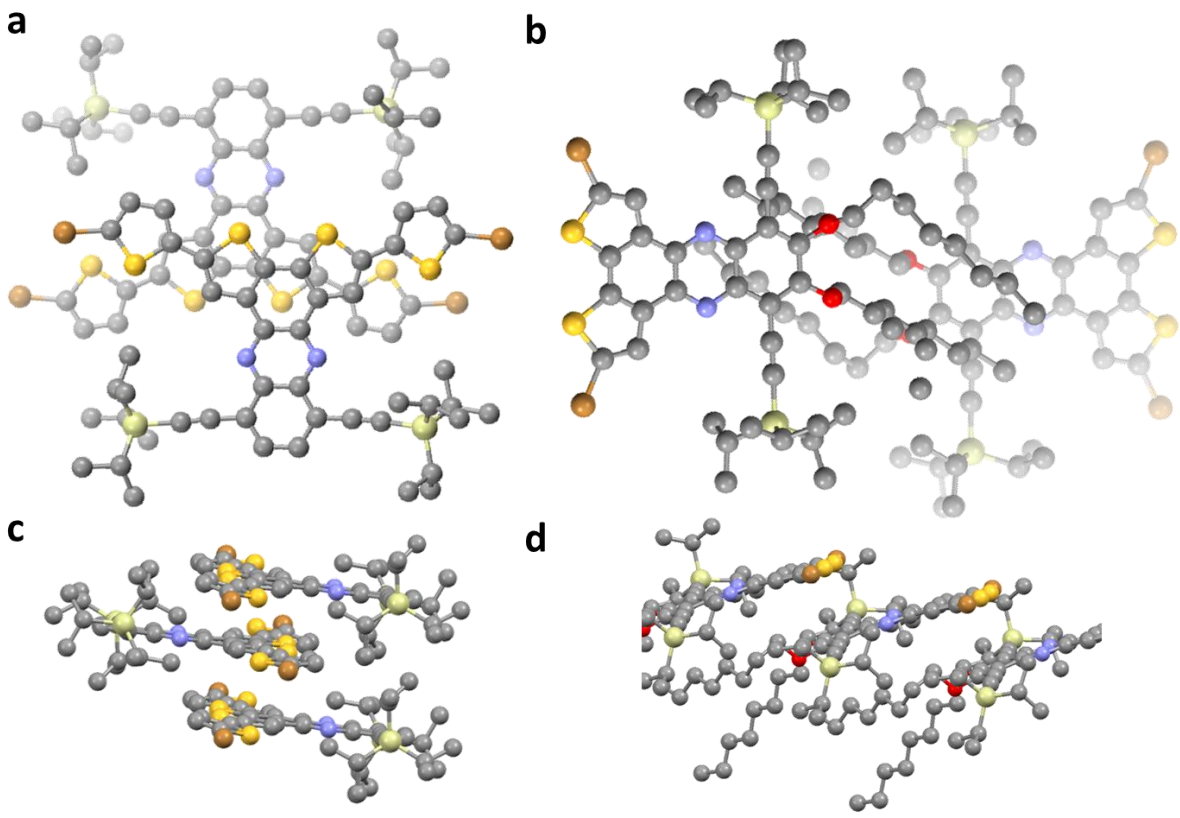

Figure 3.11. Top down view of the π stacking in single crystals of **5a** (a) and **3b** (b) and side view of the crystal packing of **5a** (c) and **3b** (d).

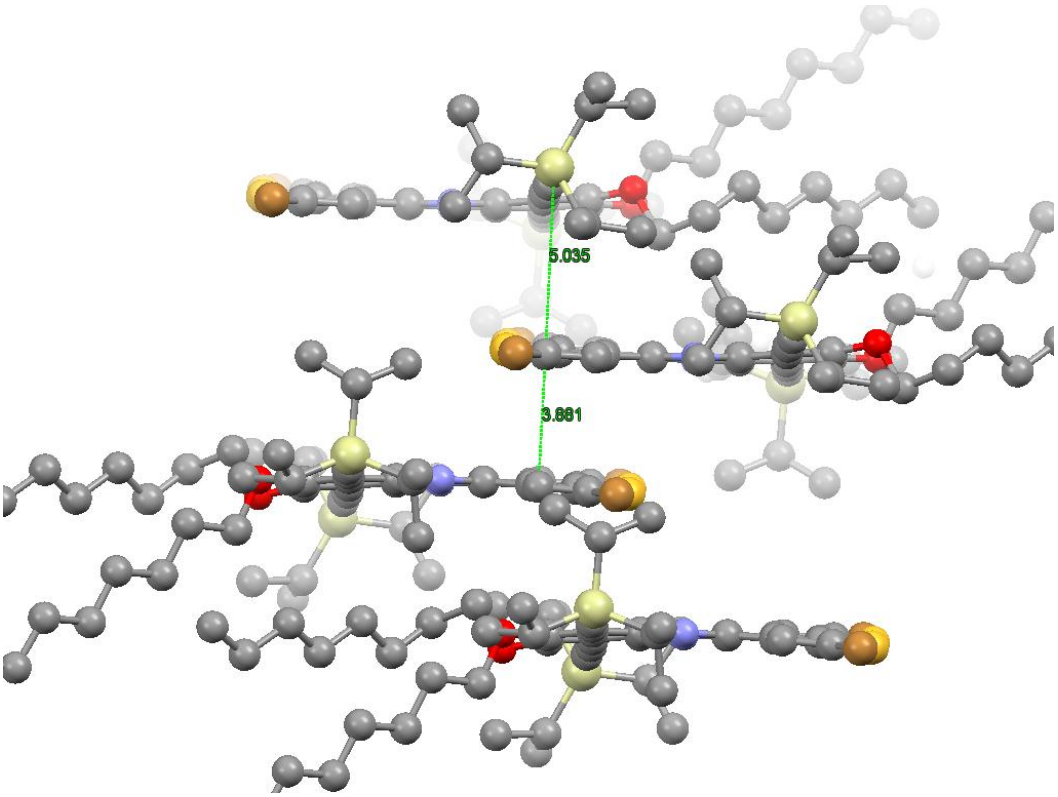

Figure 3.12. Side view of the asymmetric packing of the DTP units of **3b** caused by the steric demands of the bulky TIPS alkynyl groups

The crystal structure of monomer **3b** can also be seen in Figure 3.11. **3b** was crystallized out of a mixture of chloroform and ethanol and formed thin yellow needles. The unit cell of the single crystals was found to have triclinic symmetry and belonged to the space group *P*-1. The cell length were 8.45, 14.20, and 23.57 Å for the a, b, and c axes respectively and 100.9, 91.47 and 90.9 ° were the angles for α, β, and γ respectively. The spacings of the DTP units alternate between relatively close interactions of 3.8 Å dominated by π—π interactions between DTP units and loose interactions dominated by the alkyl—pi interaction of the bulky TIPS groups and the π system of the DTP units (Figure 3.12). It can also be seen in (Figure 3.13) that the octyloxy chains of **3b** also have strong interactions along the c axis of the unit cell. The average

carbon—carbon distances for these alkyl chains range from 3.9—5.6 Å. There are no intermolecular close contacts between the atoms comprising the aromatic core of **3b**; the closest interaction being 3.97 Å between the sulfur atoms of the benzo[3,2-a:2',3'-c]dithiophene and the carbon at the 8-position of the DTP unit. Single crystals of **3b** would not be expected to possess high mobilities due to the lack of close π-π interactions in the crystal structure.

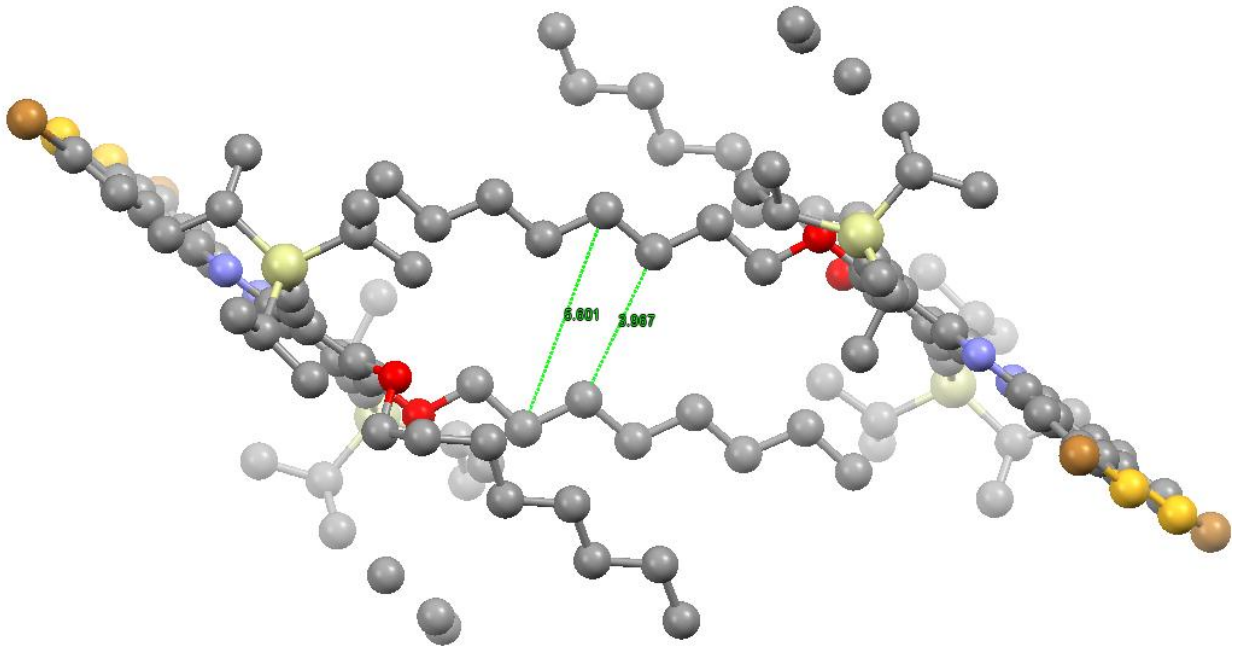

Figure 3.13. Side view of the packing of octyloxy chains in **3b** with distances ranging from 3.9 to 5.6 Å.

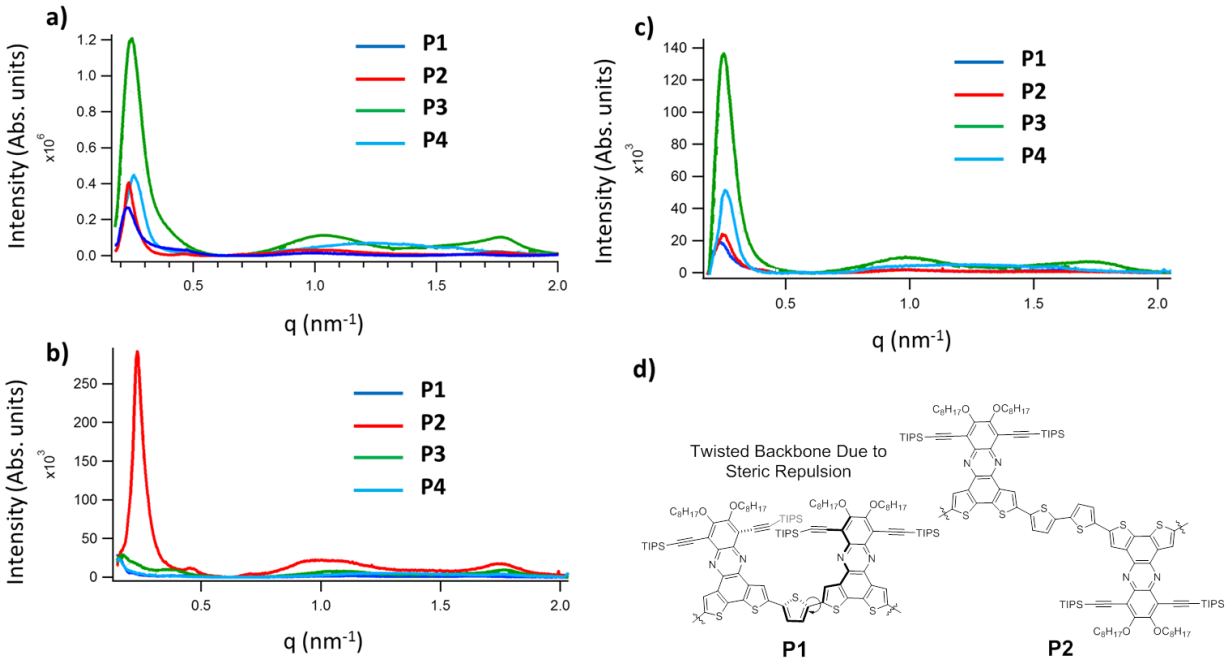

Figure 3.14. Grazing incidence wide angle x-ray scattering plots collected on thin films of **P1-P4** cast from 1,2-dichlorobenzene solutions. Plots are of a) the integrated intensity from b) the in plane integrated intensity and the c) out of plane integrated intensity for **P1** (blue) **P2** (red) **P3** (green), and **P4** (cyan). d) shows a schematic of the different steric demands of **P1** compared to **P2**.

Grazing incidence wide angle x-ray scattering (GIWAX) was collected on thin films of **P1—P4** and the integrated out-of-plane and in-plane scattering can be seen Figure 3.14, the general trend in crystallinity of the series **P1—P4** is that crystallinity increases from **P1** to **P3** as the number of thiophene spacers between DTP units increases. **P1—P4** exhibit strong scattering from the (100) peak at 0.28 $Å^{-1}$ and **P1—P3** exhibit a weak scattering peak centered a 1.1 $Å^{-1}$ and a broad scattering peak resulting from π—π stacking of polymer chains at 1.8 $Å^{-1}$. **P4** is unique in that it is the only polymer in the series which has a broad peak from 1.3—2.0 $Å^{-1}$. Very similar broad peaks from 1.3—2.0 $Å^{-1}$ are seen in other amorphous polymers such as PTB7 and PSDTTT.[41] The peaks at 1.0 A^{-1} and 1.8 A^{-1} corresponding to d spacings of 6.2 Å and 3.5 Å

respectively. This latter spacing closely matches the carbon—carbon and carbon—sulfur distances seen in the single crystal of **5a** and most likely results from the π—π stacking of the aromatic units of the polymer chains. The larger spacings corresponding to the peak at 1.0 A^{-1} match well with the spacings of the octyloxy chains seen in **3b** (carbon carbon distances in the alkyl chains of **3b** range from 3.9—5.6 Å) and thus likely result from alkyl—alkyl interactions between polymer chains. This hypothesis is strongly supported by the fact that a very similar peak at 1.3—1.4 $Å^{-1}$ is seen in GIWAXs of the polymer PBTTT resulting from diffraction resulting from interdigitated alkyl chains.[39] Similar peaks are also seen for several other conjugated polymers containing linear side chains, and these peaks disappear for these polymer upon replacement of the straight polymer chains with diastereomeric mixtures of branched alkyl chains, which prevent regular interdigitation of the alkyl chains.[42,43]

The (100) peak at 0.28 $Å^{-1}$ shows an increase in intensity in films of **P2** compared films of **P1**. This increase in crystallinity is small despite the fact that the bulky triisopropylsilyl groups of the DTP units are less sterically hindered in **P2** compared to **P1.** To elaborate on this statement, the DTP units would be expected to coplanarize with any covalently linked thienyl groups. This phenomenon is clearly seen in the thienyl groups of **5a**. However, if two DTP groups were covalently linked at the 2 and 5 positions of a single thiophene unit, as they are in **P1**, the triisopropylsilyl protected alkynyl groups substituted at the 8 and 11 positions of the DTP moieties would block coplanarization of the DTP π-system with the thiophene ring due to steric clashing of the triisopropylsilyl groups. Deplanarization of the polymer backbone should lead to more conformational disorder and therefore less scattering from peaks associated with lamellar packing of polymer chains. There is less steric clashing of the triisopropylsilyl protected alkynyl

groups when DTP units are covalently linked at the 5 and 5' positions of a 2,2'-bithiophene linkage because the two DTP units end up with a different head to tail orientation with respect to the conjugated backbone of the polymer. This steric hindrance introduces torsional strain in the polymer backbone therefore causing the polymer backbone of **P1** to deplanarize.

The more planar backbone of **P2** would be expected to possess significantly enhanced scattering from the (100) peak resulting from the lamellar packing of alkoxy chains, as can be clearly seen upon comparing the scattering of the (100) peak in **P1** and **P2** (see Figure 3.14). However, the weaker scattering intensity seen in the (100) peak of **P1** compared **P2** might also be due to the fact that **P1** has a much higher molecular weight than **P2**. Higher molecular weights often lead to a decrease in scattering intensity for most conjugated polymers.[43]

A dramatic increase in scattering from the (100) peak is also seen when comparing the relative scattering intensity of **P2** and **P3**. This increase in crystallinity for **P3** may be due to the fact that the DTP units are spaced far enough in this polymer to allow full planarization of the polymer backbone. It will be noted that in the lowest energy conformation, the DTP units would be on the same side of the polymer backbone of **P3**, but the torsional strain present in **P1** would be absent due to the greater distance between the triisopropylsilyl groups in **P3**. Surprisingly there is decrease in intensity of wide angle scattering when comparing **P3** to **P4**. This is surprising considering that the greater spacing between DTP units in **P4** would be expected to lead to more efficient packing of polymer chains and therefore lead to stronger scattering. **P4** does exhibit stronger scattering than **P2**, but this may in part be due to the fact that **P4** has a significantly lower number average molecular weight than **P2** (≈ 25%) . Another interesting feature of the x-ray scattering of **P4** is the shape of the scattering peak between 1.0-

1.7 $Å^{-1}$. Unlike **P2** and **P3** which possess two peaks in this general region, **P4** has one very broad peak, which suggests that the conjugated backbone of **P4** may possess more conformational disorder than **P2** and **P3**, thereby broadening the (010) and alkyl—alkyl peaks.

The in—plane and out—of—plane scattering from **P1**—**P4** can be seen in Figure 3.14. **P1**, **P3** and **P4** exhibit strong out-of-plane scattering for the (100) peaks while the in-plane scattering is dominated by the (010) and alkyl—alkyl peaks, suggesting that **P1**, **P3** and **P4** have a face-on orientation of the conjugated polymer backbone with respect to the substrate. In contrast, **P2** exhibits strong in—plane scattering from the (100) peak and strong out—of—plane scattering from the (010) and alkyl—alkyl peaks suggesting that the conjugated backbone of **P2** has a strong tendency towards an edge—on orientation with respect to the substrate. The DTP units of **P2** are too large to allow rotation of the DTP units around the covalent bond linking the thiophene rings to the DTP units, thus leading to a straighter polymer backbone. The fact that **P2** has a straight backbone and a more regioregular orientation of the DTP units most likely effects the relative energies between a face—on or edge—on orientation with respect to the substrate. The polymer chains of **P2** have a more regioregular arrangement of DTP units and this most likely leads to more efficient lammellar packing of polymer chains compared to the other polymers in the series. The relatively more efficient packing of polymer chains most likely results in a preference for an edge—on orientation seen in other regioregular polymers such as regioregular P3HT.[43] Kim *et al*. saw a similar trend in their study of naphtho[2,1-b:3,4-b']dithiophene based polymers.[44] For this study three polymers were synthesized consisting of naphtho[2,1-b:3,4-b']dithiophene units covalently linked by thiophene, bithiophene, and quaterthioiphene units. Polymers containing the thiophene and quaterthiophene linkages were

very amorphous and had a face—on orientation with respect to the substrate. While the polymers containing a bithiophene linkage displayed a much higher crystallinity compared to the thiophene and quaterthiophene linked polymers and had an edge-on orientation with respect to the substrate.

Electrochemical characterization of P1—P12

The electrochemical properties of **P1—P12** were measured via cyclic voltammetry (Figure 3.15 and Figure 3.16) and are summarized in

Table 3.2. CVs were obtained on films deposited on ITO glass and were measured in propylene carbonate with Li/Li^+ as the reference electrode and the ITO glass as the working electrode. The reduction peaks of **P1—P12** could not be measured possibly due to the degradation of the polymer during oxidation and because this region contains large peaks due to the ITO substrate Absolute ionization potentials were calculated using –4.3 V as the absolute

electrode potential for the standard hydrogen electrode[45] and –3.0 V as the standard reduction potential of Li/Li^+ vs. the standard hydrogen electrode.[46]

Table 3.2. Summary of cyclic voltammetry data **P1-P12**.

Polymer	IP *vs.* Li/Li^+ (V)	HOMO *vs.* vacuum level (V)	Optical Band gap (eV)	LUMO calculated (V)
P1	4.1	-5.4	1.9	-3.5
P2	3.9	-5.2	1.9	-3.3
P3	3.9	-5.2	1.8	-3.4
P4	3.8	-5.1	1.8	-3.3
P5	4.1	-5.4	1.9	-3.5
P6	4.0	-5.3	1.9	-3.4
P7	4.0	-5.3	1.8	-3.5
P8	3.9	-5.2	1.7	-3.5
P9	3.6	-4.9	1.8	-3.2
P10	3.7	-5.0	1.8	-3.2
P11	N/A	N/A	1.8	N/A
P12	3.6	-4.9	1.7	-3.2

The general trend in the polymer series **P1**—**P4** is that ionization potential decreases by 200 mV from an absolute potential of –5.4 eV *vs.* vacuum level in **P1** to a value of –5.2 eV *vs.* vacuum level in **P4**. The LUMO levels of **P1**—**P12** were calculated using the optical band gap

obtained from UV-vis absorbance spectra. The calculated LUMO levels stay somewhat consistent due to the fact that the general rise in HOMO level from **P1**—**P4** and **P5**—**P8** is somewhat offset by a general decrease in the band gap of these polymers. The LUMO levels range from –3.4 to –3.6 eV *vs.* vacuum due to these opposing trends. **P9** has a somewhat raised HOMO level due to the substitution of the weakly electron deficient TIPS alkynyl substituents at the 8 and 11 positions with relatively electron-rich thiophene groups. This substitution most likely makes the DTP unit of the polymer less electron deficient, thereby raising the HOMO of **P9** and **P12** compared to the series **P1**—**P8**.

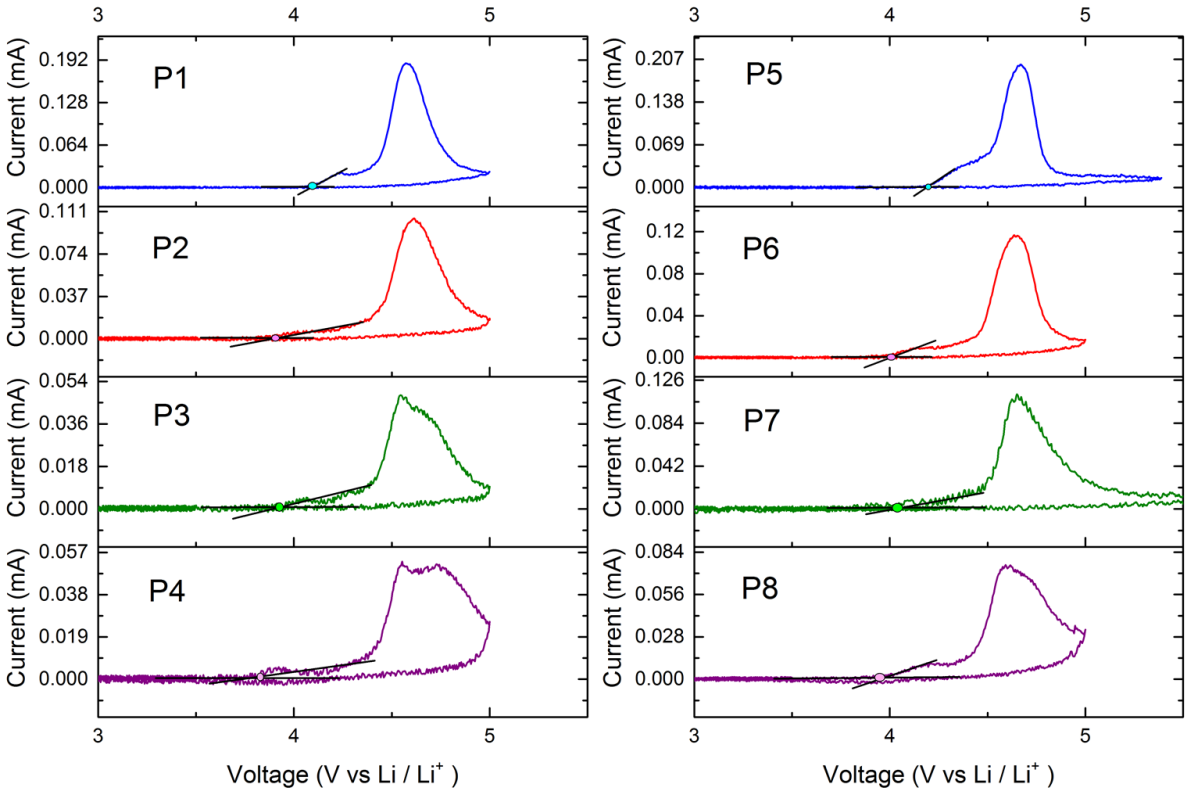

Figure 3.15. Cyclic voltammograms of films of **P1**-**P8** on ITO glass taken with Li / Li^+ reference.

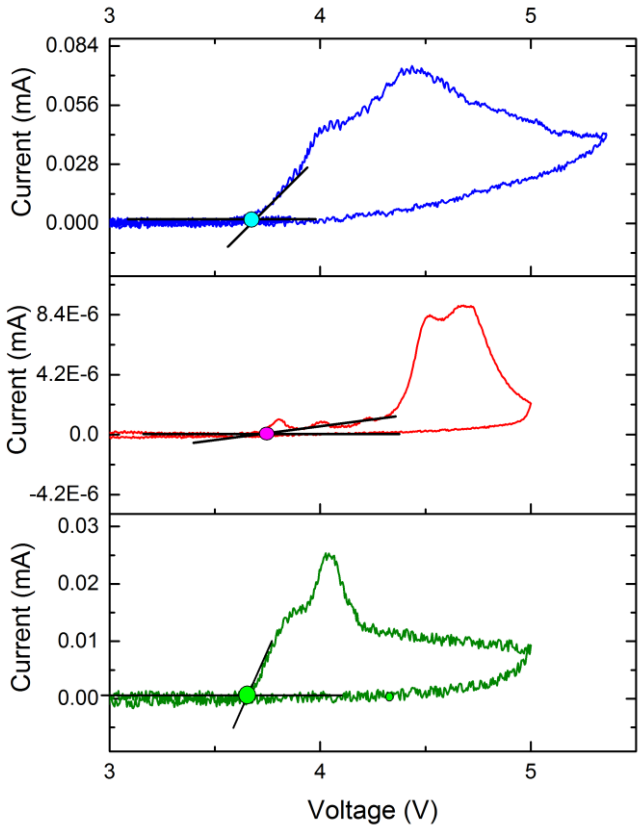

Figure 3.16. Cyclic voltammograms of **P9** (blue), **P10** (red), and **P12** (green).

As was mentioned earlier, the HOMO levels of **P1**—**P8** and were lower than the HOMO levels of the polymers containing DTP units as reported by Zhang *et al*.[34] We hypothesized that this difference was mainly due to their use of the relatively more electron-rich indenodithiophene unit. We will also note that the calculated LUMO levels of our polymer are higher than the LUMOs reported in the aforementioned study. This increase in the LUMO levels of **P1**—**P8** compared to the DTP polymers reported by Zhang *et al*. suggests that polymerization from the relatively electron deficient 8 and 11 positions of the DTP units might lead to lower LUMO levels compared to polymers resulting from polymerization at the 2 and 5 positions.

The cyclic voltammograms of **P9**, **P10** and **P12** can be seen in Figure 3.16. **P9** has a somewhat raised HOMO level due to the substitution of the weakly electron deficient TIPS alkynyl substituents at the 8 and 11 positions with relatively electron-rich thiophene groups. This substitution most likely makes the DTP unit of the polymer less electron deficient, thereby raising the HOMO of **P9** and **P12** compared to the series **P1—P8**. The cyclic voltamogram of **P12** shares many similar features with **P9**, but the onset of the oxidation peak of **P12** is 100 mV lower compared to **P9**. This difference is most likely due to the use of the relatively more electron rich cyclopentadithiophene unit being used as the comonomer in **P12**. Measurement of the oxidation potentials of **P10** and **P11** was difficult due to the swelling and subsequent delamination of these films in the ethylene carbonate/propylene carbonate solvent. Measurements of **P10** were somewhat successfull, but the measurements yielded low currents and it was difficult to measure the oxidation onset potential. Attempts to measure the oxidation onset potentials of **P11** failed, however. Solution phase measurements of the oxidation onset potentials of **P10** and **P11** will be performed in the future.

Polymers solar cell properties

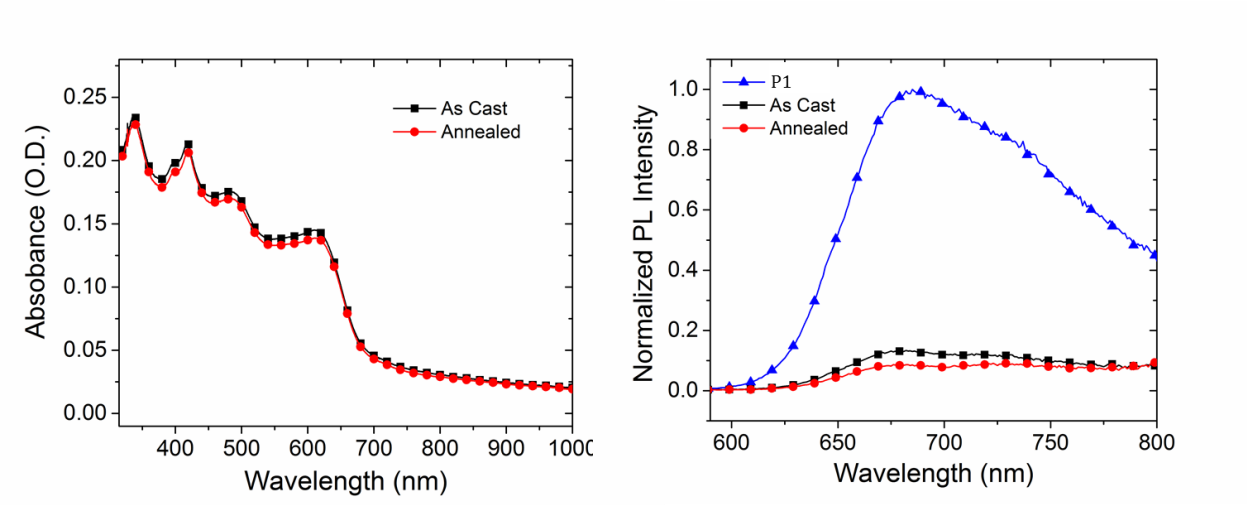

Figure 3.17. Absorption (left) and PL quenching (right) of thin films of **P1** (blue) and as cast (black) and annealed (red) films consisting as cast of (1:1) blends of **P1** and PCBM cast from *o*-DCB solutions containing 1% DIO additive.

Polymer solar cells were created from polymers **P1**, but the solubility of polymers **P2—P9** weren't high enough to cast films of a sufficient thickness needed for properly functioning solar cells. As can be seen in Figure 3.17, blends of **P1** and the fullerene derivative phenyl-C_{61}-butyric acid methyl ester (PCBM) have broad absorption extending out to 700 nm. Films were cast using 1,8-diiodooctance (DIO) solvent additive to improve the crystallinity of the polymer phases and to improve phase purity of polymer fullerene blends to improve the free carrier mobilities within these domains.[47] Films had a thickness of 70 nm and annealed films were annealed at 110 ˚C for 20 minutes . Annealed films of these blends show no marked changes in the vibronic structure of these blends which suggests that annealing has little effect at enhancing the crystallinity of the amorphous polymer **P1**. Strong fluorescence quenching in films consisting of blends of **P1** and PCBM provide evidence that **P1** can efficiently transfer

charge to PCBM upon excitation. This shows that **P1** and PCBM are intemixed on length scales of the exciton diffusion length, which for most polymers is on the order of 10 nm.[7] A small increase upon exciton quenching can be seen upon annealing blends of **P1** and PCBM which shows that annealing causes increased intermixing of the fullerene and polymer phases.

Table 3.3. Properties of solar cells consisting of (1:1) blends of **P1** and PCBM cast from an *o*-DCB solution containing 3% DIO additive.

Device	V_{OC} (V)	J_{SC} (mA/cm^2)	FF (%)	PCE (%)
P1:PCBM 3% DIO	0.77 ± 0.01	3.75 ± 0.25	44.14 ± 1.28	1.27 ± 0.08
P1:PCBM annealed	0.73	2.31	41.85	0.71

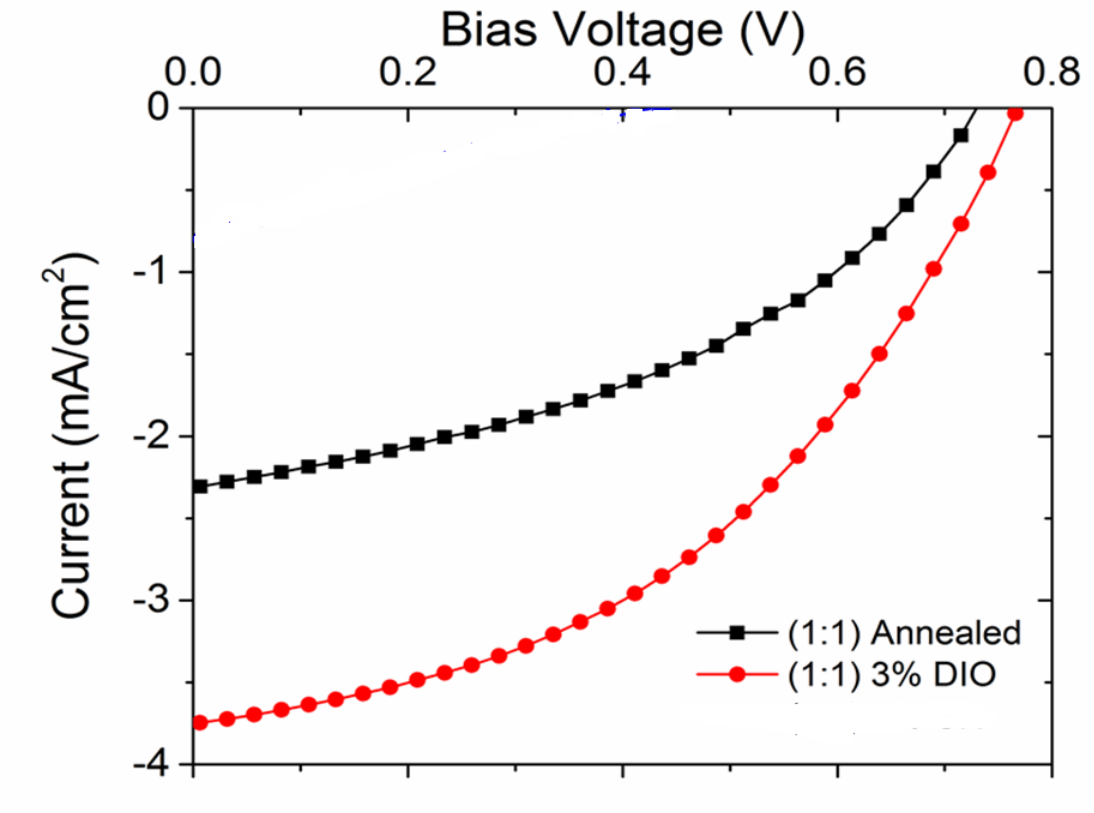

Figure 3.18. Current—voltage curves of solar cells consisting of unannealed **P1** and PCBM films in (1:1) blend ratio cast from an *o*-dichlorobenzene solution containing 3% DIO additive.

The current—voltage curves of solar cells created from 1:1 blends of **P1** and PCBM are shown in Figure 3.18**Error! Reference source not found.** and the properties of these solar cells are summarized in Table 3.3. Polymer films were cast using the same conditions used for the florescence measurements and were fabricated using the process outlined in the experimental section. These solar cells displayed relatively high open circuit voltages (V_{OC}) due to the low lying HOMO orbitals of **P1**. Films that were cast using no DIO additive and that were annealed 110 ˚C for 20 minutes showed lower short circuit currents (J_{SC}) than unannealed films processed using 3% DIO additive. This difference is most likely due over mixing of polymer and fullerene phases, leading to poor phase purity of the polymer and fullerene domains in the annealed films. Films showed relatively low short circuit currents due to the relatively thin active layers of these devices. Fill factors (FF) of these devices were also quite low, and low fill factors are often the result of recombination losses, which in this case is most likely the result impure fullerene and polymer domains. Power conversion efficiencies (PCEs) of these solar cells remained low due to the combination of these factors, achieving a PCE of 1.27% and 0.71% for the 3% DIO and annealed solar cells respectively.

Conclusion

A number of πD-πA copolymers were synthesized using 5,6-bis(alkoxy-8,11-bis((triisopropylsilyl)ethynyl)dithieno[3,2-*a*:2',3'-*c*]phenazine as the πA component of the copolymer. These polymers were found to have deep HOMO levels (–4.9 to –5.4 eV *vs*. vacuum level), broad absorption across the visible spectrum and moderately low band gaps (1.7—1.9 eV). Although the monomer units used for these polymers exhibited high crystallinity, the polymers synthesized from these units were largely amorphous. This most likely due to the

steric clashing of the TIPS alkynyl groups. Photovoltaic devices were fabricated and tested using PCBM as the electron acceptor component and **P1** as the electron donor. Devices showed a relatively high V_{OC} due to the low lying HOMO of **P1**. Optimized devices had PCEs had a high performance of 1.27%. Device performance was somewhat limited by the poor phase purity of the polymer and fullerene layers in the solar cells fabricated from these mateials and the limited solubities of these polymers, as well as the poor solubility of these polymers. Future studies will focus on the performance of the more easily processed polymers **P10—P12** which have smaller band gaps and higher solubilities than **P1—P9**.

Experimental

Unless otherwise noted all reagents and solvents were purchased and used as received from available commercial sources. 2,6-Bis(tributylstannyl)-4,4-bis(2'-ethylhexyl)-4H-cyclopenta [2,1-b:3,4-b']dithiophene was synthesized according to the literature procedure and spectra matched the reported values.[36] All NMR spectra were collected on a Varian AV500 spectrometer with a 5 mm dual cryoprobe and a Bruker DRX500 spectrometer with a 5 mm broadband probe.

For polymer molecular weight determination, polymer samples were dissolved in HPLC grade *o*-dichlorobenzene at a concentration of 0.5 mg/mL and were heated until complete dissolution and then allowed to cool to room temperature prior to filtering through a 0.2 µm PFTE filter. GPC was performed using HPLC grade *o*-dichlorobenzene at a flow rate of 0.6 ml/min one 300 X 7.8 mm TSK-Gel GMHH R-H column (Tosoh Corporation) at 65 ˚C using a Viscotek GPC Max VE 2001 separation module and a Viscotek TDA 305 RI detector. The instrument was calibrated using polystyrene standards (1,050—3,800,000 g/mol) and data was analyzed using OmniSec 4.6.0 software.

ESI mass spectra were acquired on an *Agilent 6890-5975* GC- MS and MALDI-TOF spectra were acquired on a Bruker Ultraflex MALDI-TOF-TOF instrument using a 9-nitroanthracene matrix.

2-D grazing incidence wide angle X-ray scattering (GIWAXS) experiments were performed at the Stanford Synchrotron Radiation Lightsource on beamline 11-3 using a wavelength of 0.9742 Å with an incidence angle of 0.12◦ . Fig. S3 shows the full 2-D

diffractograms of our different polymer systems. These diffractograms were radially integrated to obtain the diffraction patterns (0-10◦ for in-plane, 70-80◦ for out-of-plane, and 0-180◦ for full). The 2-D images were collected on a plate with the detector 250 mm away from the center of the measured sample. The beam spot had a width of ∼150 μm and a helium chamber was used to reduce the noise. The software package WxDiff was used to reduce the GIWAXS data and subsequent analysis was performed in IgorPro.

All substrates were cleaned by sequentially sonicating in soapy water, DI water, acetone, and isopropanol for 5-10 minutes each, then placed under rough vacuum to remove all traces of residual solvent, and finally transferred into a nitrogen glove box for use. The films were cast from *o*-dichlorobenzene solutions at a concentration of 20 mg/mL and spin cast at 1160 rpm for 20 seconds, then 3000 rpm for 1 second. This allowed for even distribution of the polymer on the substrate and removal of excess solution while leaving the film still wet.

All CVs were scanned in the oxidation direction first follow by reduction. CVs were measured in a 3 neck flask at 0.5 mV/s with Arbin BT2000. Polymer films deposited on ITO glass is used as the working electrode, Li as the reference and counter electrode and 1M $LiPF_6$ in propylene carbonate as the electrolyte. CVs of **P5**, **P7**, and **P9** exhibited shifts in the spectra due to plating of oxidized polymer on the Li reference electrodes. All spectra showed a -300 mV shift in their spectra as evidenced by a shift in the ITO peak from -4.1 V to -3.8 V *vs*. Li / Li+. Spectra were corrected so that the ITO peak appeared at -4.1 V *vs*. Li / Li+.

Solar cells were fabricated by cleaning glass substrates pre-patterned with ITO. The substrates were cleaned for approximately ten minutes each in solutions of detergent, DI

water, acetone, and isopropyl alcohol. The substrates were then placed in a plasma etcher and pumped down to 200 mTorr. Following at least 30 minutes under vacuum, the substrates were plasma etched for 15 minutes. A 35 nm layer of PEDOT:PSS (AI 4083) was deposited by spin-coating the solution in air at 5000 rpm for 30 s. The PEDOT:PSS substrates were then baked at 150 C for 20 minutes in air.

Blend-cast active layers were prepared by co-dissolving polymer and PCBM in o-dichlorobenzene with a 1:1 weight ratio. The concentration with respect to P1 was 10 mg/mL and the solutions were stirred at 55 C overnight. After cooling to room temperature, the solutions were spun successively at 1160 rpm for 20 s, followed by 3000 rpm for 5 s. For devices fabricated with 3 % (volume percent) DIO the solvent additive was added prior to solution heating. For thermally annealed films, the annealing process occurred in an argon atmosphere after BHJ formation. Films were annealed 110 C for 20 minutes.

Electrodes for devices were evaporated onto the active layers using a thermal evaporator (Angstrom Engineering). Cathodes consisted of approximately 10 nm of Ca evaporated at a rate of 0.5 Angstrom/s followed by evaporating 60 nm Al at a rate of 1 Angstrom/s. Evaporation pressures were 10^-7 Torr or less. The active areas of the resulting solar cells were 7.2 mm^2.

J-V measurements were performed in an argon atmosphere using a Keithley 2400 source meter. A xenon arc lamp equipped with an Am-1.5 filter was used as the excitation source, with an intensity calibrated to match one sun.

2,7-Dibromobenzo[2,1-b:3,4-b']dithiophene-4,5-dione (1) Compound **1** was synthesized according to the literature procedure[45] and spectra match reported values.

4,7-Bis((triisopropylsilyl)ethynyl)benzo[c][1,2,5]thiadiazole (2a)

Compound **2a** was prepared via the following procedure: 4,7-dibromobenzo[c][1,2,5]thiadiazole (17.0 mmol), 5.00 g, was dissolved in a mixture toluene (85 mL), triethylamine (13 mL) and triisopropylsilyl acetylene 9.5 mL (42.5 mmol, 2.5 eq) in a 250 mL flask with reflux condenser. This mixture was sparged for 20 minutes using argon after which time 982 mg tetrakis(triphenylphosphine)palladium(0) (0.849 mmol, 0.05 eq) and 323 mg copper iodide were added (0.636 mmol, 0.1 eq). The mixture was then sparged a second time with argon and heated to reflux for 12 hours. Upon cooling, the mixture was rotary evaporated and subsequently purified by column chromatography using SiO_2 and a mixture of 1:4 DCM to hexanes as eluent to afford 4.32 g (51%) of a fluorescent yellow solid. Spectra matched reported literature values.[35] ^{1}H NMR (500 MHz, $CDCl_3$) δ (ppm) 7.67 (s, 2H), 1.23-1.17 (m, 42H). ^{13}C NMR (125 MHz, $CDCl_3$) δ (ppm) 154.7, 132.7, 117.4, 102.3, 100.3, 18.7, 11.4.

5,6-Bis(octyloxy)-4,7-bis((triisopropylsilyl)ethynyl)benzo[*c*][1,2,5]thiadiazole (2b)

Compound **2b** was prepared via the following procedure: 4,7-dibromo-5,6-bis(octyloxy)benzo[c][1,2,5]thiadiazole (3.48 g, 6.36 mmol) was dissolved in a mixture toluene (50 mL), triethylamine (4.4 mL) and triisopropylsilyl acetylene 4.28 mL (19.1 mmol, 3 eq) in a 100 mL flask with reflux condenser. This mixture was sparged for 20 minutes using argon after

which time 367 mg tetrakis(triphenylphosphine)palladium(0) (0.318 mmol, 0.05 eq) and 121 mg copper iodide were added (0.636 mmol, 0.1 eq). The mixture was then sparged a second time with argon and heated to reflux for 12 hours. Upon cooling, the mixture was rotary evaporated and subsequently purified by column chromatography using SiO_2 and a mixture of 1:8 DCM to hexanes as eluent to afford 3.37 g of a fluorescent yellow solid (75%). ^{1}H NMR (500 MHz, $CDCl_3$) δ (ppm) 4.34 (t, *J* = 6.9 Hz, 4H), 1.87 (p, *J* = 7.6 Hz, 4H), 1.48 (p, *J* = 7.5 Hz, 4H), 1.40 – 1.18 (m, 48 H) 0.91 (t, *J* = 6.4 Hz, 6H). ^{13}C NMR (125 MHz, $CDCl_3$) δ (ppm) 157.9, 152.2, 107.9, 103.8, 98.6, 74.7, 31.7, 30.3, 29.4, 29.2, 25.8, 22.6, 18.6, 14.0, 11.3. ESI-MS: *m/z* (rel intensity) 753.5362 (77, MH+) Calculated $C_{44}H_{76}N_2O_2SSi_2H$ 753.5244.

5,6-Bis(dodecyloxy)-4,7-bis((triisopropylsilyl)ethynyl)benzo[*c*][1,2,5]thiadiazole (2c)

Compound **2c** was prepared via the following procedure: 4,7-dibromo-5,6-bis(dodecyloxy)benzo[c][1,2,5]thiadiazole (3.00 g, 4.52 mmol) was dissolved in a mixture toluene (50 mL), triethylamine (2.8 mL) and triisopropylsilyl acetylene 3.0 mL (13.6 mmol, 3 eq) in a 100 mL flask with reflux condenser. This mixture was sparged for 20 minutes using argon after which time 261 mg tetrakis(triphenylphosphine)palladium(0) (0.226 mmol, 0.05 eq) and 86 mg copper iodide were added (0.45 mmol, 0.1 eq). The mixture was then sparged a second time with argon and heated to reflux for 12 hours. Upon cooling, the mixture was rotary evaporated and subsequently purified by column chromatography using SiO_2 and a mixture of 1:8 DCM to hexanes as eluent to afford 2.50 g of a fluorescent yellow solid (2.89 mmol, 64%). ^{1}H NMR (500 MHz, $CDCl_3$) δ (ppm) 4.35 (t, *J* = 6.8 Hz, 4H), 1.88 (p, *J* = 7.0 Hz, 4H), 1.48 (p, 4H),

1.41 – 1.21 (m, 80 H), 0.89 (t, *J* = 6.9, 6H). ^{13}C NMR (125 MHz, $CDCl_3$) δ (ppm) 157.9, 152.2, 107.9, 103.7, 98.7, 74.7, 31.9, 30.3, 29.6, 29.659, 29.657, 29.656, 29.5, 29.3, 25.9, 22.6, 18.6, 14.0, 11.3. MALDI-TOF MS: *m/z* 864.070 M+ Calculated $C_{52}H_{92}N_2O_2SSi_2$ 864.642.

2,5-Dibromo-8,11-bis((triisopropylsilyl)ethynyl)dithieno[3,2-*a*:2',3'-*c*]phenazine (3a)

Compound **2a** (0.500 g, 0.841 mmol, 1 eq) was dissolved in 25 mL of dry THF and the mixture was sparged with argon for 15 minutes. Lithium aluminum hydride (128 mg, 3.37 mmol, 4 eq) was then added to the solution and the mixture was then allowed to stir for 12 hours under argon atmosphere. The mixture was then cooled to 0 °C and quenched by slowly adding 0.1 mL H_20, 0.1 mL 15% NaOH/H_2O, and 0.3 mL H_2O. The mixture was then filtered to remove inorganic salts and the filter cake was washed with 3 5 mL portions of chloroform. The filtrate was then combined with a solution of 340 mg of **1** (0.899 mmol**,** 1 eq) in an air free solution of 10 mL toluene, 0.5 mL ethanol, and 4 drops of acetic acid catalyst. The solution was refluxed until complete consumption of reagents could be seen by TLC. The mixture was then rotary evaporated and purified by SiO_2 chromatography (1:6 DCM/Hexanes), to yield 275 mg of a bright yellow solid (0.329 mmol, 39%). ^{1}H NMR (500 MHz, $CDCl_3$) δ (ppm) 8.45 (s, 2H), 8.00 (s, 2H), 1.29 (m, 42H). ^{13}C NMR (125 MHz, $CDCl_3$) δ (ppm) 141.9, 138.2, 136.1, 135.0, 133.9, 128.2, 124.1, 113.4, 103.4, 100.2, 18.9, 11.6. ESI-MS: *m/z* (rel intensity) 808.8820 (48, MH+) Calculated $C_{38}H_{46}Br_2N_2S_2Si_2$ 809.101

2,5-Dibromo-9,10-bis(octyloxy)-8,11-bis((triisopropylsilyl)ethynyl)dithieno[3,2-a:2',3'-

c]phenazine (3b)

3b was prepared using the procedure outlined for the synthesis of **3a**: Compound **2b** (1.25 g, 1.66 mmol, 1.0 eq) and 0.600 g of **1** (1.66 mmol, 1.0 eq) were used and the stoichiometry of the other reagents were unaltered. 0.858 g of a bright canary yellow solid was isolated (0.81 mmol, 47%). ^{1}H NMR (500 MHz, $CDCl_3$) δ (ppm) 8.45 (s, 2H), 4.42 (t, *J* = 6.9 Hz, 4H), 1.93 (quintet, *J* = 7.3 Hz, 4H), 1.52 .(quintet, *J* = 7.2 Hz, 4H), 1.28-1.34 (m, 58H), 0.90 (t, *J* = 7.0 Hz, 6H). ^{13}C NMR (125 MHz, $CDCl_3$) δ (ppm) 158.7, 140.7, 137.2, 135.3, 135.1, 128.1, 115.3, 113.0, 104.6, 99.5, 75.0, 31.9, 30.6, 29.6, 29.3, 26.0, 22.7, 19.0, 14.1, 11.6. ESI-MS: *m/z* (rel intensity) 1065.3962 (42, MH+) Calculated $C_{54}H_{78}Br_2N_2O_2S_2Si_2H$ 1065.3488.

2,5-Dibromo-9,10-bis(dodecyloxy)-8,11-bis((triisopropylsilyl)ethynyl)dithieno[3,2-a:2',3'-c]phenazine (3c)

Compound **3c** was prepared using the procedure outlined for the synthesis of **3a**: Compound **2c** (1.51 g, 1.72 mmol, 1.0 eq) and 0.650 g of **1** (1.72 mmol, 1.0 eq) were used and the stoichiometry of the other reagents was unaltered. 0.781 g of a canary yellow solid was isolated (0.662 mmol, 38%) ^{1}H NMR (500 MHz, $CDCl_3$) δ (ppm) 8.40 (s, 2H), 4.44 (t, *J* = 6.9 Hz, 4H), 1.94 (p, *J* = 7.1 Hz, 4H), 1.51 (p, *J* = 7.7 Hz, 4H), 1.46 – 1.30 (m, 74H), 0.89 (t, *J* = 6.8 Hz, 6H). ^{13}C NMR (125 MHz, $CDCl_3$) δ (ppm) 158.7, 140.7, 137.1, 135.1, 135.0, 128.0, 115.4, 113.0, 104.5, 99.6, 75.0, 32.0, 30.6, 29.8, 29.73, 29.67, 29.4, 26.1, 22.7, 19.0, 14.2, 11.6. ESI-MS: *m/z* (rel intensity) 1177.0271 (40, MH+) Calculated $C_{62}H_{94}Br_2N_2O_2S_2Si_2H$ 1177.4740.

2,7-Bis-(2-thienyl-5-bromo)-[2,1-*b*:3,4-*b'*]dithiophene-4,5-dione (4)

2b was synthesized from **2a** through a 4 step reaction. The four sequential steps were as follows: the protection of the dione as a ketal, a Suzuki cross coupling reaction of the ketal with thiophene-2-boronic acid pinacol ester, bromination, and deprotection of the ketal with trifluoromethanesulfonic acid. The intermediates were taken on as crude products due to the fact that first ketalization resulted in a mixture of the monoketal and the two bisketal regioisomers.

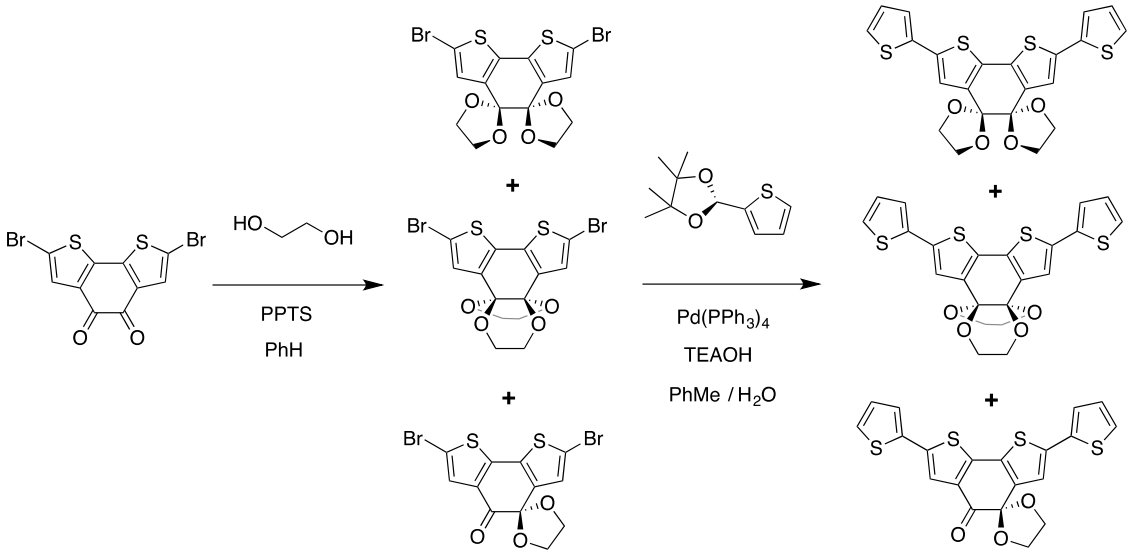

Figure 3.19. Synthesis of first and second intermediate of **2a**.

Compound **2a** (1.00 g, 2.6 mmol, 1 eq) was dissolved in 30 mL of freshly distilled toluene, 0.968 g of ethylene glycol (15.6 mmol, 6 eq), and 0.266 g of pyridinium p-toluenesulfonate (1.06 mmol, 0.40 eq) in a 50 mL flask. The reaction mixture was connected to a dean-stark apparatus,

and refluxed under argon atmosphere for 48 hours. The reaction was then cooled to room temperature and extracted with water and brine. The organic layer was then dried using magnesium sulfate and rotary evaporated under reduced pressure to yield 0.936 g of a crude brownish yellow solid.

The crude product from the previous reaction (0.936 g, 2.01 mmol, 1.0 eq) was combined in 50 mL flask with 1.27 g of thiophene-2-boronic acid pinacol ester (6.02 mmol, 3.0 eq) and 10 mL of toluene and 2 mL of a 25% tetraethyl ammonium hydroxide solution in water. The solution was sparged with argon for 15 minutes, after which time, 116 mg of tetrakis(triphenylphosphine) palladium (0) (0.101 mmol, 0.05 eq) was added to the flask. The flask was then connected to a reflux condenser, sparged with argon, and refluxed for 12 hours. The solution was then cooled to room temperature, and extracted with water and brine. The organic layer was then dried using magnesium sulfate and rotary evaporated under reduced pressure. The resulting crude product was then purified using SiO_2 chromatography using a 1:1 mixture of $CHCl_3$ / PhMe to yield 0.737 g of an orange solid.

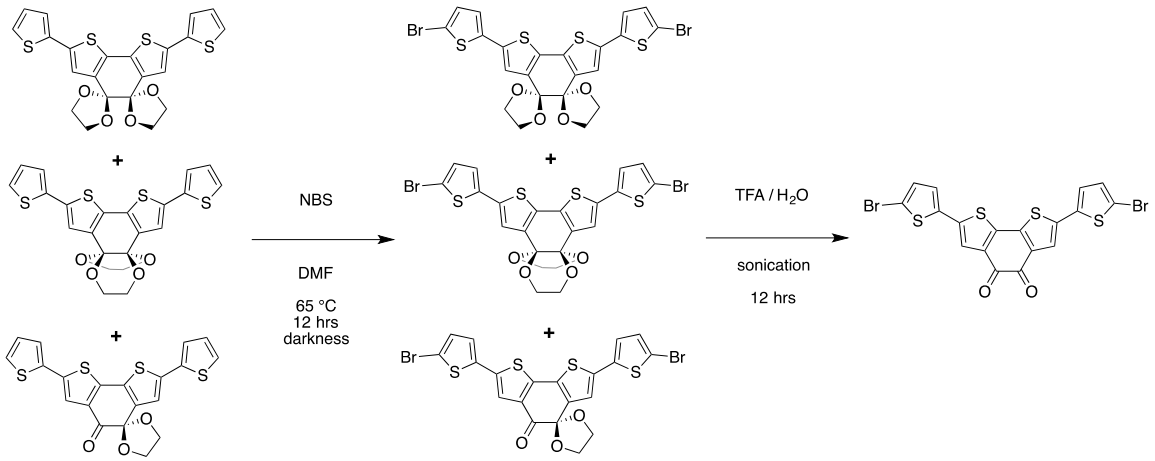

Figure 3.20. Synthesis of third intermediate and product **2a**.

The orange solid (0.737 g, 1.56 mmol, 1.0 eq) was then added to a 50 mL round-bottom flask and dispersed in 20 mL of *N*,*N*-dimethylformamide. The reaction mixture was heated to 65 °C until the orange solid fully dissolved and then 0.583 g of *N*-bromosuccinimide(3.28 mmol, 2.1 eq) was then added to the flask. The flask was then covered in aluminum foil and heated at 65 °C for 12 hours. The reaction was then poured into 200 mL of a 10% solution of sodium thiosulfate solution and extracted with 3 20mL portions of toluene. The organic layer was washed with 100 mL 1 M NaOH in water and 100 mL of brine and dried with magnesium sulfate. The solution was filtered and rotary evaporated under reduced pressure to yield 0.928 g of an orange-red solid.

The orange solid, 0.928 g, was then added to 30 mL of a 9:1 mixture of trifluoroacetic acid / water in a 50 mL round-bottom flask. The suspension was sonicated for 12 hours and filtered through a fine fritted filter and washed with water. The resulting navy blue solid was then dried under high vacuum to yield 0.685 g of the final product (1.26 mmol, 48% over 4 steps). ^{1}H NMR

(500 MHz, $CDCl_3$) δ (ppm) 7.44 (s, 2H), 7.24 (d, *J* = 3.9 Hz, 2H), 6.99 (d, *J* = 3.9 Hz). ^{13}C NMR (125 MHz, $CDCl_3$) δ (ppm) 174.0, 141.6, 137.0, 136.2, 135.9, 131.1, 125.6, 123.1, 113.7. MALDI-TOF MS: *m/z* found 539.663 M+ Calculated $C_{18}H_6Br_2O_2S_4$ 539.76.

2,5-Bis(5-bromothiophen-2-yl)-8,11-bis((triisopropylsilyl)ethynyl)dithieno[3,2-a:2',3'-c]phenazine (5a)

Compound **5a** was prepared by dissolving 250 mg of **2a** (0.496 mmol, 1.0 eq) in 10 mL of dry, air free THF. 76 mg of lithium aluminum hydride was added slowly to the solution (2.0 mmol, 4.0 eq) and the mixture was allowed to stir under argon atmosphere for 12 hours. The mixture was then cooled to 0 °C and quenched by slowly adding 0.1 mL H_20, 0.1 mL 15% NaOH/H_2O, and 0.3 mL H_2O. The mixture was then filtered to remove inorganic salts and the filter cake was washed with 3, 5 mL portions of chloroform. The filtrate was then combined with a solution of 270 mg of **4** (0.501 mmol**,** 1 eq) in an air free solution of 10 mL toluene, 0.5 mL ethanol, and 4 drops of acetic acid catalyst. The solution was refluxed until complete consumption of reagents could be seen by TLC. The mixture was then rotary evaporated and purified by SiO_2 chromatography (1:6 DCM/Hexanes), to yield 131 mg of a bright red solid (0.128 mmol, 26%).^1H NMR (500 MHz, $CDCl_3$) δ (ppm) 8.40 (s, 2H), 7.08 (d, J = 3.7 Hz, 2H), 7.05 (d, *J* = 3.7 Hz), 1.34-1.28 (m, 55H integral off because of residual solvent). ^{13}C NMR (125 MHz, $CDCl_3$) δ (ppm) 141.8, 139.5, 138.3, 136.0, 135.6, 134.6, 133.8, 130.9, 125.1, 124.1, 121.1, 112.7, 103.8, 100.0, 19.0, 11.6. MALDI-TOF MS: *m/z* 971.683 M+ Calculated $C_{46}H_{50}Br_2N_2S_4Si_2$ 972.076.

X-Ray crystal data given in second supplementary information

2,5-Bis(5-bromothiophen-2-yl)-9,10-bis(octyloxy)-8,11-bis((triisopropylsilyl)ethynyl)dithieno[3,2-a:2',3'-c]phenazine (5b)

Compound **5b** was prepared by dissolving 421 mg of **2b** (0.563 mmol, 1.0 eq) in 10 mL of dry, air free THF. lithium aluminum hydride (85 mg) was added slowly to the solution and the mixture was allowed to stir under argon atmosphere for 12 hours. The mixture was then cooled to 0 °C and quenched by slowly adding 0.1 mL H_20, 0.1 mL 15% NaOH/H_2O, and 0.3 mL H_2O. The mixture was then filtered to remove inorganic salts and the filter cake was washed with 3, 5 mL portions of chloroform. The filtrate was then combined with a solution of 300 mg of **4** (0.556 mmol**,** 1 eq) in an air free solution of 10 mL toluene, 0.5 mL ethanol, and 4 drops of acetic acid catalyst. The solution was refluxed until complete consumption of reagents could be seen by TLC. The mixture was then rotary evaporated and purified by SiO_2 chromatography (1:6 DCM/Hexanes), to yield 329 mg of a bright red solid (0.27 mmol, 48%). ^{1}H NMR (500 MHz, $CDCl_3$) δ (ppm) 8.34 (s, 2H), 7.02 (m, 4H), 4.41 (t, *J* = 6.9 Hz, 4H), 1.93 (p, *J* = 7.1 Hz, 4H), 1.51–1.29 (m, 62H), 0.90 (t, *J* = 6.6 Hz, 6H). ^{13}C NMR (125 MHz, $CDCl_3$) δ (ppm) 158.6, 140.5, 138.41, 138.40, 138.4, 136.0, 135.3, 133.7, 130.8, 124.9, 121.0, 115.5, 112.4, 104.4, 99.7, 74.9, 31.9, 30.6, 29.6, 29.3, 26.0, 22.7, 19.0, 14.1, 11.7, 11.6. ESI-MS: *m/z* (rel intensity) 1229.3668 (22, MH+) Calculated $C_{62}H_{82}Br_2N_2O_2S_4Si_2H$ 1229.3243.

2,5-bis(5-bromothiophen-2-yl)-9,10-bis(octyloxy)-8,11-bis((triisopropylsilyl)ethynyl)dithieno[3,2-a:2',3'-c]phenazine (5c)

Compound **5c** was prepared by dissolving 401 mg of **2c** (0.509 mmol, 1.00 eq**)** in 25 mL of dry, air free THF. Lithium aluminum hydride (78 mg, 4.08 mmol, 4.00 eq) was added slowly to the solution and the mixture was allowed to stir under argon atmosphere for 12 hours. The mixture was then cooled to 0 °C and quenched by slowly adding 0.2 mL H_20, 0.2 mL 15% NaOH/H_2O, and 0.6 mL H_2O. The mixture was then filtered to remove inorganic salts and the filter cake was washed with 3, 5 mL portions of chloroform. The filtrate was then combined with a solution of 274 mg of **4** (0.509 mmol**,** 1.00 eq) in an air free solution of 10 mL toluene, 0.5 mL ethanol, and 4 drops of acetic acid catalyst. The solution was refluxed until complete consumption of reagents could be seen by TLC. The mixture was then rotary evaporated and purified by SiO_2 chromatography (1:6 DCM/Hexanes), to yield 0.359 g of a bright red solid (0.26 mmol, 52%). ^{1}H NMR (500 MHz, $CDCl_3$) 8.42 (s, 2H), 7.11 (d, *J* = 3.8 Hz, 2H), 7.07 (d, *J* = 3.8 Hz, 2H), 4.41 (t, *J* = 6.9 Hz, 4H), 1.92 (quintuplet, *J* = 7.0 Hz, 4H), 1.30 (m, 4H), 1.4-1.2 (m, 92H) 0.88 (t, *J* = 6.9 Hz, 6H) ^{13}C NMR (125 MHz, $CDCl_3$) δ (ppm) 158.6, 140.5, 138.5, 138.4, 136.1, 135.3, 133.8, 130.9, 125.0, 121.1, 115.5, 112.5, 104.4, 99.7, 74.9, 31.9, 30.6, 29.73, 29.69 (3C), 29.65, 29.4, 26.0, 22.7, 19.0, 14.1, 11.6 MALDI-TOF MS: *m/z* 1340.287 M+ Calculated $C_{70}H_{98}Br_2N_2O_2S_4Si_2$ 1340.442.

5,6-Bis(dodecyloxy)-4,7-di(thiophen-2-yl)benzo[c][1,2,5]thiadiazole (6)

4,7-dibromo-5,6-bis(dodecyloxy)benzo[c][1,2,5]thiadiazole (1.50 g, 2.33 mmol, 1 eq) and 1.43 g of 4,4,5,5-Tetramethyl-2-(2-thienyl)-1,3,2-dioxaborolane (6.79 mmol, 3.0 eq) were dissolved in 20 mL of toluene and 1 mL of a 20% aqueous solution of tetrabutylammonium hydroxide. The

solution was sparged with argon for 15 min, whereupon, 159 mg of tetrakis(triphenylphosphine)palladium (0) was added (0.226 mmol, 0.1 eq). The solution was sparged again with argon and refluxed under inert atmosphere for 12 hours. The organic layer was then separated from the aqueous layer, dried using $MgSO_4$, and rotary evaporated to dryness. The crude product was purified using SiO_2 column chromatography (5:1 Hexanes:DCM) to afford a 1.0 g of a bright yellow solid (1.5 mmol, 65%). ^{1}H NMR (500 MHz, $CDCl_3$) δ (ppm) 8.48 (d, *J* = 3.7 Hz, 2H), 7.50 (d, *J* = 5.1 Hz, 2H), 7.23 (t, *J* = 4.5 Hz, 2H), 4.11 (t, *J* = 7.1 Hz, 4H), 1.93 (p, *J* = 7.3 Hz, 4H), 1.44 (q, *J* = 7.4 Hz, 4H), 1.39 –1.28 (m, 34H), 0.89 (t, *J* = 6.7 Hz, 3H). ^{13}C NMR (125 MHz, $CDCl_3$) δ (ppm) 151.9, 151.0, 134.1, 130.6, 127.3, 126.8, 117.6, 74.4, 32.0, 30.4, 29.75, 29.71(2C), 29.68, 29.60, 29.42, 26.0, 22.7, 14.2. MALDI-TOF MS: *m/z* 668.362 M+ Calculated $C_{38}H_{56}N_2O_2S_3$ 668.350.

2,5-dibromo-9,10-bis(dodecyloxy)-8,11-di(thiophen-2-yl)dithieno[3,2-a:2',3'-c]phenazine (7)

Compound **7** was prepared by dissolving 383 mg of **6** (0.572 mmol, 1 eq) in 10 mL dry, air free THF. 130 mg of lithium aluminum hydride (3.43 mmol, 6 eq) was then slowly added and the mixture was heated to reflux for 12 hours. The mixture was then cooled to 0 °C and quenched by slowly adding 0.1 mL H_20, 0.1 mL 15% NaOH/H_2O, and 0.3 mL H_2O. The mixture was then filtered to remove inorganic salts and the filter cake was washed with 3, 5 mL portions of chloroform. The filtrate was then combined with a solution of 216 mg of **1** (0.572 mmol**,** 1 eq) in an air free solution of 10 mL toluene, 0.5 mL ethanol, and 4 drops of acetic acid catalyst. The solution was refluxed until complete consumption of reagents could be seen by TLC. The

mixture was then rotary evaporated and purified by SiO_2 chromatography (1:6 DCM/Hexanes), to yield 289 mg of a red-orange solid (0.287 mmol, 51%). ^{1}H NMR (500 MHz, $CDCl_3$) δ (ppm) 8.19 (s, 2H), 8.12 (d, *J* = 3.6 Hz, 2H), 7.67 (d, *J* = 5.1 Hz, 2H), 7.29 (dd, *J* = 5.1, 3.7 Hz, 2H), 4.07 (t, *J* = 6.7 Hz, 4H), 1.82 (p, *J* = 6.9 Hz, 4H), 1.43 (p, *J* = 11.5, 7.0 Hz, 4H), 1.36 – 1.23 (m, 32H), 0.89 (t, *J* = 6.8 Hz, 6H) ^{13}C NMR (125 MHz, $CDCl_3$) δ (ppm) 153.6, 137.8, 135.8, 135.0, 134.8, 133.4, 130.9, 128.2, 128.0, 126.0, 123.7, 113.1, 74.2, 32.0, 30.5, 29.8, 29.71, 29.69 (2C), 29.56, 29.41, 26.1, 22.7, 14.2. MALDI-TOF MS: *m/z* 980.254 M+ Calculated $C_{48}H_{58}Br_2N_2O_2S_4$ 980.175.

Poly{((5,6-bis(octyloxy)-(8,11-bis((triisopropylsilyl)ethynyl)dithieno[3,2-*a*:2',3'-*c*]phenazine)-2,5-diyl)-*alt*-(thiophene-2,5-diyl) (**P1**)

Polymer **P1** was prepared by dissolving 175 mg of **3b** (0.164 mmol, 1.0 eq.) and 109 mg (0.090 mL, 0.164 mmol, 1 eq.) of 2,5-bis(tributylstannyl)thiophene in 15 mL of toluene. The mixture was then sparged using argon for 15 minutes, and then 10 mg of tetrakistriphenylphosphine palladium (0) was added to the solution (0.0082 mmol, 0.05 eq.) the solution was then connected to a reflux condenser and sparged for 10 minutes. The solution was then refluxed under argon atmosphere for 3 days. The solution was poured into 100 mL of a 1% HCl solution in methanol and stirred for 15 minutes. The solution was then filtered and the filtered powder was then soxholet extracted using methanol, then acetone, then hexanes to yield 111 mg of a black solid (≈ 68%). ^{1}H NMR (500 MHz, Cl_2CD-$CDCCl_2$) 8.55 (s, 2H), 7.44 (s, 2H), 4.46 (s, 4H), 1.98 (s, 4H) 1.6-0.4 (m, 66H). GPC (ODCB solvent, M_w compared to PS std) M_n = 11,089 Da, PDI = 1.57.

Poly{((5,6-bis(octyloxy)-8,11-bis((triisopropylsilyl)ethynyl)dithieno[3,2-*a*:2',3'-*c*]phenazine)-2,5-diyl)-*alt*-(2,2'-bithiophene-5,5'-diyl) (**P2**)

Polymer **P2** was prepared by dissolving 175 mg of **3c** (0.164 mmol, 1.0 eq.) and 122 mg (0.10 mL, 0.164 mmol, 1 eq.) of 5,5'-bis(tributylstannyl)2,2'-bithiophene in 15 mL of toluene. The mixture was then sparged using argon for 15 minutes, and then 10 mg of tetrakistriphenylphosphine palladium (0) was added to the solution (0.0082 mmol, 0.05 eq.) the solution was then connected to a reflux condenser and sparged for 10 minutes. The solution was then refluxed under argon atmosphere for 3 days. The solution was poured into 100 mL of a 1% HCl solution in methanol and stirred for 15 minutes. The solution was then filtered and the filtered powder was then soxholet extracted using methanol, then acetone, and hexanes to yield 128 mg of a black powder (≈ 72%). ^{1}H NMR (500 MHz, Cl_2CD-$CDCCl_2$) 8.33 (s, 2H), 6.99 (m, 4H), 4.43 (s, 4H), 1.98 (s, 4H), 1.6-1.1 (m, 62H), 0.94 (s, 6H). GPC (ODCB, compared to PS std) M_n = 4317 Da, PDI = 1.33.

Poly{((5,6-bis(octyloxy)-8,11-bis((triisopropylsilyl)ethynyl)dithieno[3,2-*a*:2',3'-*c*]phenazine)-2,5-diyl)-*alt*-(2,2':5',2'':terthiophene-5,5''-diyl) (**P3**)

Polymer **P3** was prepared by dissolving 175 mg of **5b** (0.142 mmol, 1.0 eq.) and 94 mg (0.078 mL, 0.142 mmol, 1 eq.) of 2,5-bis(tributylstannyl)thiophene in 15 mL of toluene. The mixture was then sparged using argon for 15 minutes, and then 8 mg of tetrakistriphenylphosphine palladium (0) was added to the solution (0.0082 mmol, 0.05 eq.) the solution was then

connected to a reflux condenser and sparged with argon for 10 minutes. The solution was then refluxed under argon atmosphere for 3 days. The solution was poured into 100 mL of a 1% HCl solution in methanol and stirred for 15 minutes. The solution was then filtered and the filtered powder was then soxholet extracted using methanol, then acetone, and hexanes and 134 mg of a black powder was recovered (≈ 82%). ^{1}H NMR (500 MHz, Cl_2CD-$CDCCl_2$) 8.48 (s, 2H), 7.17 (s, 6H), 4.46 (s, 4H), 1.94 (s, 4H), 1.5-1.1 (m, 62H), 0.93 (s, 6H). GPC (ODCB, compared to PS std) M_n = 5886 Da, PDI = 3.50.

Poly{((5,6-bis(octyloxy_-8,11-bis((triisopropylsilyl)ethynyl)dithieno[3,2-*a*:2',3'-*c*]phenazine)-2,5-diyl)-*alt*-(2,2':5',2'':5'',2'''-quaterthiophene-5,5'''-diyl) (**P4**)

Polymer **P4** was prepared by dissolving 200 mg of **5c** (0.162 mmol, 1.0 eq.) and 121 mg (0.100 mL, 0.162 mmol, 1 eq.) of 5,5'-bis(tributylstannyl)2,2'-bithiophene in 20 mL of toluene. The mixture was then sparged using argon for 15 minutes, and then 9 mg of tetrakistriphenylphosphine palladium (0) was added to the solution (0.016 mmol, 0.05 eq.) the solution was then connected to a reflux condenser and sparged with argon for 10 minutes. The solution was then refluxed under argon atmosphere for 3 days. The solution was poured into 100 mL of a 1% HCl solution in methanol and stirred for 15 minutes. The solution was then filtered and the filtered powder was then soxholet extracted using methanol, then acetone, and hexanes to yield 151 mg of a black powder (≈ 75%). ^{1}H NMR (500 MHz, Cl_2CD-$CDCCl_2$) 8.54 (s, 2H), 8.1-6.9 (m, 8H), 4.48 (s, 4H), 1.97 (s, 4H), 1.5-1.2 (m, 62H), 0.88 (s, 6H). GPC (ODCB, compared to PS std) M_n = 3849 Da, PDI = 1.84.

Poly{((5,6-bis(dodecyloxy)-(8,11-bis((triisopropylsilyl)ethynyl)dithieno[3,2-*a*:2',3'-*c*]phenazine)-2,5-diyl)-*alt*-(thiophene-2,5-diyl) (**P5**)

Polymer **P5** was prepared via an analogous procedure to **P1**: 0.175 g of **3c** (0.148 mmol, 1.0 eq) and 0.097 g of 2,5-tributylstannylthiophene (0.148 mmol, 1.0 eq) were used for the reaction. 0.095 g of a black powder was isolated (≈ 58%). ^{1}H NMR (500 MHz, $CDCl_3$) 8.48 (s, 2H), 7.15 (s, 2H), 4.42 (s, 4H), 1.94 (s, 4H), 1.5-1.1 (m, 74H), 0.89 (m, 10H). GPC (ODCB, compared to PS std) M_n = 6232 Da, PDI = 1.25.

Poly{((5,6-bis(dodecyloxy)-8,11-bis((triisopropylsilyl)ethynyl)dithieno[3,2-*a*:2',3'-*c*]phenazine)-2,5-diyl)-*alt*-(2,2'-bithiophene-5,5'-diyl) (**P6**)

Polymer **P6** was prepared via an analogous procedure to **P2**: 0.175 g of **3c** (0.148 mmol, 1.0 eq) and 0.110 g of 5,5'-bis(tributylstannyl)2,2'-bithiophene (0.148 mmol, 1.0 eq) were used for the reaction. 0.115 g of a black powder was isolated (≈ 65%). ^{1}H NMR (500 MHz, $CDCl_3$) 8.29 (s, 2H), 7.03 (s, 4H), 4.44 (s, 4H), 1.93 (s, 4H), 1.5-0.4 (m, 86H). GPC (ODCB, compared to PS std) M_n = 3849 Da, PDI = 1.57.

Poly{((5,6-bis(dodecyloxy)-8,11-bis((triisopropylsilyl)ethynyl)dithieno[3,2-*a*:2',3'-*c*]phenazine)-2,5-diyl)-*alt*-(2,2':5',2'':-terthiophene-5,5''-diyl) (**P7**)

Polymer **P7** was prepared via an analogous procedure to **P3**: 0.175 g of **5c** (0.130 mmol, 1.0 eq)

and 0.086 g of 2,5-tributylstannylthiophene (0.130 mmol, 1.0 eq) were used for the reaction. 0.132 g of a black powder was isolated (≈ 80%). ^{1}H NMR (500 MHz, Cl_2CD-$CDCCl_2$) 8.44 (s, 2H), 7.14 (s, 6H), 4.44 (s, 4H), 1.95 (s, 4H), 1.5-0.6 (m, 84H). GPC (ODCB solvent, compared to PS std) M_n = 6242 Da, PDI = 2.05.

Poly{((5,6-bis(dodecyloxy)-8,11-bis((triisopropylsilyl)ethynyl)dithieno[3,2-*a*:2',3'-*c*]phenazine)-2,5-diyl)-*alt*-(2,2':5',2'':5'',2'''-quaterthiophene-5,5'''-diyl) (**P8**)

Polymer **P8** was prepared via an analogous procedure to **P4**: Compound **3c** (0.175 g of 0.130 mmol, 1.0 eq) and 0.097 g of 5,5'-bis(tributylstannyl)2,2'-bithiophene (0.130 mmol, 1.0 eq) were used for the reaction. 0.140 g of a black powder was isolated (≈ 79%). ^{1}H NMR (500 MHz, Cl_2CD-$CDCCl_2$) 8.48 (s, 2H), 7.10 (s, 8H), 4.40 (s, 4H), 1.95 (s, 4H), 1.5-0.6 (m, 84H). GPC (ODCB solvent, compared to PS std) M_n = 4871 Da, PDI = 1.93.

Poly{(9,10-bis(dodecyloxy)-8,11-di(thiophen-2-yl)dithieno[3,2-a:2',3'-c]phenazine)-2,5-diyl)-*alt*-(thiophene-2,5-diyl)} (**P9**)

Polymer **P9** was prepared via an analogous procedure to **P1**: 0.175 g of **7** (0.178 mmol, 1.0 eq) and 0.118 g of 2,5-tributylstannylthiophene (0.178 mmol, 1.0 eq) were used for the reaction. 0.129 g of a black powder was isolated (≈ 80%). ^{1}H NMR (500 MHz, Cl_2CD-$CDCCl_2$) 8.9-5.6 (broad s, 10H), 4.40 (s, 4H), 1.5-0.6 (m, 46H). GPC (ODCB solvent, compared to PS std) M_n = 3630 Da, PDI = 3.64.

Poly{((9,10-bis(dodecyloxy)-(8,11-bis((triisopropylsilyl)ethynyl)dithieno[3,2-*a*:2',3'-*c*]phenazine)-2,5-diyl)-*alt*-((4,4-bis(2'-ethylhexyl)-4H-cyclopenta[2,1-b:3,4-b']dithiophene)-2,6-diyl)} (P10)

Polymer **P10** was prepared by dissolving 150 mg of **3c** (0.127 mmol, 1.0 eq.) and 125 mg (0.127 mmol, 1.0 eq.) of 2,6-bis(tributylstannyl)-4,4-bis(2'-ethylhexyl)-4H-cyclopenta[2,1-b:3,4-b']dithiophene in 15 mL of toluene. The mixture was then sparged using argon for 15 minutes, and then 8 mg of tetrakistriphenylphosphine palladium (0) was added to the solution (0.0069 mmol, 0.05 eq.) the solution was then connected to a reflux condenser and sparged for 10 minutes. The solution was then refluxed under argon atmosphere for 3 days. The solution was poured into 100 mL of a 1% HCl solution in methanol and stirred for 15 minutes. The solution was then filtered and the filtered powder was then soxholet extracted using methanol, then acetone, and hexanes for 2 extractions to yield 89 mg of a black solid (≈ 49%). ^{1}H NMR (500 MHz, $CDCl_3$) 8.5-8.4 (broad s, 2H), 7.3-6.9 (m, 2H) 4.41 (s, 4H), 1.9 (br s, 10H), 1.7-1.5 (m, 12H), 1.4-1.2 (m, 40H), 1.2-0.5 (m, 60H) GPC (ODCB solvent, compared to PS std) M_n = 4652 Da, PDI = 1.87.

Poly{(9,10-bis(dodecyloxy)-8,11-bis((triisopropylsilyl)ethynyl)dithieno[3,2-a:2',3'-c]phenazine)-2,5-diyl)-*alt*-((4,4-bis(2'-ethylhexyl)-2,6-(thiophen-2-yl)-4H-cyclopenta[2,1-b:3,4-b']dithiophene)-5,5'-diyl)} (P11)

Polymer **P11** was prepared by dissolving 100 mg of **5c** (0.127 mmol, 1.0 eq.) and 73 mg (0.127

mmol, 1.0 eq.) of 2,6-bis(tributylstannyl)-4,4-bis(2'-ethylhexyl)-4H-cyclopenta[2,1-b:3,4-b']dithiophene in 10 mL of toluene. The mixture was then sparged using argon for 15 minutes, and then 4 mg of tetrakistriphenylphosphine palladium (0) was added to the solution (0.004 mmol, 0.05 eq.) the solution was then connected to a reflux condenser and sparged for 10 minutes. The solution was then refluxed under argon atmosphere for 3 days. The solution was poured into 100 mL of a 1% HCl solution in methanol and stirred for 15 minutes. The solution was then filtered and the filtered powder was then soxholet extracted using methanol, then acetone, and hexanes for 2 extractions to yield 70 mg of a black solid (≈ 60%). ^{1}H NMR (500 MHz, $CDCl_3$) 8.5-8.4 (m, 2H), 8.0-6.8 (m, 6H), 4.35 (s, 4H), 1.87 (m, 10H), 1.62 (m, 12H), 1.4-1.1 (m, 40H), 1.1-0.5 (m, 60H). GPC (ODCB solvent, compared to PS std) M_n = 4480 Da, PDI = 1.16.

Poly{(9,10-bis(dodecyloxy)-8,11-di(thiophen-2-yl)dithieno[3,2-a:2',3'-c]phenazine)-2,5-diyl)-*alt*-((4,4-bis(2'-ethylhexyl)-4H-cyclopenta[2,1-b:3,4-b']dithiophene)-2,6-diyl)} (P12)

Polymer **P12** was prepared by dissolving 125 mg of **7** (0.127 mmol, 1.0 eq.) and 125 mg (0.127 mmol, 1.0 eq.) of 2,6-bis(tributylstannyl)-4,4-bis(2'-ethylhexyl)-4H-cyclopenta[2,1-b:3,4-b']dithiophene in 15 mL of toluene. The mixture was then sparged using argon for 15 minutes, and then 8 mg of tetrakistriphenylphosphine palladium (0) was added to the solution (0.0069 mmol, 0.05 eq.) the solution was then connected to a reflux condenser and sparged for 10 minutes. The solution was then refluxed under argon atmosphere for 3 days. The solution was poured into 100 mL of a 1% HCl solution in methanol and stirred for 15 minutes. The solution was then filtered and the filtered powder was then soxholet extracted using methanol, then

acetone, and hexanes for 2 extractions to yield 100 mg of a black solid (≈ 64%). ^{1}H NMR (500 MHz, $CDCl_3$) 8.5-7.2 (m, 10H) 4.03 (s, 4H), 1.87 (broad s, 4H), 1.7-1.2 (m, 44H), 1.2-0.6 (m, 32H). GPC (ODCB solvent, compared to PS std) M_n = 10,700 Da, PDI = 1.38.

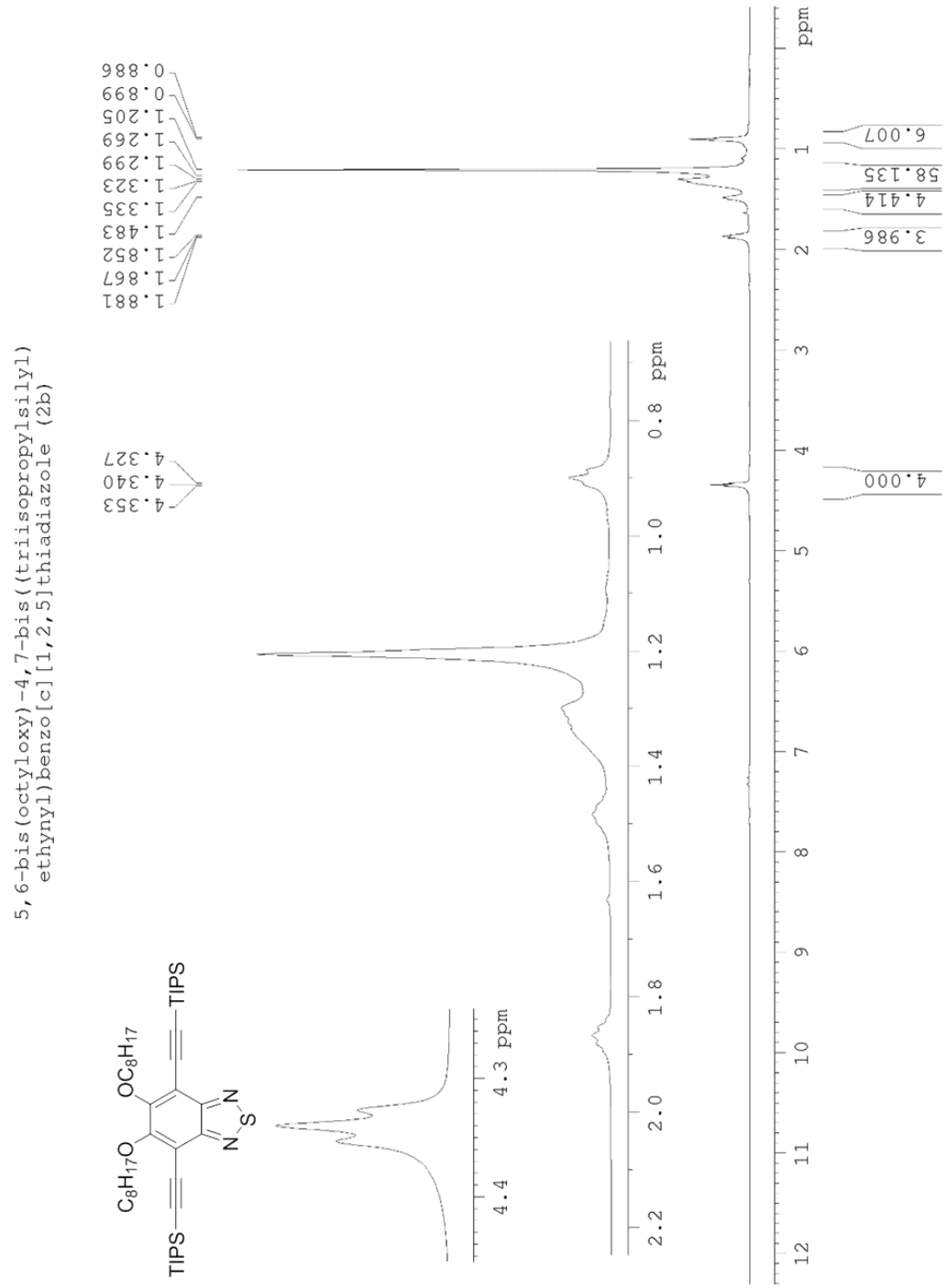

Figure 3.21. ^{1}H NMR spectrum of **2b**.

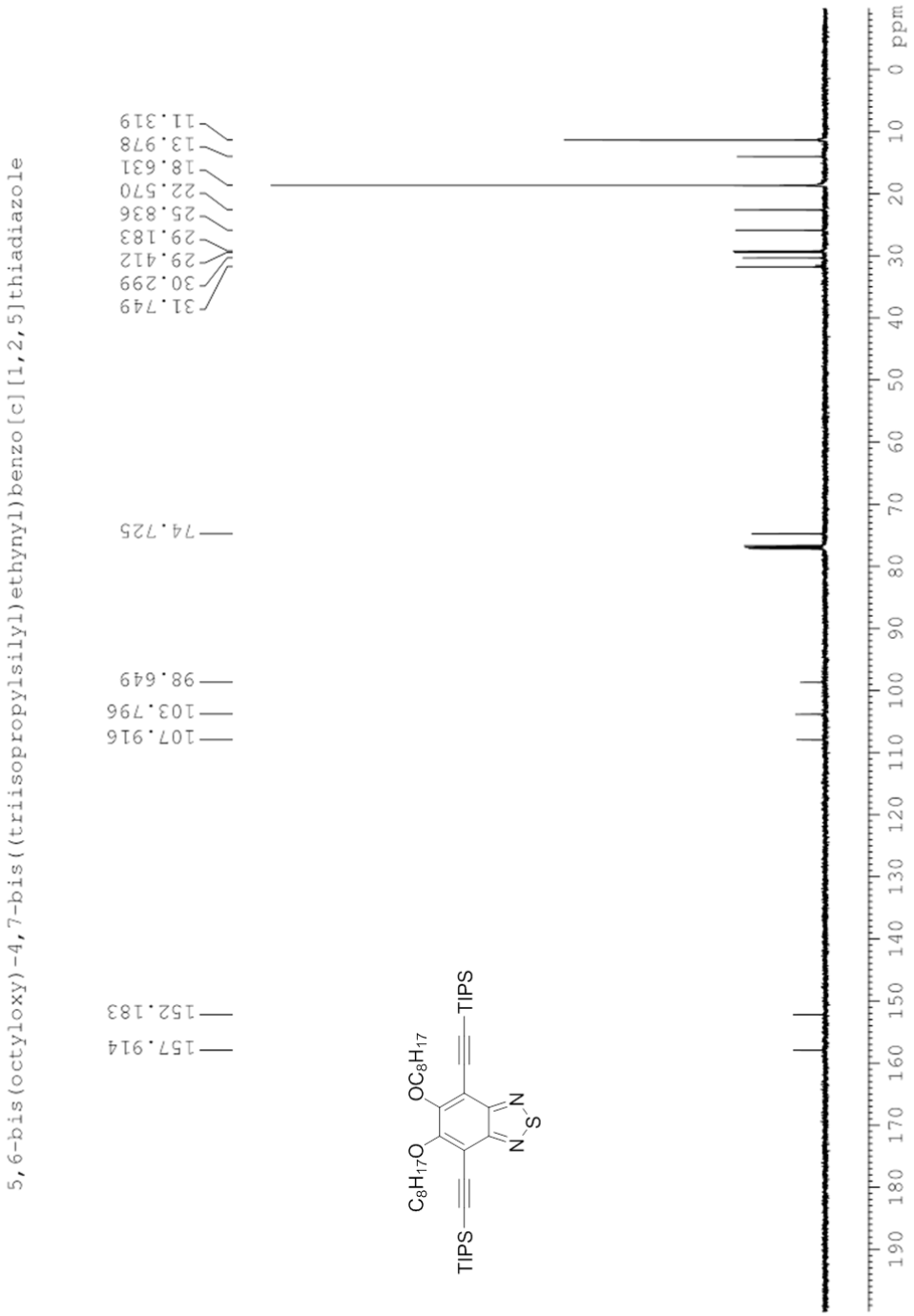

Figure 3.22. ^{13}C NMR of **2b**.

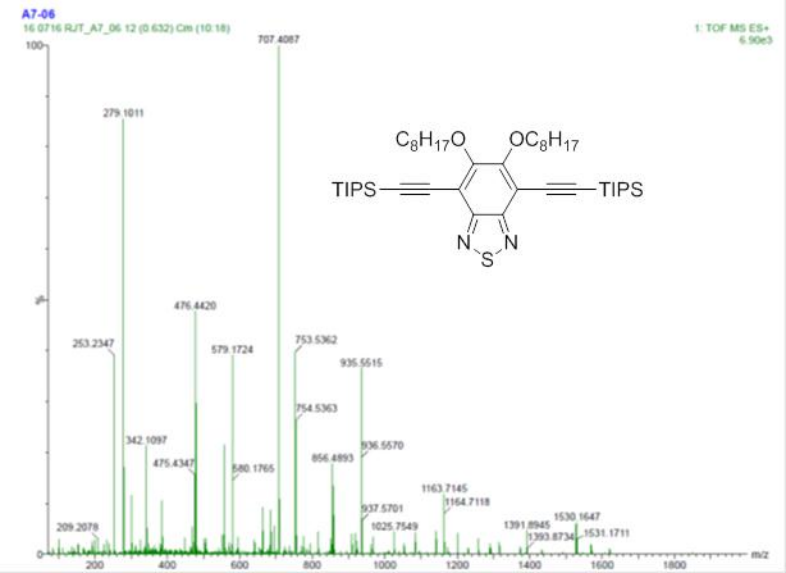

Figure 3.23. Full MALDI_TOF spectrum of **2b**.

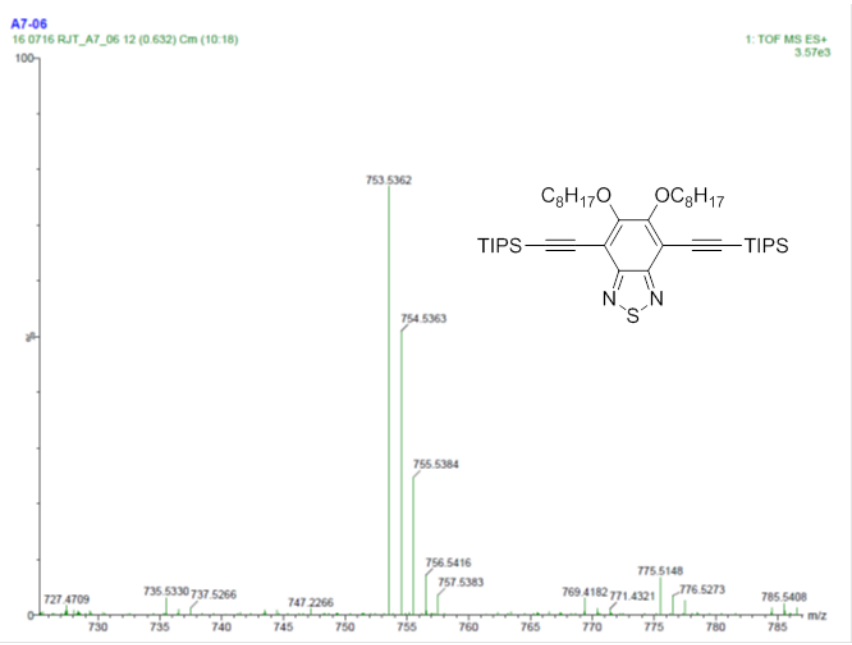

Figure 3.24. MALDI-TOF spectrum of parent ion of **2b**.

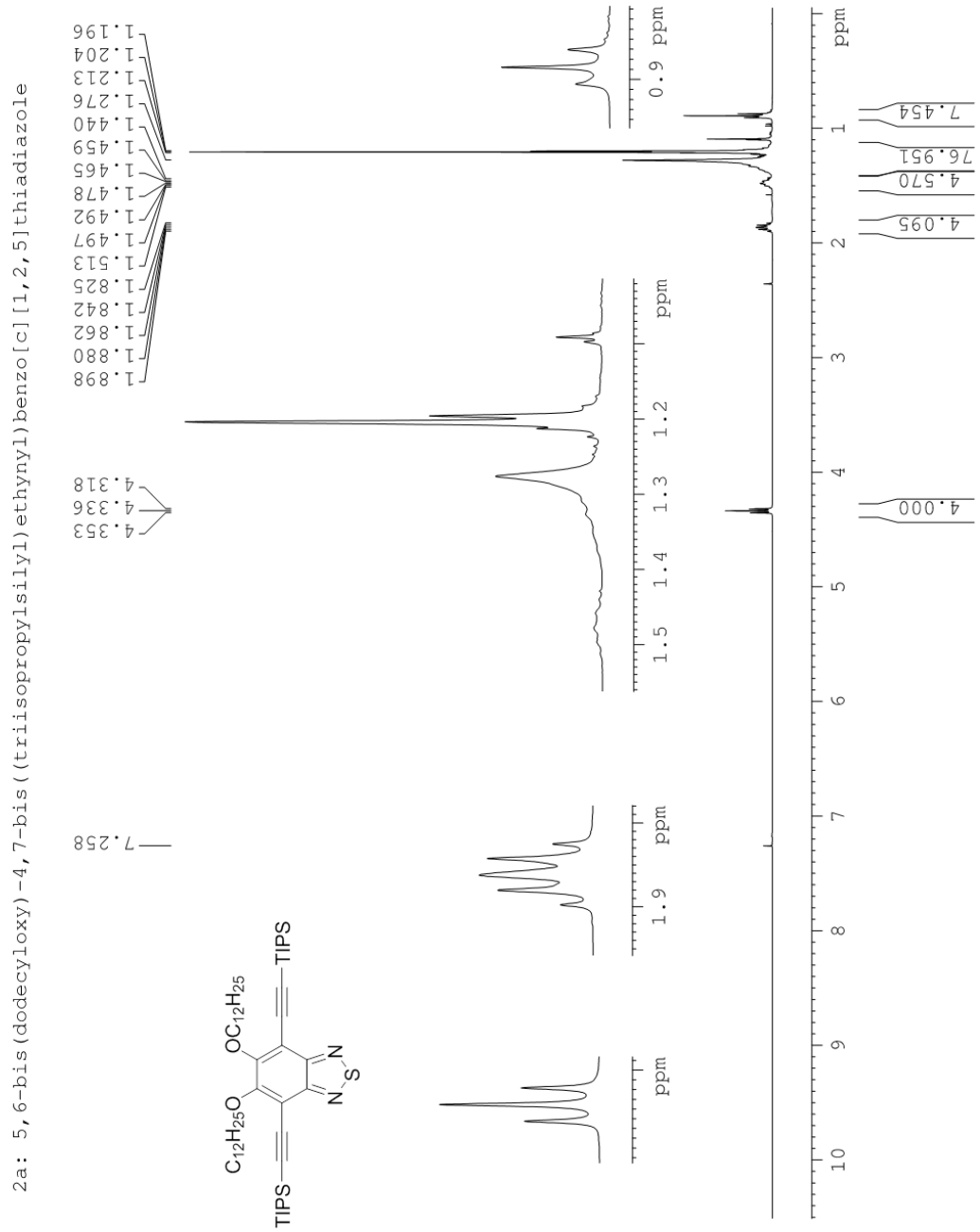

Figure 3.25. ^{1}H NMR spectrum of **2c.**

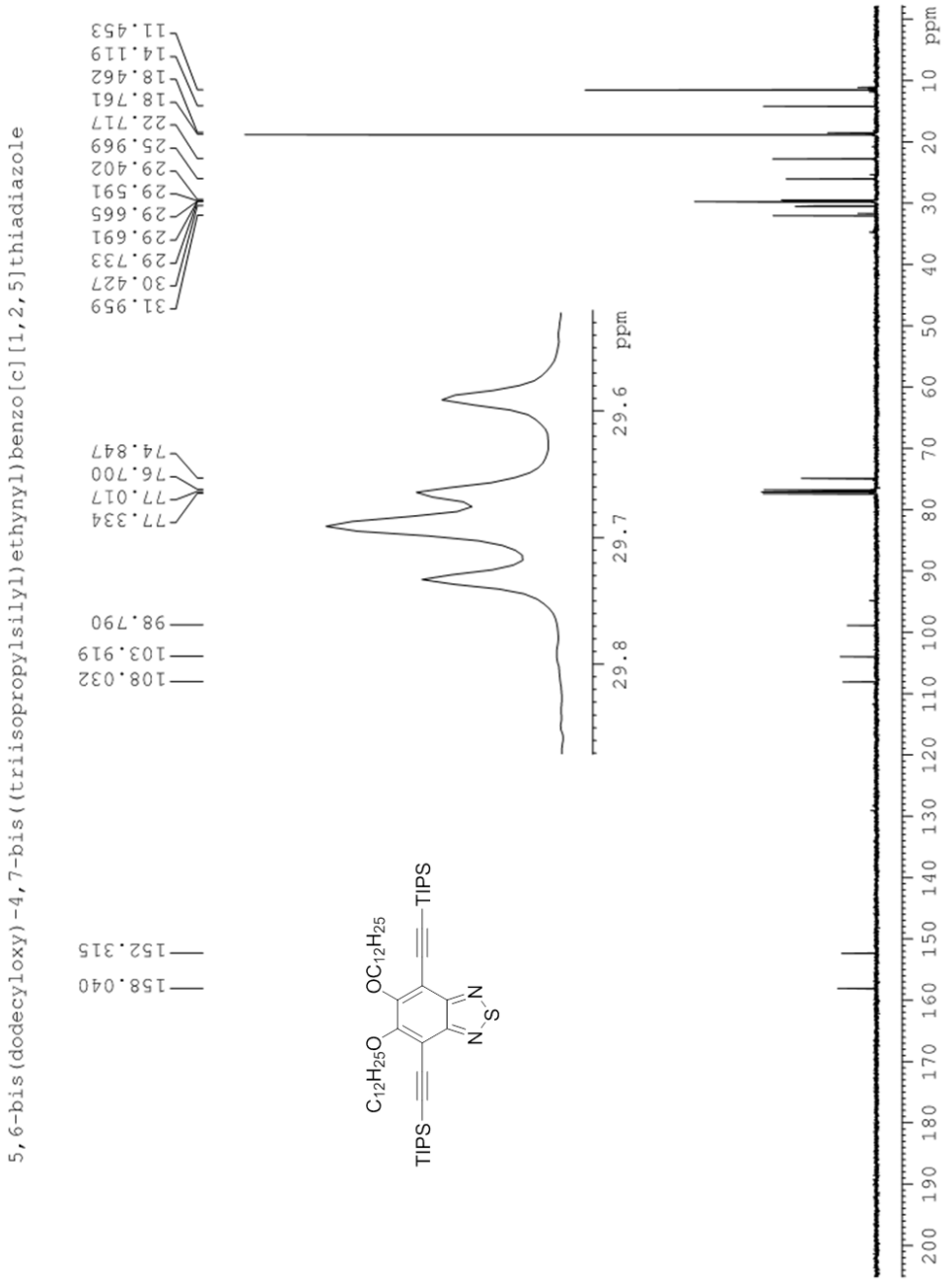

Figure 3.26. ^{13}C NMR spectrum of **2c.**

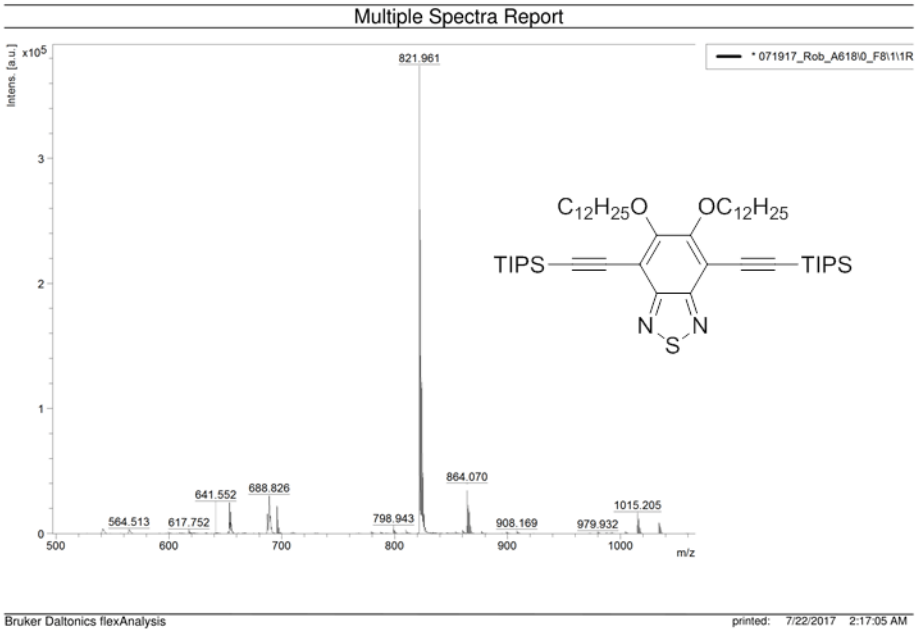

Figure 3.27. Full MALDI-TOF spectrum of **2c**.

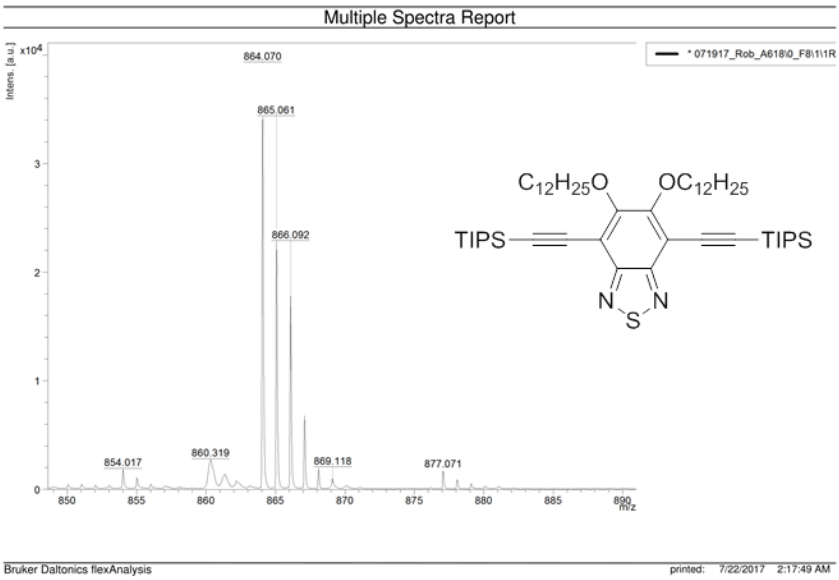

Figure 3.28. MALDI-TOF parent ion of **2c**.

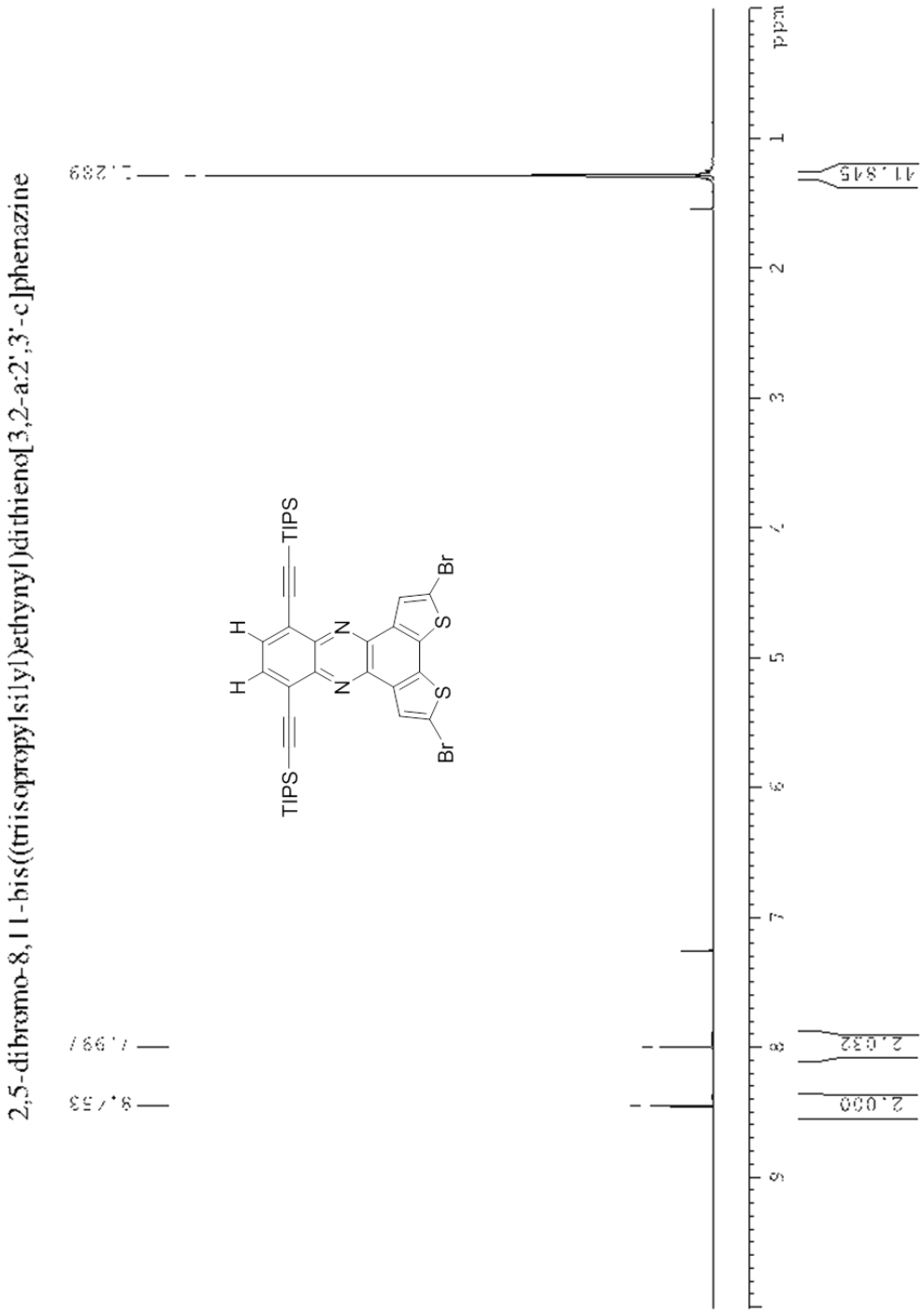

Figure 3.29. ^{1}H NMR spectrum of **3a.**

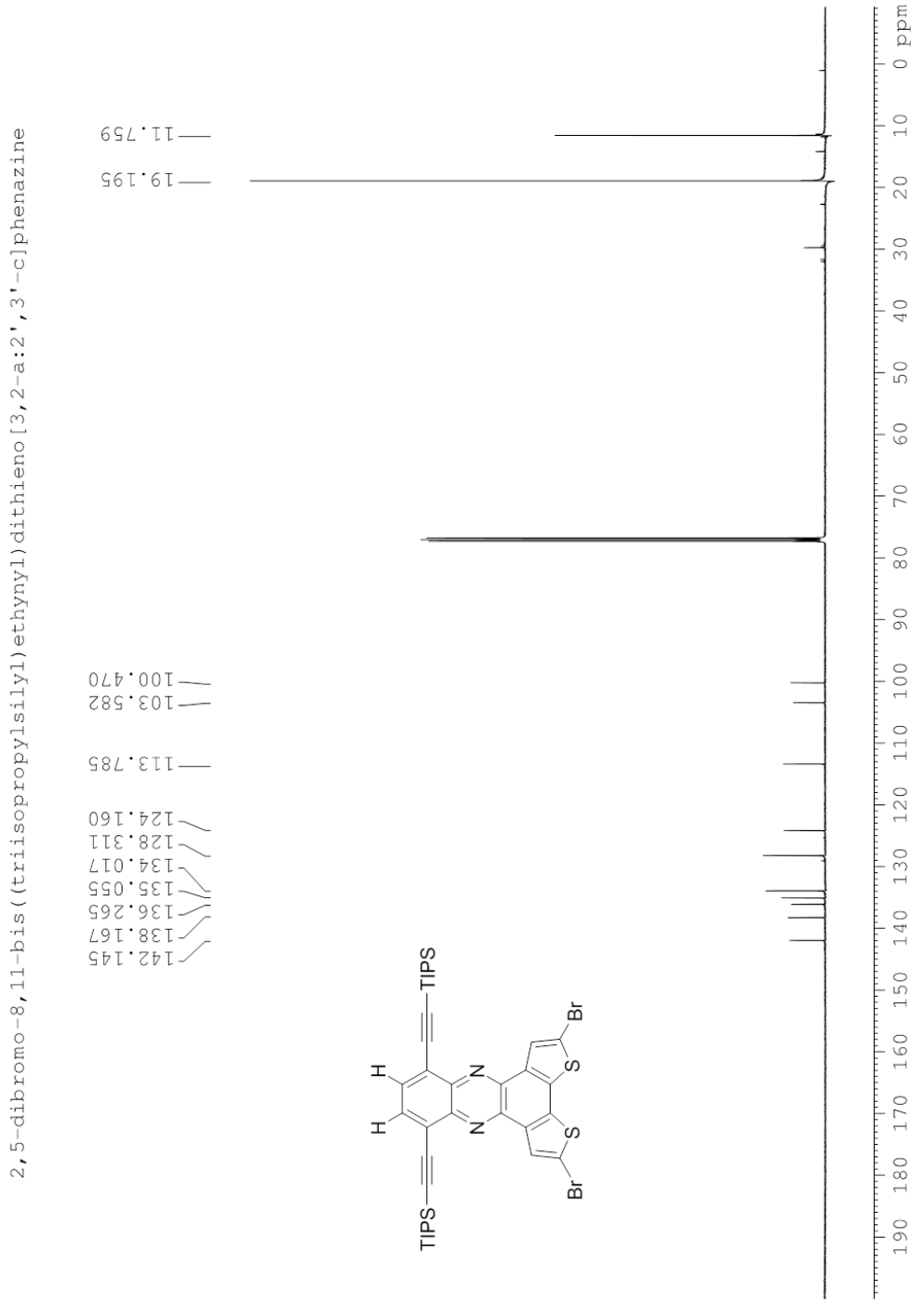

Figure 3.30. ^{13}C NMR spectrum of **3a**.

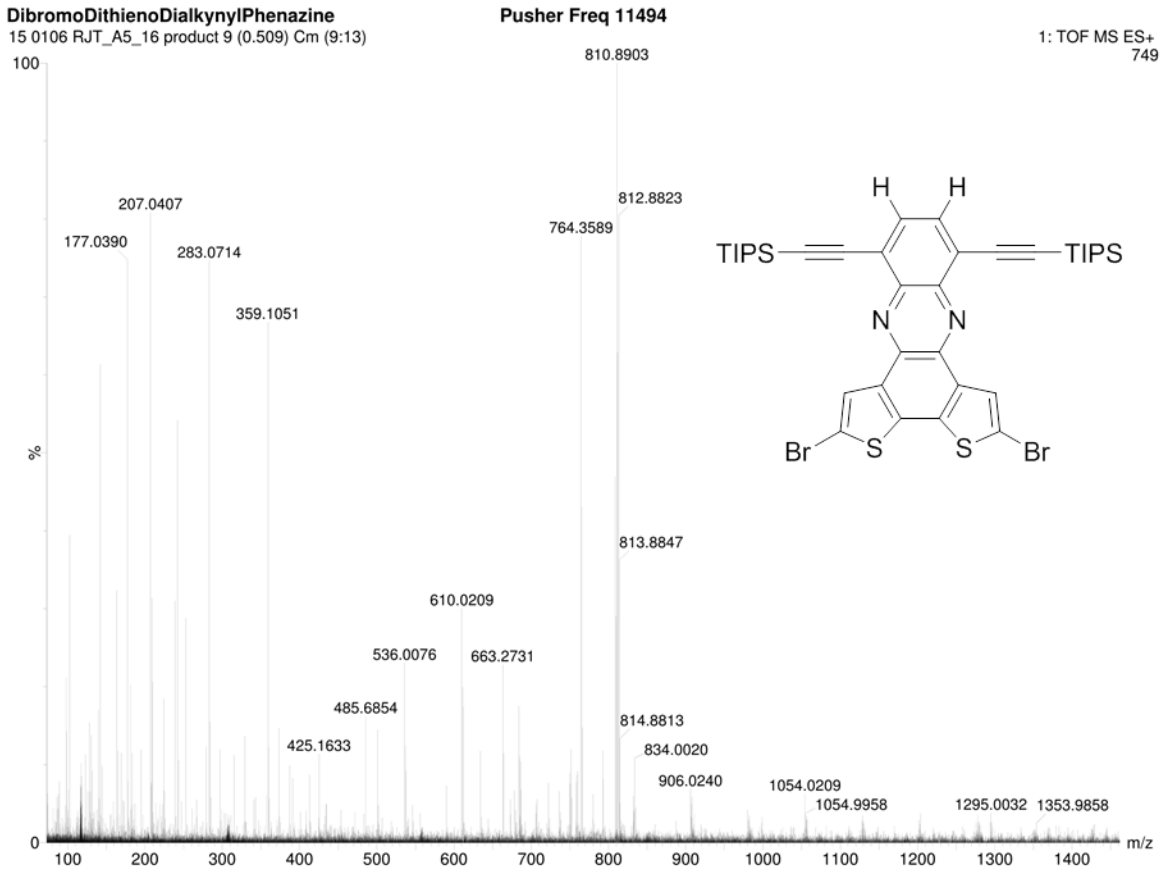

Figure 3.31. ESI-MS spectrum of **3a**.

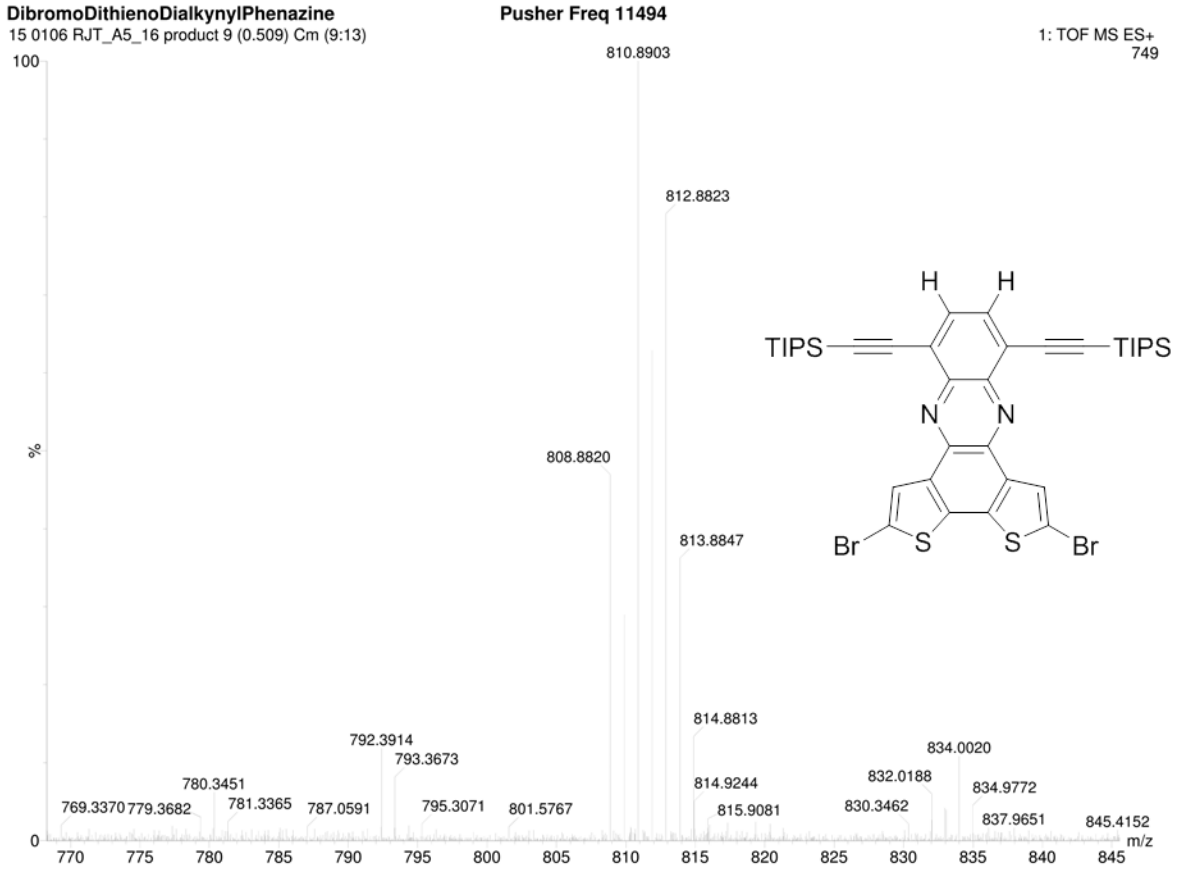

Figure 3.32. ESI-MS of **3a** parent ion.

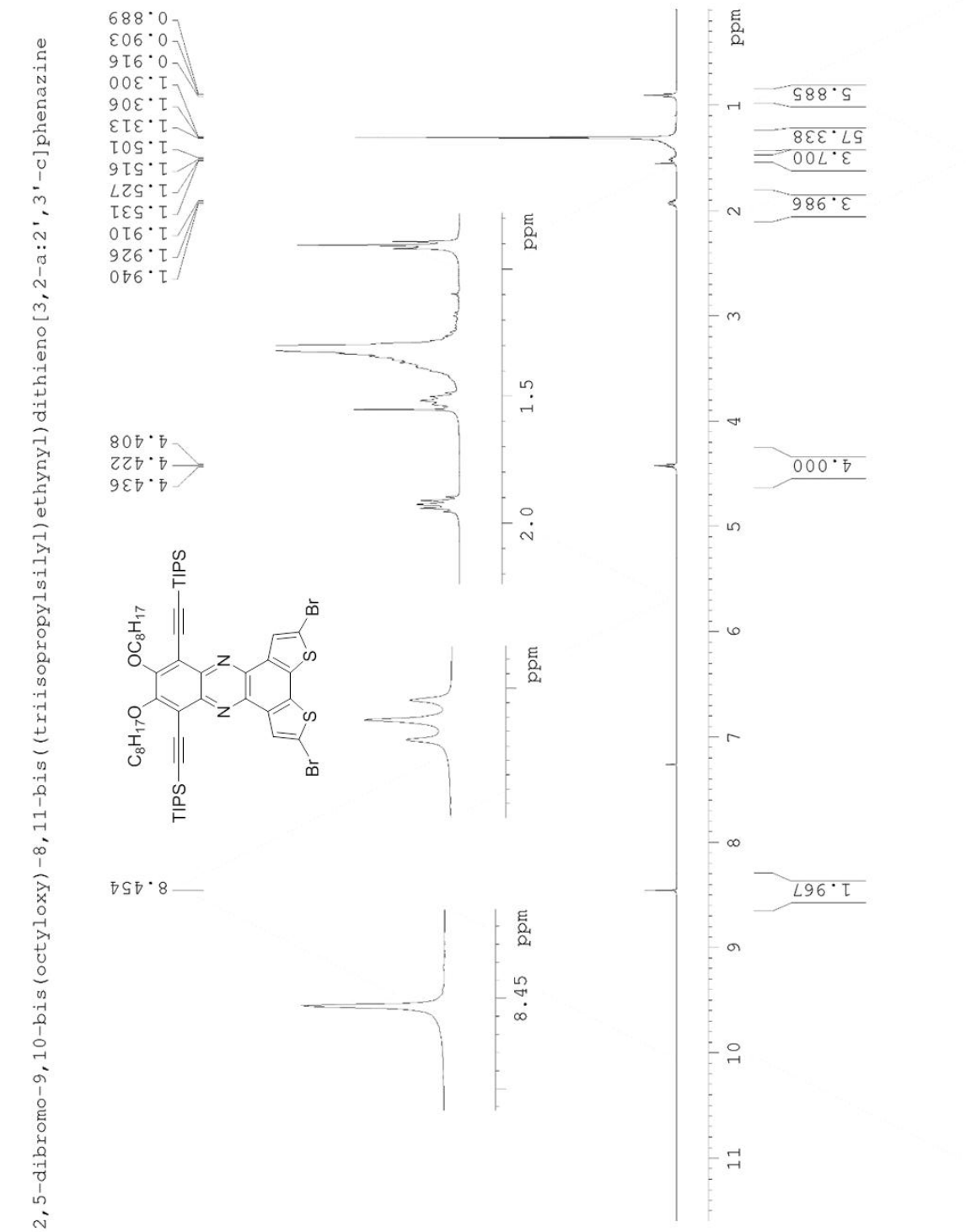

Figure 3.33. ^{1}H NMR spectrum of **3b**.

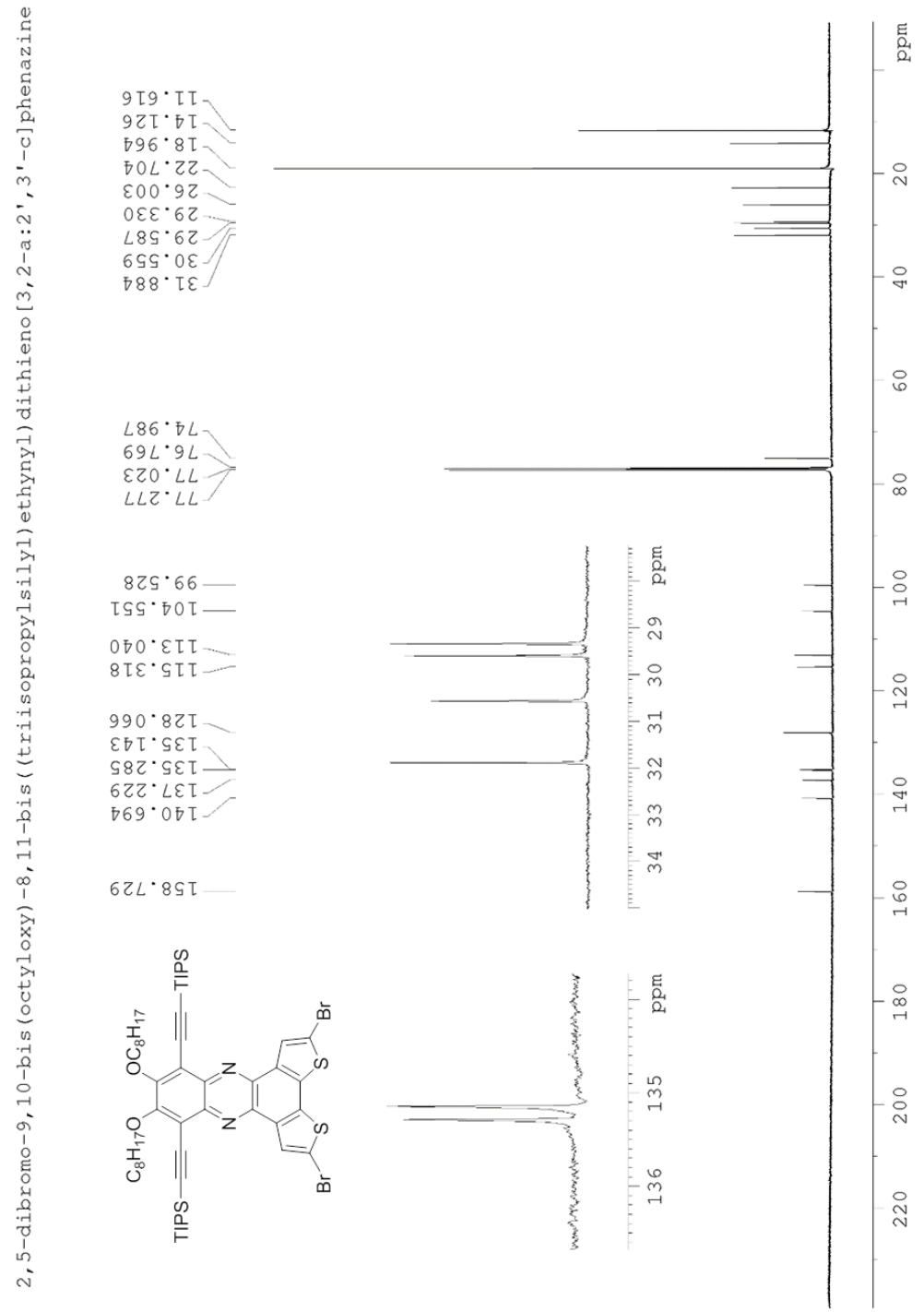

Figure 3.34. ^{13}C NMR spectrum of **3b**.

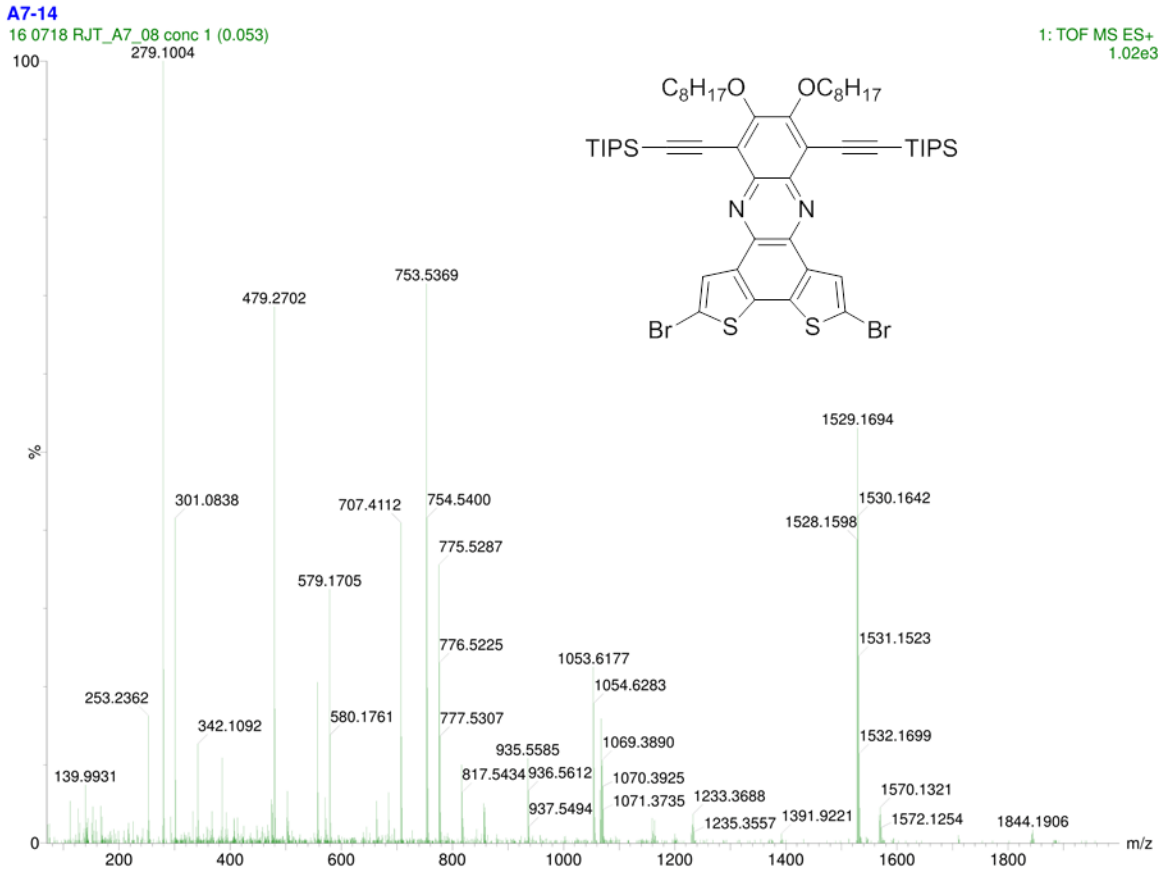

Figure 3.35. ESI-MS of **3b**.

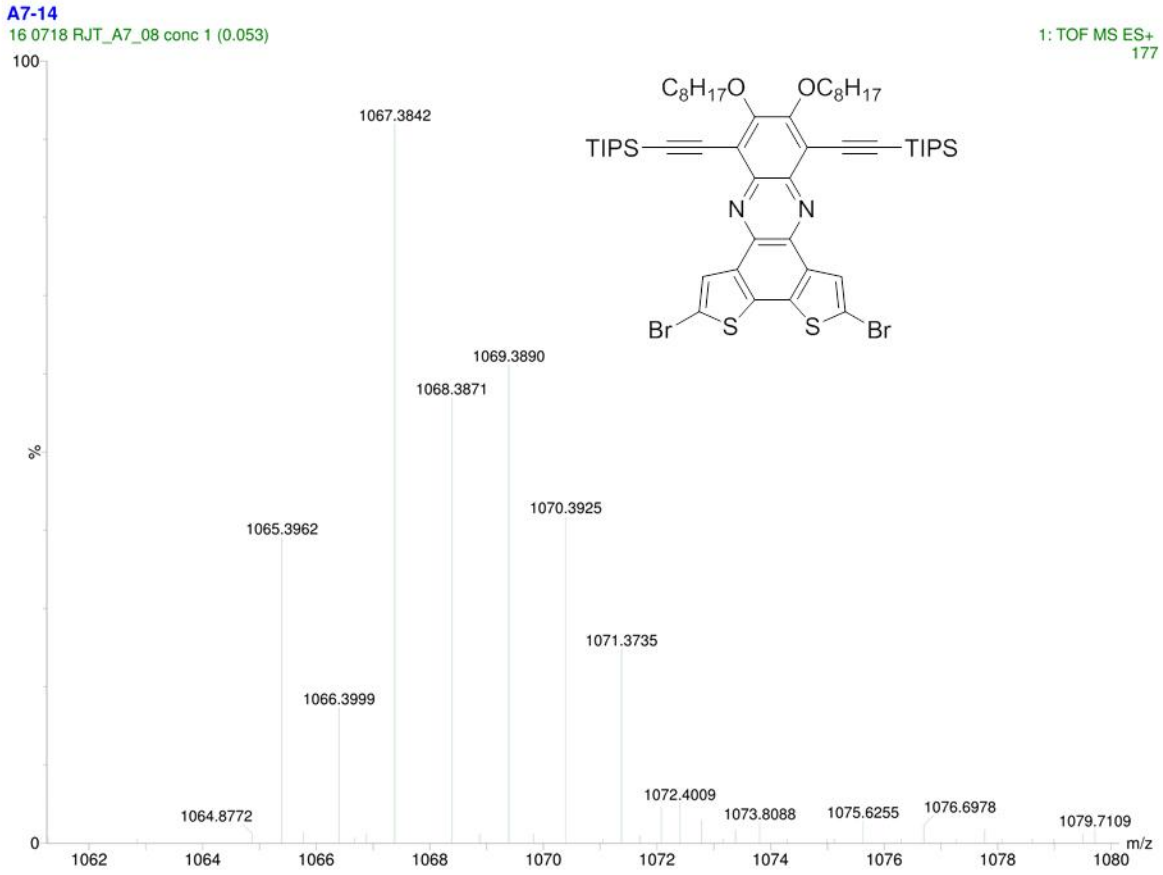

Figure 3.36. ESI-MS of **3b** parent ion.

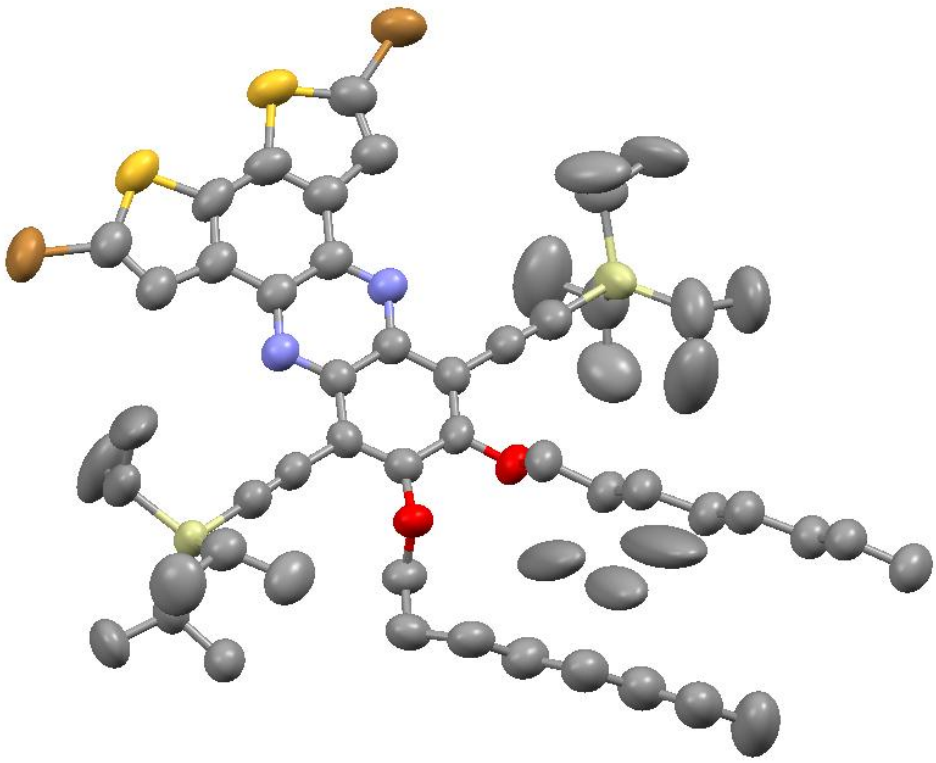

Figure 3.37. crystal structure of **3b** displaying 95% probability ellipsoids (note that the 3 carbon atoms in the background are due to positional disorder in the TIPS alkynyl groups).

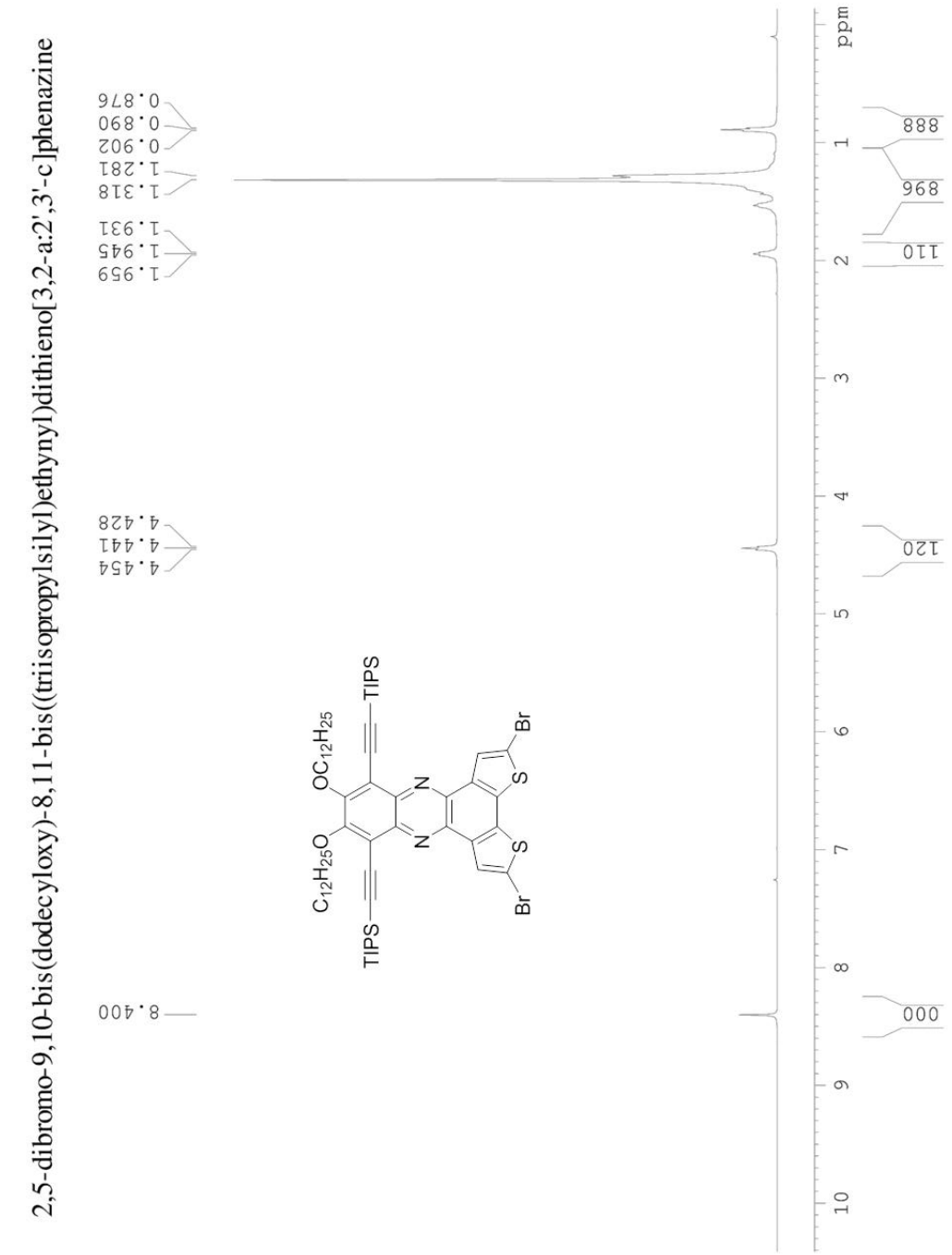

Figure 3.38. ^{1}H NMR spectrum of **3c**.

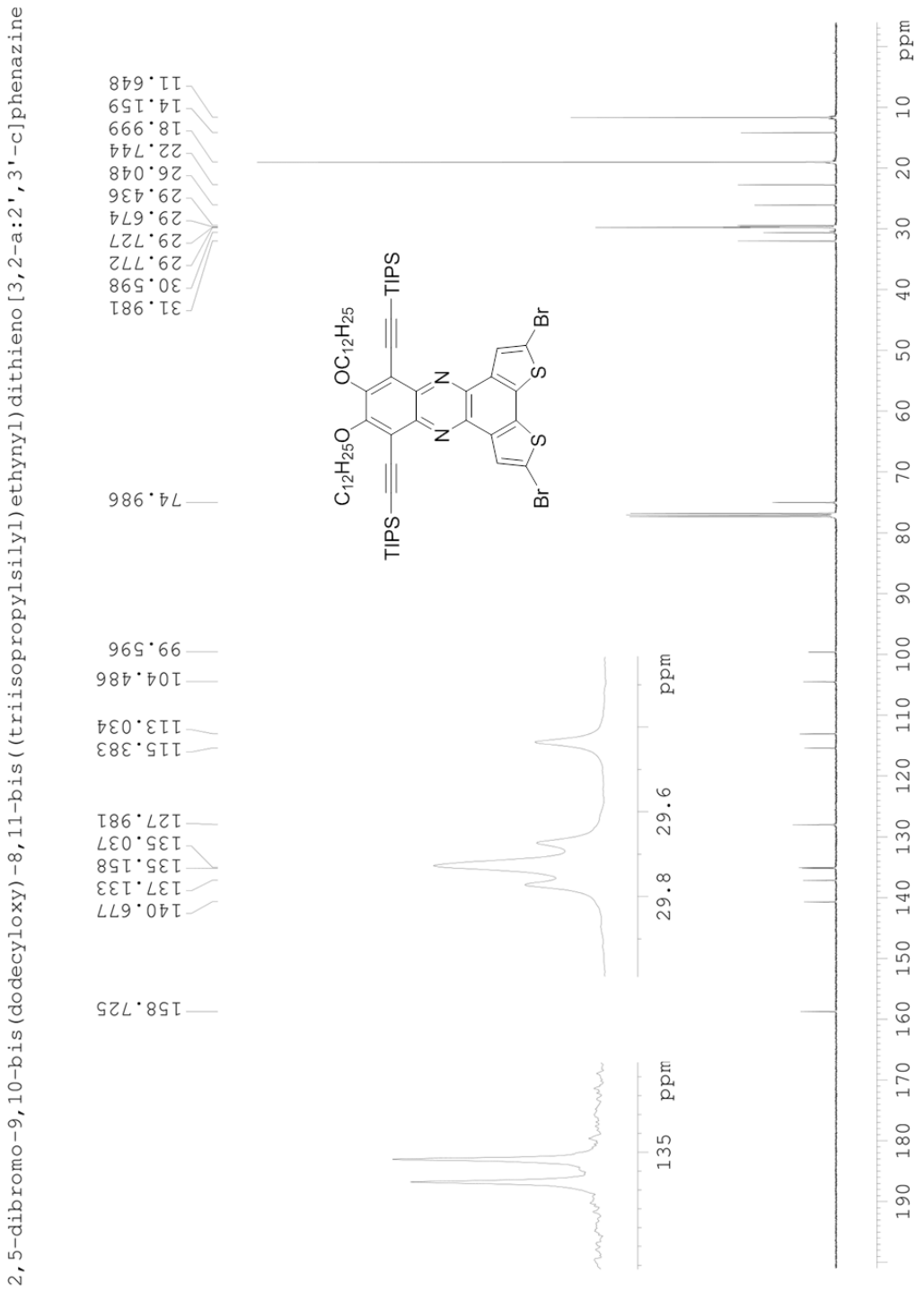

Figure 3.39. ^{13}C NMR spectrum of **3c**.

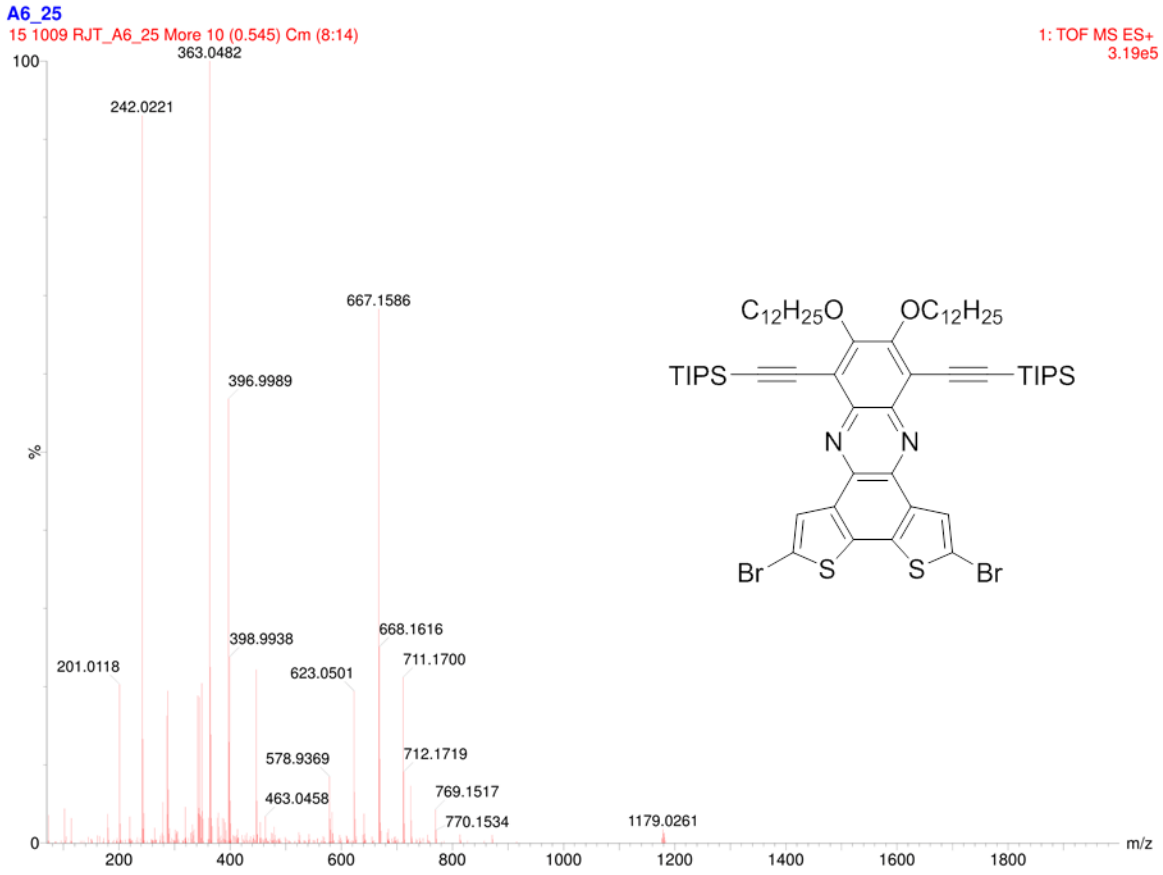

Figure 3.40. ESI-MS spectrum of **3c**.

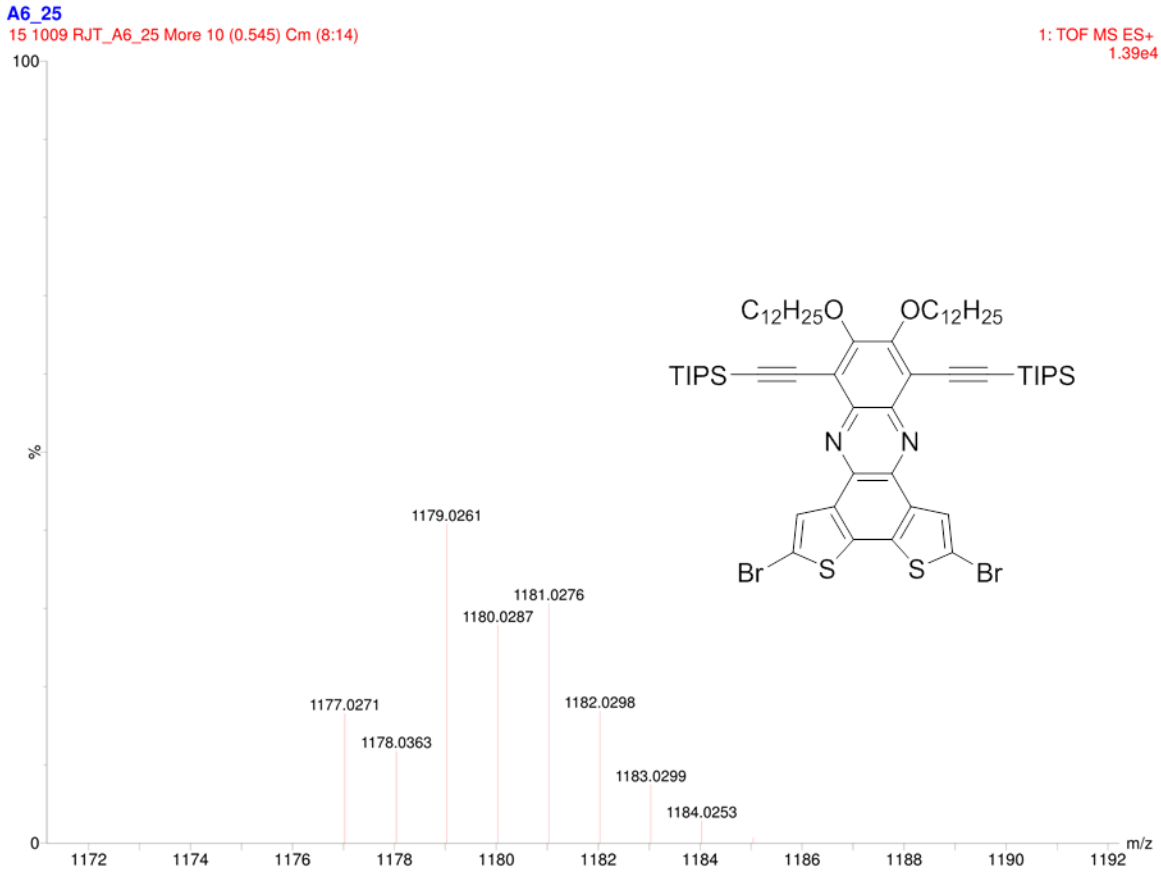

Figure 3.41. ESI-MS of **3c** parent ion.

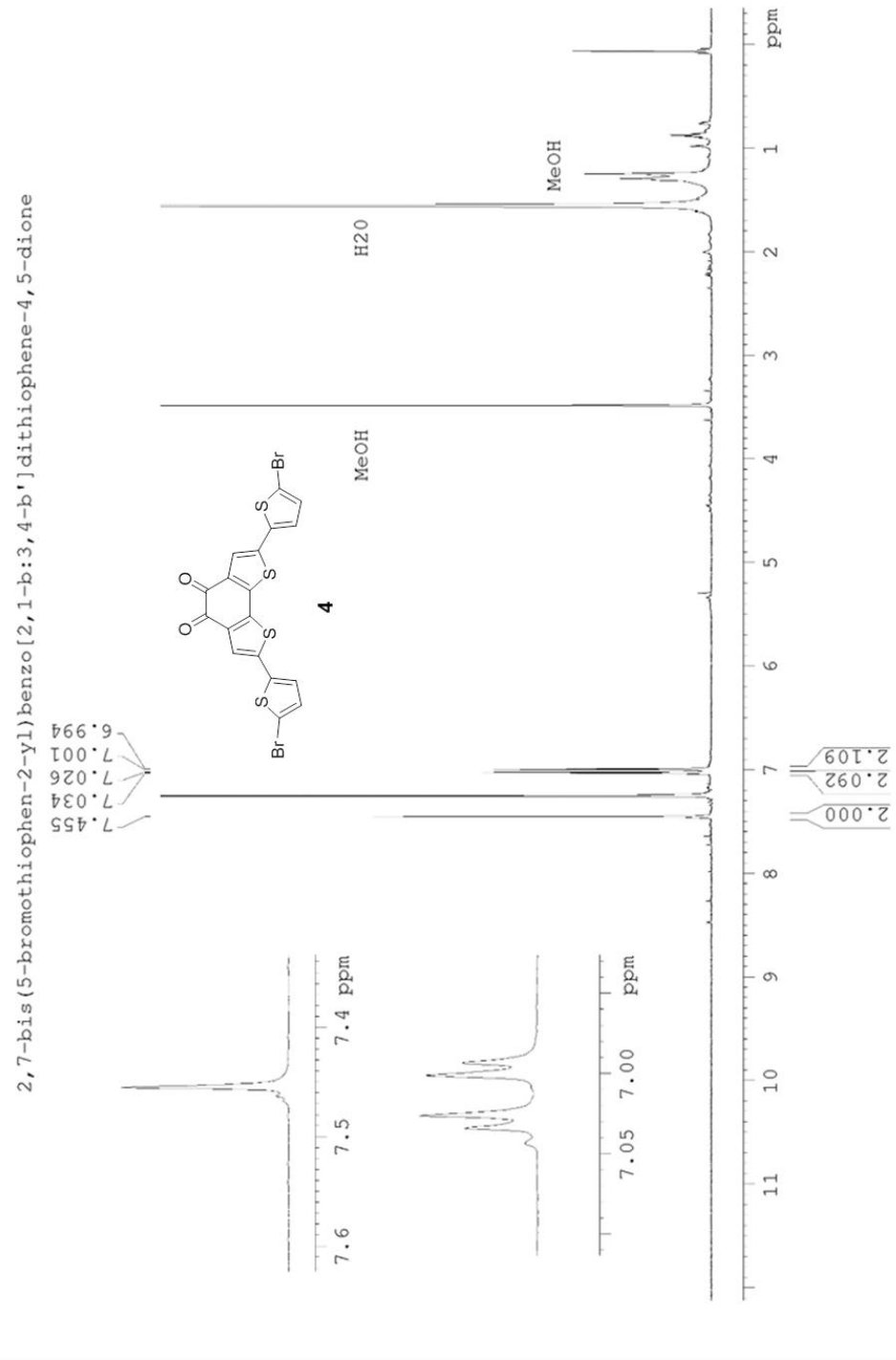

Figure 3.42. ^{1}H NMR of **4**.

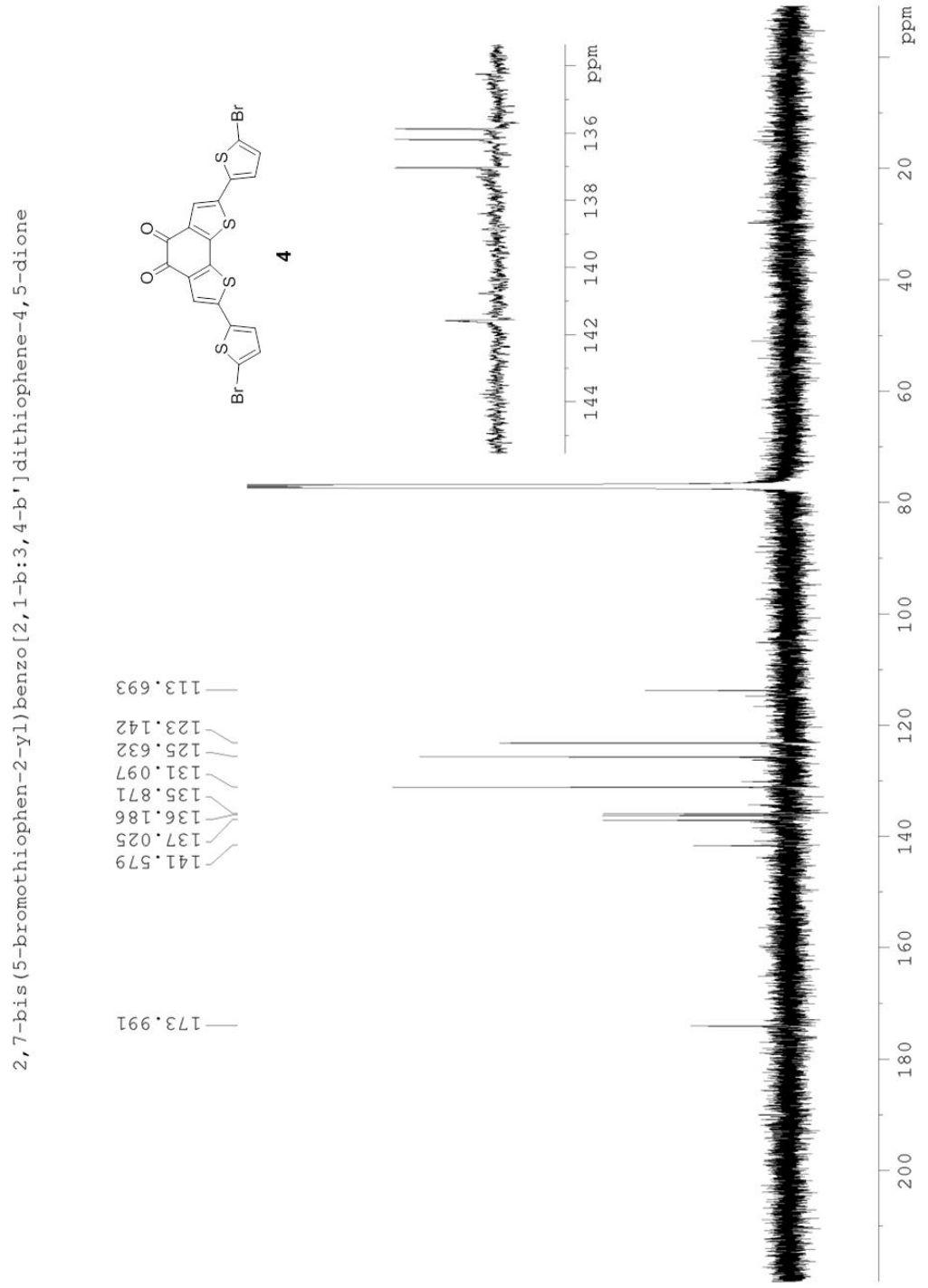

Figure 3.43. ^{13}C NMR of **4**.

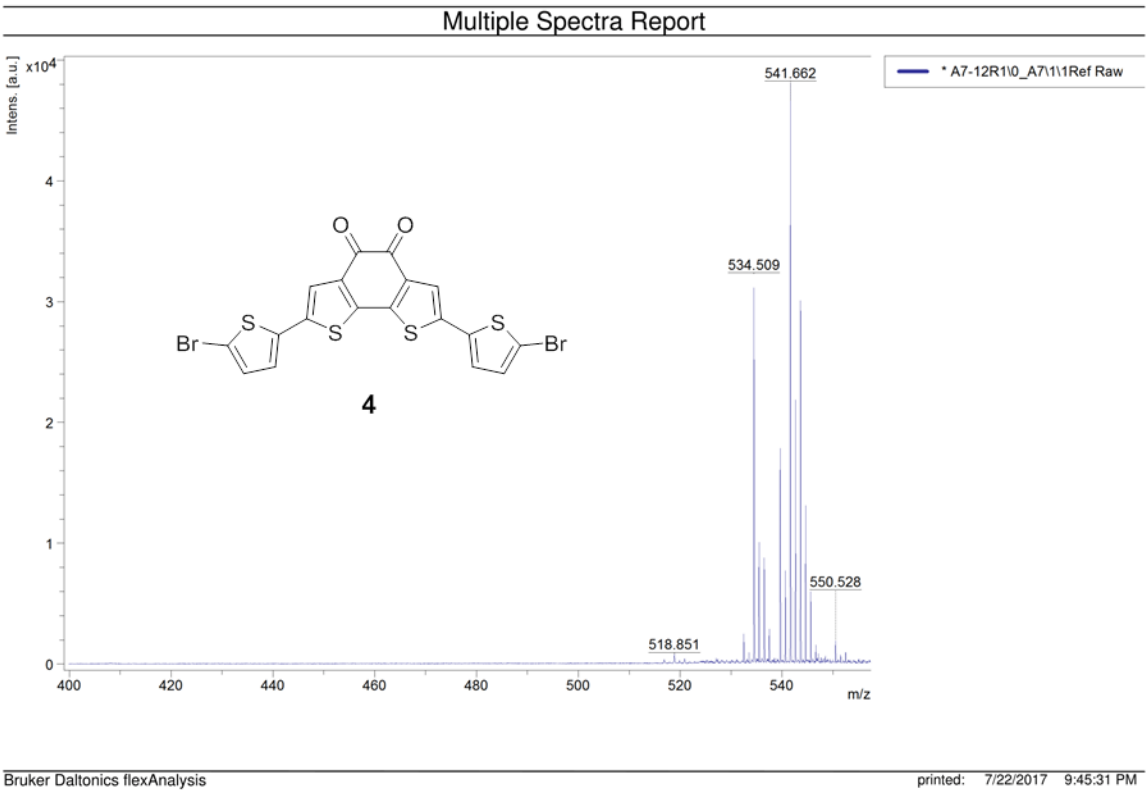

Figure 3.44. MALDI-TOF spectrum of **4**.

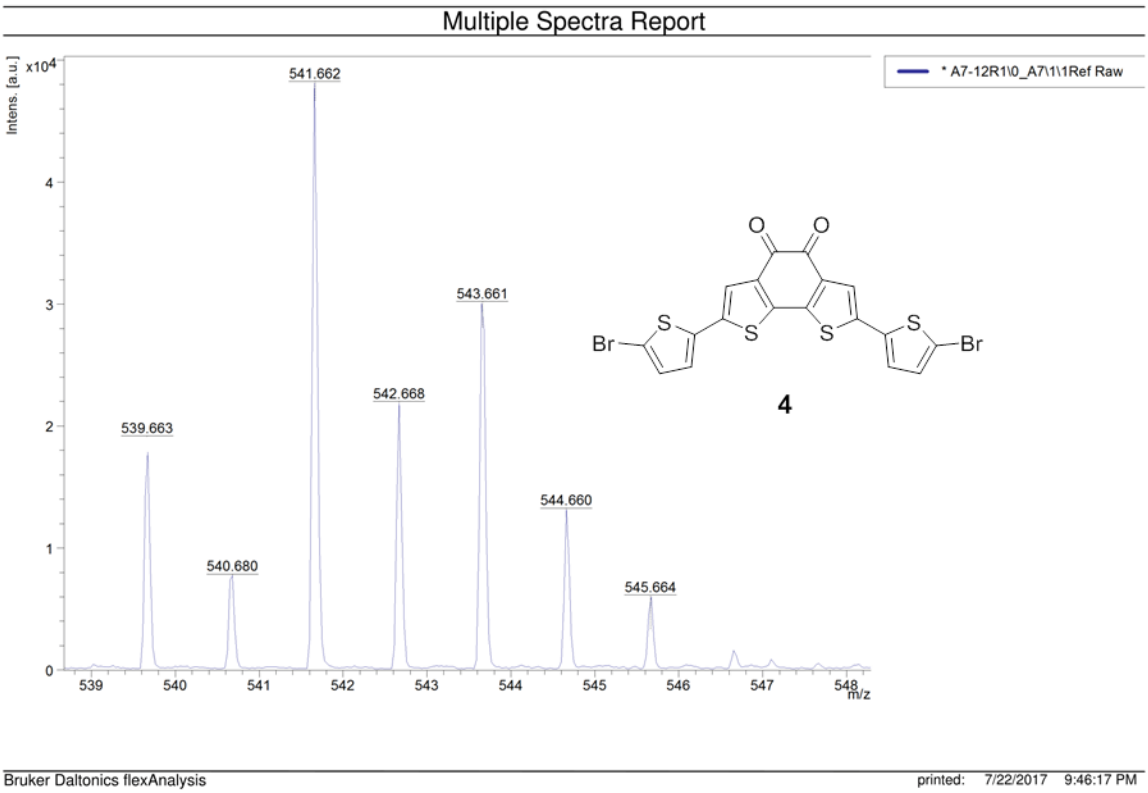

Figure 3.45. MALDI-TOF spectrum of **4** parent ion.

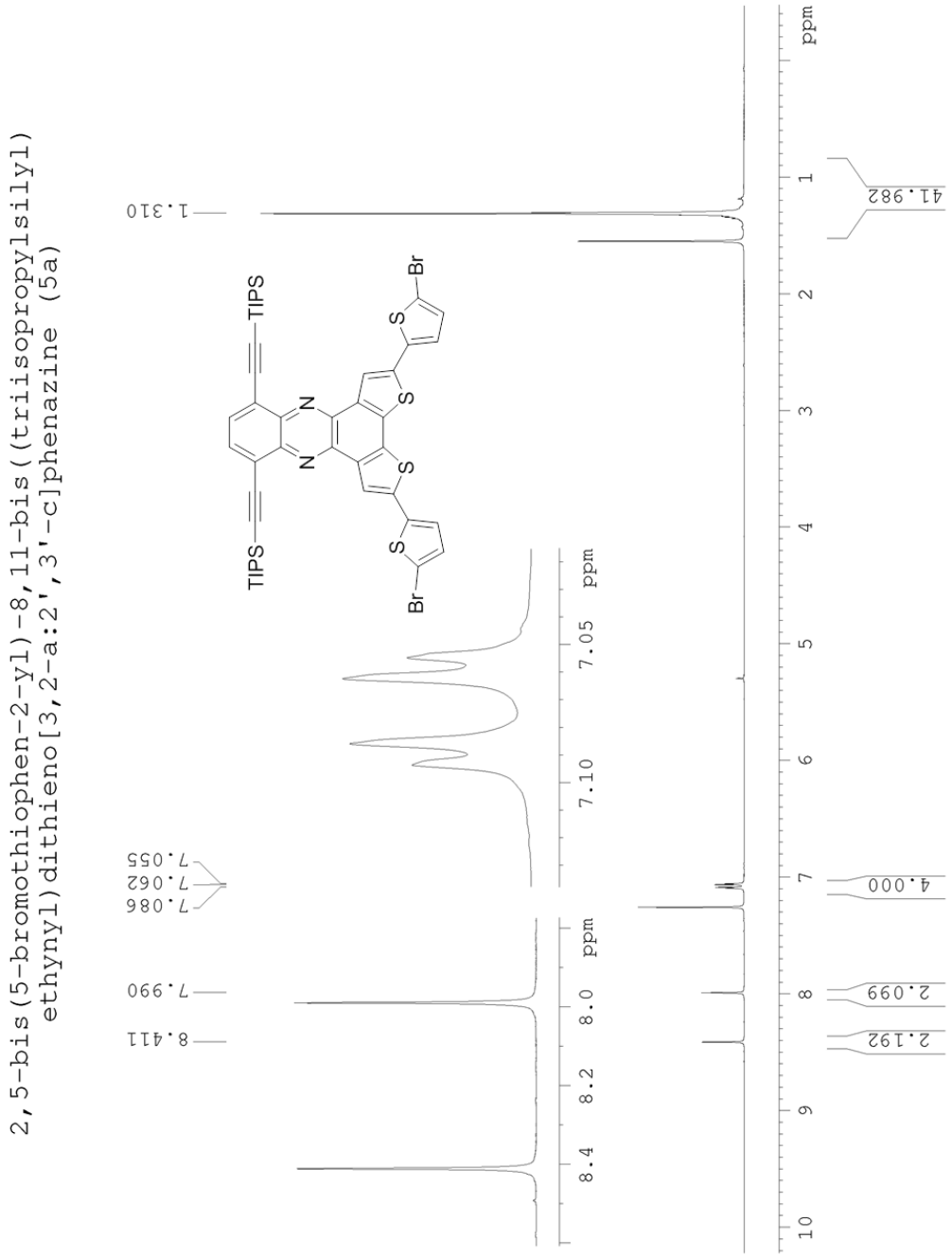

Figure 3.46. ^{1}H NMR spectrum of **5a**.

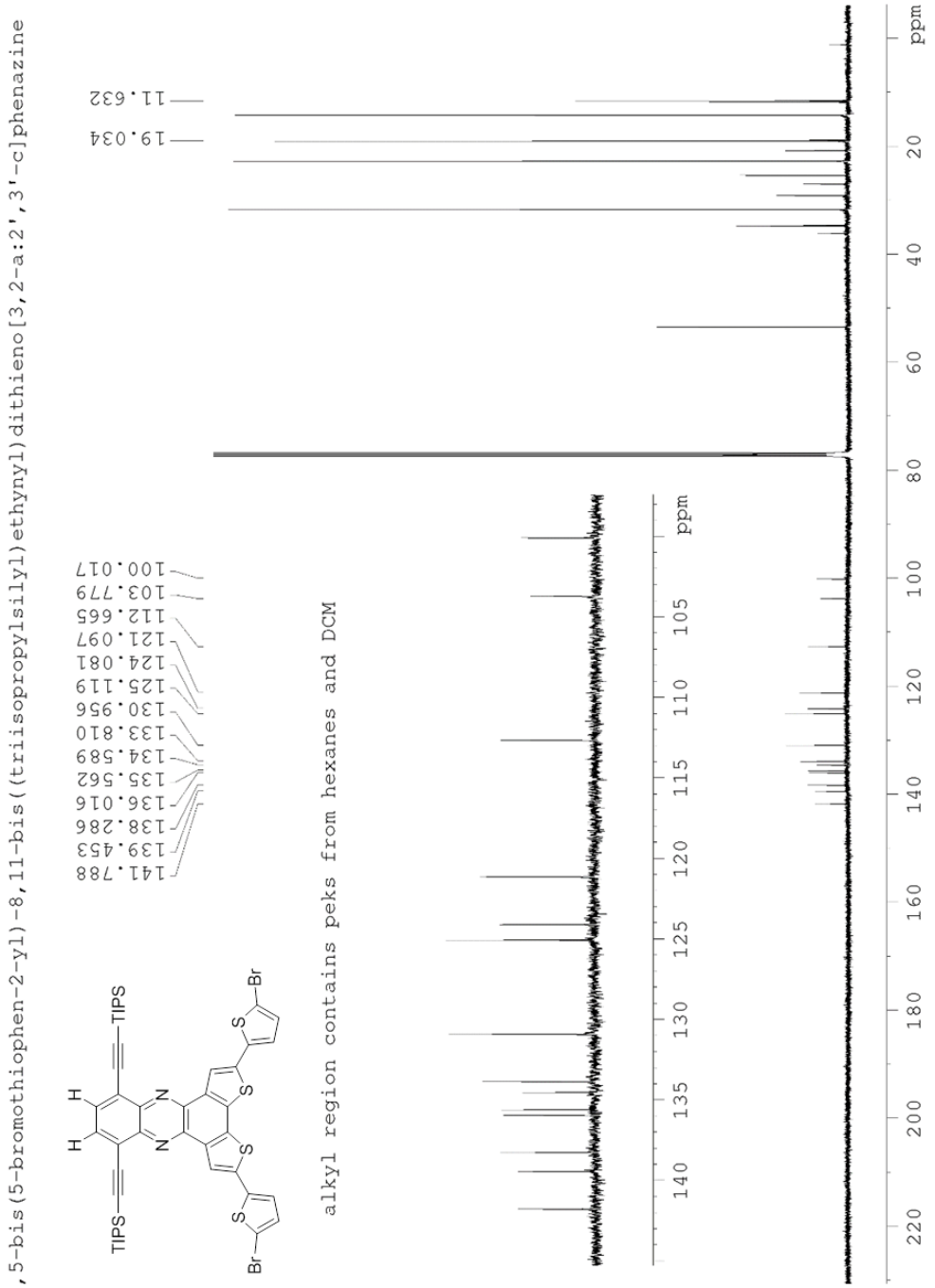

Figure 3.47. ^{13}C NMR of **5a**.

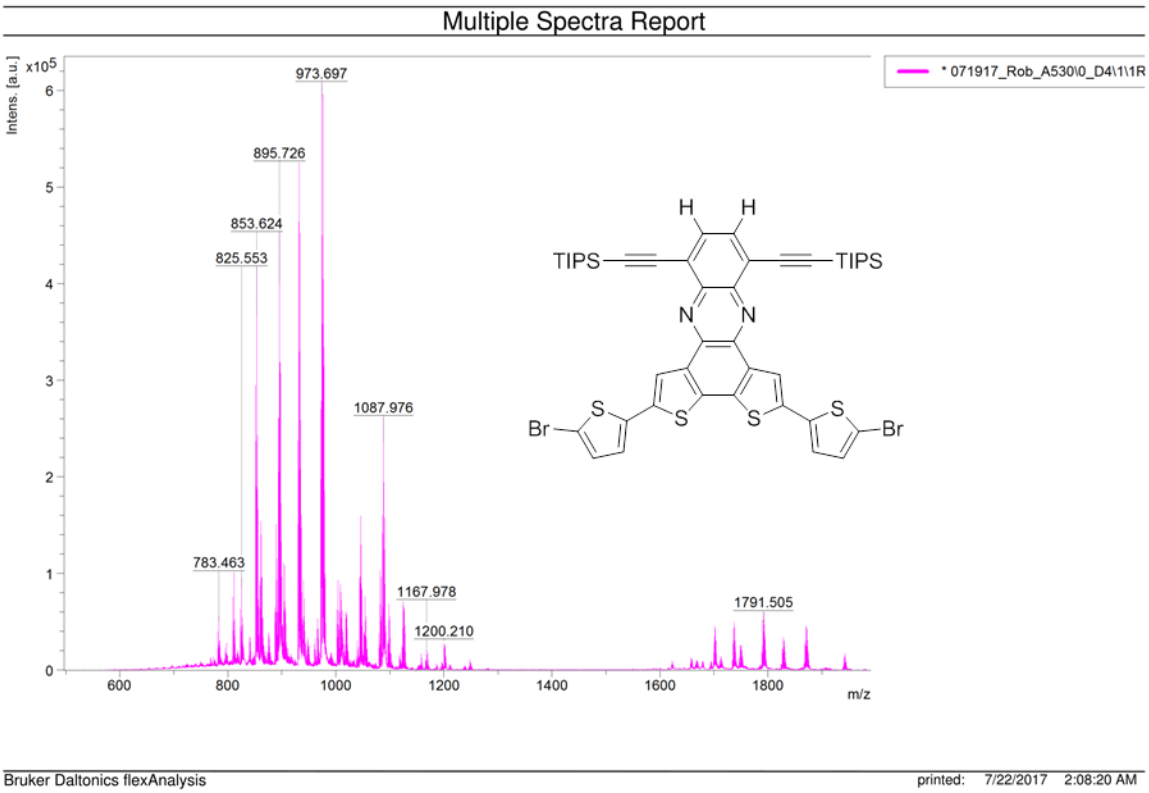

Figure 3.48. MALDI-TOF spectrum of **5a**.

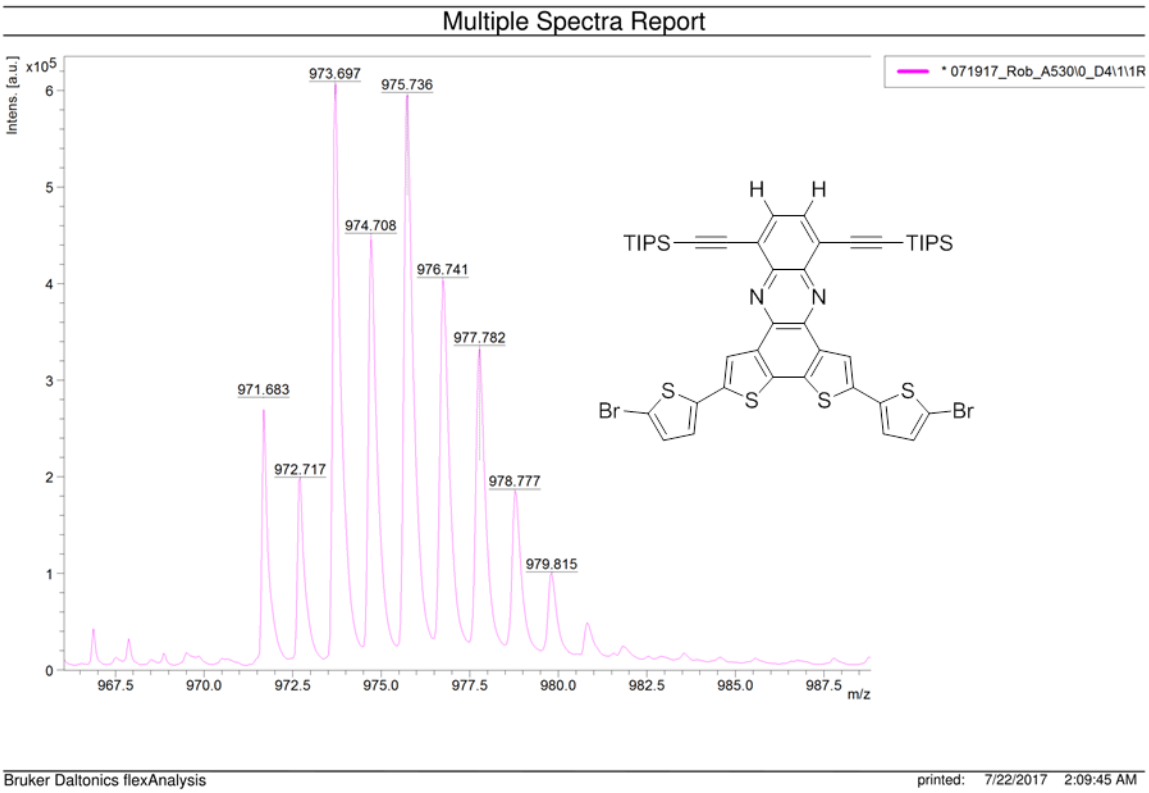

Figure 3.49. MALDI-TOF spectrum of **5a** parent ion.

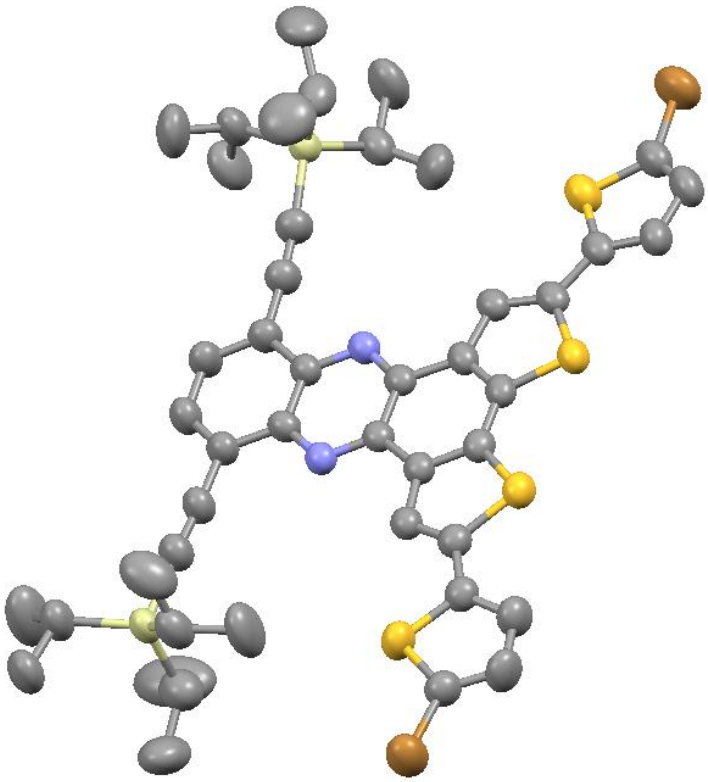

Figure 3.50. Crystal structure of **5a** with ellipsoids displaying 50% probability.

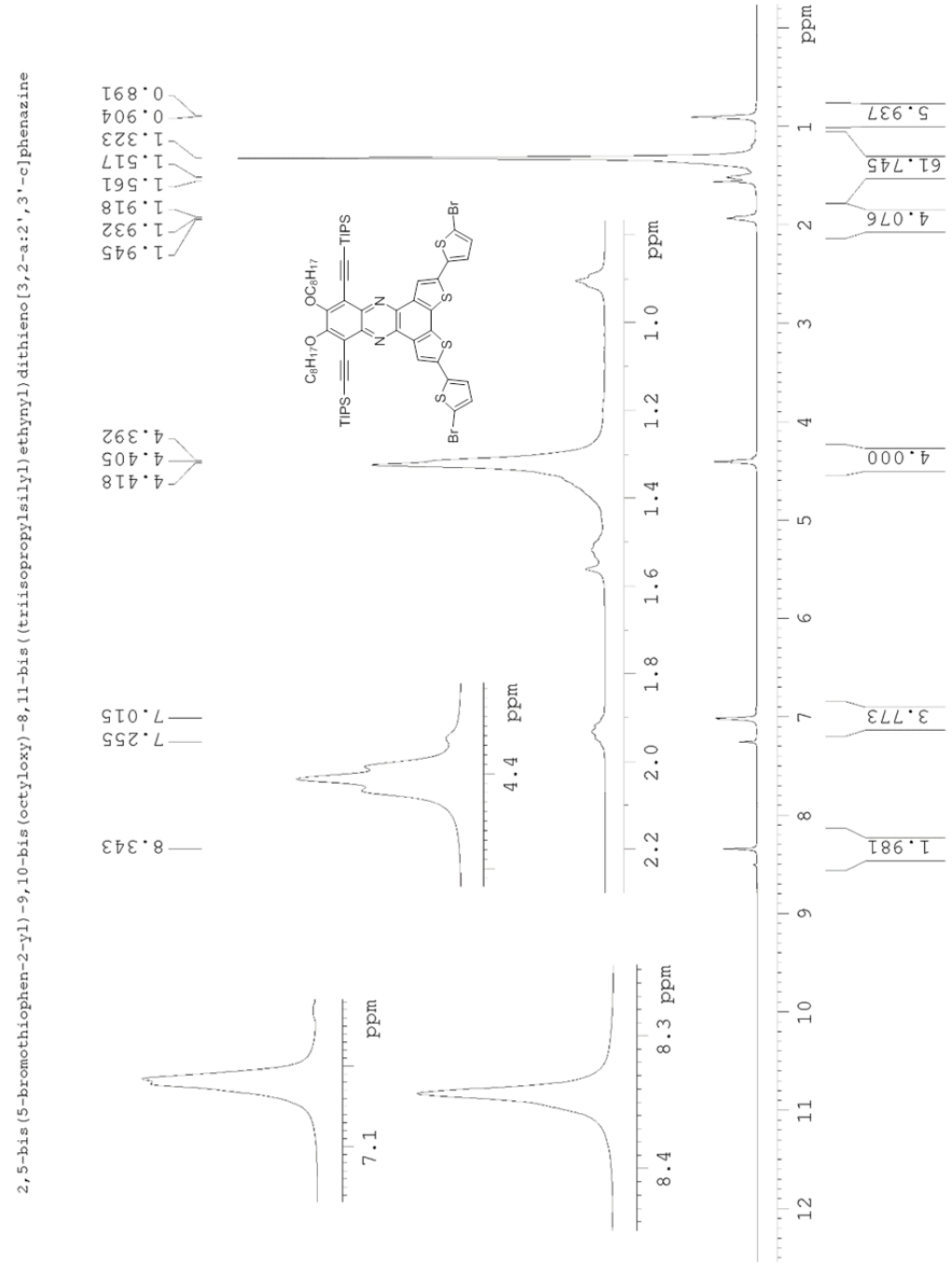

Figure 3.51. ^{1}H NMR spectrum of **5b**.

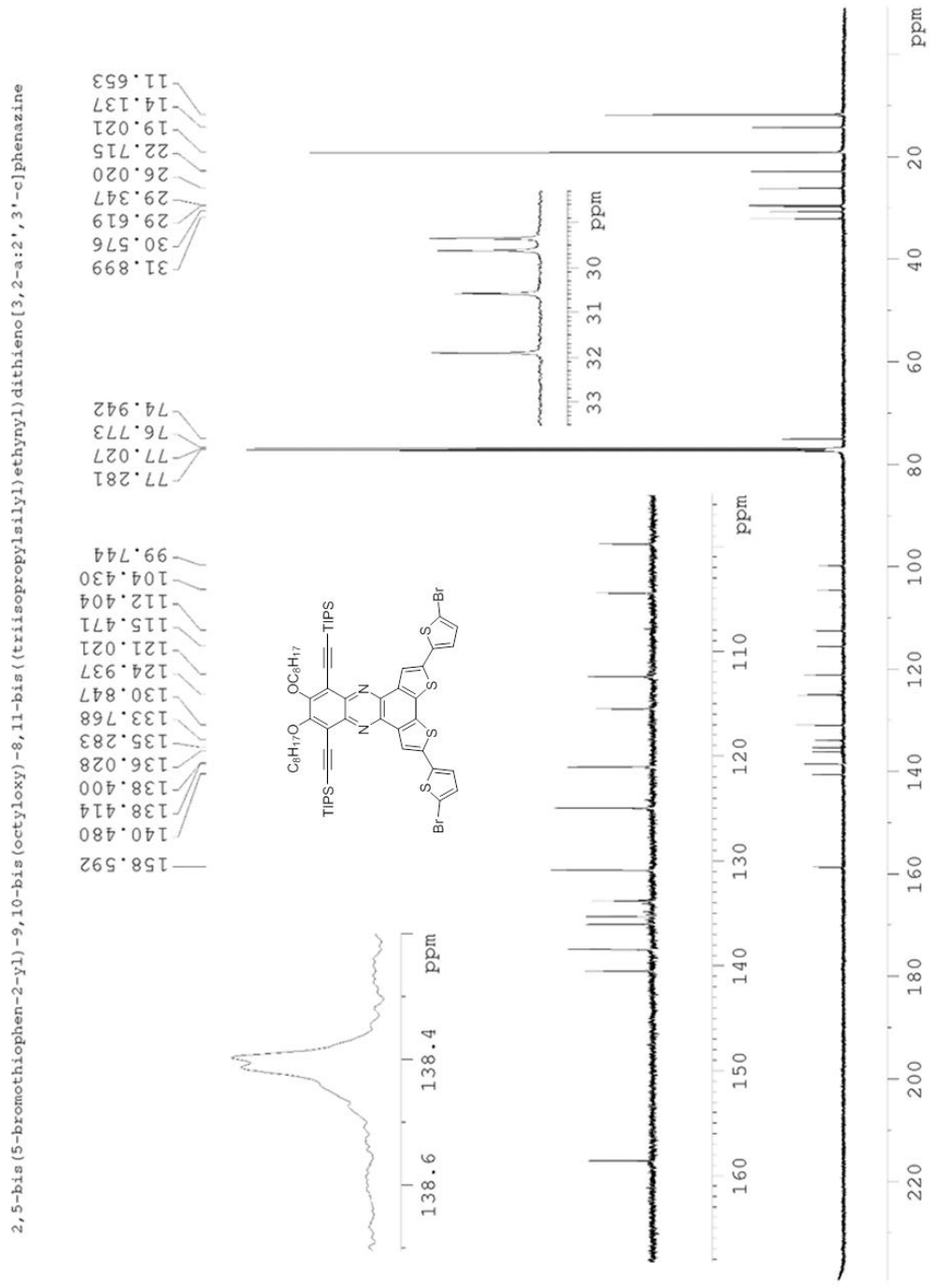

Figure 3.52. ^{13}C NMR of **5b**.

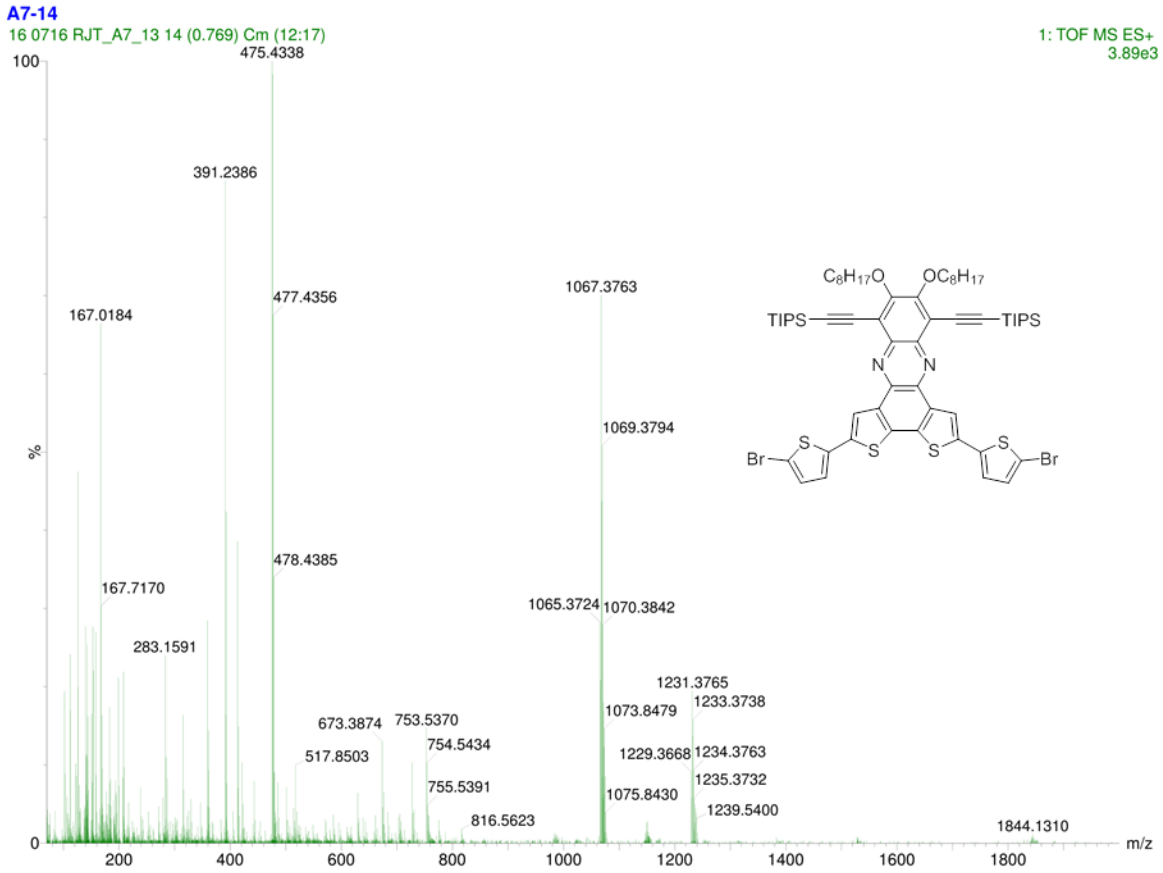

Figure 3.53. ESI-MS of **5b**.

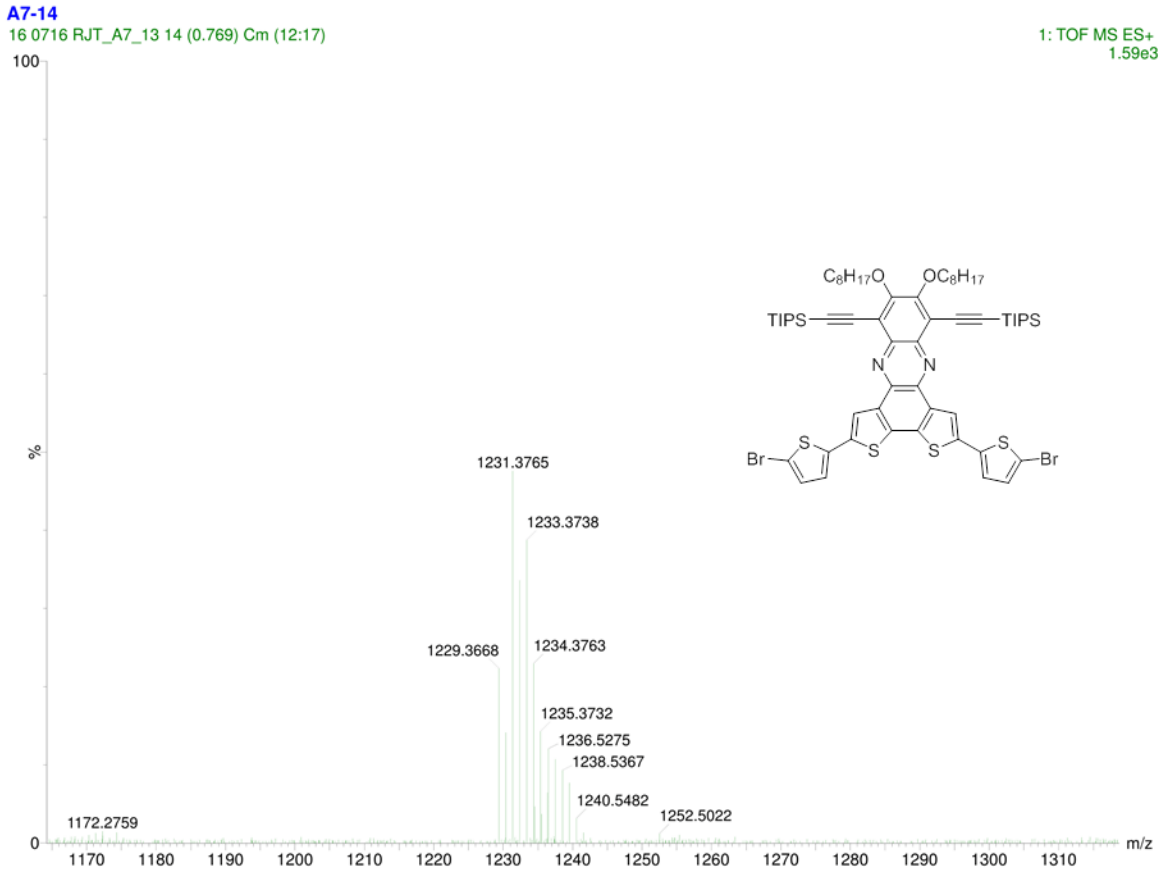

Figure 3.54. ESI-MS of **5b** parent ion.

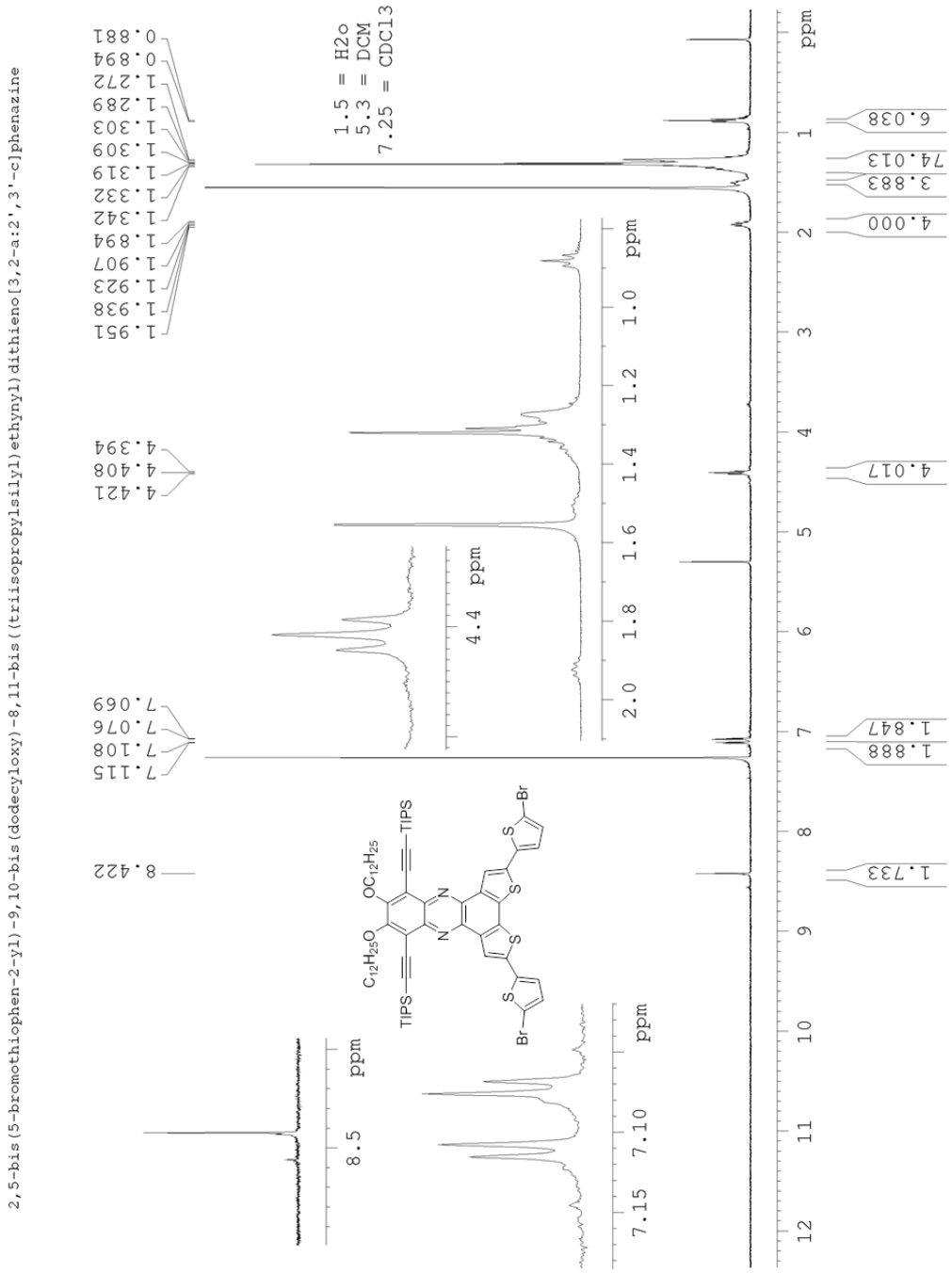

Figure 3.55. ^{1}H NMR spectrum of **5c**.

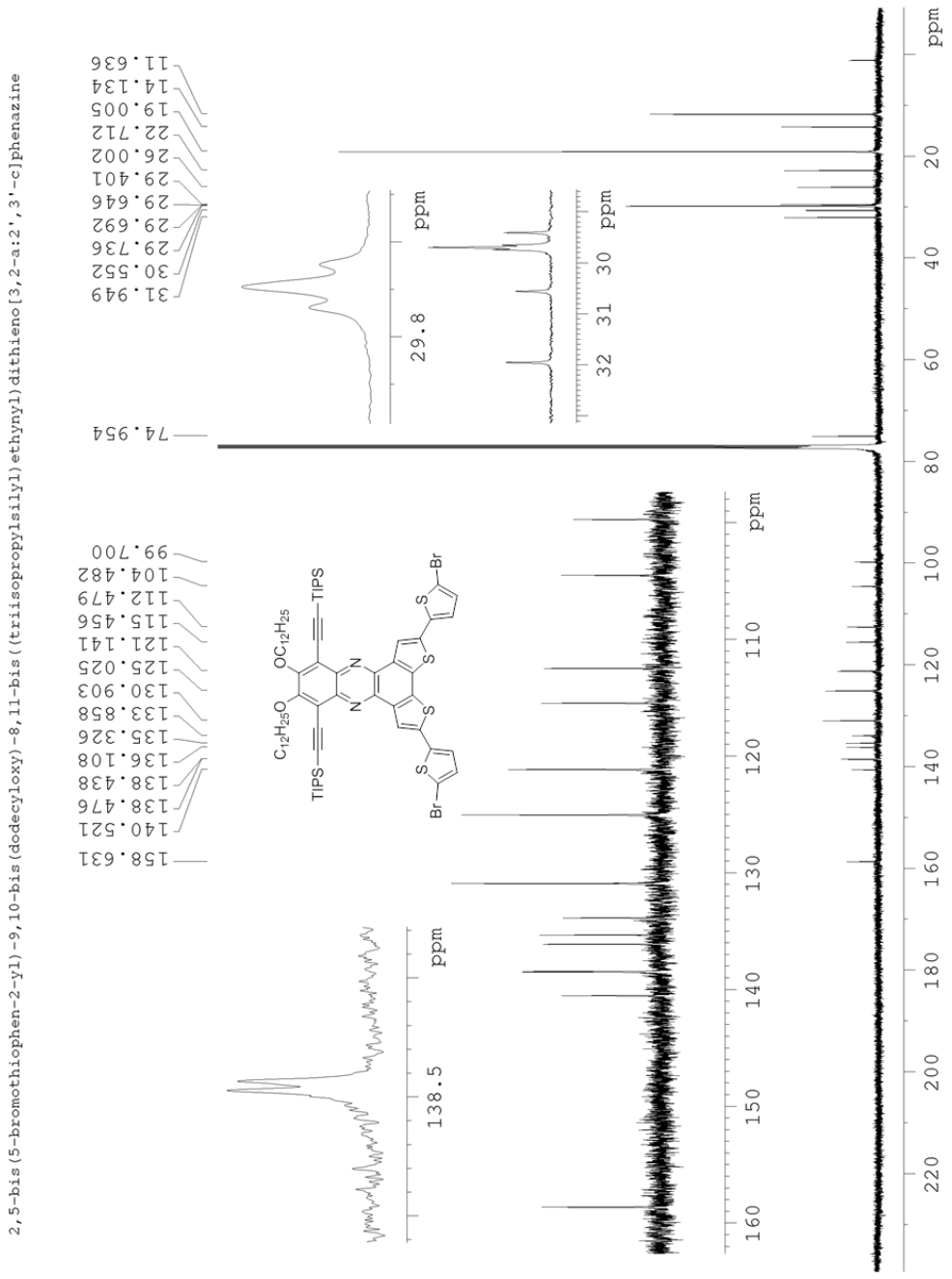

Figure 3.56. ^{13}C NMR of **5c**.

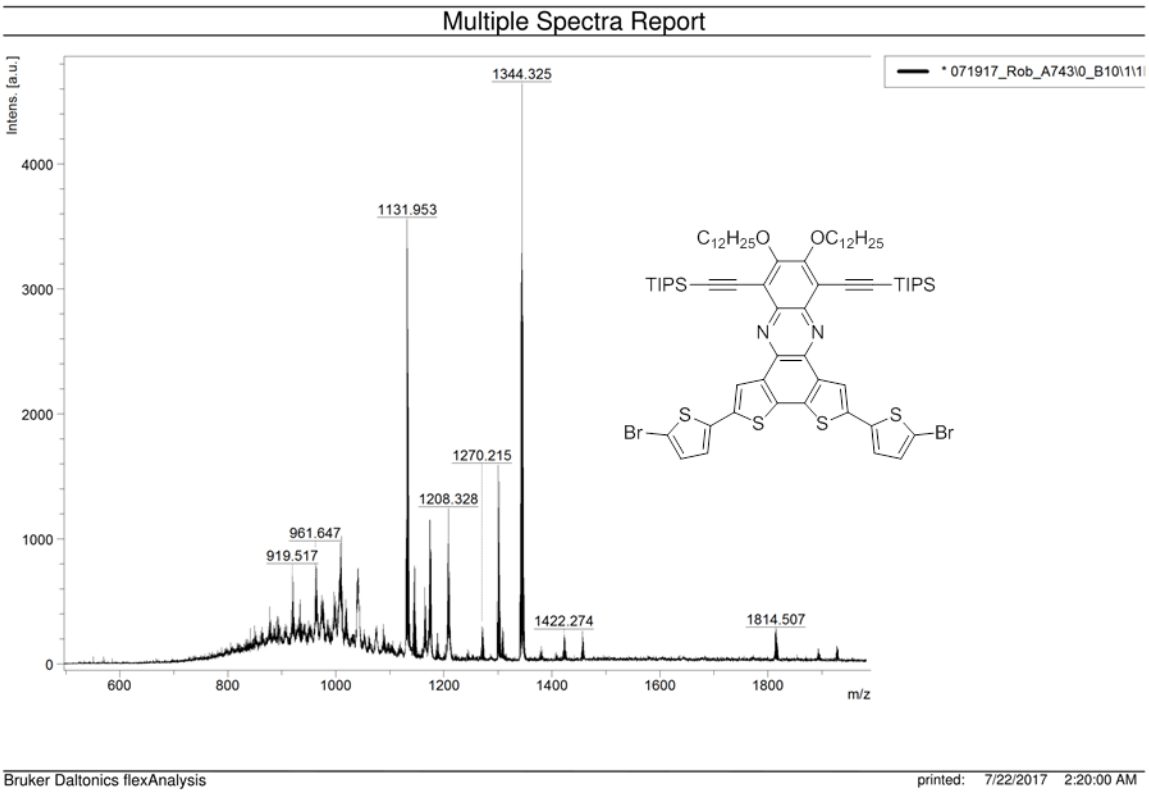

Figure 3.57. MALDI-TOF spectrum of **5c**.

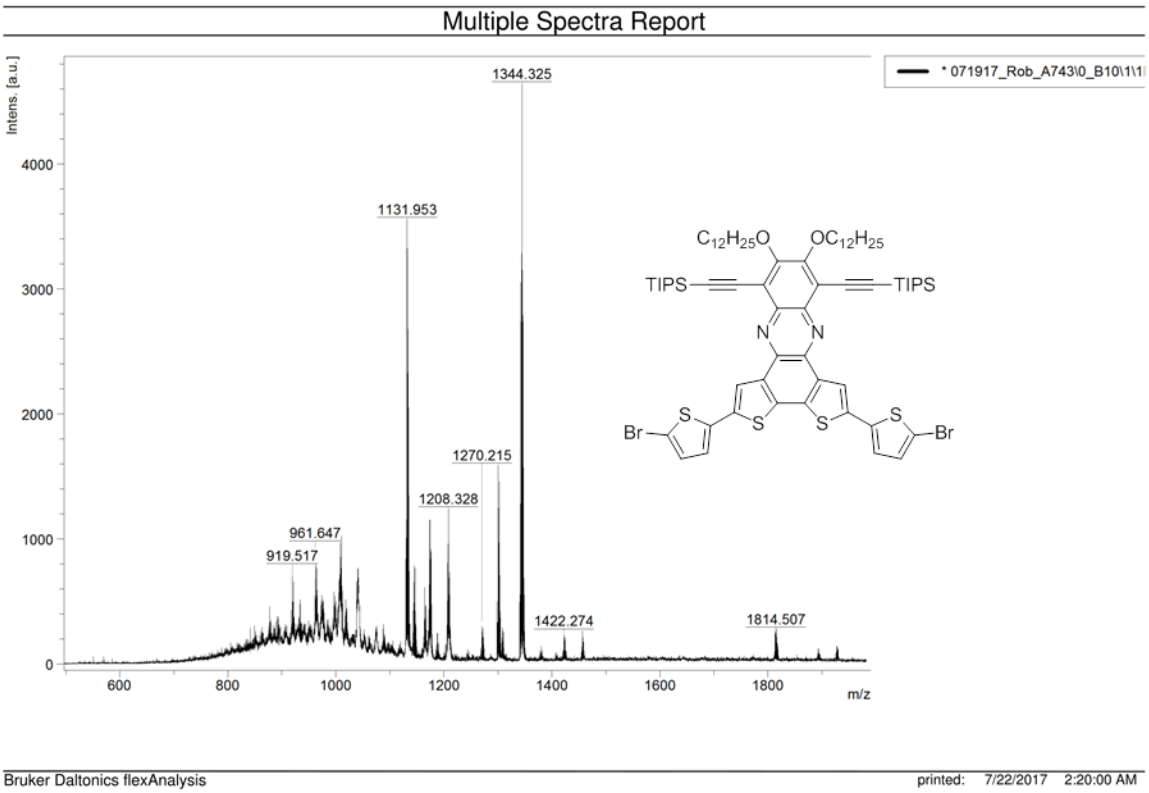

Figure 3.58. MALDI-TOF spectrum of **5c** parent ion.

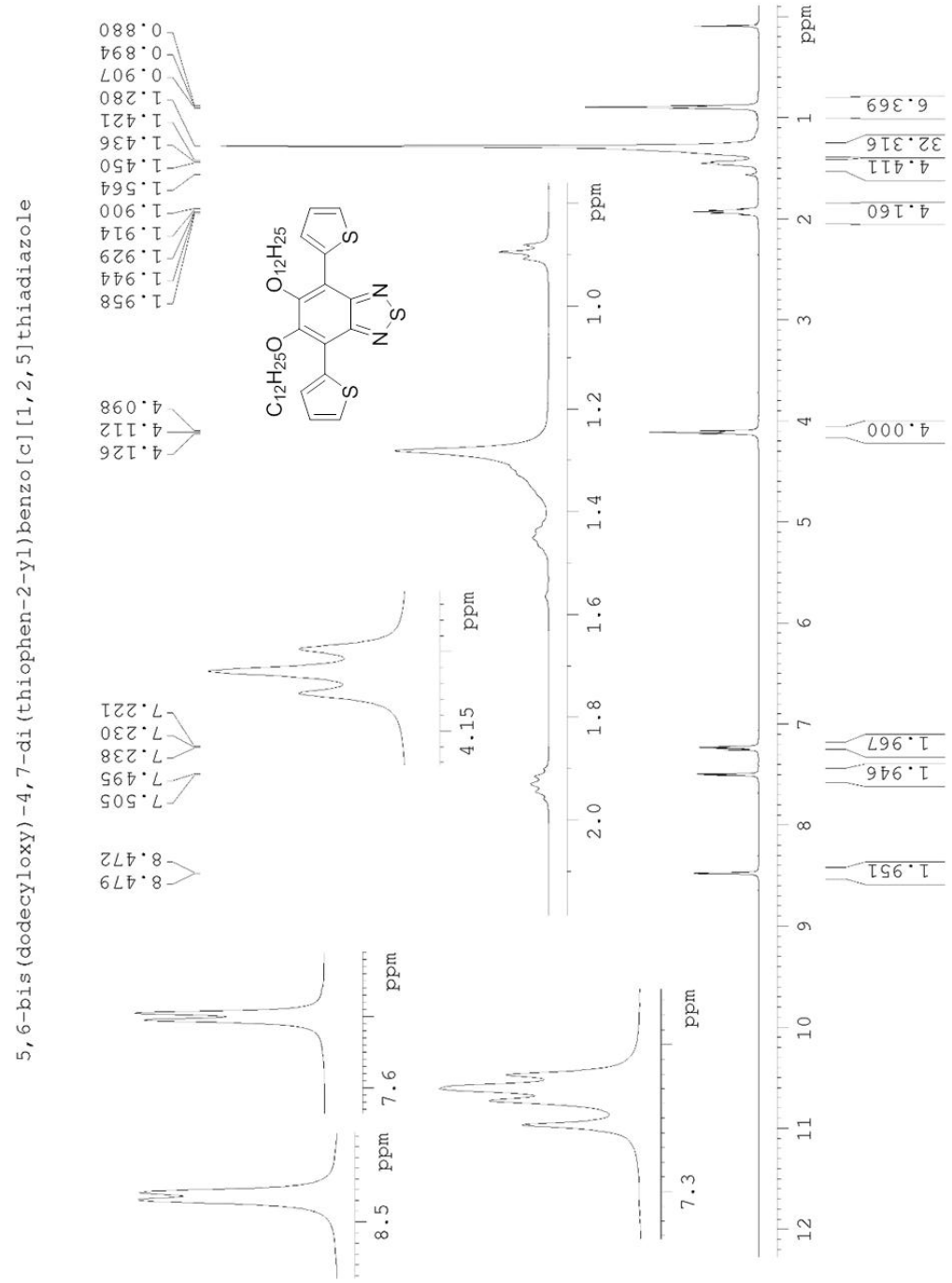

Figure 3.59. ^{1}H NMR spectrum of **6**.

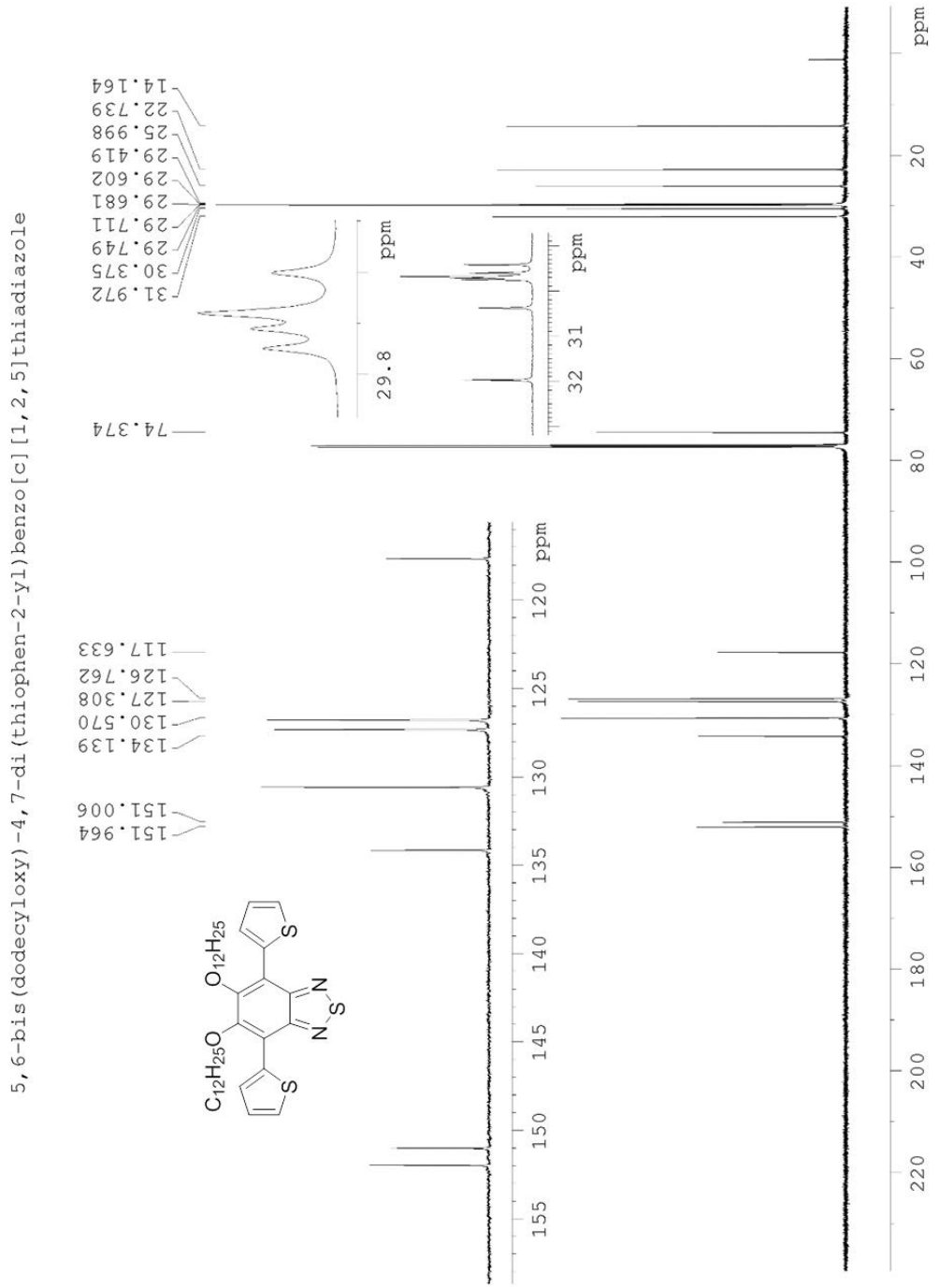

Figure 3.60. ^{13}C NMR of **6**.

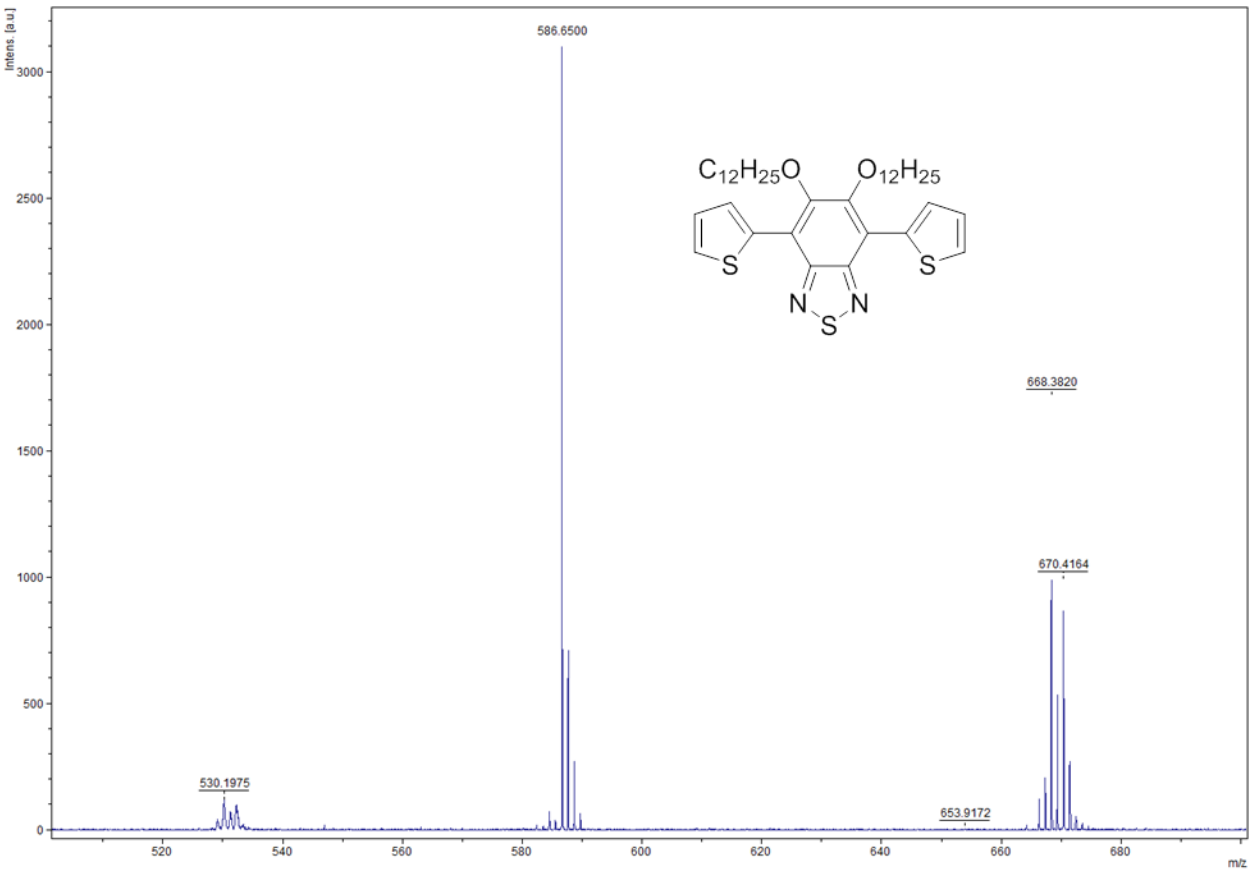

Figure 3.61. MALDI-TOF spectrum of **6**.

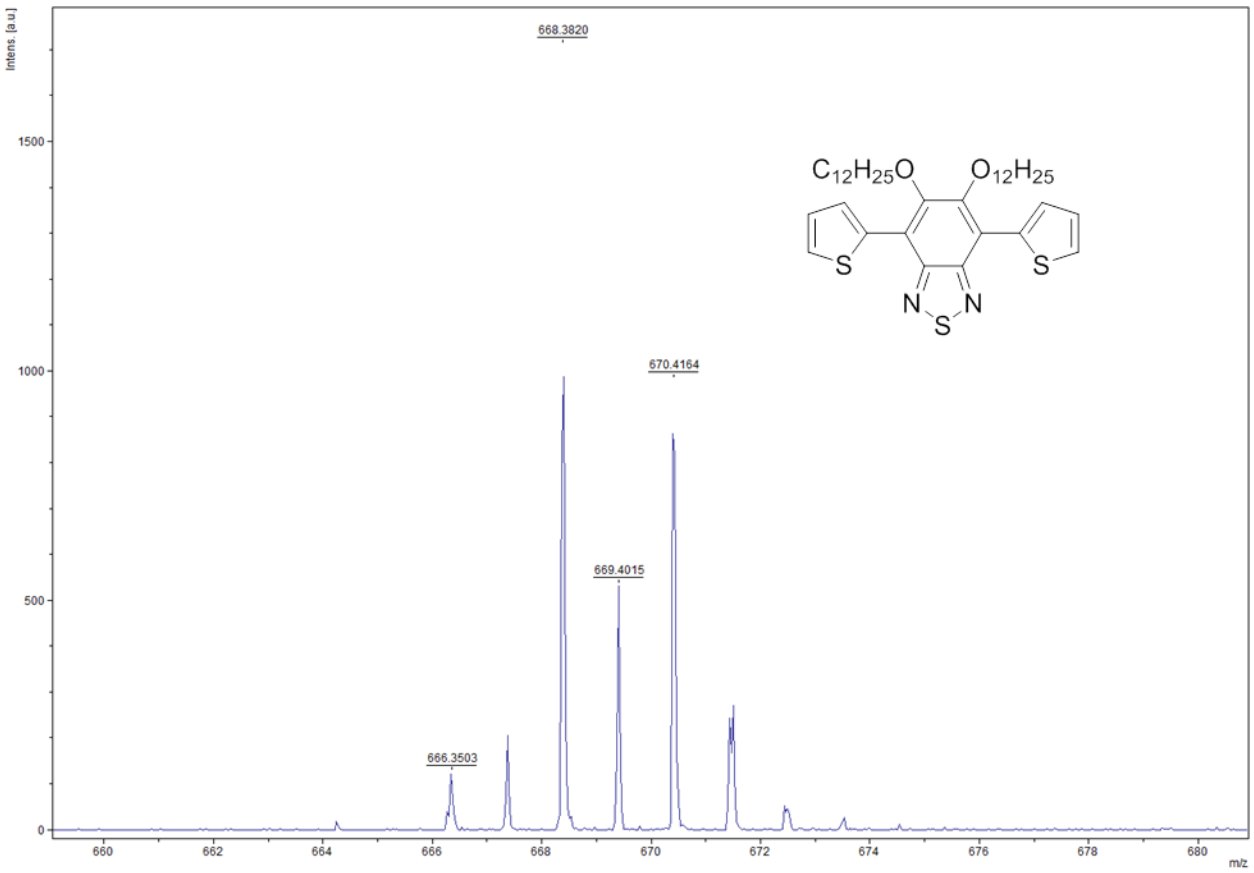

Figure 3.62. MALDI-TOF spectrum of **6** parent ion.

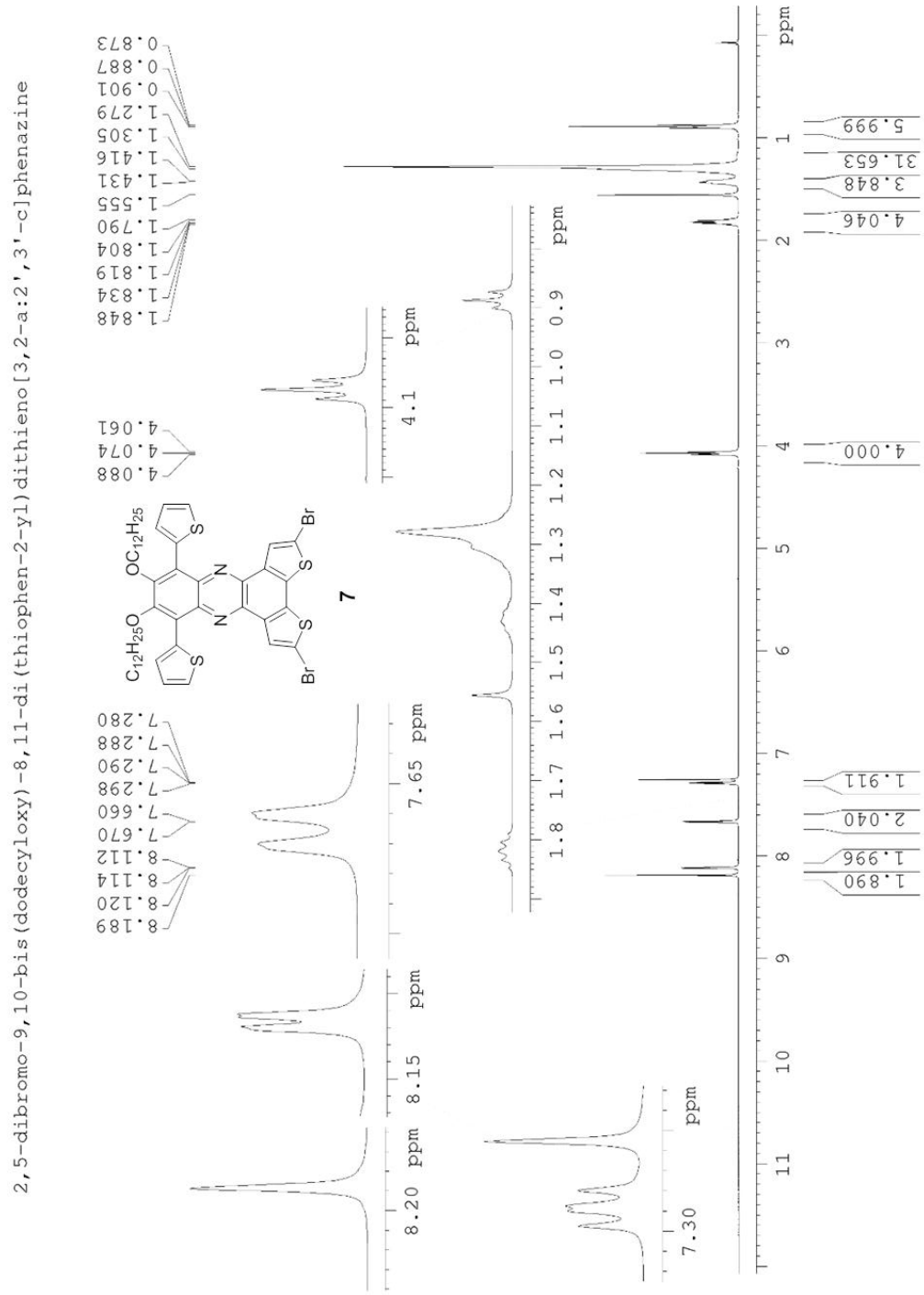

Figure 3.63. ^{1}H NMR spectrum of **7**.

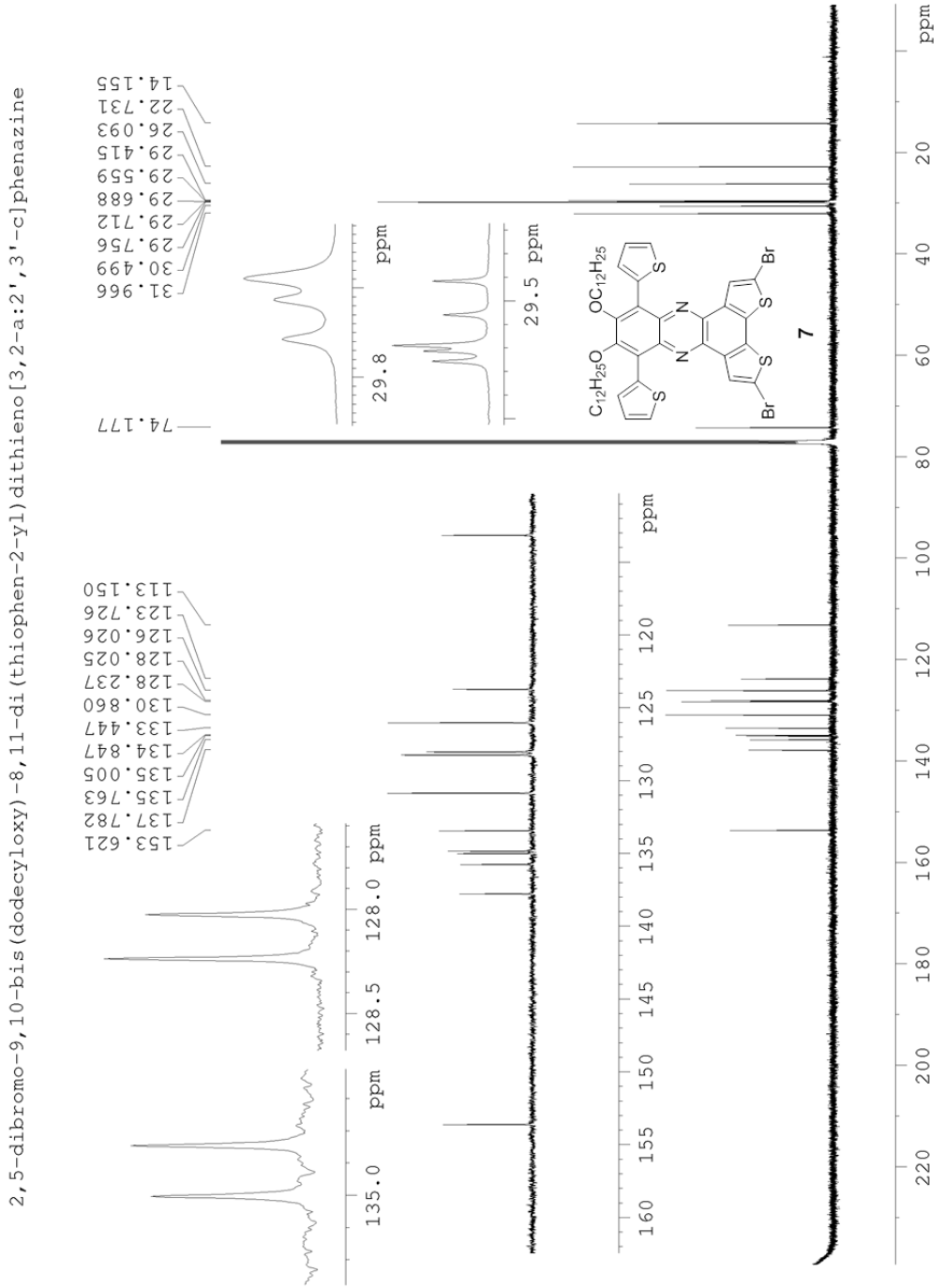

Figure 3.64. ^{13}C NMR spectrum of **7**.

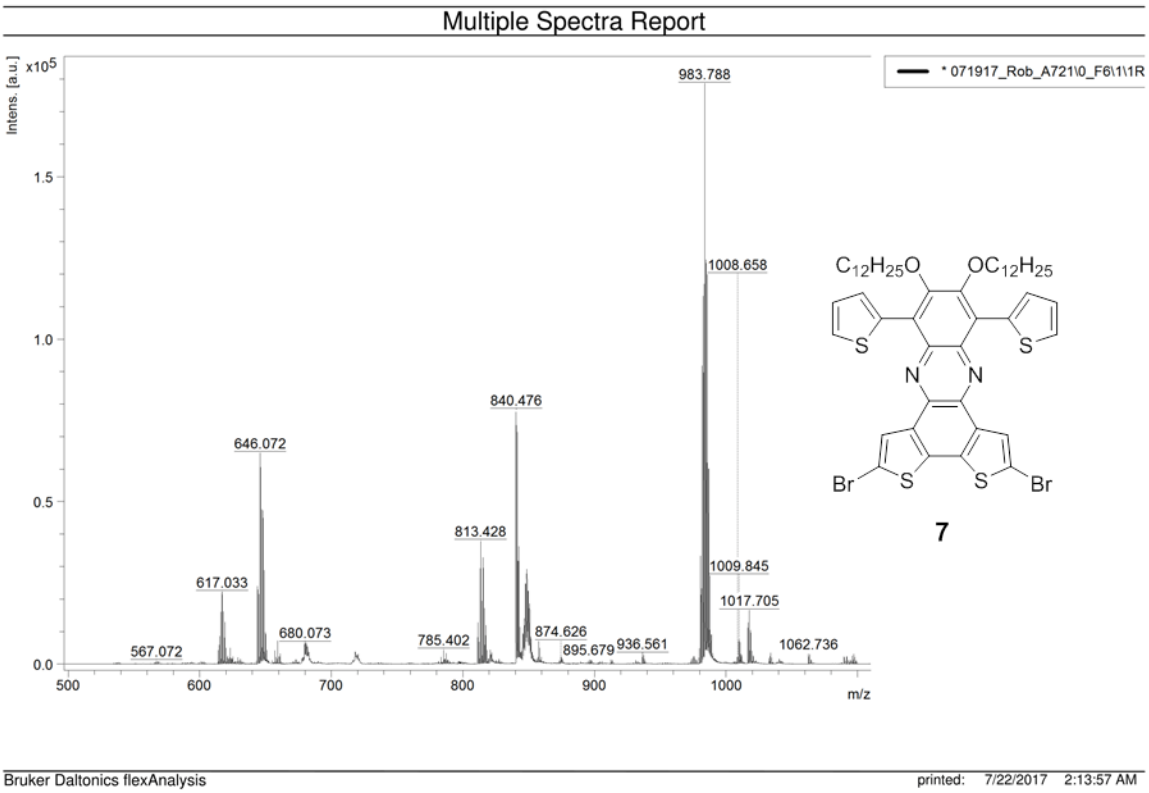

Figure 3.65. MALDI-TOF spectrum of **7**.

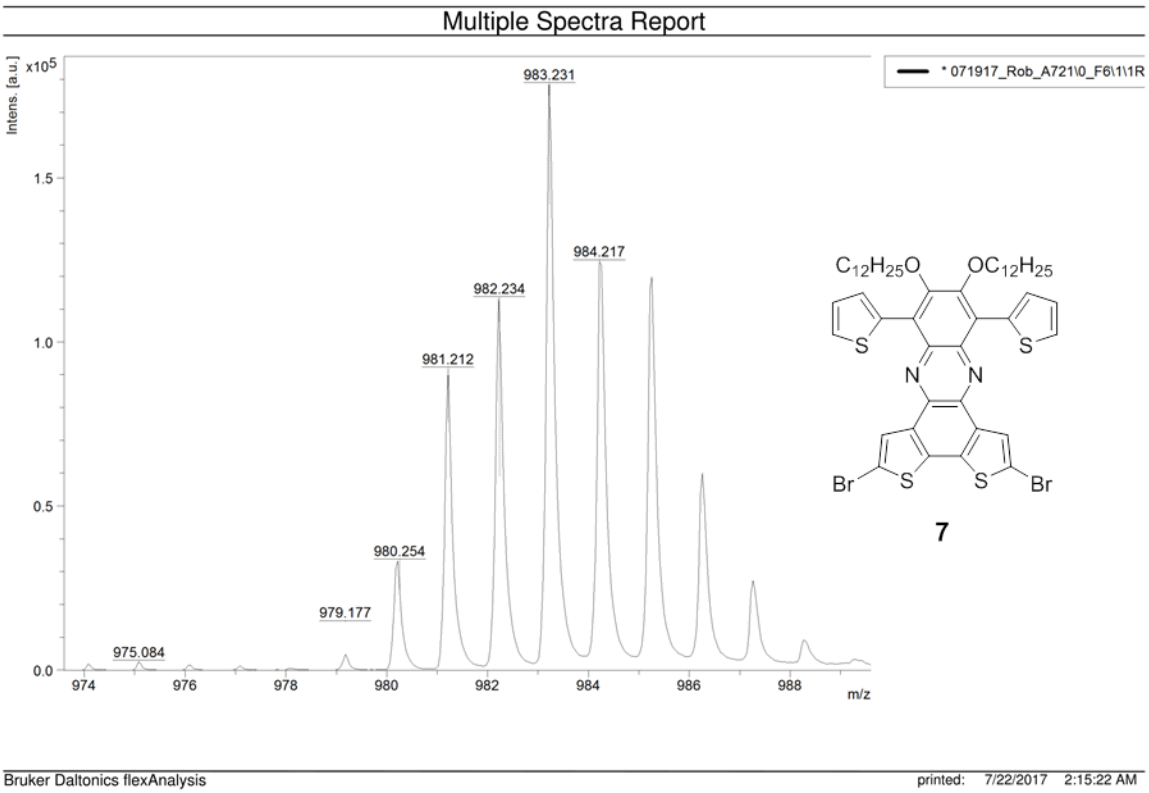

Figure 3.66. MALDI-TOF spectrum of **7** parent ion**.**

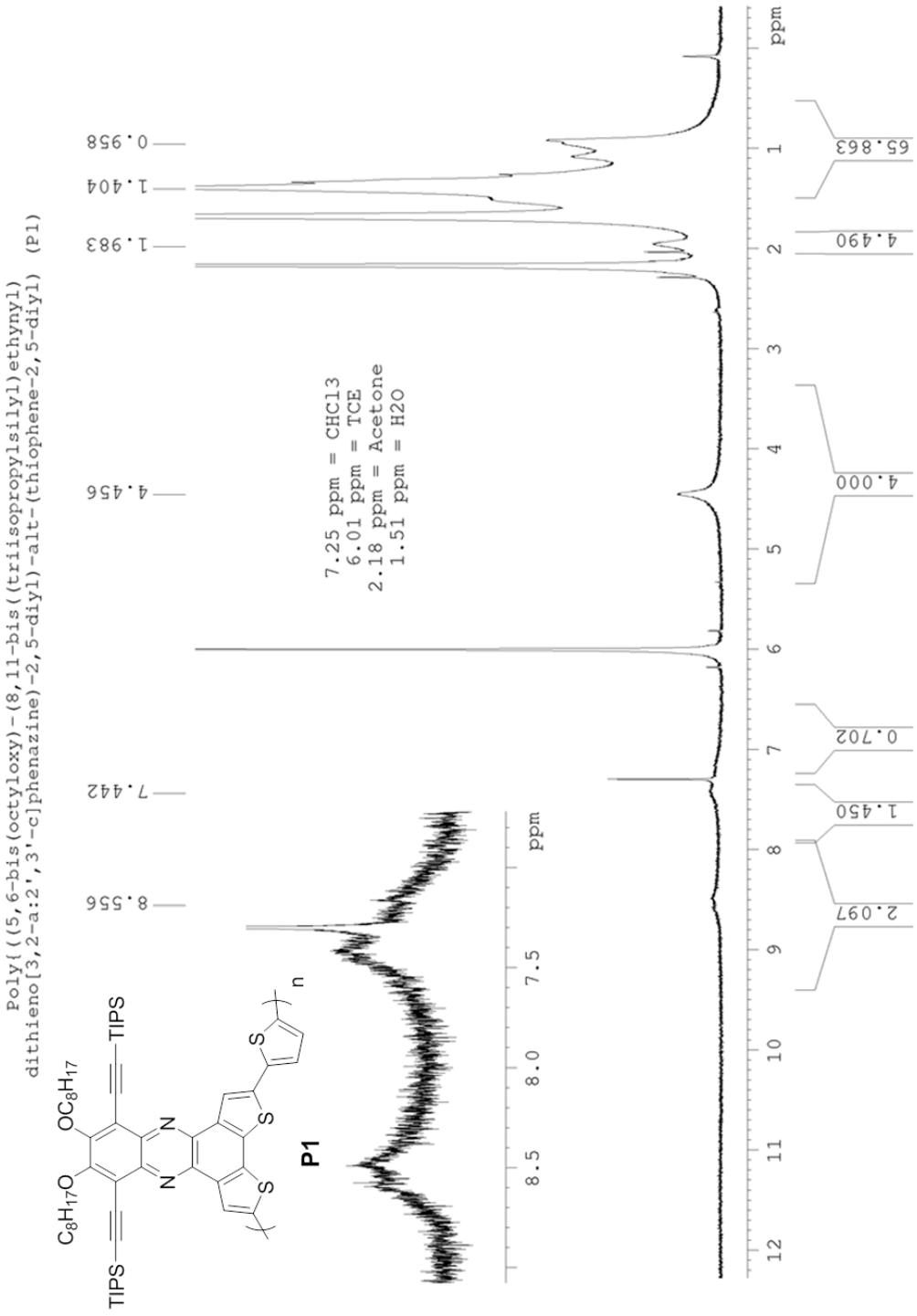

Figure 3.67. ^{1}H NMR spectrum of **P1**.

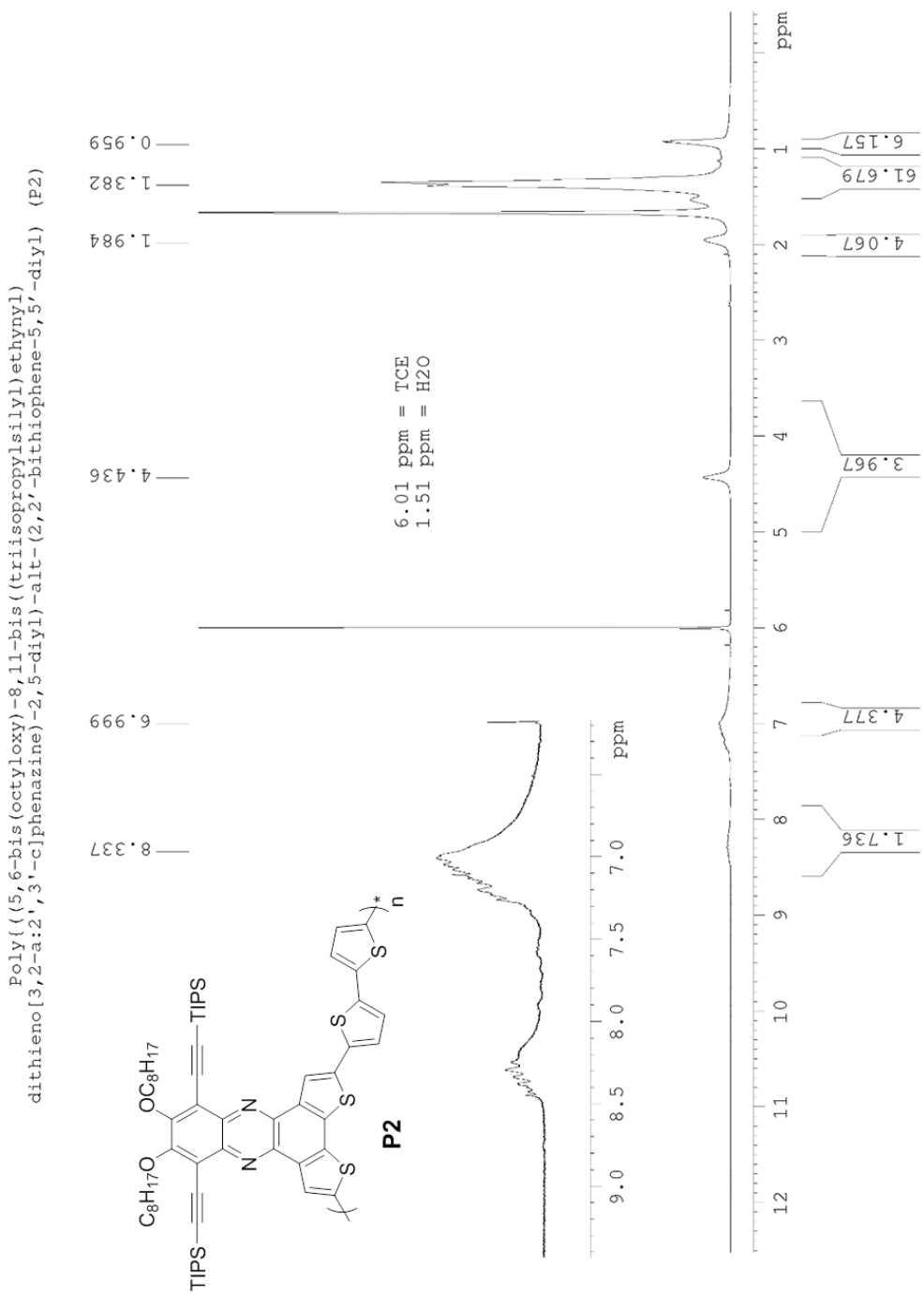

Figure 3.68. ^{1}H NMR spectrum of **P2**.

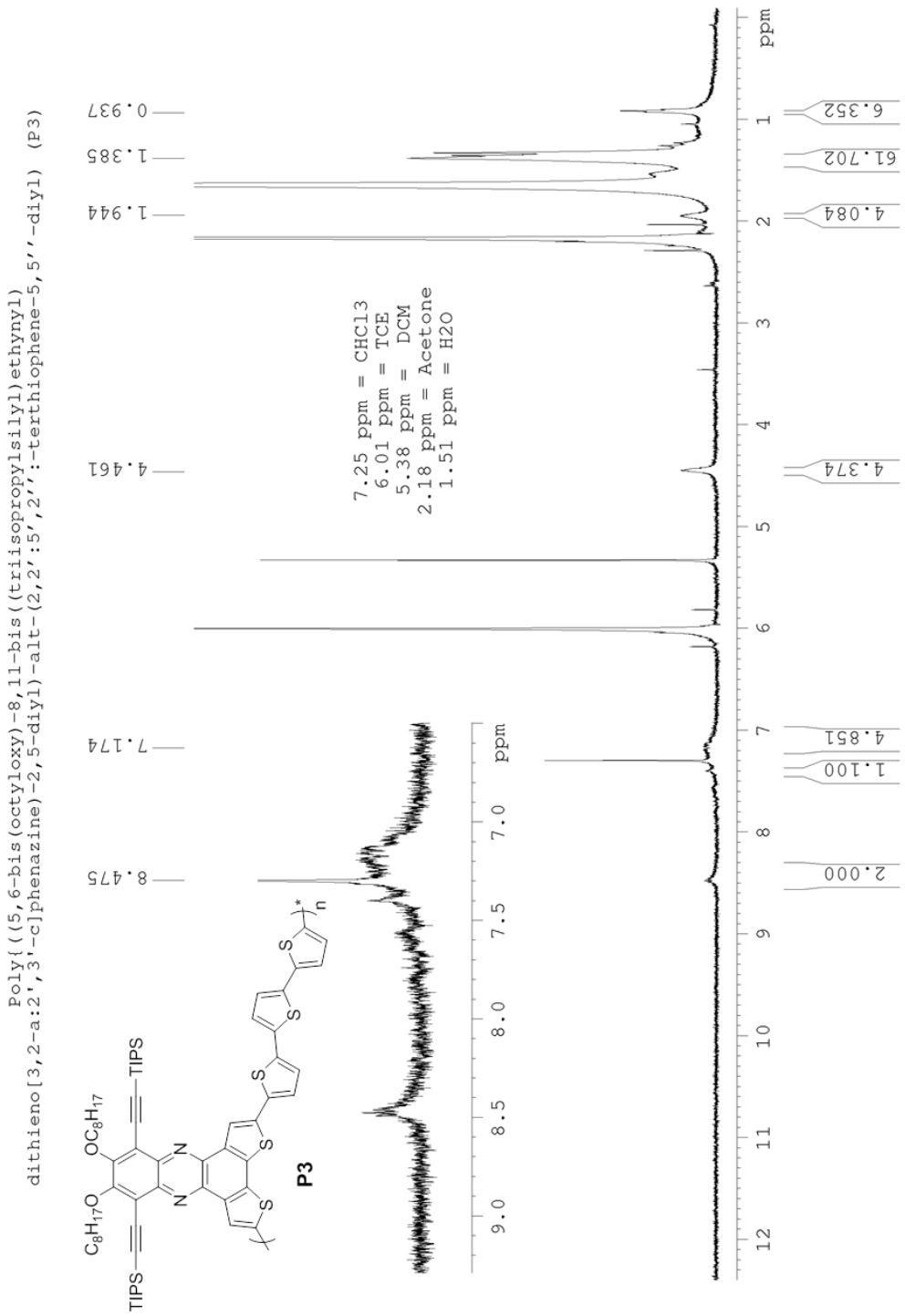

Figure 3.69. ^{1}H NMR of **P3**.

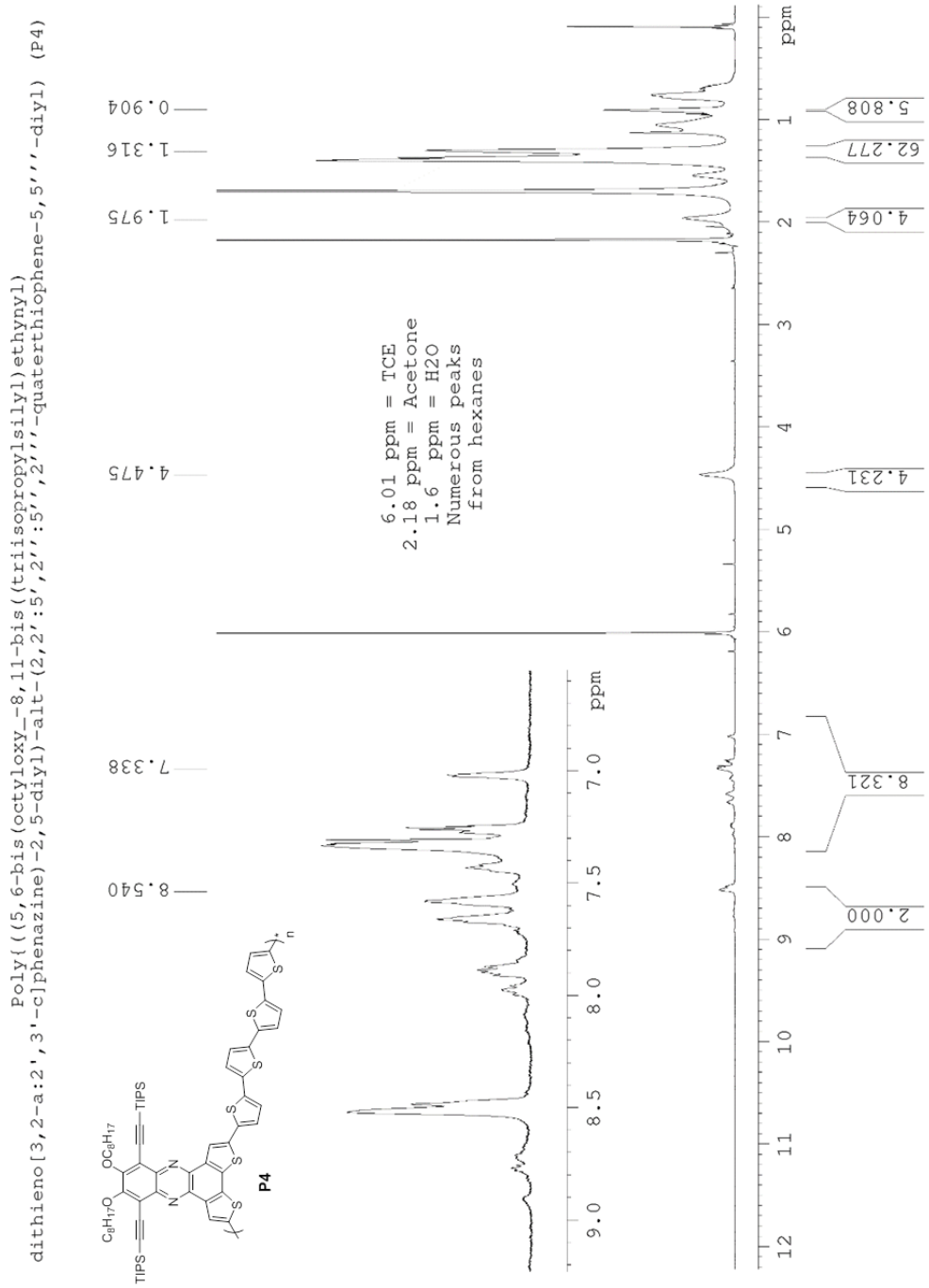

Figure 3.70. ^{1}H NMR of **P4**.

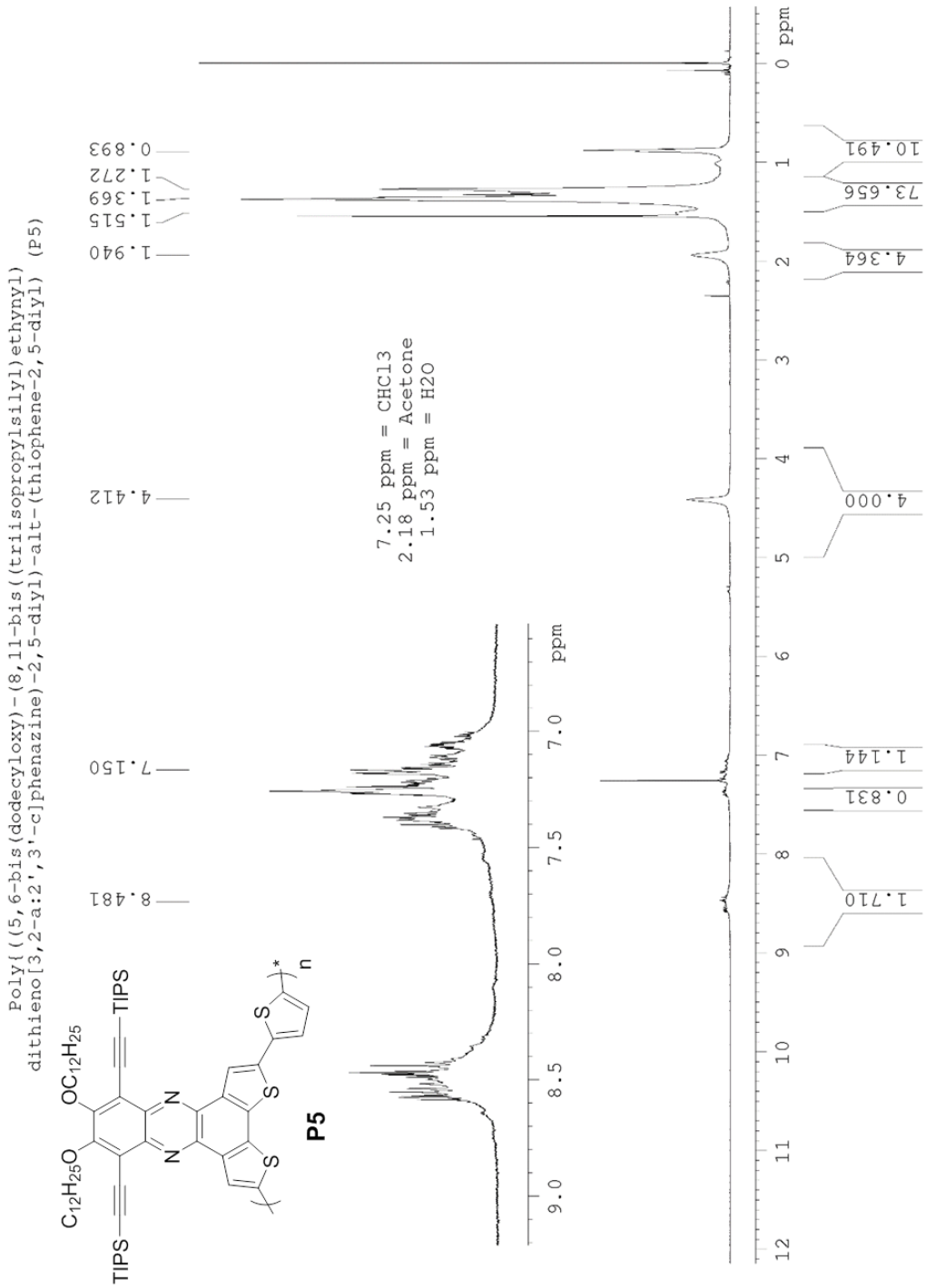

Figure 3.71. ^{1}H NMR spectrum of **P5**.

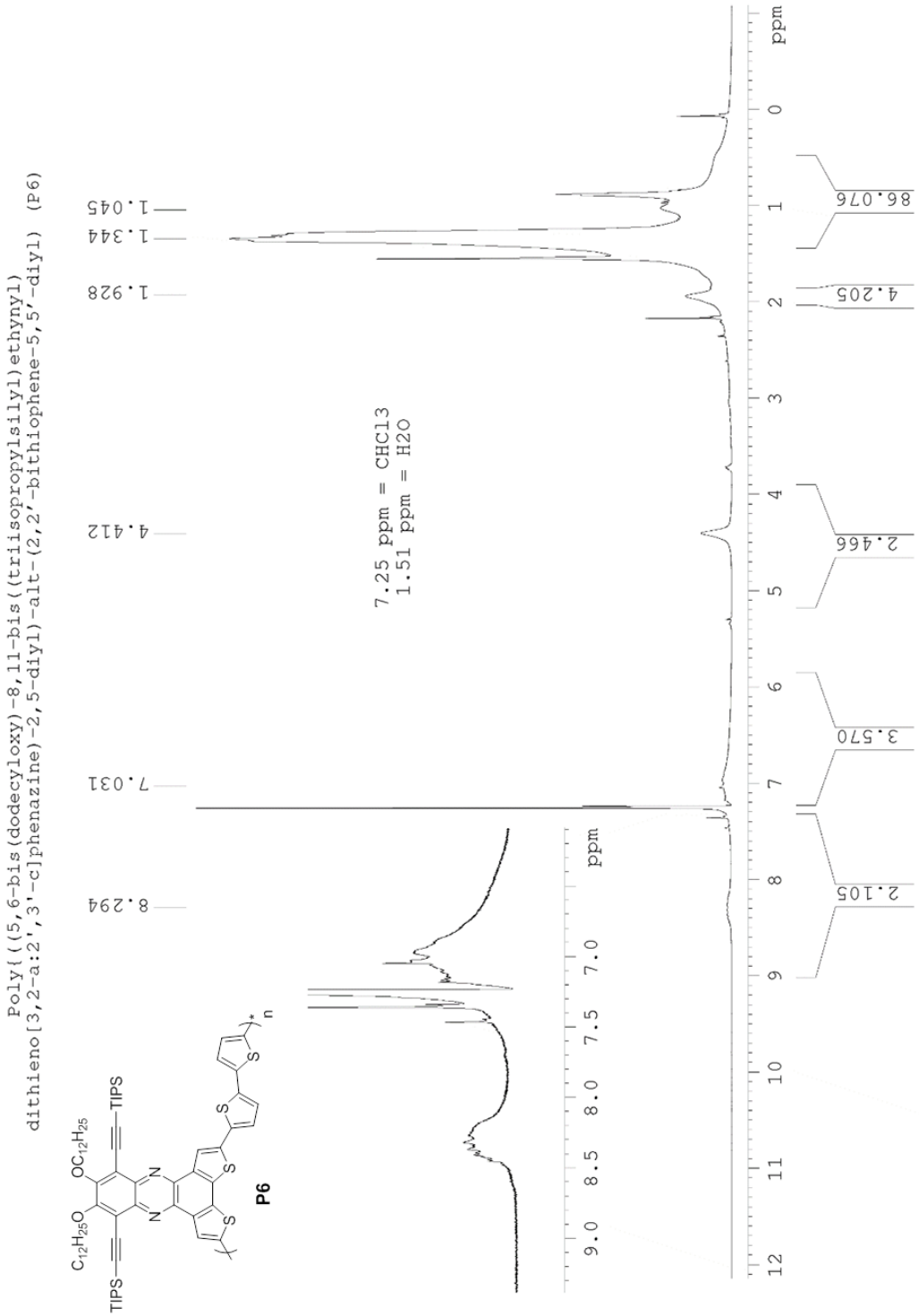

Figure 3.72. ^{1}H NMR spectrum of **P6**.

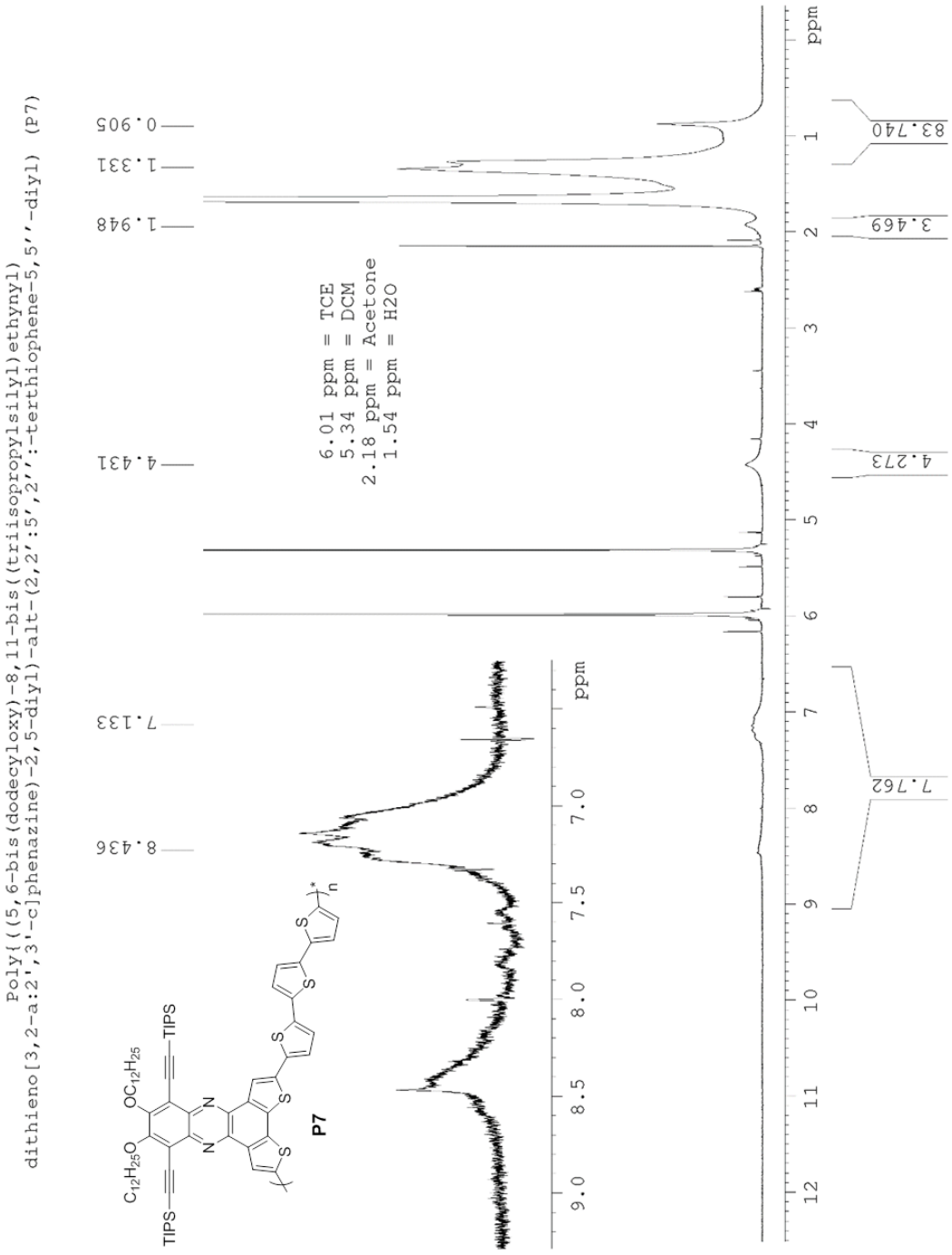

Figure 3.73. ^{1}H NMR spectrum of **P7.**

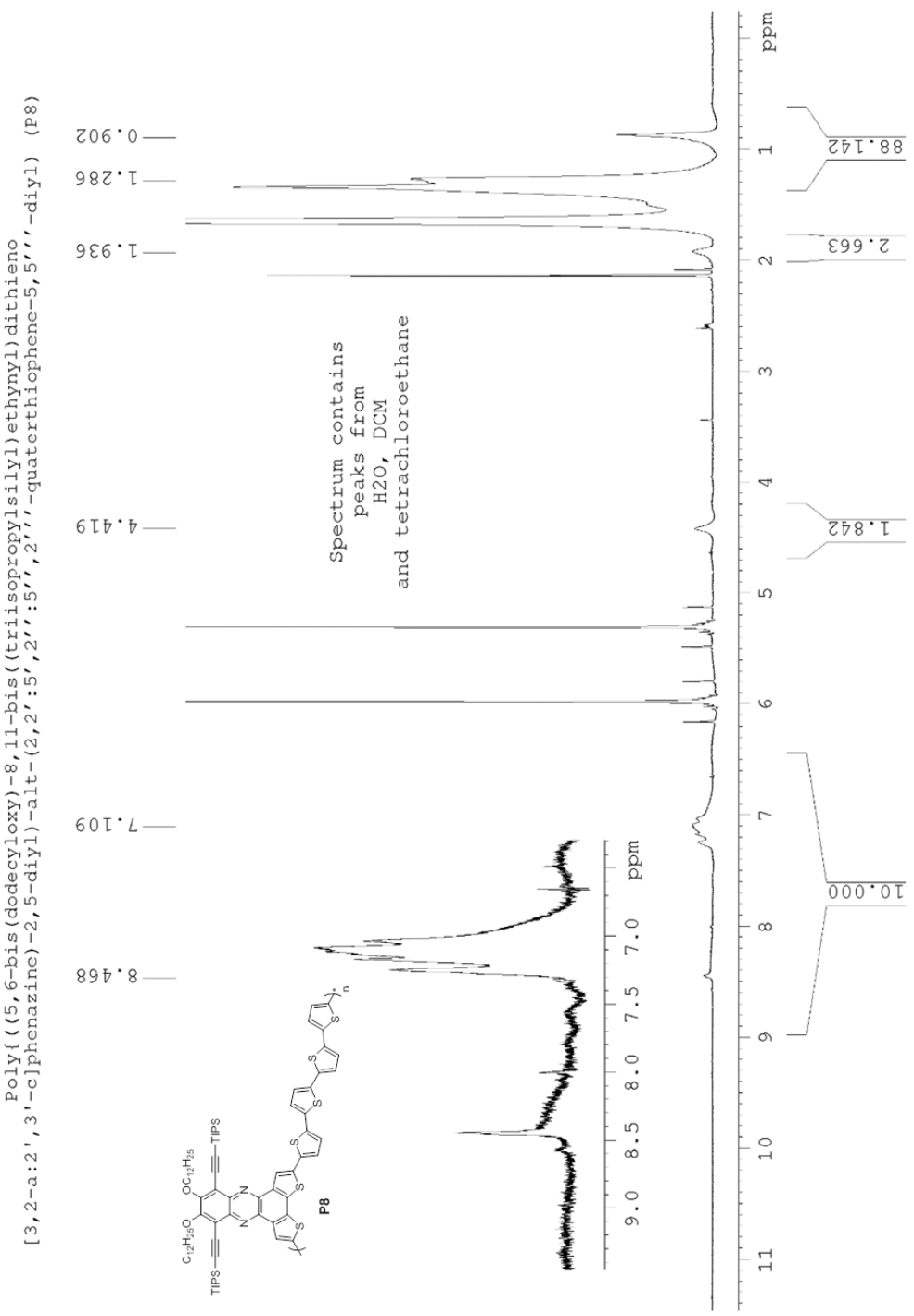

Figure 3.74. ^{1}H NMR spectrum of **P8**.

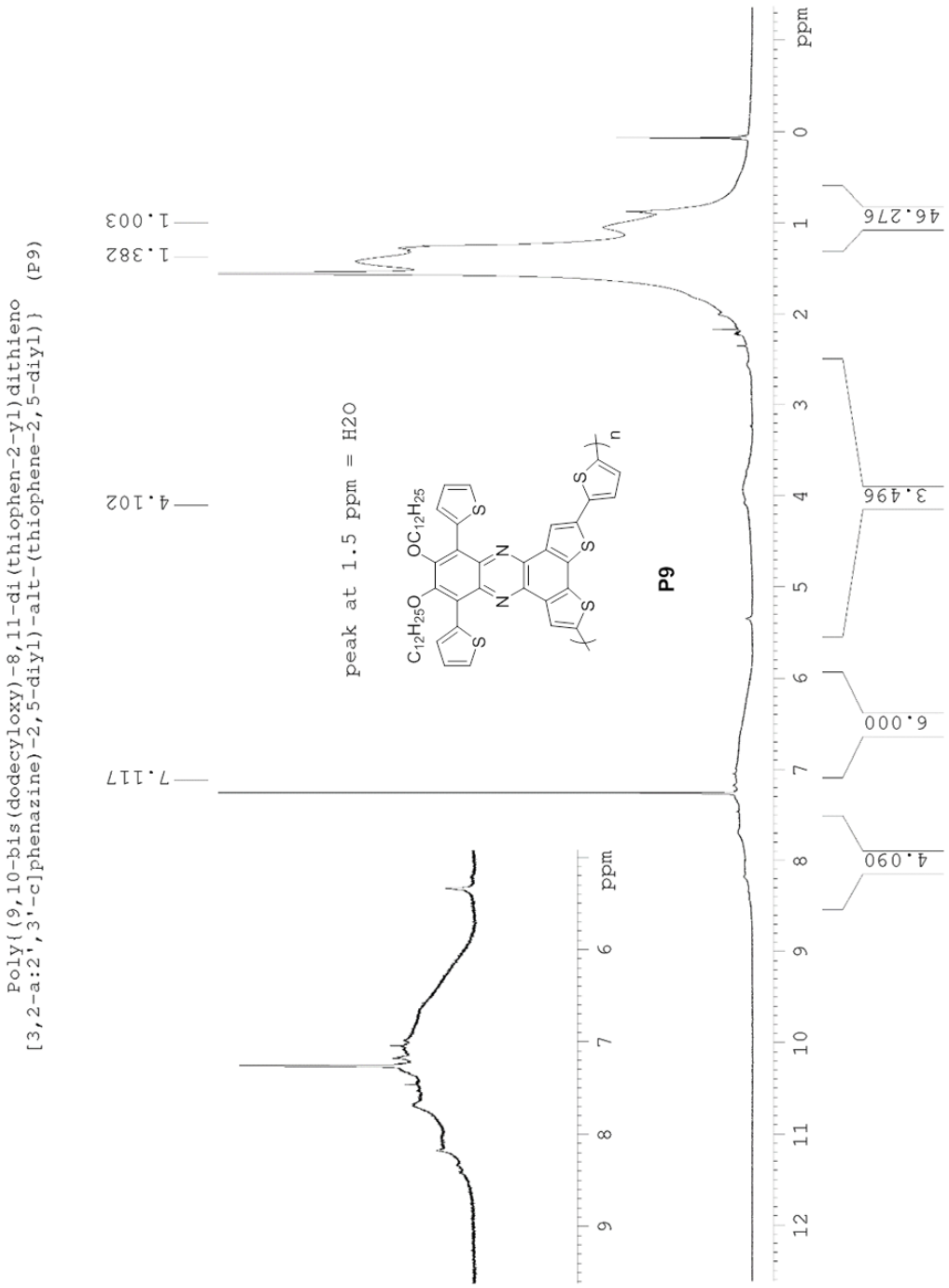

Figure 3.75. ^{1}H NMR spectrum of **P9**.

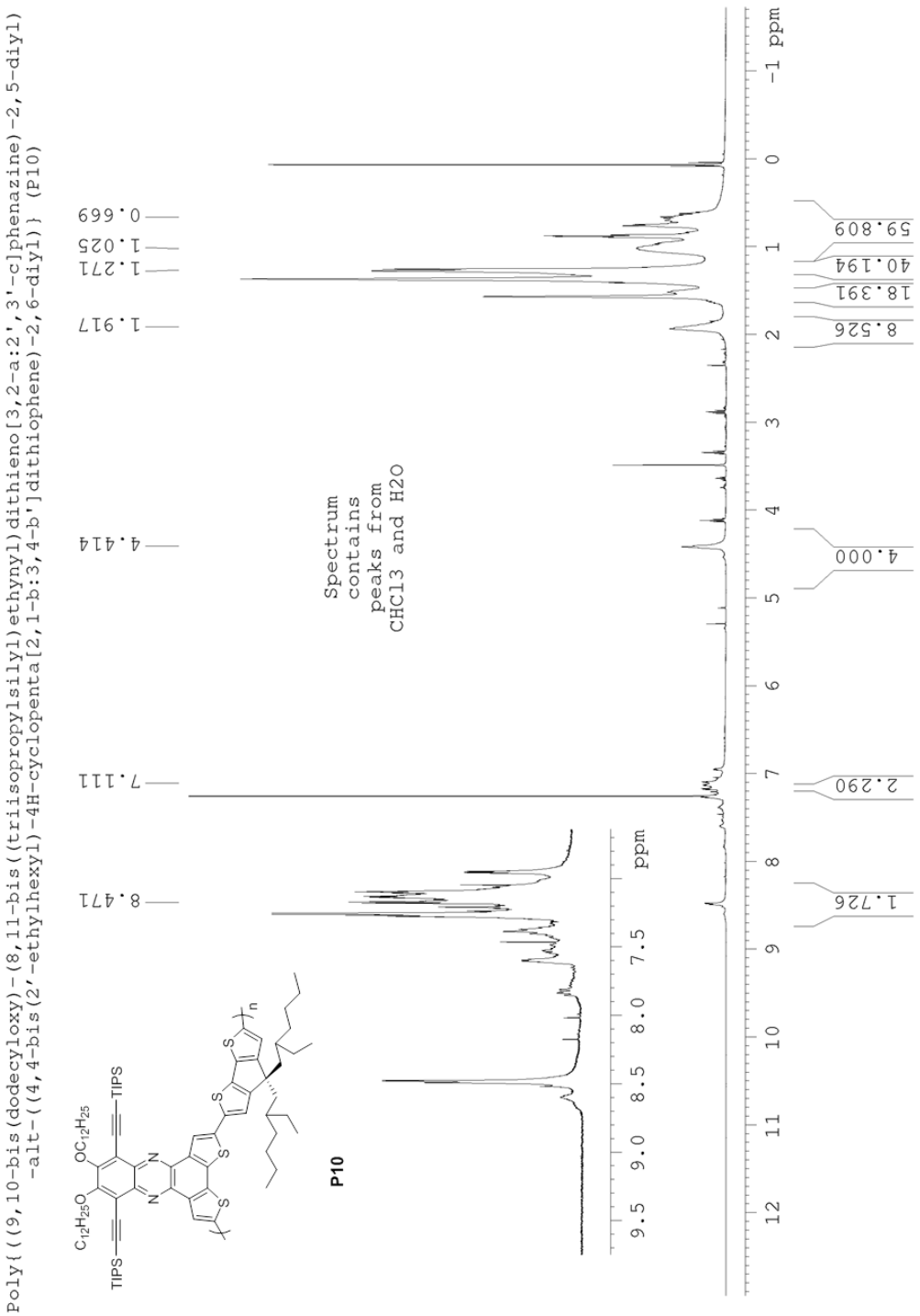

Figure 3.76. ^{1}H NMR of **P10**.

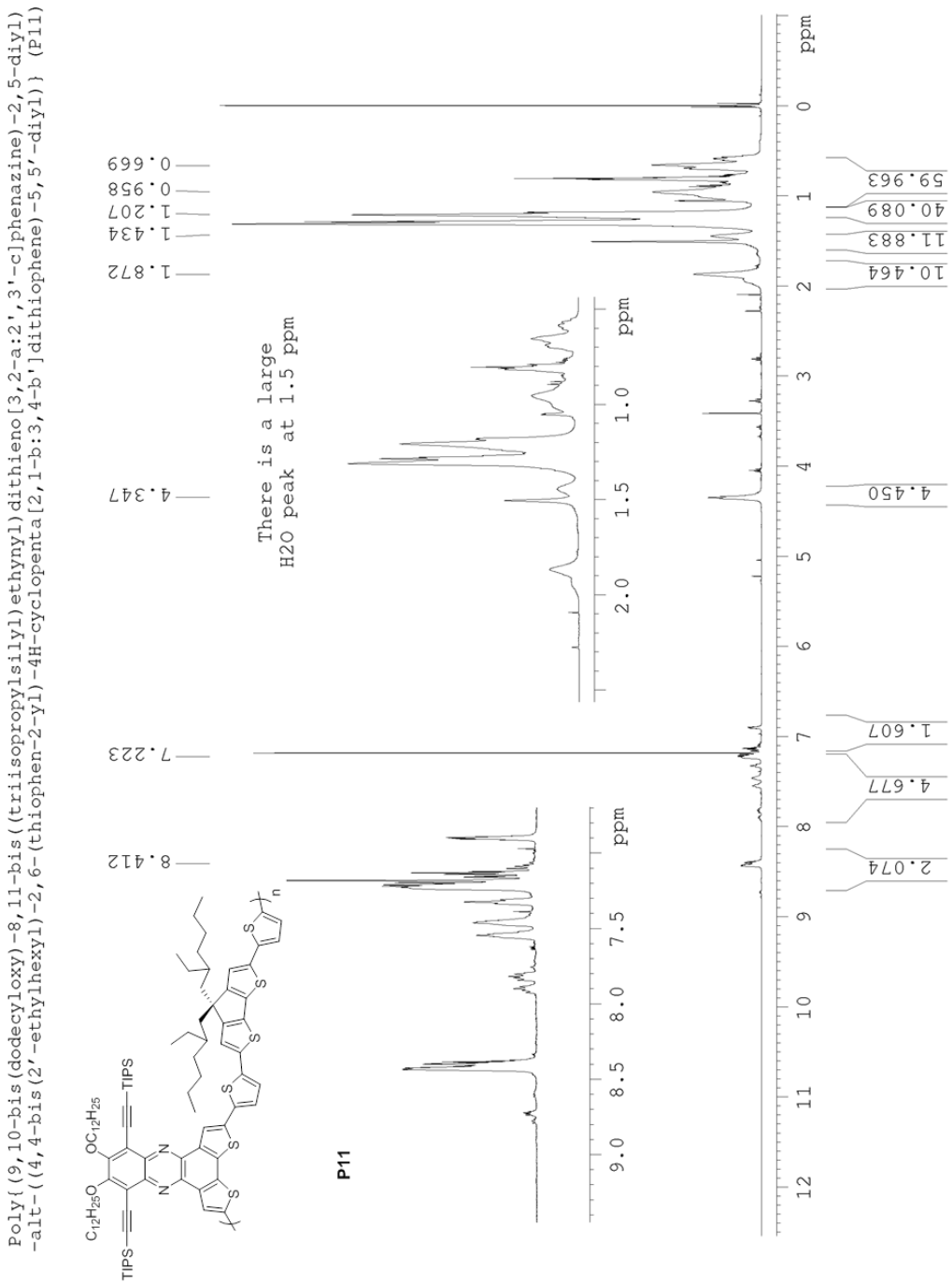

Figure 3.77. ^{1}H NMR **P11**.

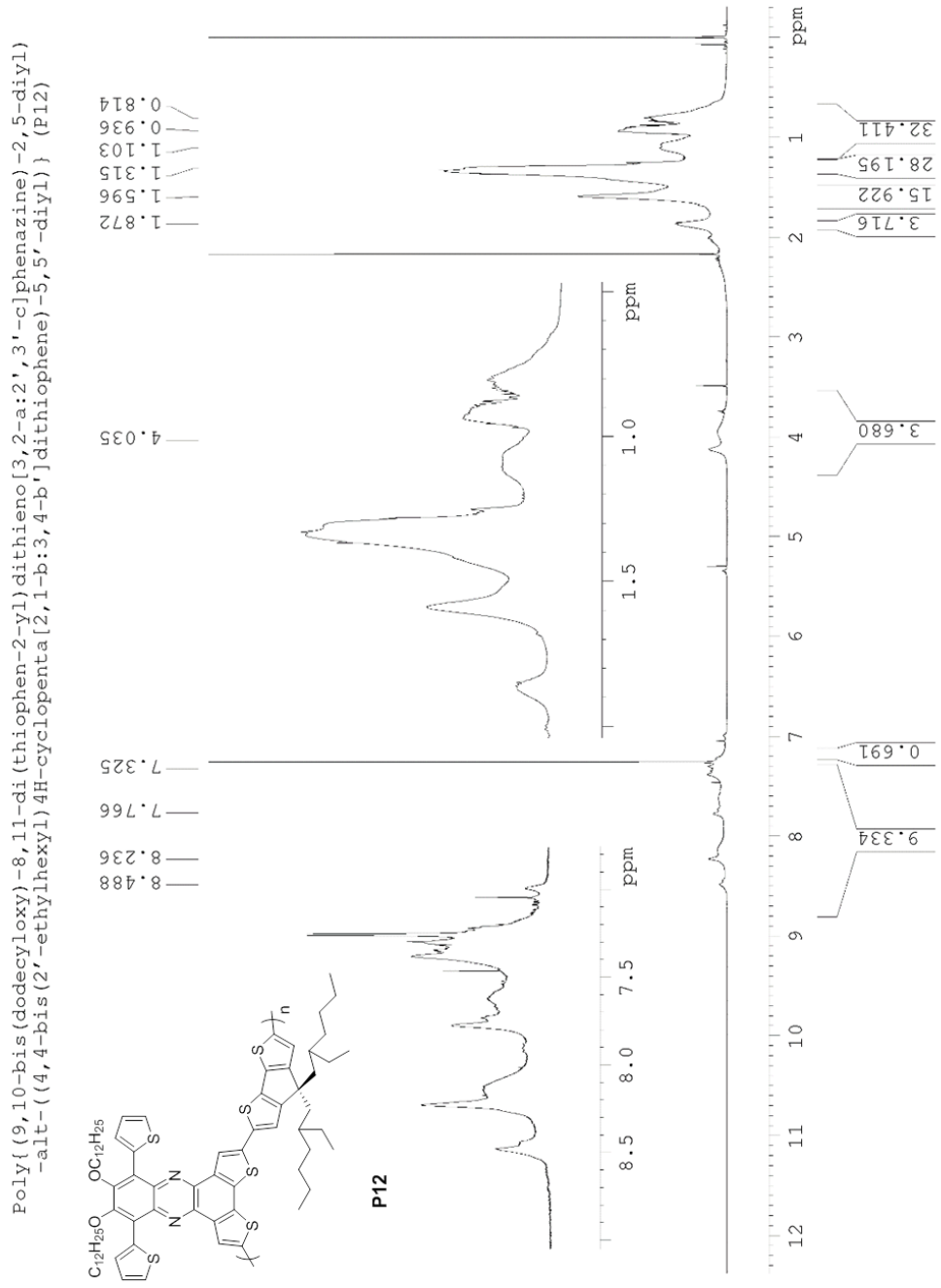

Figure 3.78. ^{1}H NMR of **P12**.

References

(1) Grimsdale, A. C.; Chan, K. L.; Martin, R. E.; Jokisz, P. G.; Holmes, A. B. Synthesis of Light-Emitting Conjugated Polymers for Applications in Electroluminescent Devices Synthesis of Light-Emitting Conjugated Polymers for Applications in Electroluminescent Devices. **2009**, *109*, 897–1091. DOI: 10.1021/cr000013v.

(2) Arias, A. C.; MacKenzie, J. D.; McCulloch, I.; Rivnay, J.; Salleo, A. Materials and applications for large area electronics: Solution-based approaches. *Chem. Rev.* **2010**, *110*, 3–24. DOI: 10.1021/cr900150b.

(3) Sirringhaus, H. 25th anniversary article: Organic field-effect transistors: The path beyond amorphous silicon. *Advanced Materials*. **2014**, *26*, 1319–1335.

(4) Forrest, S. R. The path to ubiquitous and low-cost organic electronic appliances on plastic. *Nature* **2004**, *428*, 911–918. DOI: 10.1038/nature02498.

(5) Li, C.; Liu, M.; Pschirer, N. G.; Baumgarten, M.; Müllen, K. Polyphenylene-Based Materials for Organic Photovoltaics. *Chem. Rev.* **2010**, *110*, 6817.

(6) Scharber, M. C.; Sariciftci, N. S. Progress in Polymer Science Efficiency of bulk-heterojunction organic solar cells. *Prog. Polym. Sci.* **2013**, *38*, 1929–1940. DOI: 10.1016/j.progpolymsci.2013.05.001.

(7) Li, G.; Zhu, R.; Yang, Y. Polymer solar cells. *Nat. Photonics* **2012**, *6*, 153–161. DOI: 10.1038/nphoton.2012.11.

(8) Kulkarni, A. P.; Tonzola, C. J.; Babel, A.; Jenekhe, S. A. Electron transport materials for organic light-emitting diodes. *Chem. Mater.* **2004**, *16*, 4556–4573. DOI: 10.1021/cm049473l.

(9) Thompson, B. C.; Kim, Y. G.; McCarley, T. D.; Reynolds, J. R. Soluble narrow band gap and blue propylenedioxythiophene-cyanovinylene polymers as multifunctional materials for photovoltaic and electrochromic applications. *J. Am. Chem. Soc.* **2006**, *128*, 12714–12725. DOI: 10.1021/ja061274a.

(10) Liu, Y.; Zhao, J.; Li, Z.; Mu, C.; Ma, W.; Hu, H.; Jiang, K.; Lin, H. Aggregation and morphology control enables multiple cases of high-efficiency polymer solar cells. *Nat. Commun.* **2014**, *5*, 1–8. DOI: 10.1038/ncomms6293.

(11) Kline, R. J.; DeLongchamp, D. M.; Fischer, D. A.; Lin, E. K.; Richter, L. J.; Chabinyc, M. L.; Toney, M. F.; Heeney, M.; McCulloch, I. Critical role of side-chain attachment density on the order and device performance of polythiophenes. *Macromolecules* **2007**, *40*, 7960–7965. DOI: 10.1021/ma0709001.

(12) Zhang, X.; Richter, L. J.; Delongchamp, D. M.; Kline, R. J.; Hammond, M. R.; McCulloch, I.; Heeney, M.; Ashraf, R. S.; Smith, J. N.; Anthopoulos, T. D.; et al. Molecular packing of high-mobility diketo pyrrolo-pyrrole polymer semiconductors with branched alkyl side chains. *J. Am. Chem. Soc.* **2011**, *133*, 15073–15084. DOI: 10.1021/ja204515s.

(13) Bronstein, H.; Leem, D. S.; Hamilton, R.; Woebkenberg, P.; King, S.; Zhang, W.; Ashraf, R. S.; Heeney, M.; Anthopoulos, T. D.; Mello, J. De; et al. Indacenodithiophene- co -benzothiadiazole Copolymers for High Performance Solar Cells or Transistors via Alkyl

Chain Optimization. *Macromolecules* **2011**, *44*, 6649–6652. DOI: 10.1021/ma201158d.

(14) Chen, Z.; Lee, M. J.; Shahid Ashraf, R.; Gu, Y.; Albert-Seifried, S.; Meedom Nielsen, M.; Schroeder, B.; Anthopoulos, T. D.; Heeney, M.; McCulloch, I.; et al. High-performance ambipolar diketopyrrolopyrrole-thieno[3,2-b]thiophene copolymer field-effect transistors with balanced hole and electron mobilities. *Adv. Mater.* **2012**, *24*, 647–652. DOI: 10.1002/adma.201102786.

(15) Tsao, H. N.; Cho, D. M.; Park, I.; Hansen, M. R.; Mavrinskiy, A.; Yoon, D. Y.; Graf, R.; Pisula, W.; Spiess, H. W.; Müllen, K. Ultrahigh mobility in polymer field-effect transistors by design. *J. Am. Chem. Soc.* **2011**, *133*, 2605–2612. DOI: 10.1021/ja108861q.

(16) Xu, T.; Yu, L. How to design low bandgap polymers for highly efficient organic solar cells. *Mater. Today* **2014**, *17*, 11–15. DOI: 10.1016/j.mattod.2013.12.005.

(17) Holliday, S.; Li, Y.; Luscombe, C. K. Recent advances in high performance donor-acceptor polymers for organic photovoltaics. *Prog. Polym. Sci.* **2017**, *70*, 34–51. DOI: 10.1016/j.progpolymsci.2017.03.003.

(18) Facchetti, A. Semiconductors for organic transistors. *Mater. Today* **2007**, *10*, 28–37. DOI: 10.1016/S1369-7021(07)70017-2.

(19) Facchetti, A. Polymer donor-polymer acceptor (all-polymer) solar cells. *Mater. Today* **2013**, *16*, 123–132. DOI: 10.1016/j.mattod.2013.04.005.

(20) Li, Y. Molecular design of photovoltaic materials for polymer solar cells: Toward suitable electronic energy levels and broad absorption. *Acc. Chem. Res.* **2012**, *45*, 723–733. DOI:

10.1021/ar2002446.

(21) An, C.; Puniredd, S. R.; Guo, X.; Stelzig, T.; Zhao, Y.; Pisula, W.; Baumgarten, M. Benzodithiophene-Thiadiazoloquinoxaline as an acceptor for ambipolar copolymers with deep LUMO level and distinct linkage pattern. *Macromolecules* **2014**, *47*, 979–986. DOI: 10.1021/ma401938m.

(22) Ye, Q.; Chang, J.; Huang, K. W.; Chi, C. Thiophene-fused tetracene diimide with low band gap and ambipolar behavior. *Org. Lett.* **2011**, *13*, 5960–5963. DOI: 10.1021/ol202357f.

(23) Wu, W.; Liu, Y.; Zhu, D. π-Conjugated molecules with fused rings for organic field-effect transistors: design, synthesis and applications. *Chem. Soc. Rev.* **2010**, *39*, 1489–1502. DOI: 10.1039/B813123F.

(24) Wang, E.; Hou, L.; Wang, Z.; Hellstrőm, S.; Mammo, W.; Zhang, F.; Inganős, O.; Andersson, M. R. Small band gap polymers synthesized via a modified nitration of 4,7-dibromo-2,1,3-benzothiadiazole. *Org. Lett.* **2010**, *12*, 4470–4473. DOI: 10.1021/ol1020724.

(25) Hasegawa, T.; Ashizawa, M.; Aoyagi, K.; Masunaga, H.; Hikima, T.; Matsumoto, H. Thiadiazole-fused Quinoxalineimide as an Electron-deficient Building Block for N-type Organic Semiconductors. *Org. Lett.* **2017**, *19*, 3275–3278. DOI: 10.1021/acs.orglett.7b01424.

(26) Planells, M.; Nikolka, M.; Hurhangee, M.; Tuladhar, P. S.; White, A. J. P.; Durrant, J. R.; Sirringhaus, H.; McCulloch, I. The effect of thiadiazole out-backbone displacement in indacenodithiophene semiconductor polymers. *J. Mater. Chem. C* **2014**, *2*, 8789–8795. DOI: 10.1039/C4TC01500B.

(27) An, C.; Li, M.; Marszalek, T.; Li, D.; Berger, R.; Pisula, W.; Baumgarten, M. Thiadizoloquinoxaline-based low-bandgap conjugated polymers as ambipolar semiconductors for organic field effect transistors. *Chem. Mater.* **2014**, *26*, 5923–5929. DOI: 10.1021/cm502563t.

(28) Mondal, R.; Becerril, H. a.; Verploegen, E.; Kim, D.; Norton, J. E.; Ko, S.; Miyaki, N.; Lee, S.; Toney, M. F.; Brédas, J.-L.; et al. Thiophene-rich fused-aromatic thienopyrazine acceptor for donor–acceptor low band-gap polymers for OTFT and polymer solar cell applications. *J. Mater. Chem.* **2010**, *20*, 5823. DOI: 10.1039/c0jm00903b.

(29) Zhang, Y.; Zou, J.; Yip, H.; Chen, K.; Davies, J. A.; Sun, Y.; Jen, A. K.-Y. Synthesis, Characterization, Charge Transport, and Photovoltaic Properties of Dithienobenzoquinoxaline- and Dithienobenzopyridopyrazine-Based Conjugated Polymers. *Macromolecules* **2011**, *44*, 4752–4758. DOI: 10.1021/ma2008699.

(30) Kauffmann, T.; Greving, B.; König, J.; Mitschker, A.; Woltermann, A. Synthese heterocyclischer Cyclopolyaromaten mit gleichartigen aromatischen Ringgliedern. *Angew. Chem.* **1975**, *87*, 745–746. DOI: 10.1002/ange.19750872011.

(31) Guégano, X.; Kanibolotsky, A. L.; Blum, C.; Mertens, S. F. L.; Liu, S. X.; Neels, A.; Hagemann, H.; Skabara, P. J.; Leutwyler, S.; Wandlowski, T.; et al. Pronounced electrochemical amphotericity of a fused donor-acceptor compound: A planar merge of TTF with a TCNQ-Ttype bithienoquinoxaline. *Chem. - A Eur. J.* **2009**, *15*, 63–66. DOI: 10.1002/chem.200802011.

(32) Meyer, A.; Sigmund, E.; Luppertz, F.; Schnakenburg, G.; Gadaczek, I.; Bredow, T.; Jester,

S. S.; Höger, S. Syntheses and properties of thienyl-substituted dithienophenazines. *Beilstein J. Org. Chem.* **2010**, *6*, 1180–1187. DOI: 10.3762/bjoc.6.135.

(33) Chen, Y.; Lu, X.; Xiang, C.; Ling, Y.; Zhou, G. Charge Transfer Through Dithieno[2,3-a:3,2-c]phenazine: Effect of Substitution Pattern on the Optoelectronic Properties of Regioisomeric Luminophores. *Chem. - An Asian J.* **2016**, *11*, 874–881. DOI: 10.1002/asia.201501389.

(34) Du, C.; Li, W.; Li, C.; Bo, Z. Ethynylene-containing donor-acceptor alternating conjugated polymers: Synthesis and photovoltaic properties. *J. Polym. Sci. Part A Polym. Chem.* **2013**, *51*, 383–393. DOI: 10.1002/pola.26396.

(35) Coombs, B. A.; Lindner, B. D.; Edkins, R. M.; Rominger, F.; Beeby, A.; Bunz, U. H. F. Photophysical property trends for a homologous series of bis-ethynyl-substituted benzochalcogendiazoles. *New J. Chem.* **2012**, *36*, 550–553. DOI: 10.1039/C2NJ20847D.

(36) Zhang, Y.; Zou, J.; Yip, H.-L.; Sun, Y.; Davies, J. a.; Chen, K.-S.; Acton, O.; Jen, A. K.-Y. Conjugated polymers based on C, Si and N-bridged dithiophene and thienopyrroledione units: synthesis, field-effect transistors and bulk heterojunction polymer solar cells. *J. Mater. Chem.* **2011**, *21*, 3895. DOI: 10.1039/c0jm03927f.

(37) Würthner, F.; Kaiser, T. E.; Saha-Möller, C. R. J-aggregates: From serendipitous discovery to supramolecular engineering of functional dye materials. *Angew. Chemie - Int. Ed.* **2011**, *50*, 3376–3410. DOI: 10.1002/anie.201002307.

(38) Aguirre, J. C.; Hawks, S. A.; Ferreira, A. S.; Yee, P.; Subramaniyan, S.; Jenekhe, S. A.; Tolbert, S. H.; Schwartz, B. J. Sequential processing for organic photovoltaics: Design

rules for morphology control by tailored semi-orthogonal solvent blends. *Adv. Energy Mater.* **2015**, *5*, 1–11. DOI: 10.1002/aenm.201402020.

(39) Cho, E.; Risko, C.; Kim, D.; Gysel, R.; Cates Miller, N.; Breiby, D. W.; McGehee, M. D.; Toney, M. F.; Kline, R. J.; Bredas, J. L. Three-dimensional packing structure and electronic properties of biaxially oriented poly(2,5-bis(3-alkylthiophene-2-yl)thieno[3,2- b]thiophene) films. *J. Am. Chem. Soc.* **2012**, *134*, 6177–6190. DOI: 10.1021/ja210272z.

(40) Cabanetos, C.; El Labban, A.; Bartelt, J. A.; Douglas, J. D.; Mateker, W. R.; Fréchet, J. M. J.; McGehee, M. D.; Beaujuge, P. M. Linear side chains in benzo[1,2-b:4,5-b']dithiophene-thieno[3,4-c] pyrrole-4,6-dione polymers direct self-assembly and solar cell performance. *J. Am. Chem. Soc.* **2013**, *135*, 4656–4659. DOI: 10.1021/ja400365b.

(41) Yiu, A. T.; Beaujuge, P. M.; Lee, O. P.; Woo, C. H.; Toney, M. F.; Fréchet, J. M. J. Side-chain tunability of furan-containing low-band-gap polymers provides control of structural order in efficient solar cells. *J. Am. Chem. Soc.* **2012**, *134*, 2180–2185. DOI: 10.1021/ja2089662.

(42) Kim, C. H.; Hlaing, H.; Carta, F.; Bonnassieux, Y.; Horowitz, G.; Kymissis, I. Templating and charge injection from copper electrodes into solution-processed organic field-effect transistors. *ACS Appl. Mater. Interfaces* **2013**, *5*, 3716–3721. DOI: 10.1021/am400325k.

(43) Kline, R. J.; McGehee, M. D.; Kadnikova, E. N.; Liu, J.; Fréchet, J. M. J. Controlling the field-effect mobility of regioregular polythiophene by changing the molecular weight. *Adv. Mater.* **2003**, *15*, 1519–1522. DOI: 10.1002/adma.200305275.

(44) Kim, Y. J.; Cheon, Y. R.; Back, J. Y.; Kim, Y.-H.; Chung, D. S.; Park, C. E. Naphtho[2,1- *b* :3,4- *b* ']dithiophene-based Bulk Heterojunction Solar Cells: How Molecular Structure

Influences Nanoscale Morphology and Photovoltaic Properties. *ChemPhysChem* **2014**, *15*, 3626–3633. DOI: 10.1002/cphc.201402295.

(45) Isse, A. A.; Gennaro, A. Absolute Potential of the Standard Hydrogen Electrode and the Problem of Interconversion of Potentials in Different Solvents. *J. Phys. Chem. B* **2010**, *114*, 7894–7899. DOI: 10.1021/jp100402x.

(46) Haynes W. M. *CRC Handbook of Chemistry and Physics, 97th Edition*; 2017.

(47) Lee, J. K.; Ma, W. L.; Brabec, C. J.; Yuen, J.; Moon, J. S.; Kim, J. Y.; Lee, K.; Bazan, G. C.; Heeger, A. J. Processing Additives for Improved Efficiency from Bulk Heterojunction Solar Cells. *J. Am. Chem. Soc.* **2008**, *130*, 3619–3623. DOI: 10.1021/ja710079w.

(48) Arroyave, F. A.; Richard, C. A.; Reynolds, J. R. Efficient Synthesis of Benzo[1,2-b:6,5-b']dithiophene-4,5-dione (BDTD) and Its Chemical Transformations into Precursors for π-Conjugated Materials. *Org. Lett.* **2012**, *14*, 6138–6141. DOI: 10.1021/ol302704v.

Acknowledgements

CV data was collected by Terri Lin, GIWAXs data was collected and reduced by KJ Winchell and Patrick Yee. Single crystal diffractometry data was collected and analyzed by Saeed Khan. Mathew Fontana was responsible for fabricating and collecting data on solar cells created from **P1** and PCBM. The author would also like to thank professor Barry Thompson and his student Betsy Melenbrink for help with gel permeation chromatography measurements and use of their laboratory.

Chapter 4 : Synthesis and characterization of novel polymers and small molecules based on fused heteroacenes

Fused π-donor π-acceptor semiconductors based on benzodithiophene fused *N*-heteroacenes

There is a significant amount of literature on fused π-donor π-acceptor small molecules consisting of an electron rich unit (usually a thiophene, or thiophene derivative) and an electron deficient unit (usually a *N*-heteroacene, or thiadiazole derivative) fused through two or more covalent linkages.[1,2,3,4] In terms of chemical and physical properties, perhaps the simplest and most stereotypical example of such a fused π-donor π-acceptor small molecule would be thieno[3,4-b]pyrazine. Figure 4.1 shows the two resonance structures inherent to the fused rings of thieno[3,4-b]pyrazine. It can be seen that the thiophene ring in the "aromatic" resonance structure contains a formal aromatic sextet of electrons (2 π bonds and one lone pair localized on the sulfur atom) while the pyrazine ring in the "quinoidal" resonance structure of thieno[3,4-b]pyrazine contains a formal aromatic sextet of electrons (3 π bonds). The quinoidal resonance structure of thieno[3,4-b]pyrazine is stabilized due to the aromatization of the pyrazine ring, and this strong quinoidal character imparted to thieno[3,4-b]pyrazine by this resonance stabilization allows thieno[3,4-b]pyrazine to function as a π acceptor unit in copolymers consisting of alternating π-donor and π-acceptor (πD-πA) units.[5,6,7] Thieno[3,4-b]pyrazine containing πD-πA copolymers often have narrow band gaps, semi-reversible oxidation and reduction behavior, low HOMO levels compared to P3HT, and moderate PCEs when incorporated as the electron donating component of organic photovoltaic devices (high of 2.4%).[8]

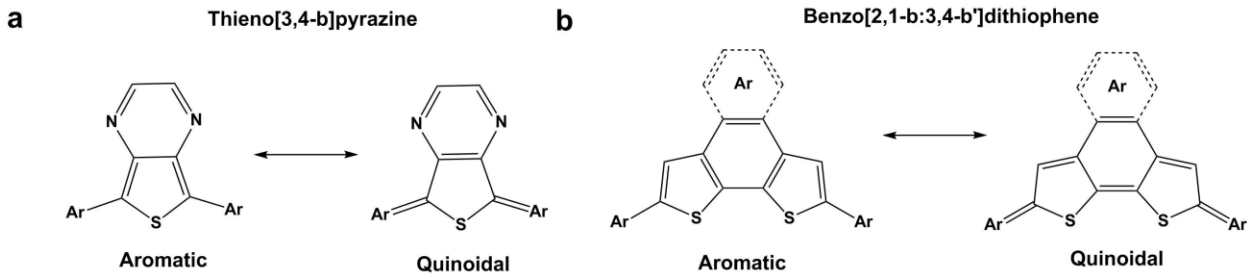

Figure 4.1. Comparison of the aromatic and quinoidal resonance structures of a) thieno[3,4-b]pyrazine and b) benzo[2,1-b:3,4-b']dithiophene.

Benzodithiophenes are electron rich systems often employed in πD-πA copolymers. There are two regioisomers of benzodithiophene: benzo[1,2-b:4,5-b']dithiophene and benzo[2,1-b:3,4-b']dithiophene This chapter focuses on the former of the two regioisomers, but it will be noted that the latter regioisomer has been studied extensively elsewhere in the literature.[9,10,11] As can be seen in Figure 4.1, benzo[2,1-b:3,4-b']dithiophene has a more stabilized aromatic resonance structure compared to the quinoidal resonance structure because aromaticity is lost in the central benzene ring in the quinoidal form, thereby destabilizing it. The relative stability of the aromatic resonance structure compared to the quinoidal resonance structure therefore causes benzodithiophenes to be electron rich. One way of destabilizing the aromaticity of the central benzene ring in benzo[2,1-b:3,4-b']dithiophene is to fuse an aromatic unit at the 4 and 5 positions. Extending the aromatic π system in such a way decreases the relative stability of the aromatic *vs*. quinoidal resonance structure because the quinoidal resonance structure creates a formal aromatic sextet of pi π electrons in the aromatic ring fused at the 4 and 5 positions.

This decrease in the relative stability of the quinoidal *vs.* the aromatic resonance structure decreases the band gap of benzo[2,1-b:3,4-b']dithiophene and also makes the unit less electron rich. If the aromatic group substituted at the 4 and 5 positions is an electron deficient aromatic group such as a [2,1,3] thiadiazole unit or an *N*-heteroacene, the quinoidal resonance structure can be further stabilized and the resulting monomer unit can function as a π acceptor in πD-πA copolymers.

Electron deficient monomer units utilizing dithieno[3',2':3,4;2'',3'':5,6]benzo[1,2-c][1,2,5]thiadiazole (see Figure 4.2) were first reported by Mei *et al.*[12] and πD-πA copolymers based on this monomer unit polymerized at the 5 and 8 positions exhibit very deep HOMO levels (—5.6 eV *vs.* vacuum level), broad visible absorption (E_g = 1.6 eV) and achieved a power conversion efficiencies of 4.4 % when blended with $PC_{61}BM$. Several other groups have also published work based on πD-πA copolymers containing dithieno[3',2':3,4;2'',3'':5,6]benzo[1,2-c][1,2,5]thiadiazole and have explored their use in organic photovoltaic devices as well. The synthesized polymers possess many of the same attractive features such as deep HOMO levels and band gaps near 1.5 eV. Efrem *et al.* achieved power conversion efficiencies of 2.2% in photovoltaic devices using a copolymer consisting of dithieno[3',2':3,4;2'',3'':5,6]benzo[1,2-c][1,2,5]thiadiazole and alkylated quaterthiophene,[13] and Planells et. al. reported a power conversion efficiency of 2.2 % using a copolymer consisting of dithieno[3',2':3,4;2'',3'':5,6] benzo[1,2-c][1,2,5]thiadiazole and indacenodithiophene.[14]

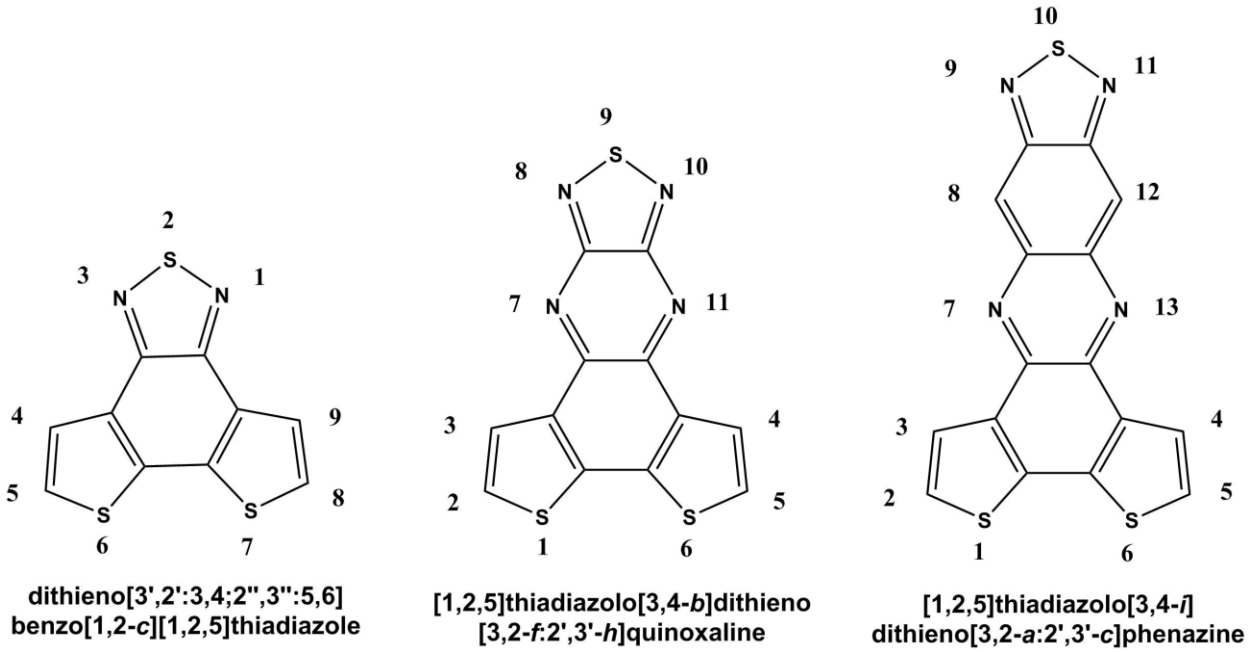

Figure 4.2. Electron deficient monomers based on fused heteroacene derivatives of benzo[2,1-b:3,4-b']dithiophene and the IUPAC numbering of the positions of these derivatives.

Extending the π conjugation of dithieno[3',2':3,4;2'',3'':5,6]benzo[1,2-c][1,2,5]thiadiazole by inserting a pyrazine ring between the benzene ring and the [2,1,3]thiadiazole unit further increases the π acceptor character of the benzodithiophene unit (see Figure 4.2). Planells *et al.* also reported the synthesis of πD-πA copolymers consisting of the monomer unit [1,2,5]thiadiazolo[3,4-b]dithieno[3,2-f:2',3'-h]quinoxaline copolymerized with indacenodithiophene.[14] Polymers synthesized from the [1,2,5]thiadiazolo[3,4-b]dithieno[3,2-f:2',3'-h]quinoxaline monomer unit have a slightly higher HOMO level than polymers synthesized from the dithieno[3',2':3,4;2'',3'':5,6]benzo[1,2-c][1,2,5]thiadiazole unit (-5.43 compared -5.47 eV *vs.* vacuum level), but polymers based on the former polymer had significantly reduced band gaps with respect to the latter polymer (1.38 eV *vs.* 2.02 eV) due to the addition of a pyrazine unit and subsequent extension of the π system. The

thiadiazoloquinoxaline based copolymers also exhibited an intermolecular charge transfer band in solution owing to intermolecular charge transfer from the benzodithiophene unit to the thiadiazoloquinoxaline unit. Indacenodithiophene-[1,2,5]thiadiazolo[3,4-b]dithieno[3,2-f:2',3'-h]quinoxaline copolymers exhibited lower power conversion efficiencies compared to the indacenodithiophene-dithieno[3',2':3,4;2'',3'':5,6]benzo[1,2-c][1,2,5]thiadiazole copolymers (1.34% *vs.* 2.2%), mostly due to the decreased solubility of the former polymer compared to the latter.

Baumgarten *et al.* explored the properties of [1,2,5]thiadiazolo[3,4-i]dithieno[3,2-a:2',3'-c]phenazine derivatives and closely related aryl substituted thiadiazoloquinoxaline in a series of several papers.[15,16,17,18,19] Small molecules derivatives of [1,2,5]thiadiazolo[3,4-i]dithieno[3,2-a:2',3'-c]phenazine substituted at the 8 and 12 positions with alkynyl[18] and thienyl[20] substituents exhibited small band gaps (1.86 and 1.6 eV respectively) and low lying HOMO (-5.7 and -5.1 eV *vs.* vacuum level) and LUMO orbitals (-3.92 and -3.44). Both of these derivatives displayed high crystallinity in the solid state resulting from strong intermolecular π-π interactions. An *et al.* reported the synthesis of a series of copolymers consisting of [1,2,5]thiadiazolo[3,4-i]dithieno[3,2-a:2',3'-c]phenazine covalently linked at the 8 and 12 positions with alkylated quaterthiophenes (see Figure 4.3). These copolymers were found to have high field effect mobilities of 0.22 cm^2 V^{-1} s^{-1}, narrow optical band gaps (0.76 eV) and moderately low lying HOMO orbitals (-5.05 eV *vs.* vacuum level) and ambipolar charge transport. An et. al. also reported the properties of two copolymers consisting of an alkylated derivative of [1,2,5]thiadiazolo[3,4-i]dithieno[3,2-a:2',3'-c]phenazine covalently linked at the 8 and 12 positions with alkylated quaterthiophenes, and a 8 and 12 thienyl substituted of

[1,2,5]thiadiazolo[3,4-i]dithieno[3,2-a:2',3'-c]phenazine derivative copolymerized at the 2 and 5 positions with 2,2'-bithiophene. These polymers exhibited narrow band gaps (1.64 and 1.47 for the former and the latter respectively) and low lying HOMO (-5.50 and -5.48 eV *vs.* vacuum level for the former and the latter respectively) and LUMO levels (-3.86 and -4.01 eV *vs.* vacuum level respectively). Interestingly the copolymer resulting from the polymerization at the 8 and 12 positions of the [1,2,5]thiadiazolo[3,4-i]dithieno[3,2-a:2',3'-c]phenazine showed ambipolar charge transport measured in OFET devices (1.2 X 10^{-3} and 6.0 X 10^{-4} cm^2 V^{-1} s^{-1} for holes and electrons respectively), while the copolymer resulting from substitution at the 2 and 5 positions had no measurable field effect response. Based on the exciting materials properties of these copolymers reported by An *et al.* we decided to synthesis synthetically similar copolymers for use in OPVs.

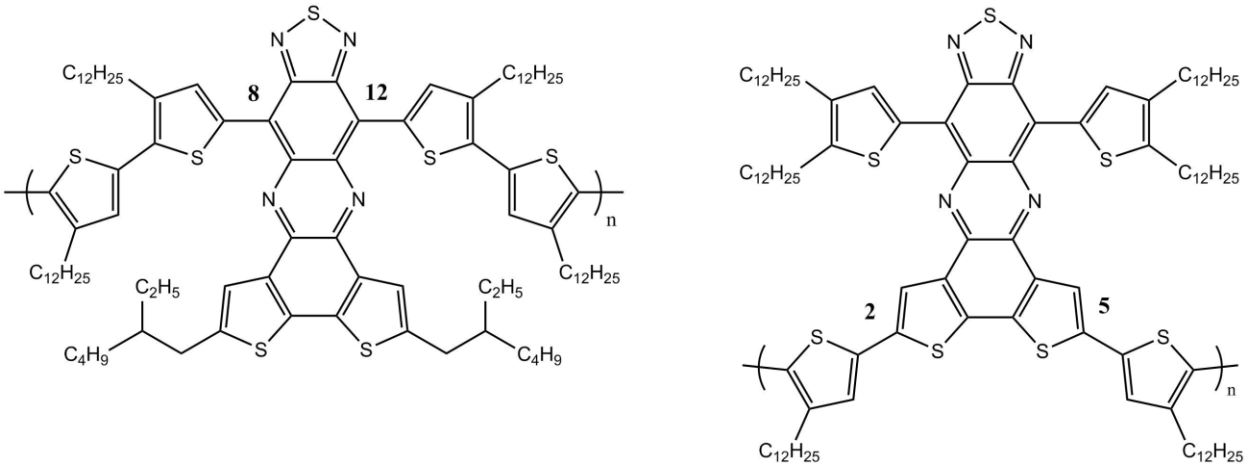

Figure 4.3. πD-πA copolymers containing [1,2,5]thiadiazolo[3,4-i]dithieno[3,2-a:2',3'-c]phenazine reported by An *et al*.

This chapter outlines the synthesis and physical properties of πD-πA copolymers containing dithieno[3',2':3,4;2'',3'':5,6]benzo[1,2-c][1,2,5]thiadiazole as a π acceptor unit, as well as πD-πA copolymers containing [1,2,5]thiadiazolo[3,4-i]dithieno[3,2-a:2',3'-c]phenazine as the acceptor unit. It also contains the synthesis of and physical properties of soluble small molecule acceptors consisting of pyrene units fused at the 4, 5, 9, and 10 positions with alkynyl substituted [1,2,5]thiadiazolo[3,4-g]quinoxaline. These materials exhibit similar electrochemical and photophysical characteristics of similar previously reported derivatives consisting of aryl substituted [1,2,5]thiadiazolo[3,4-g]quinoxalines fused to pyrene molecules.[21] Finally the chapter reviews synthesis and physical characteristics of small molecule donor molecules consisting of π extended derivatives of dithieno[3,2-a:2',3'-c]phenazine.

Synthesis of π extended derivate of alkynyl substituted [1,2,5]thiadiazolo[3,4-g]quinoxaline derivatives

The general strategy employed for the synthesis many of the molecules studied in this paper utilizes the condensation of 4,7-bis((triisopropylsilyl)ethynyl)benzo[c][1,2,5]thiadiazole-5,6-diamine with various *o*-diketones. 5,6-dinitro-4,7-bis((triisopropylsilyl)ethynyl)benzo[c][1,2,5]thiadiazole (**1**) can be selectively reduced using iron powder in slightly acidic media to yield the aforementioned diamine (Figure 4.4). 4,7-Bis((triisopropylsilyl)ethynyl)benzo[c][1,2,5]thiadiazole-5,6-diamine is relatively air stable, but degrades slowly at room temperature over the course of several days; therefore, the compound was used soon after it was produced to limit the amount of difficult to separate side products in subsequent reactions.

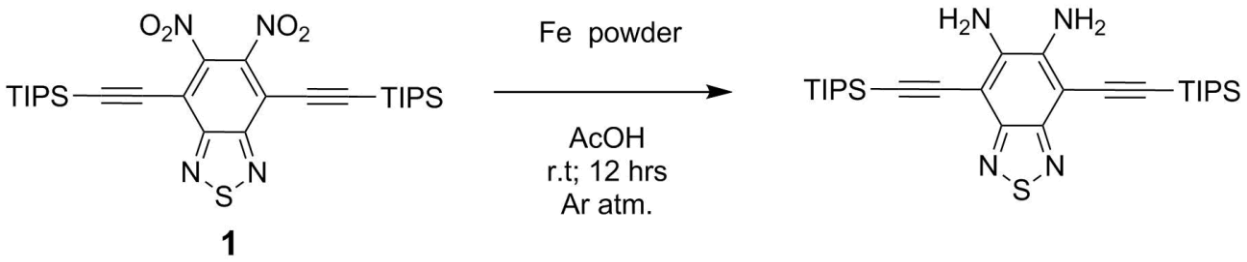

Figure 4.4. Selective reduction of *ortho*-dinitrobenzenes to *ortho*-phenylenediamines in the presence of substituted benzo[c][1,2,5]thiadiazoles.

Bis((triisopropylsilyl)ethynyl)benzo[c][1,2,5]thiadiazole-5,6-diamine was condensed onto 2,7-dibromobenzo[2,1-b:3,4-b']dithiophene-4,5-dione (**2**) using acetic acid as a catalyst to generate 2,5-dibromo-8,12-bis((triisopropylsilyl)ethynyl)-[1,2,5]thiadiazolo[3,4-i]dithieno[3,2-a:2',3'-c]phenazine (**3**) (Figure 4.5). Interestingly use of stronger acids such as sulfuric acid or polystyrene sulfonic acid retarded the condensation reaction, presumably because stronger acids were able to protonate the *o*-diamines producing the corresponding ammonium salts, thereby decreasing the nucleophilicity of the *o*-diamine. Yields of the product **3** were generally quite low due to the fact that both reagents slowly decomposed at the high temperatures required for the reaction.

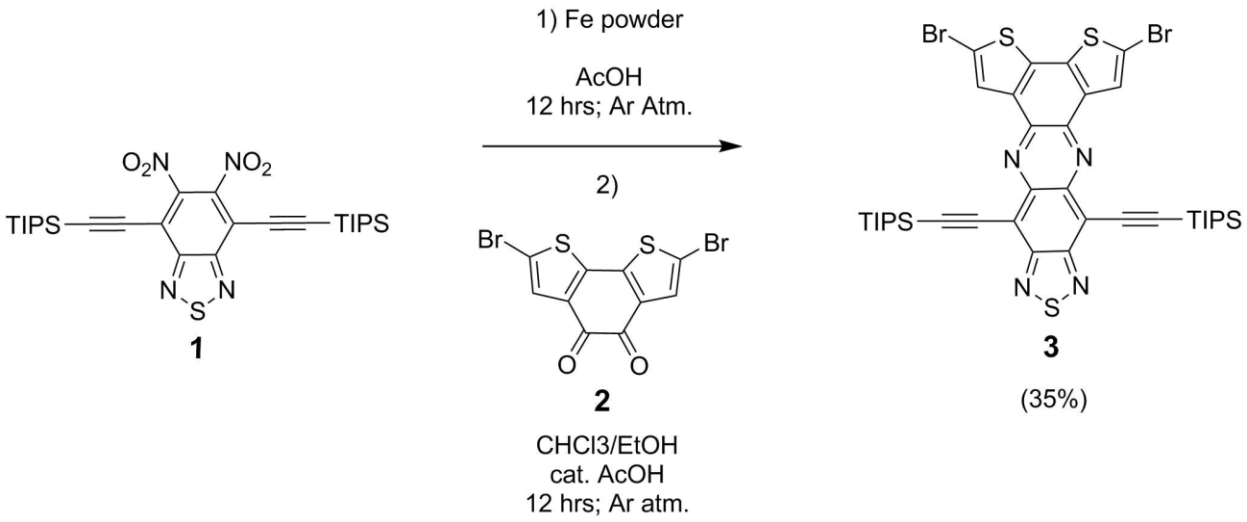

Figure 4.5. Synthesis of compound **3.**

The success of the condensation of **1** with **3** led our group to attempt a condensation with other *o*-diketone derivatives. Bis((triisopropylsilyl)ethynyl)benzo[c][1,2,5]thiadiazole-5,6-diamine was combined in a 1:2 stoichiometric ratio with 2,7-di-tert-butylpyrene-4,5,9,10-tetraone (**4**) to produced two new compounds via TLC: a strongly fluorescent, bright pink compound with a high R_f, (2,12-di-tert-butyl-5,9,15,19tetrakis((triisopropylsilyl)ethynyl) [1,2,5]thiadiazolo[3'',4'':6',7']quinoxalino[2',3':9,10]phenanthro[4,5-abc][1,2,5]thiadiazolo[3,4-i]phenazine (**5**) and a brown colored compound with a relatively low R_f, (2,7-di-tert-butyl-10,14-bis((triisopropylsilyl)ethynyl)phenanthro[4,5-abc][1,2,5]thiadiazolo[3,4-i]phenazine-4,5-dione (**6**). The intermediate **6** was produced in a much higher yield than the target compound **5**. Attempts were made to condense dione **5** with benzo[2,1-b:3,4-b']dithiophene-4,5-diamine (**7**) (Figure 4.6), and a new bright pink compound with a high R_f was observed by TLC. A pink solid was isolated, but yields of the product were too low to fully characterize the new compound.

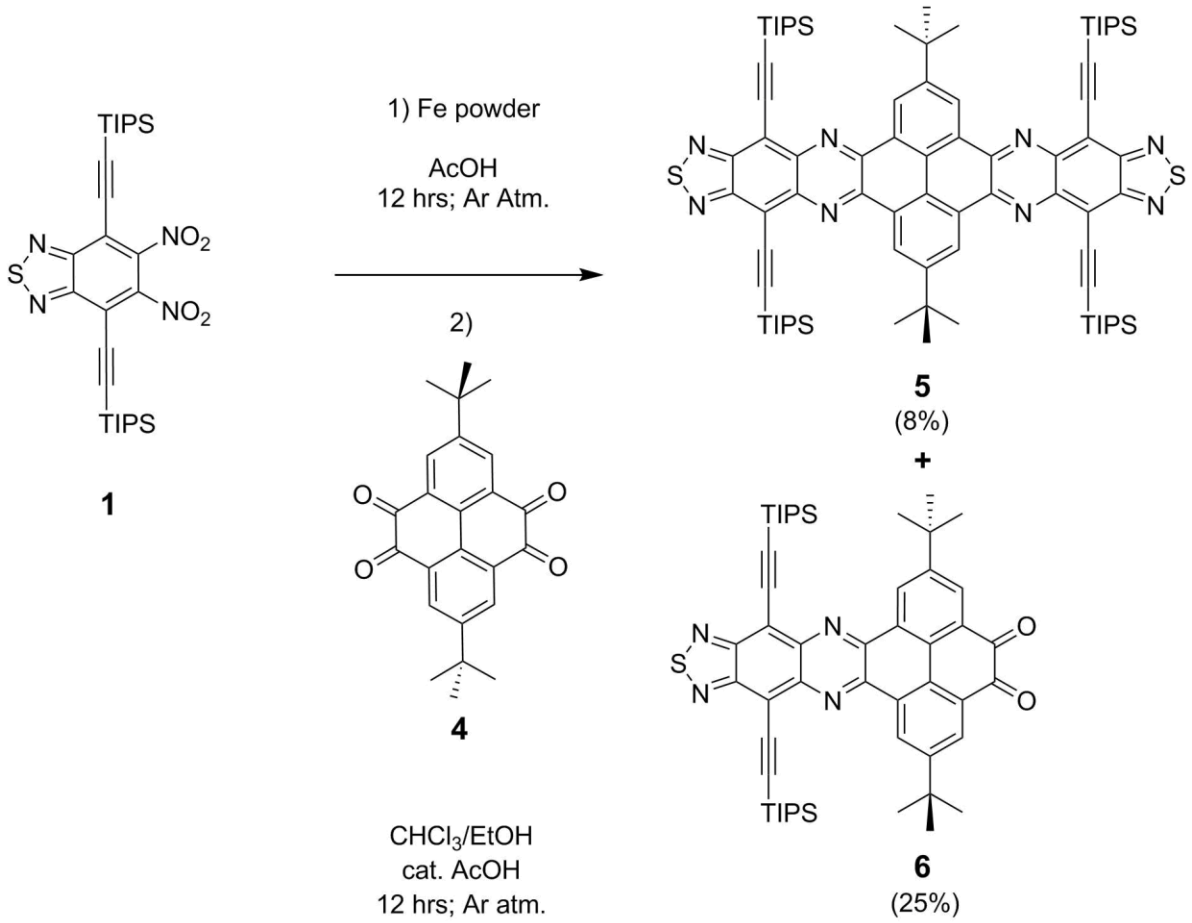

Figure 4.6. Synthesis of **5** and **6.**

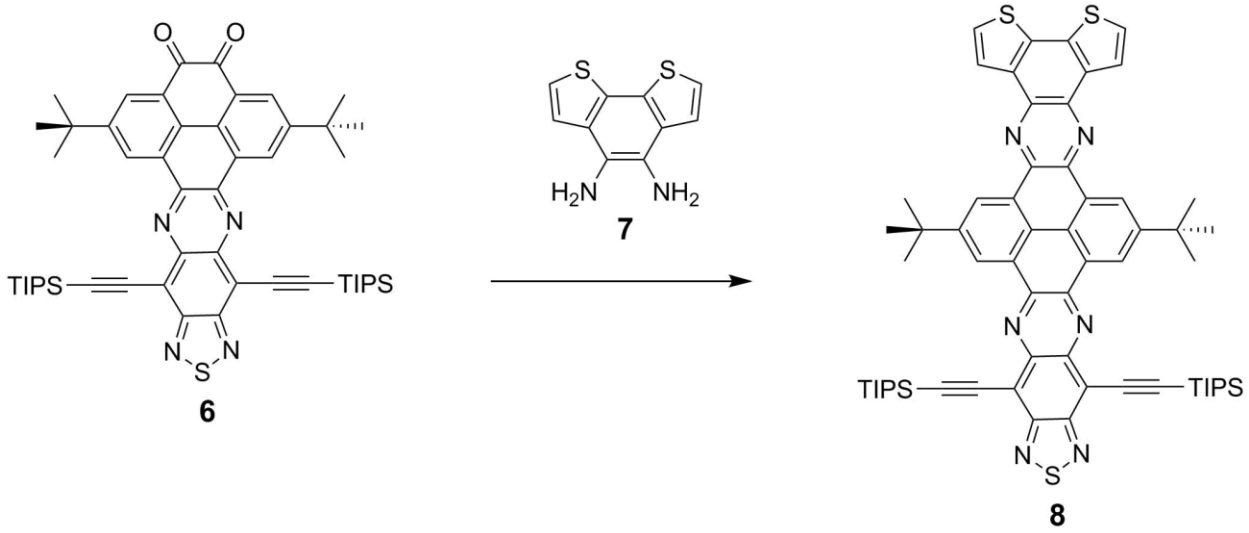

Figure 4.7. Attempted synthesis of **8.**

Synthesis of several derivatives of benzo[2,1-b:3,4-b']dithiophene-4,5-diamine

Benzo[2,1-b:3,4-b']dithiophene-4,5-diamine (**7**) was used for condensation reactions with *o*-diketones as can be seen in Figure 4.8. **7** was easily condensed with sulfur monochloride and brominated using molecular bromine using the literature procedures to yield 5,8-dibromo dithieno[3',2':3,4;2'',3'':5,6]benzo[1,2-c][1,2,5]thiadiazole (**9b**). Monomer **9b** was later copolymerized with cyclopentadithiophene to produce semiconducting polymers. **7** was also condensed onto **2** using literature procedures[22] to produce **10a**, which was further derivatized using the Sonagashira reaction to yield the small molecule **10b**. Bromination of **10b** was attempted at the 9 and 12 positions of **10b** using *N*-bromosuccinimide and molecular bromine, but deprotection of triisopropylsilyl groups occurred under these conditions. Condensation of **7** with 2,3,6,7-tetrakis(dodecyloxy)phenanthrene-9,10-dione lead to the formation of **11** in good yield. Compound **11** appeared as a greenish yellow solid, and formed organogels at low concentration in mixtures of chloroform and ethanol. The structure of this organogel will be characterized in later studies, but it will be noted that organogels have been previously reported by Kato *et al.*[23] for derivatives of tetraalkoxyphenanthrene-fused thiadiazoloquinoxalines, which are closely related to **11** in structure.

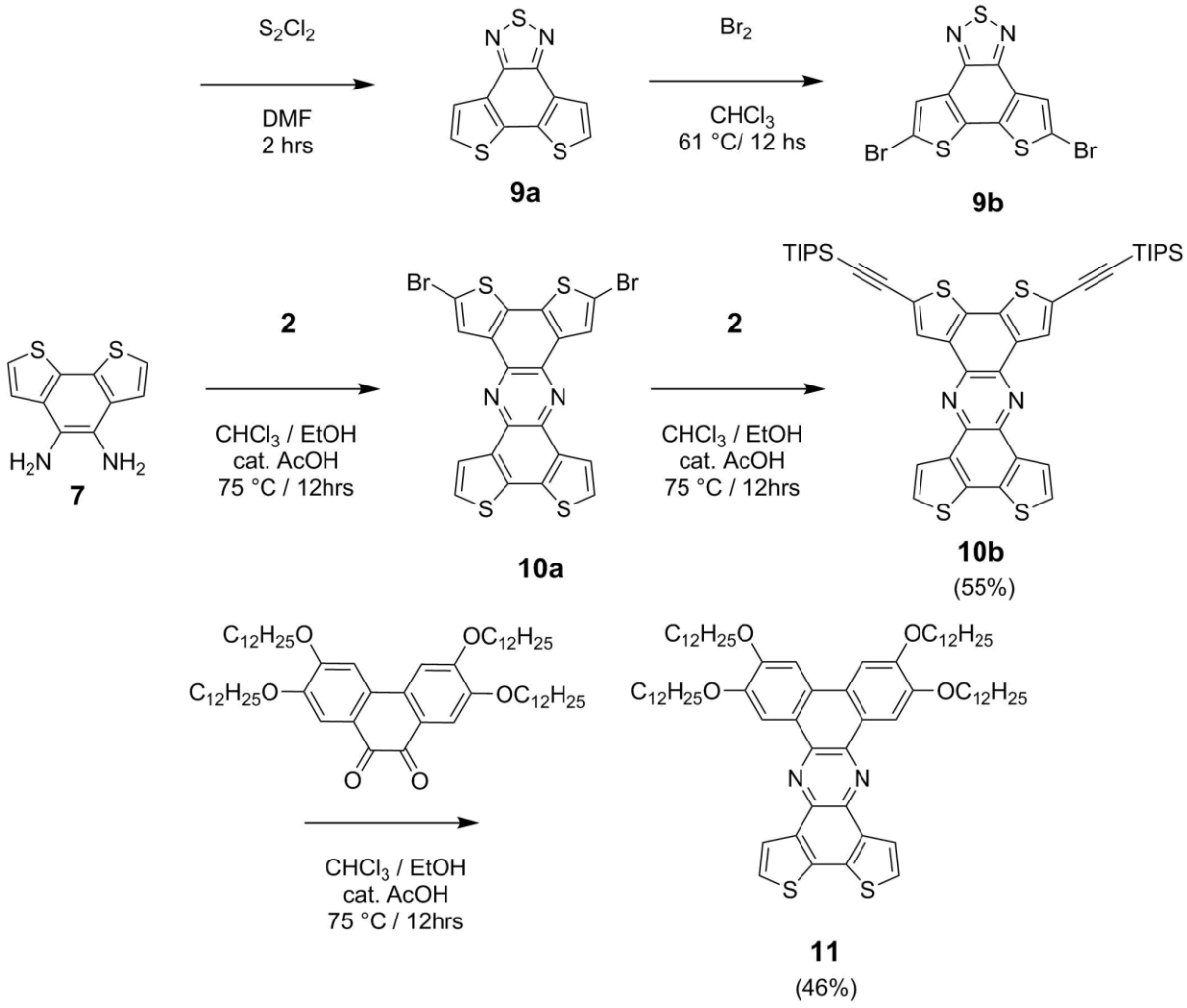

Figure 4.8. Preparation of several derivatives of Benzo[2,1-b:3,4-b']dithiophene-4,5-diamine (7) via condensation reactions with *o*-diketones and sulfur monochloride.

Synthesis of π-donor π-acceptor conjugated alternating co-polymers containing electron deficient thiadiazole units

Several π-donor π-acceptor copolymers were synthesized using palladium catalyzed Stille cross-coupling reactions (Figure 4.9). Monomer **3** was copolymerized with 2,7-bis(tributylstannyl)-9,9-bisoctylfluorene and 2,6-bis(tributylstannyl)-4,4-bis(2'-ethylhexyl)-4H-

cyclopenta[2,1-b:3,4-b']dithiophene to yield **P1** and **P2** respectively. Monomer **9b** was copolymerized with 2,6-bis(tributylstannyl)-4,4-bis(2'-ethylhexyl)-4H-cyclopenta[2,1-b:3,4-b']dithiophene to yield **P3**. The molecular weights and dispersities of **P1**-**P3** are summarized in Table 4.1. Low degrees of polymerization were achieved because palladium catalyzed polymerization reactions are relatively slow using tributylstannyl Stille coupling reagents compared to the more commonly employed but much more toxic trimethylstannyl coupling reagents. The author will note that higher apparent molecular weights c.a. 100,000 Da were observed by GPC using solvents such as tetrahydrofuran and chloroform due to aggregation of the polymers in these solvents. These findings are notable considering that other groups synthesizing similar polymers recorded GPC values using tetrahydrofuran as eluent.[16,19]

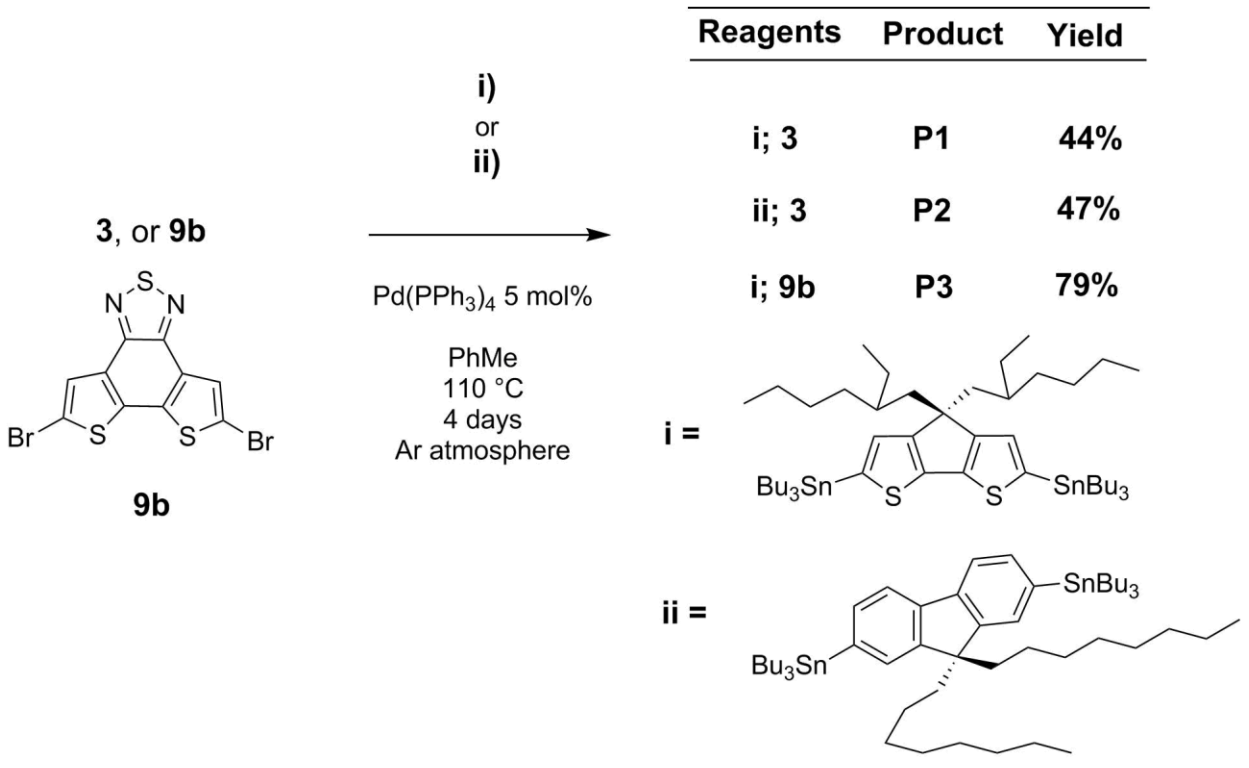

Figure 4.9. Synthesis of **P1**, **P2**, **P3.**

Table 4.1. Summary of GPC results for **P1**-**P3** using 1,2-dichlorobenzene as eluent.

Polymer	M_n	Dispersity	DP_n
P1	3566	1.71	6.4
P2	4526	1.75	8.2
P3	3800	1.66	11.6

Photophysical properties of P1-P3 and small molecules 3 and 5.

The absorbance and photoluminescence properties of **3**, **5**, and **P1**-**P3** are summarized in Table 4.2. Monomer **3** has an emerald green appearance and has a strong absorbance at 420 nm and two weaker absorbance bands centered at 620 nm as can be seen in Figure 4.10. Excitation of **3** at 450 nm leads to a strong fluorescence peak at 680 nm, while excitation of the weaker peaks at 650 nm also leads to photoluminescence at 680 nm. The strong π-donor character of the benzo[2,1-b:3,4-b']dithiophene and the strong π-acceptor character of the [1,2,5]thiadiazolo[3,4-g]quinoxaline lead us to hypothesis that the pair of weak peaks at 590 and 650 nm arise from an intramolecular charge transfer band (ICT). ICT bands have been reported for similar compounds which suggests that this may be the case for compound **3**. [14,20]

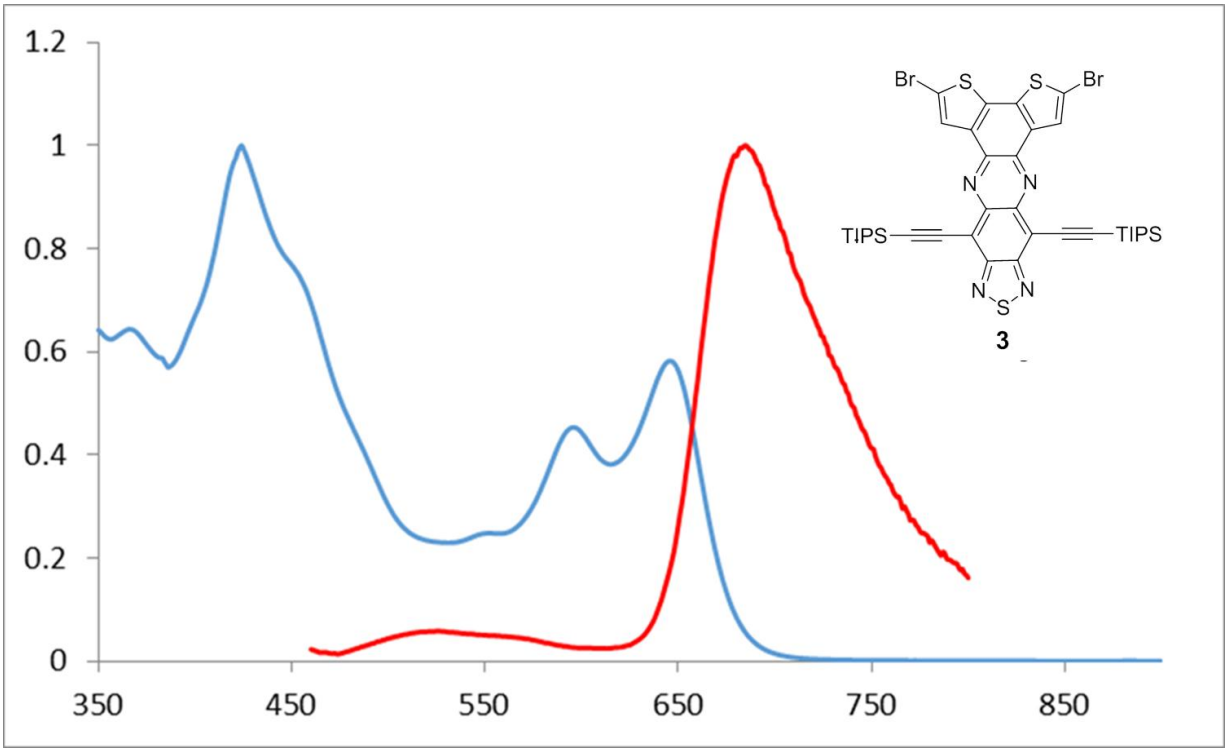

Figure 4.10. Normalized absorbance (blue) and normalized PL (red, excitation 450 nm) of **3** in chloroform solution.

Compound **5** appears as a fluorescent pink solution when dissolved in chloroform and its normalized absorbance and PL data can be seen in Figure 4.11. It can be seen that the absorbance of **5** consists of four closely spaced peaks between 450 and 650 nm. Excitation of **5** at 485 nm leads to two peaks at 620 nm and 650 nm. The splitting of the fluorescence peaks may arise from the fact that there are two overlapping excitation bands at 485 nm. The absorbance and photoluminescence of compound **5** is significantly different from the [1,2,5]thiadiazolo[3'',4'':6',7']quinoxalino[2',3':9,10]phenanthro[4,5-abc][1,2,5]thiadiazolo[3,4-i]phenazine derivatives reported by Luo et. al.[21] The aforementioned derivatives have strongly electron donating aromatic groups substituted at the 5,9,15, and 19 positions, so the molecules exhibit very strong intramolecular charge transfer character and absorption into the near IR.

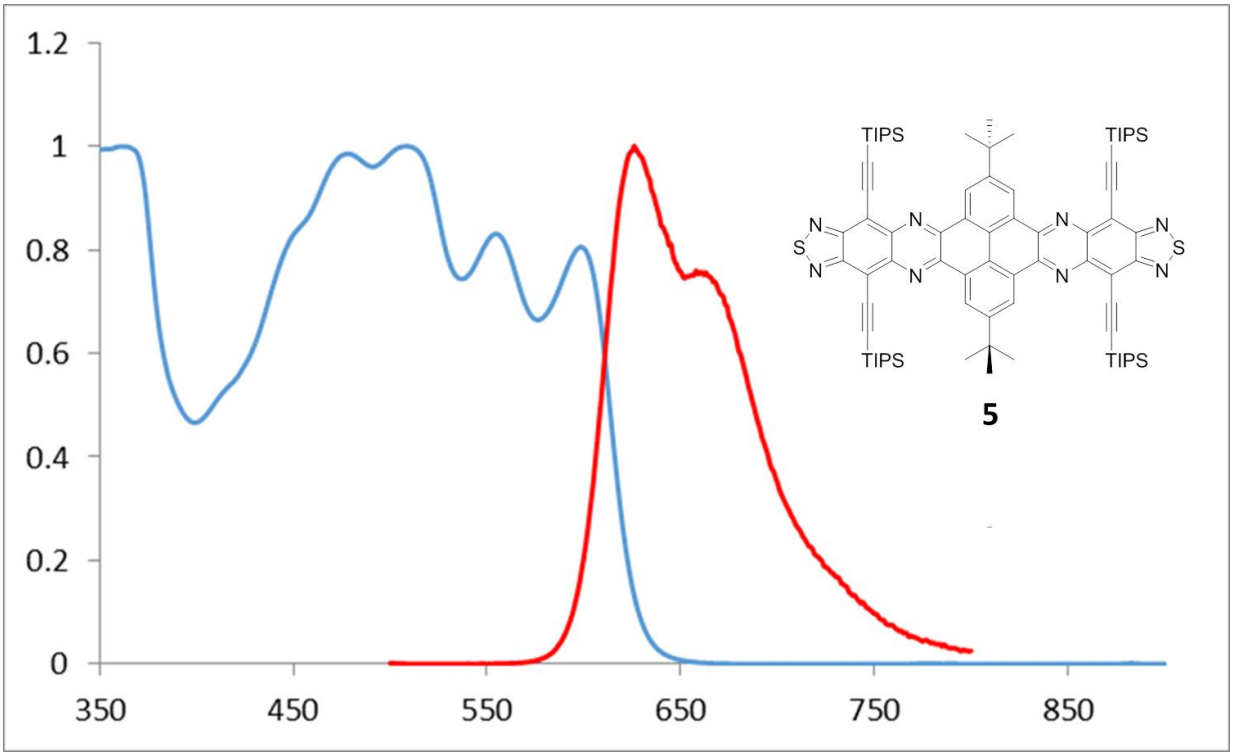

Figure 4.11. Normalized absorbance (blue) and normalized PL (red, excitation 485 nm) of **5.**

The absorbance and PL data of **P1**-**P3** can be seen in Figure 4.12. **P1** and **P2** both use 8,12-bis((triisopropylsilyl)ethynyl)-[1,2,5]thiadiazolo[3,4-i]dithieno[3,2-a:2',3'-c]phenazine as the π-acceptor unit of the alternating co-polymer, but differ in the π-donor unit. **P1** contains a fluorene as the π-donor species, while **P2** contains a cyclopenta[2,1-b:3,4-b']dithiophene unit as the electron donating species. Cyclopenta[2,1-b:3,4-b']dithiophene units possess higher HOMO levels than fluorenyl units causing a decrease in the band gap and an increase in the wavelength of the maximum absorption peaks arising from the excitation of the π conjugated backbone (450nm for **P1** and 550 nm for **P2**). Both **P1** and **P2** have weak absorption bands that extend into redder frequencies of light than the stronger absorptions arising from excitation of the polymer backbone (700 and 810nm). These weak absorptions were ascribed to ICT bands

for an analogous set of polymers and we have thus putatively assigned these peaks as ICT bands as well. These ICT bands most likely result from charge transfer from the excited state of the electron rich benzo[2,1-b:3,4-b']dithiophene moiety to the electron poor [1,2,5]thiadiazolo[3,4-g]quinoxaline moiety. We hypothesized that this ICT band may aid in electron transfer to fullerene derivatives by funneling negative charges to the [1,2,5]thiadiazolo[3,4-g]quinoxaline units, which lie on the periphery of the polymer backbone.

Absorption and PL data were also collected for **P1** and **P2** in thin films of these compounds. The absorbance of both compounds remained essentially unchanged except for a small bathochromic shift of the main absorption peaks due to the higher dielectric constant of the film compared to the solution. Interestingly there was a small hypsochromic shift of the putative ICT absorption band of **P2** in films, while **P1** displayed a large bathochromic shift of this peak. The author has no explanation for this discrepancy, but differences in the conformation of the backbone of these polymers may play a role. The absorbance spectrum of **P2** closely resembles the spectra of a similar copolymer reported by An *et al.* consisting of a bisthienyl substituted [1,2,5]thiadiazolo[3,4-i]dithieno[3,2-a:2',3'-c]phenazine covalently linked to an alkyl substituted quaterthiophene at the 2 and 5 positions.[16] The main absorption peak at 520, 550, and 810 in **P2** exhibited hypsochromic shifts in comparison with the main absorption peaks reported for the polymer synthesized by An et. al. This is most likely due to the extended pi systems of the polymers synthesized by An et al.

The max absorbance of **P3** arising from the excitation of the polymer backbone is red shifted compared to **P2** (550 nm for **P3** compared to 520 for **P2**). This is significant because the

LUMO levels of fused 4,7-dithienyl[2,1,3]benzothiadiazoles tend to be higher than [1,2,5]thiadiazolo[3,4-g]quinoxalines and would therefore be expected to have a lower band gap than **P2**. This discrepancy can easily be explained if the excitations from which the max absorbance at 440 nm in **P2** and 550 in **P3** are considered to be mainly localized on the series of conjugated bonds along the benzo[2,1-b:3,4-b']dithiophene and cyclopenta[2,1-b:3,4-b']dithiophene moieties contained within these polymers. The π-acceptor unit in **P3** would be expected to be slightly more electron deficient than **P2** because fused [1,3,2]thiadazoles are slightly more electron deficient units than fused [3,4]quinoxalines. This hypothesis would also explain why the putative ICT bands of **P1** and **P2** would red shift in comparison to the putative ICT bands of **3**: The HOMO level of **P1** and **P2** would be expected to increase as the conjugation of the polymer backbone is extended thereby decreasing the HOMO-LUMO gap of the putative ICT bands. The absence of an ICT band in **P3** also suggests that the ICT band in **P1** and **P2** may exist as a localized negative charge residing on the [1,2,5]thiadiazolo[3,4-g]quinoxaline unit and a delocalized positive charge residing on the polymer backbone. The absorbance spectra of **P3** strongly resembles the spectra of other πD-πA copolymers containing a dithieno[3',2':3,4;2'',3'':5,6]benzo[1,2-c][1,2,5]thiadiazole unit in terms of the optical band gap and the general shape of the absorbance peaks.[12,13,24]

Table 4.2. Summary of absorbance and photoluminescence data of **3**, **5**, and **P1**-**P3.**

Compound	peak abs. (vis, nm)	PL exc. λ (nm)	PL emis. λ (nm)
3	420, 590, 660	450	680
5	520, 600	485	620, 680
P1	440, (700 weak)	450	620, 650
P1 film	450 (750 weak)	450	520
P2	520, 550, (810 weak)	490	580, 620
P2 film	540, 570 (790 weak)	560	610
P3	560	580	650

The PL of **P1**-**P3** seen in Figure 4.12 shows the photoluminescence of excitations resulting from the polymer backbone. Photoluminescence from the putative ICT bands of these polymers was not explored in this study due to limitations of our instrumentation. **P1** shows an unexpectedly large stokes shift of 170 nm in solution when excited at 450 nm. The resulting emission of **P1** displays a broad shoulder at longer wavelengths due to vibronic transitions. The photoluminescence of **P1** in films is drastically decreased, suggesting that non-radiative pathways dominate in the solid state. There is a dramatic hypsochromic shift in the emission wavelength of **P1** in films, shifting to 520 nm using an excitation wavelength of 450 nm. **P2** possesses more typical fluorescence behavior. Excitation of **P2** at 490 nm leads to an emission at 580 and with strong vibronic structure. Films of **P2** showed a drastic decrease in photoluminescence and there was a bathochromic shift in the emission wavelength to 610 nm. **P3** showed similar behavior to **P2** with a peak emission of 650 nm resulting from an excitation of 580 nm.

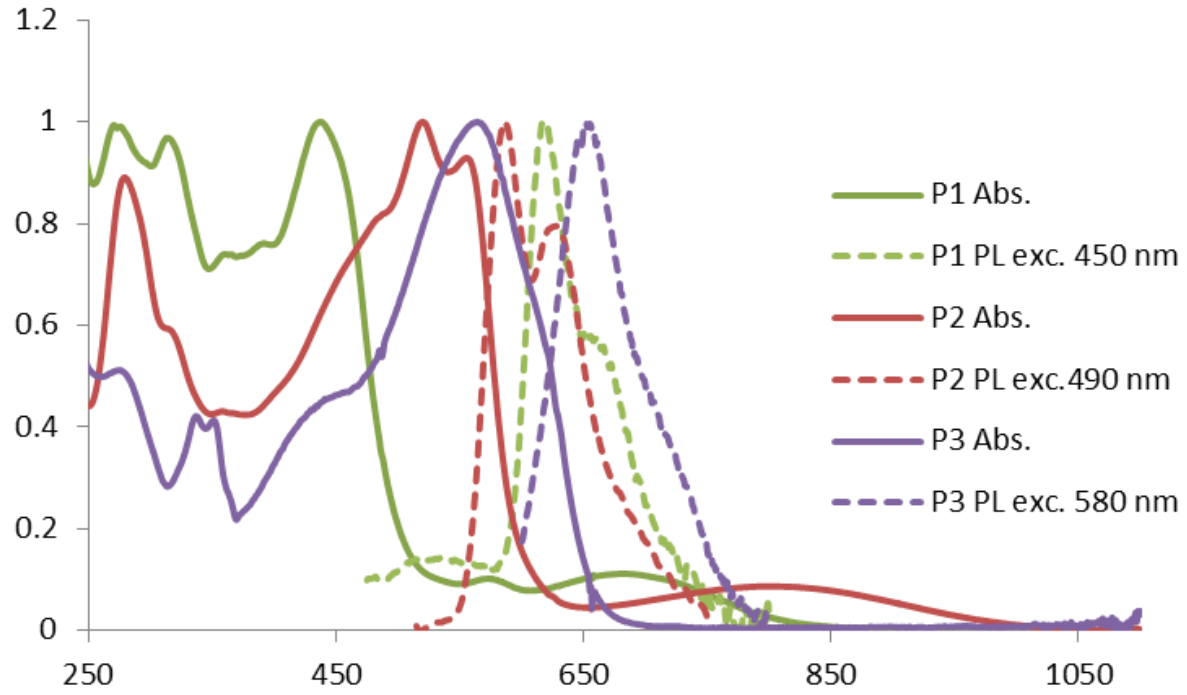

Figure 4.12. Normalized absorbance (solid lines) and normalized PL (dashed lines) for **P1** (green, exc. 450 nm), **P2** (red, exc. 490 nm), and **P3** (purple, exc. 580 nm).

The differences in photoluminescence behavior of **P1** and **P2** can be explained in context of the theoretical calculations performed by Planells *et al*. in their theoretical studies of polymers containing [1,2,5]thiadiazolo[3,4-b]dithieno[3,2-f:2',3'-h]quinoxaline which also showed a strong ICT band.[14] Density functional theory (DFT) calculations on models of these polymers showed that HOMO orbitals consisted of a delocalized state extending over several monomer units of the polymer backbone. There were two closely spaced LUMO orbitals which consisted of a higher energy orbital (LUMO + 1) that was localized on the polymer backbone and a slightly lower energy orbital (LUMO) localized mainly on the [1,2,5]thiadiazolo[3,2-f:2',3'-h]quinoxaline unit of the [1,2,5]thiadiazolo[3,4-b]dithieno[3,2-f:2',3'-h]quinoxaline monomer.

These calculations showed that the ICT band resulted mainly from the transition from the HOMO to the LUMO transition and time dependent DFT calculations showed that the ICT excitation had a much lower oscillator strength compared to the HOMO to LUMO + 1 transition. Photoluminescence spectra of these polymers using an excitation of the HOMO to LUMO + 1 transition revealed a spectrum that had a very similar stokes shift to **P2** and had minimal overlap with the ICT band. As can be seen in Figure 4.12 **P2** also displays an emission band that had a small overlap with the ICT band.

Excitation of the polymer backbone of **P1** at 450 nm on the other hand displays an emission which has a very strong overlap with ICT band. This behavior is similar to the fluorescence seen in **3** which also shows strong relaxation to the ICT band upon excitation of the main π—π* transition. This change in emission behavior possibly results from the use of the relatively weak fluorene πD unit in **P1**. Fluorene is a much weaker electron donor unit than benzo[2,1-b:3,4-b']dithiophene, therefore the HOMO and LUMO + 1 of **P1** is probably more localized on the benzo[2,1-b:3,4-b']dithiophene units. This increased localization on the benzo[2,1-b:3,4-b']dithiophene units most likely leads to more efficient relaxation from the LUMO + 1 to the LUMO orbital. The increased localization of excitations on the [1,2,5]thiadiazolo[3,2-f:2',3'-h]quinoxaline unit of **P1** compared to **P2** will most likely have a drastic effect on the electron transfer between these polymers and phenyl-C_{61}-butyric acid methyl ester although it is unclear whether this effect would be detrimental or beneficial.

Crystallographic properties of 3, P1, and P2

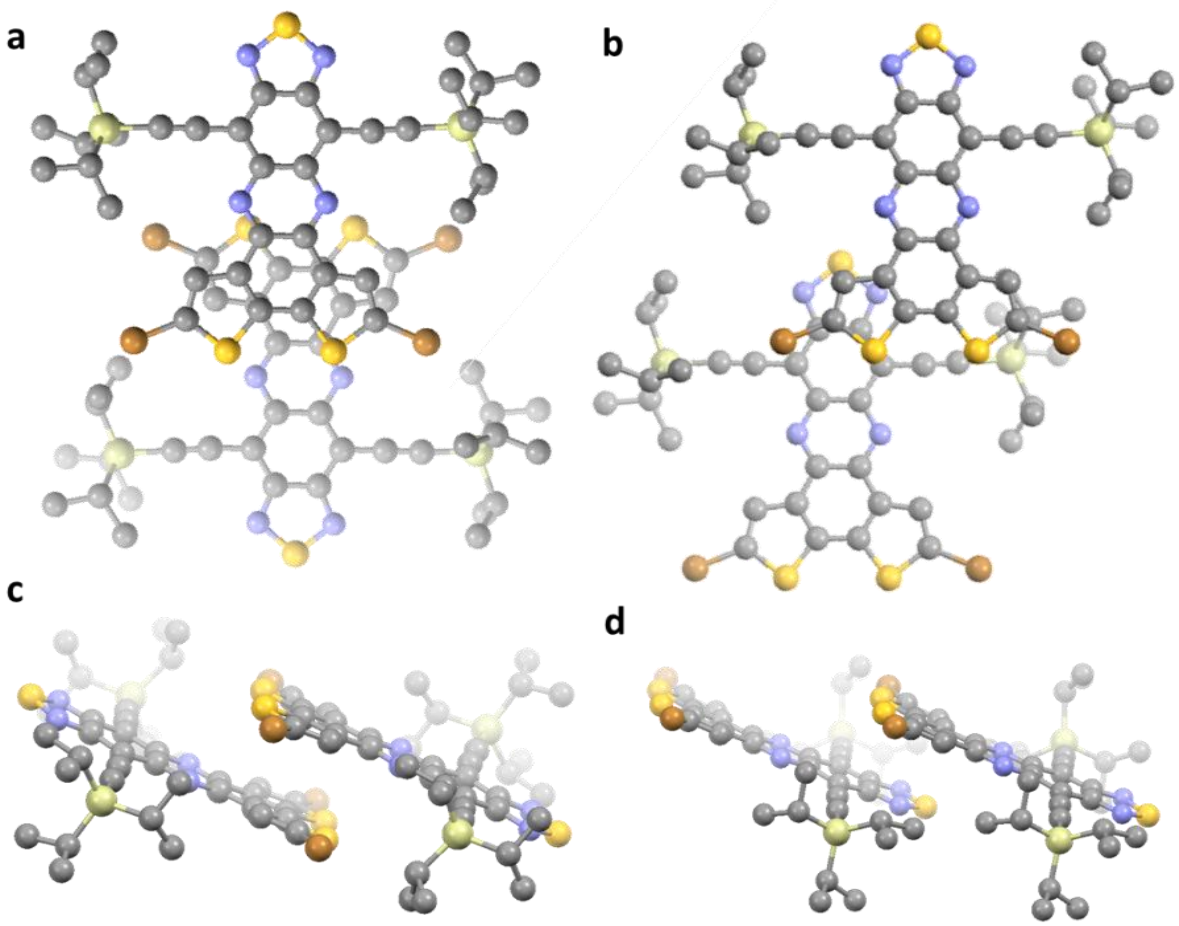

Figure 4.13. π stacking of **3** viewed along the c-axis of the unit cell of the single crystal showing interactions between a) two benzo[2,1-b:3,4-b']dithiophene units and b) one thiadiazole unit and a benzo[2,1-b:3,4-b']dithiophene unit and side views of these interactions c) and d).

Single crystals of monomer **3** were formed from $CHCl_3$/EtOH and diffraction data was collected on the crystals. The unit cell structure can be seen in Figure 4.14. The unit cell was found to belong to the triclinic space group *P*-1. The a,b, and c axes if the unit cell have lengths of 8.90, 14.95, and 15.66 Å respectively and the angles α, β, and γ are 80.8, 77.1,and 86.5 °

respectively. The packing of **3** in the solid state can be roughly described as consisting of π stacked monomer units which are stacked "head-to-tail" so that the benzo[2,1-b:3,4-b']dithiophene of one molecule is rotated 180° in relation to the molecule directly below it and above it. These observations are in close agreement with the crystal structures of the debrominated analog of **3**. The atoms of the two benzo[2,1-b:3,4-b']dithiophene units are slightly offset in the crystal structure and the distances between the 8 carbon atoms of the benzo[2,1-b:3,4-b']dithiophene units are between 3.7-3.4 Å and there is one close contact (3.5 Å) between one sulfur atom of the benzo[2,1-b:3,4-b']dithiophene of one molecule and a carbon atom in the quinoxaline ring of the molecule comprising the dimer. These molecules also contain a second π-π interaction between the electron deficient thiadiazole unit and the electron rich benzo[2,1-b:3,4-b']dithiophene. There are close contacts between the atoms comprising the thiadiazole and one of the thiophene rings, and there are also close contacts between the sulfur atoms of one thiophene ring and the carbon atoms of the alkynyl group.

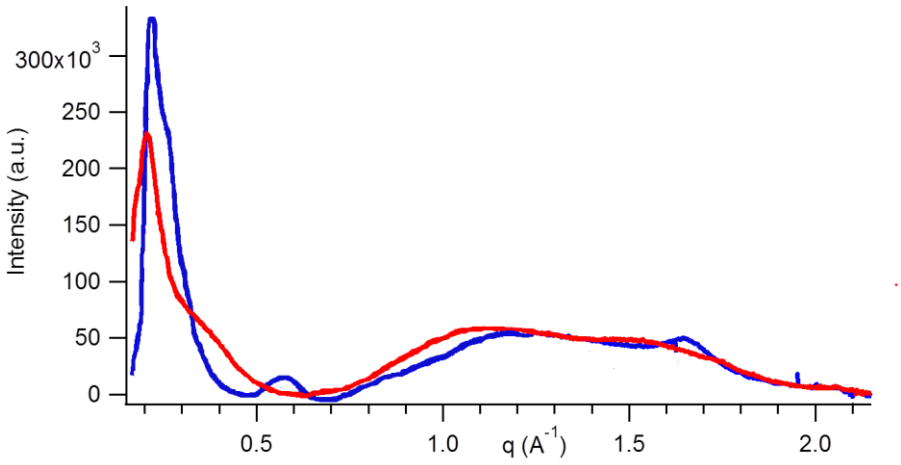

Figure 4.14. Reduced, thickness normalized GIWAX scattering plots collected on thin films of **P1** (red) and **P2** (blue).

Grazing incident wide angle x-ray scattering (GIWAXs) data was collected on spin coated films of **P1** and **P2** and the integrated plots of the 2-D data can be seen in Figure 4.14. The films revealed very weak and broad isotropic scattering at 0.2 A^{-1} which likely results from the lamellar packing of polymer chains and two peaks at 1.0 and 1.6 $Å^{-1}$ which likely result from scattering from several convoluted peaks. Very similar broad peaks at 1.0 1.6 $Å^{-1}$ are seen in other amorphous polymers containing cyclopentadithiophene units such as PSDTTT[25] and PSEHTT.[26] The scattering at lower q values 1.0 $Å^{-1}$ correspond to spacings of 6.4 Å and likely result from alkyl-alkyl interactions between the alkyl chains located on the florenyl and cyclopenta[2,1-b:3,4-b']dithiophene (Figure 4.15). The scattering at higher q values (1.4-2.0 $Å^{-1}$) correspond to typical spacings from π—π interactions and likely result from stacking of the conjugated backbones of these polymers.

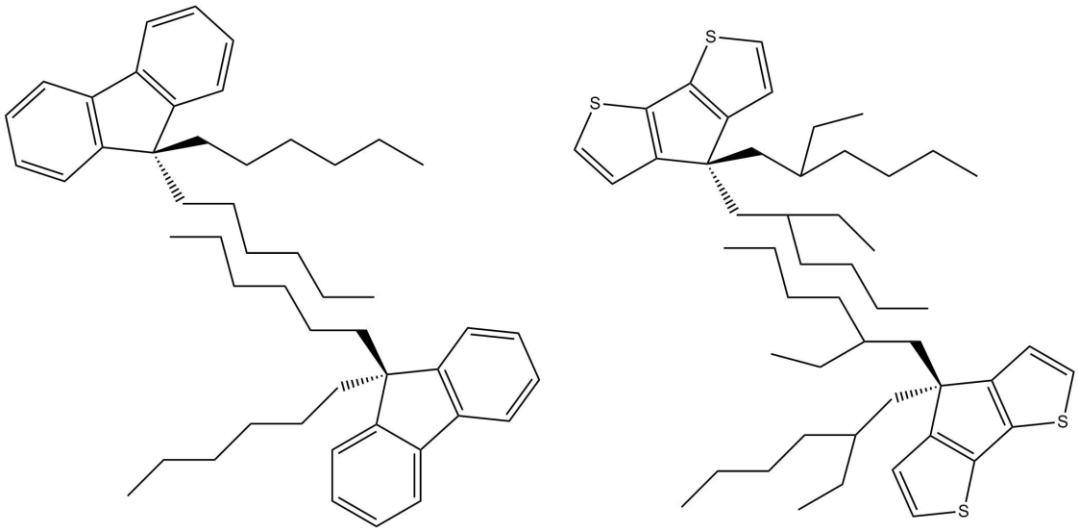

Figure 4.15. Depiction of the putative alkyl-alkyl interactions between the florenyl and cyclopenta[2,1-b:3,4-b']dithiophene units of **P1** and **P2**.

The weak intensity of the scattering from films of **P1** and **P2** suggests that backbone of these polymers are highly disordered and that the polymers are both amorphous. The high amount of disorder is likely the result of the fact that the octyl chains 9 position of the fluorene unit in **P1** and 2-ethylhexyl chains substituted at the 4 position of the cyclopenta[2,1-b:3,4-b']dithiophene unit of **P2** extend above and below the conjugated backbone of these polymers. This most likely increases disorder in these polymers by frustrating the efficient lamellar packing of polymer chains and by frustrating π-π interactions between the relatively electron rich cyclopenta[2,1-b:3,4-b']dithiophene and fluorene units with the relatively electron deficient [1,2,5]thiadiazolo[3,4-i]dithieno[3,2-a:2',3'-c]phenazine unit.

Electrochemical characterization of 3, 5, and P1-P3

Table 4.3: Electrochemical properties of **3**, **5**, and **P1**-**P3**.

Compound	I.P. *vs.* Li/Li+	HOMO *vs.* vacuum level	Optical Band gap	LUMO calculated
3	4.4 V	-5.7 eV	1.7 eV	-4.0 eV
5	4.4 V	-5.7 eV	1.9 eV	-3.8 eV
P1	4.2 V	-5.5 eV	1.5 eV	-4.0 eV
P2	3.9 V	-5.3 eV	1.3 eV	-4.0 eV
P3	3.7 V	-5.0 eV	1.9 eV	-3.1 eV

The electrochemical properties of **3**, **5**, and **P1**-**P3** were measured via cyclic voltammetry (Figure 4.16) and are summarized in **Error! Reference source not found.**. CVs were obtained on films deposited on ITO glass at 0.5 mV/s and were measured in propylene carbonate with Li/Li^+ as the reference electrode and the ITO glass as the working electrode. Absolute ionization potentials were calculated using -4.3 V as the absolute electrode potential for the standard

hydrogen electrode[28] and -3.0 V as the standard reduction potential of Li / Li^+ *vs.* the standard hydrogen electrode.[29]

Monomer **3** has a very low HOMO level of -5.7 eV and a very low lying calculated LUMO of -4.0 eV *vs.* vacuum level. These values match closely with the measured reduction potentials of reported by An et for the debrominated analog of **3** (the LUMO was calculated to have an absolute reduction potential of -3.92 eV vs. vacuum level).[18] This data suggests that **3** can possibly function as a competent electron acceptor in photovoltaic cells. Compound **5** has the same oxidation potential as **3**, but the calculated LUMO of **5** is significantly higher than that of **3**, due to the fact that **5** has a wider band gap than **3**. The calculated LUMO of **5** is close to the measured reduction potentials of aryl substituted [1,2,5]thiadiazolo[3'',4'':6',7']quinoxalino [2',3':9,10]phenanthro[4,5-abc][1,2,5]thiadiazolo[3,4-i]phenazine derivatives reported by Luo *et al.*(3.73 and 3.86 eV vs vacuum level).[21] Both **3** and 5 have calculated LUMO orbitals that are in the same range as **P1** and **P2** have similar HOMO levels, which is expected considering that they share the same electron deficient unit.

The HOMO level of **P1** is slightly lower than the HOMO level of **P2** because cyclopenta[2,1-b:3,4-b']dithiophene units are stronger electron donors than fluorene units. **P3** has a higher HOMO value *vs.* vacuum level than **P1** and **P2**. This suggests that [1,2,5]thiadiazolo[3,4-i]dithieno[3,2-a:2',3'-c]phenazines are more electron deficient than dithieno[3',2':3,4;2'',3'':5,6]benzo[1,2-c][1,2,5]thiadiazoles. The reductions of **P1**-**P3** were not observed using the set up employed for the oxidation of these polymers. However, the LUMO levels were calculated from the experimentally observed oxidations and the optical band gaps.

The calculated LUMO levels of **P1** and **P2** are quite similar while **P3** has a LUMO level that is substantially higher than the other two polymers. The experimentally obtained HOMO levels and the calculated LUMO levels of **P1** and **P2** closely match the values reported by An *et al.* for copolymers consisting of bisthienyl substituted [1,2,5]thiadiazolo[3,4-i]dithieno[3,2-a:2',3'-c]phenazines and bithiophene (-5.50 eV and -3.86 eV *vs.* vacuum level for the HOMO and LUMO respectively).

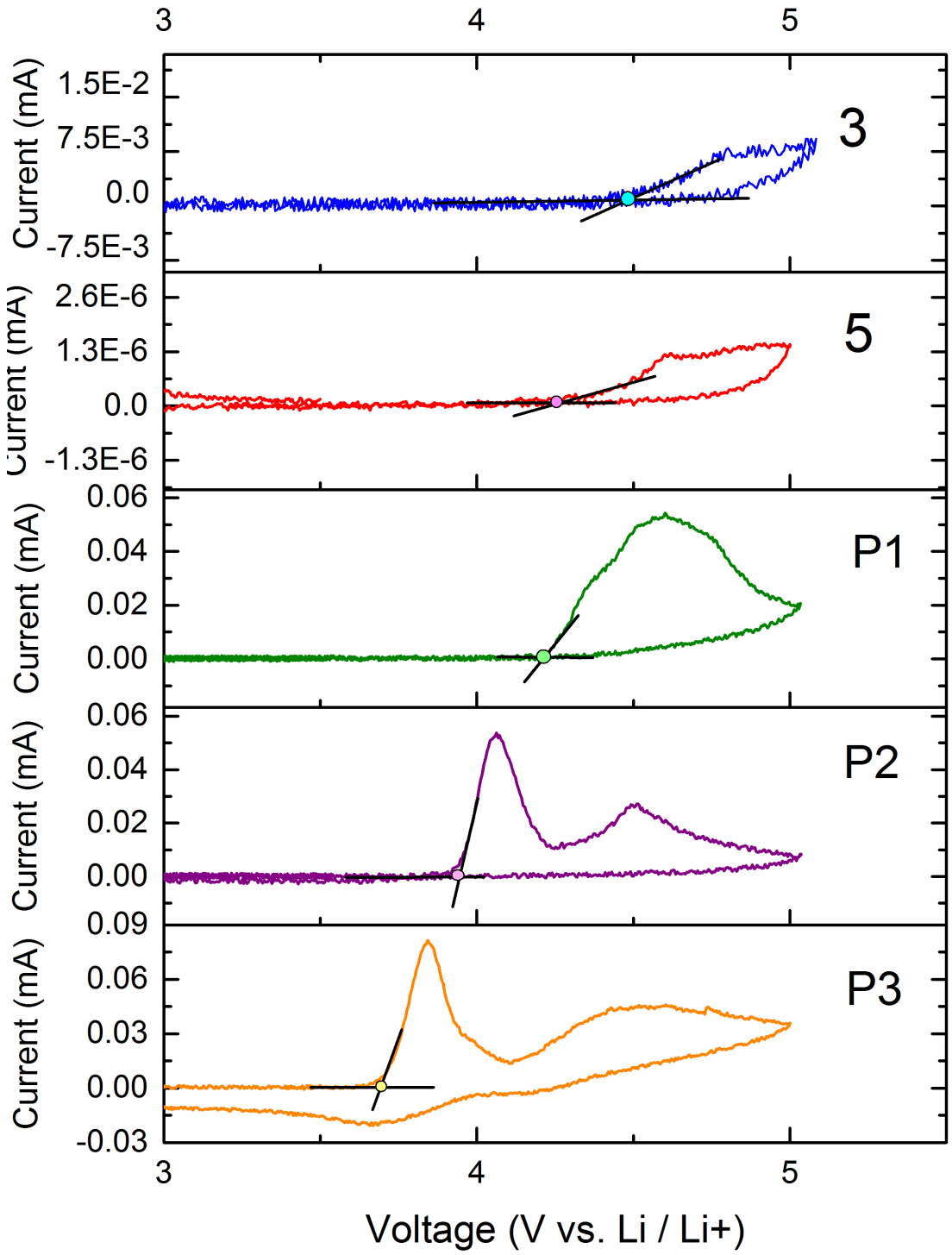

Figure 4.16. Cyclic voltammograms of **3** (blue), **5** (red), **P1** (green), **P2** (purple), **P3** (orange).

We will note that the LUMO levels of **P1** and **P2** were calculated using the weak absorptions centered at 700 m, and 810 nm respectively. This is significant because these absorptions that we have putatively assigned as ICT bands have weak cross sections in comparison to the peaks centered at 440 nm for **P1** and 540 nm for **P2**. An *et al.* reported a 500 mV difference between the optical band gap of copolymers containing [1,2,5]thiadiazolo[3,4-i]dithieno[3,2-a:2',3'-c]phenazine and the HOMO-LUMO gap directly measured via cyclic voltammetry.[16] They attributed this difference to the exciton binding energy of the copolymer, but we will note that the band gap as measured by cyclic voltammetry matches the optical band gap of the strongest excitations of the polymer, which they assigned to the π-π* transition of the conjugated backbone of the polymer. The optical band gap that An *et al.* reported, however, was derived from the band edge of the excitation which they assigned to an intramolecular charge transfer band. This is significant because we have calculated the LUMO orbital of **P1** and **P2** using the band edge of the intramolecular charge transfer band. If, however, the band edges of the main absorption bands at 440 nm and 540 nm were used to calculate the band gap of these polymers (530 nm, 2.3 eV for **P1** and 650 nm, 1.9 eV for **P2**), much higher LUMO levels would be derived (-3.2 and -3.4 eV *vs.* vacuum level for **P1** and **P2** respectively). If we were to assume that the strong excitations of these polymers at 440 and 540 nm did in fact arise from π-π* transitions along the polymer backbone and the weak absorptions centered at 700 at 810 nm were from an excitation resulting from intramolecular charge transfer, the values of -3.2 and -3.4 eV *vs*. vacuum level may be a more accurate estimate of the LUMO potentials of **P1** and **P2**.

If the calculated LUMO values of **P1** and **P2** are in fact accurate they may be sufficiently low enough to allow them to function as electron accepting polymers in polymer solar cells, but may be too low to be employed as an electron donor to fullerene acceptors. The LUMO level of the most commonly employed fullerene electron acceptor in organic photovoltaic cells, phenyl-C_{61}-butyric acid methyl ester (PCBM) has a LUMO ranging from -3.7 - -4.0 eV v vacuum level as measured by CV.[30] Therefore excitations arising from the intramolecular charge transfer band would therefore not have a thermodynamically favorable charge transfer of electrons to PCBM, while excitations arising from the much stronger excitations centered at 440 nm and 550 nm for **P1** and **P2** would presumably have sufficient energy to drive a thermodynamically favorable charge transfer. It will also be noted that use of non-fullerene acceptors with deeper LUMO levels could such as bis-perylene diimides[31] could serve as competent electron acceptors for **P1** and **P2**.

Conclusion

We have reported the synthesis of several novel polymers and small molecules based on the condensation reactions between various *o*-aryl diamines and *o*-aryl diketones. We have synthesized three new πD-πA copolymers containing electron deficient 8,12-bis((triisopropylsilyl)ethynyl)-[1,2,5]thiadiazolo[3,4-i]dithieno[3,2-a:2',3'-c]phenazine and dithieno[3',2':3,4;2'',3'':5,6]benzo[1,2-c][1,2,5]thiadiazole units (**P1**-**P3**). These polymers possess deep HOMOs, broad absorption across the visible spectrum, and narrow band gaps. Future studies will focus on the photovoltaic and conductive properties of these new polymers. We have also reported the synthesis as well as the photochemical and electrochemical properties of a new small molecule acceptor, 2,12-di-tert-butyl-5,9,15,19-tetrakis((tri-

isopropylsilyl)ethynyl) [1,2,5]thiadiazolo[3'',4'':6',7']quinoxalino[2',3':9,10]phenanthro[4,5-abc] [1,2,5]thiadiazolo[3,4-i]phenazine (**5**). **5** has a deep lying LUMO as well as broad visible absorption and a reasonably narrow band gap. Future studies will explore the photovoltaic as well as the conductive properties of this molecule. Finally, we reported the synthesis of the novel gelling donor small molecule 9,10,13,14-tetrakis(dodecyloxy)dibenzo[a,c]dithieno[3,2-h:2',3'-j]phenazine **(11).** Future studies will explore the nanoscale structure of the gels formed by this small molecule as well as the photochemical behavior of mixtures of **11** and polycationic fullerene species.

Experimental

Unless otherwise noted all reagents and solvents were purchased and used as received from available commercial sources. 2,6-Bis(tributylstannyl)-4,4-bis(2'-ethylhexyl)-4H-cyclopenta [2,1-b:3,4-b']dithiophene was synthesized according to the literature procedure and spectra matched the reported values.[36] All NMR spectra were collected on a Varian AV500 spectrometer with a 5 mm dual cryoprobe and a Bruker DRX500 spectrometer with a 5 mm broadband probe.

For polymer molecular weight determination, polymer samples were dissolved in HPLC grade *o*-dichlorobenzene at a concentration of 0.5 mg/mL and were heated until complete dissolution and then allowed to cool to room temperature prior to filtering through a 0.2 µm PFTE filter. GPC was performed using HPLC grade *o*-dichlorobenzene at a flow rate of 0.6 ml/min one 300 X 7.8 mm TSK-Gel GMHH R-H column (Tosoh Corporation) at 65 ˚C using a Viscotek GPC Max VE 2001 separation module and a Viscotek TDA 305 RI detector. The instrument was calibrated using polystyrene standards (1,050—3,800,000 g/mol) and data was analyzed using OmniSec 4.6.0 software.

ESI mass spectra were acquired on an *Agilent 6890-5975* GC- MS and MALDI-TOF spectra were acquired on a Bruker Ultraflex MALDI-TOF-TOF instrument using a 9-nitroanthracene matrix.

2-D grazing incidence wide angle X-ray scattering (GIWAXS) experiments were performed at the Stanford Synchrotron Radiation Lightsource on beamline 11-3 using a wavelength of 0.9742 Å with an incidence angle of 0.12◦ . Fig. S3 shows the full 2-D

diffractograms of our different polymer systems. These diffractograms were radially integrated to obtain the diffraction patterns (0-10◦ for in-plane, 70-80◦ for out-of-plane, and 0-180◦ for full). The 2-D images were collected on a plate with the detector 250 mm away from the center of the measured sample. The beam spot had a width of ∼150 μm and a helium chamber was used to reduce the noise. The software package WxDiff was used to reduce the GIWAXS data and subsequent analysis was performed in IgorPro.

All substrates were cleaned by sequentially sonicating in soapy water, DI water, acetone, and isopropanol for 5-10 minutes each, then placed under rough vacuum to remove all traces of residual solvent, and finally transferred into a nitrogen glove box for use. The films were cast from *o*-dichlorobenzene solutions at a concentration of 20 mg/mL and spin cast at 1160 rpm for 20 seconds, then 3000 rpm for 1 second. This allowed for even distribution of the polymer on the substrate and removal of excess solution while leaving the film still wet.

All CVs were scanned in the oxidation direction first follow by reduction. CVs were measured in a 3 neck flask at 0.5 mV/s with Arbin BT2000. Polymer films deposited on ITO glass were used as the working electrode, Li as the reference and counter electrode and 1M $LiPF_6$ in propylene carbonate as the electrolyte.

5,6-Dinitro-4,7-bis((triisopropylsilyl)ethynyl)benzo[c][1,2,5]thiadiazole (1)

Triisopropylsiliylacetylene 0.766 g of (4.2 mmol, 2.1 eq) was dissolved in 10 mL of dry, degassed tetrahydrofuran in a flame dried 50 mL round-bottom flask charged with a magnetic stir bar

under an argon atmosphere. The solution was cooled to 0 °C using an ice bath, and 1.68 mL of a 2.5 M n-butyl lithium solution in hexanes (4.2 mmol, 2.1 eq) was added drop wise under stirring. 0.838 g of copper (I) iodide (4.4 mmol, 2.2 eq) was then added to the solution, which immediately turned a lime green. The solution was then stirred for 15 minutes. A solution of 0.768 g 4,7-dibromo-5,6-dinitrobenzo[c][1,2,5]thiadiazole dissolved in 5 mL of tetrahydrofuran was then quickly added to the copper acetylide solution. The solution immediately turned deep red and was stirred for 1 hour. 20 g of silica was then added to the solution and the solution was rotary evaporated to dryness under reduced pressure. The compound was then purified via silica flash chromatography using a 1:1 mixture of dichloromethane/hexanes. The product was isolated as a bright fluorescent yellow solid: 0.846 g (34%). Spectra matched reported values.[18] ^{1}H NMR (500 MHz, $CDCl_3$) δ 1.20-1.15 (m, 42H) ^{13}C NMR (126 MHz, $CDCl_3$) δ 153.1, 145.8, 115.3, 112.6, 94.8, 18.5, 11.2.

2,7-Dibromobenzo[2,1-b:3,4-b']dithiophene-4,5-dione (2)

Compound **2** was synthesized according to the literature procedure, and spectra matched literature values.[22]

2,5-Dibromo-8,12-bis((triisopropylsilyl)ethynyl)-[1,2,5]thiadiazolo[3,4-*i*]dithieno[3,2-*a*:2',3'-*c*]phenazine (**3**)

Compound **3** was synthesized by dissolving 500 mg of (**1**) (0.850 mmol, 1.0 eq) in 8 mL of degassed glacial acetic acid in a 25 mL tear-drop flask charged with a magnetic stir-bar under an argon atmosphere. 570 mg of freshly reduced iron powder (10.2 mmol, 12.0 eq) was then added to the solution and the solution immediately turned a dark crimson. The solution was stirred for 4 hours until the crimson color was replaced by a deep yellow. The solution was then diluted with 15 mL of chloroform and filtered through a plug of celite. The celite plug was then washed with two 10 mL portions of chloroform until the filtrate became colorless. The filtrate was then rotary evaporated under reduced pressure with light heating until a wet yellow solid was isolated (some residual acetic acid is desirable). The solid was then dissolved in 15 mL of a degassed 1:1 mixture of ethanol/chloroform. 320 mg of **2** (0.850 mmol, 1 eq) was then added to the solution and the mixture was then sparged with argon for 10 minutes. The solution was then heated to reflux for 12 hours or until the starting reagents were fully consumed by TLC. The mixture was then rotary evaporated to dryness and was purified using SiO_2 flash chromatography using a 1:4 mixture of dichloromethane/hexanes to yield 266 mg of an emerald green solid (0.303 mmol, 35%).^{1}H NMR (500 MHz, $CDCl_3$) δ 8.41 (s, 2H), 1.6-1.3 (m, 42H) ^{13}C NMR (126 MHz, $CDCl_3$) δ 154.6, 141.4, 140.4, 137.3, 134.9, 128.6, 114.2, 113.7, 110.8, 101.6, 19.0, 11.6. MALDI-TOF MS: *m/z* found 869.058 calculated for $C_{38}H_{44}Br_2N_4S_3Si_2$ 868.956.

Poly{(8,12-bis((triisopropylsilyl)ethynyl)-[1,2,5]thiadiazolo[3,4-*i*]dithieno[3,2-*a*:2',3'-*c*]phenazine)-2,5-diyl)- *alt*-(9,9-dioctyl-9H-fluorene-2,7-diyl)} (P1)

Polymer **P1** was synthesized via the following procedure: Compound **3** (100 mg, 0.115 mmol, 1.0 eq) and 110 mg (0.115 mmol, 1.0 eq) of 2,7-tributylstannyl-9,9-bisoctylfluorene were dissolved in 8 mL toluene in a 25 mL round-bottom flask charged with a magnetic stir bar. The mixture was sparged with argon for 15 minutes and 6.5 mg of tetrakis(triphenylphosphine)palladium (0) (0.0062 mmol, 0.05 eq) was then added to the solution. The round-bottom flask was then sparged with argon for 10 minutes and the mixture was heated to reflux for 4 days. The mixture was then cooled and poured into 100 mL of a 1% HCl solution in methanol. The mixture was stirred for 30 minutes until a fine precipitate formed. The precipitate was then filtered using a fine fritted filter and the filter cake was soxholet extracted using methanol, acetone, and hexanes until the eluent ran nearly colorless to yield 59 mg of a black powder (47%).^{1}H NMR (500 MHz, $CDCl_3$) δ 8.9-8.3 (s, 2H), 8.0-7.6 (m, 4H), 7.2-7.1 (m 2H) 2.2-1.8 (s, 4H), 1.8-1.3 (m, 28H), 1.3-0.9 (m, 28H), 0.9-0.5 (m, 16H). GPC (ODCB solvent, calibrated using PS std) M_n = 3566 PDI = 1.71

Poly{*(*8,12-bis((triisopropylsilyl)ethynyl)-[1,2,5]thiadiazolo[3,4-*i*]dithieno[3,2-*a*:2',3'-*c*]phenazine)-2,5-diyl)-*alt*-((4,4-bis(2'-ethylhexyl)-4H-cyclopenta[2,1-b:3,4-b']dithiophene)-2,6-diyl)} (P2)

Polymer **P2** was synthesized via the following procedure: 125 mg of **3** (0.144 mmol, 1.0 eq) and 141 mg (0.144 mmol, 1.0 eq) of 2,6-tributylstannyl-4,4-bis(2'-ethylhexyl)-4H-cyclopenta[2,1-b:3,4-b']dithiophene were dissolved in 10 mL toluene in a 25 mL round-bottom flask charged with a magnetic stir bar. The mixture was sparged with argon for 15 minutes and 12 mg of

tetrakis(triphenylphosphine)palladium (0) (0.011 mmol, 0.075 eq) was then added to the solution. The round-bottom flask was then sparged with argon for 10 minutes and the mixture was heated to reflux for 4 days. The mixture was then cooled and poured into 100 mL of a 1% HCl solution in methanol. The mixture was stirred for 30 minutes until a fine precipitate formed. The precipitate was then filtered using a fine fritted filter and the filter cake was soxholet extracted using methanol, acetone, and hexanes until the eluent ran nearly colorless to yield 71 mg of a black powder (44%). ^{1}H NMR (500 MHz, $CDCl_3$) δ 8.6-8.4 (broad s.; 2H), 7.4-7.1 (m, 2H), 2.1-1.8 (m, 4H), 1.5-1.3 (m, 42H), 1.2-0.9 (m, 16H) 0.8-0.6 (m, 14H) GPC (ODCB solvent, calibrated using PS std.): M_n = 4,526, PDI = 1.75

2,7-Di-tert-butylpyrene-4,5,9,10-tetraone (4)

4 was synthesized according to the literature procedure and the spectra matched literature values.[34]

2,12-Di-tert-butyl-5,9,15,19-tetrakis((triisopropylsilyl)ethynyl)-[1,2,5]thiadiazolo[3'',4'':6',7']quinoxalino[2',3':9,10]phenanthro[4,5-abc][1,2,5]thiadiazolo[3,4-i]phenazine (5)

Compound **5** was synthesized by dissolving 500 mg of **1** (0.850 mmol, 2.0 eq) in 8 mL of degassed glacial acetic acid in a 25 mL tear-drop flask charged with a magnetic stir-bar under an argon atmosphere. 570 mg of freshly reduced iron powder (10.2 mmol, 12.0 eq) was then

added to the solution and the solution immediately turned a dark crimson. The solution was stirred for 4 hours until the crimson color was replaced by a deep yellow. The solution was then diluted with 15 mL of chloroform and filtered through a plug of celite. The celite plug was then washed with two 10 mL portions of chloroform until the filtrate became colorless. The filtrate was then rotary evaporated under reduced pressure with light heating until a wet yellow solid was isolated (some residual acetic acid is desirable).). The solid was then dissolved in 15 mL of a degassed 1:1 mixture of ethanol/chloroform. 159 mg of **4** (0.425 mmol, 1.0 eq) was then added to the solution and the mixture was then sparged with argon for 10 minutes. The solution was then heated to reflux for 48 hours. TLC revealed the formation of two products: a red/pink product with an r_f of 0.91 1:1 hexanes/DCM and a reddish/brown product with R_f of 0.36. The mixture was then rotary evaporated to dryness and was purified using SiO_2 flash chromatography using a 1:3 mixture of dichloromethane/hexanes to yield 48 mg of a pink/red solid **5** (8.0%).^{1}H NMR (500 MHz, $CDCl_3$) δ 9.86 (s, 4H), 1.71 (s, 18H), 1.5-1.3 (m, 84H)^{13}C NMR (126 MHz, $CDCl_3$) δ 155.5, 151.8, 145.3, 141.4, 129.3, 127.6, 127.5, 114.4, 110.5, 101.9, 35.7, 31.6, 19.0, 11.7 MALDI-TOF MS: *m/z* found 1354.677 calculated for $C_{80}H_{106}N_8S_2Si_4$ 1354.706.

2,7-Di-tert-butyl-10,14-bis((triisopropylsilyl)ethynyl)phenanthro[4,5-abc][1,2,5]thiadiazolo[3,4-i]phenazine-4,5-dione (6)

Compound **6** was recovered as a by-product of the reaction to synthesize **5**. **6** was recovered as a brown/red solid and contained a small amount of impurities from the desilylation of the triisopropylsilyl groups. 93 mg of **6** was isolated (25%).^{1}H NMR (500 MHz, $CDCl_3$) δ 8.62 (d, *J* =

2.0 Hz, 2H), 7.23 (d, *J* = 2.0 Hz, 2H), 1.56 (s, 18H), 1.4-1.2 (m, 42H).[13]C NMR (126 MHz, $CDCl_3$) δ 179.9, 155.6, 153.1, 143.8, 141.0, 131.3, 131.1, 130.2, 130.1, 129.6, 114.7, 111.2, 101.7, 35.5, 31.2, 19.0, 11.6198 MALDI-TOF MS: *m/z* found 863.932 calculated for $C_{52}H_{64}N_4O_2SSi_2$ 864.429.

Benzo[2,1-b:3,4-b']dithiophene-4,5-diamine (7)

Compound **7** was synthesized according to the literature procedure, and spectra matched literature values.[22] [1]H NMR (500 MHz, $CDCl_3$) δ 7.35 (d, *J* = 5.4 Hz, 2H), 7.32 (d, *J* = 5.4 Hz, 2H), 3.69 (broad s, 4H) [13]C NMR (126 MHz, $CDCl_3$) δ 130.3, 125.8, 124.9, 123.7, 120.1

9,19-Di-tert-butyl-12,16-bis((triisopropylsilyl)ethynyl)-[1,2,5]thiadiazolo[3'',4'':6',7']quinoxalino[2',3':9,10]phenanthro[4,5-abc]dithieno[3,2-h:2',3'-j]phenazine (8)

Compound **8** was synthesized according to the literature procedure, and spectra matched literature values.[22]

Dithieno[3',2':3,4;2'',3'':5,6]benzo[1,2-c][1,2,5]thiadiazole (9a)

Compound **9a** was synthesized according to the literature procedure, and spectra matched literature values.[22]

5,8-Dibromodithieno[3',2':3,4;2'',3'':5,6]benzo[1,2-c][1,2,5]thiadiazole (9b)

Compound **9b** was synthesized according to the literature procedure, and spectra matched literature values.[22]

2,5-Dibromotetrathieno[3,2-a:2',3'-c:3'',2''-h:2''',3'''-j]phenazine (10a)

Compound **10a** was synthesized according to the literature procedure, and spectra matched literature values.[22]

2,5-Bis((triisopropylsilyl)ethynyl)tetrathieno[3,2-a:2',3'-c:3'',2''-h:2''',3'''-j]phenazine (10b)

Compound **10b** was synthesized via the following procedure: 500 mg of **10a** (0.886 mmol, 1.0 eq) and 486 mg of triisopropylsiliylacetylene (2.74 mmol, 3.0 eq) were added to a 100 mL round-bottom flask charged with a magnetic stir-bar and the mixture was suspended in 50 mL of toluene and 1 mL of triethylamine. The suspension was sparged with a stream of argon for 15 minutes. 34 mg of copper (I) iodide (0.18 mmol, 0.2 eq) and 100 mg of tetrakis(triphenylphosphine)palladium (0) (0.089 mmol, 0.1 eq), was then added to the suspension and the round-bottom flask was connected to a reflux condenser and sparged with a stream of argon for 10 minutes. The mixture was then heated to reflux for 12 hours. The solution was cooled and rotary evaporated under reduced pressure and the crude product was purified using SiO_2 flash chromatography using a 1:5 mixture of DCM/hexanes as eluent. 379 mg of **10b** was recovered as a yellow solid (55%).^{1}H NMR (500 MHz, $CDCl_3$) δ 8.22 (s, 2H), 8.18

(d, *J* = 5.1 Hz, 2H), 7.45 (d, *J* = 5.1 Hz, 2H), 1.25 (m, 42H).^{13}C NMR (126 MHz, $CDCl_3$) δ 137.3, 136.5, 135.2, 134.9, 134.6, 134.3, 129.4, 124.6, 124.2, 122.6, 99.4, 98.8, 18.8, 11.4.

9,10,13,14-tetrakis(dodecyloxy)dibenzo[a,c]dithieno[3,2-h:2',3'-j]phenazine (11)

Compound **11** was synthesized via the following procedure: 100 mg of benzo[2,1-b:3,4-b']dithiophene-4,5-diamine (0.45 mmol) and 418 mg of 2,3,6,7-tetrakis(dodecyloxy)phenanthrene-9,10-dione (0.44 mmol) were added to a 50 mL round-bottom flask charged with a magnetic stir-bar and the solids were dissolved in 20 mL of a 1:1 mixture of chloroform/ethanol and a drop of acetic acid was added as catalyst. The mixture was connected to a reflux condenser and the mixture was sparged with a stream of argon for 10 minutes. The reaction was refluxed under an argon atmosphere for 48 hours and the reaction mixture was cooled and rotary evaporated under reduced pressure. The crude mixture was then purified using SiO_2 chromatography using 1;5 mixture of DCM/hexanes as eluent to yield 230 mg of a greenish yellow solid (46%).^{1}H NMR (500 MHz, $CDCl_3$) δ 8.80 (s, 2H), 8.44 (d, J = 5.2 Hz, 2H), 7.69 (s, 2H), 7.56 (d, *J* = 5.3 Hz, 2H), 4.35 (t, *J* = 6.5 Hz, 4H), 4.26 (t, *J* = 6.5 Hz, 4H), 1.99 (m, 8H), 1.61 (m, 8H), 1.46 (m, 8H), 1.4-1.2 (56H), 0.87 (t, *J* = 7.1 Hz, 12H).^{13}C NMR (126 MHz, $CDCl_3$) δ 151.4, 149.2, 139.3, 137.1, 135.3, 134.6, 126.1, 124.6, 124.1, 124.0, 108.3, 106.2, 69.6, 69.1, 29.79, 29.76, 29.72, 29.63, 29.61 (29.9-29.5 relative integration is 30C), 29.45, 29.42, 29.39 (29.5-29.3 relative integration is 12C), 26.3, 26.2. MALDI-TOF MS: *m/z* found 1128.841 calculated for $C_{72}H_{108}N_2O_4S_2$ 1128.775.

Poly{dithieno[3',2':3,4;2'',3'':5,6]benzo[1,2-c][1,2,5]thiadiazole)-5,8-diyl)-*alt*-((4,4-bis(2-ethylhexyl)-4H-cyclopenta[2,1-b:3,4-b']dithiophene)-2,6-diyl)} (**P3)**

Polymer **P3** was synthesized via the following procedure: 75 mg of **9a** (0.186 mmol, 1.0 eq) and 182 mg of 2,6-tributylstannyl-4,4-bis(2'-ethylhexyl)-4H-cyclopenta[2,1-b:3,4-b']dithiophene (0.186 mmol, 1.0 eq) were added to a 25 mL round-bottom flask charged with a magnetic stir bar and the compounds were suspended in 15 mL of toluene and the suspension was sparged with argon for 15 minutes. 11 mg of tetrakis(triphenylphosphine)palladium (0) (0.0093 mmol, 0.05 eq) was then added to the suspension and the suspension was sparged with argon for 10 minutes. The flask was then heated to reflux under an argon atmosphere for 4 days. The mixture was then poured into 100 mL 1% solution of HCl in methanol and the mixture was stirred for 30 minutes until a fine black precipitate formed. The precipitate was filtered using a fine fritted filter and the black solid was purified via soxholet extraction using subsequent washes of methanol, acetone, and hexanes. Soxholet extractions were terminated once the filtrate ran nearly colorless. 95 mg of a black solid was isolated (≈ 79%).^{1}H NMR (500 MHz, $CDCl_3$) δ 8.1-6.9 (m,4H), 2.3-1.8 (br. s, 4H), 1.8-1.5 (m, 6H), 1.5-0.4 9 (m, 24H).GPC (ODCB solvent compared to PS standard), M_n = 3800 PDI = 1.66

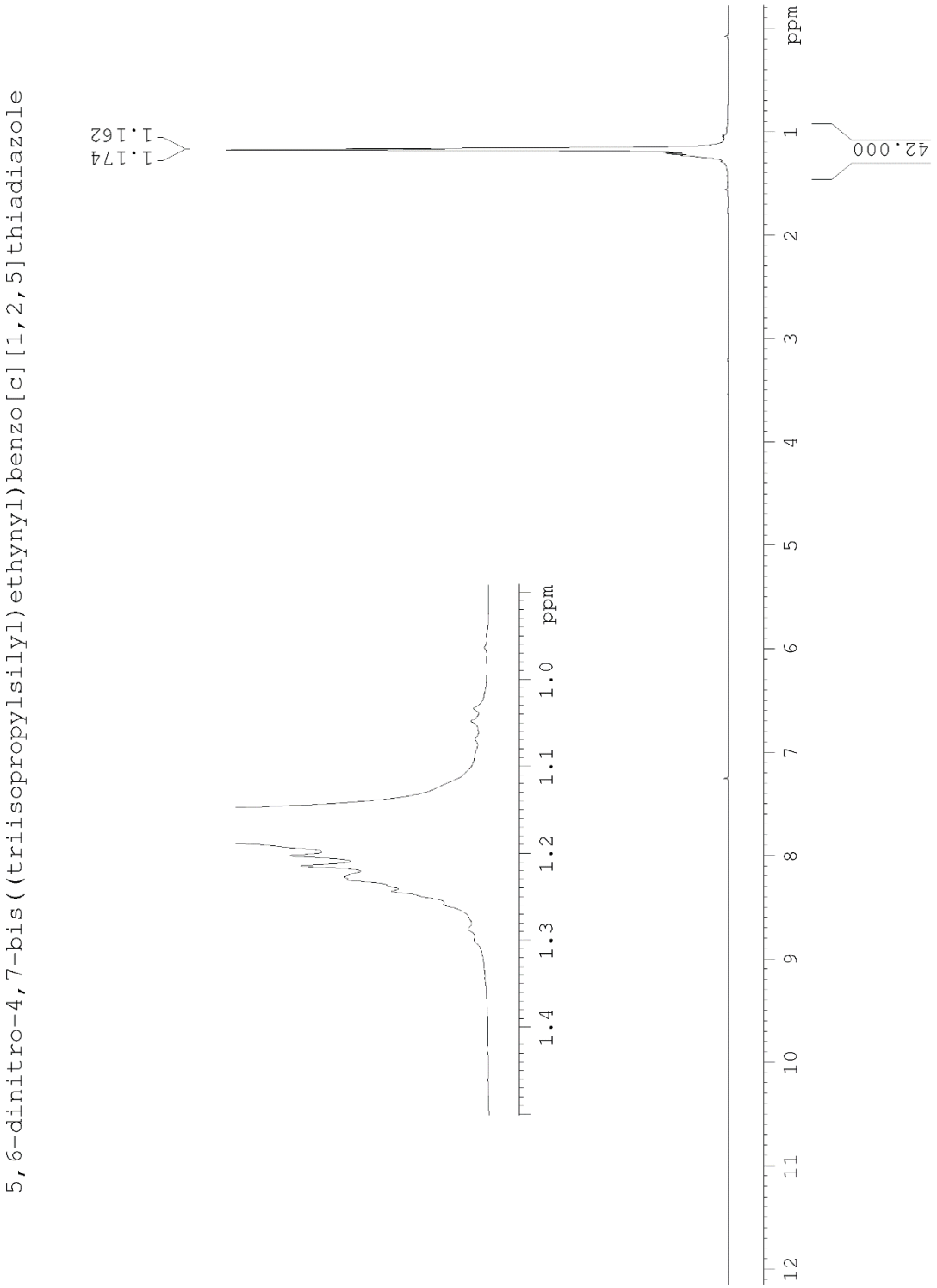

Figure 4.17. ^{1}H NMR spectrum of **1.**

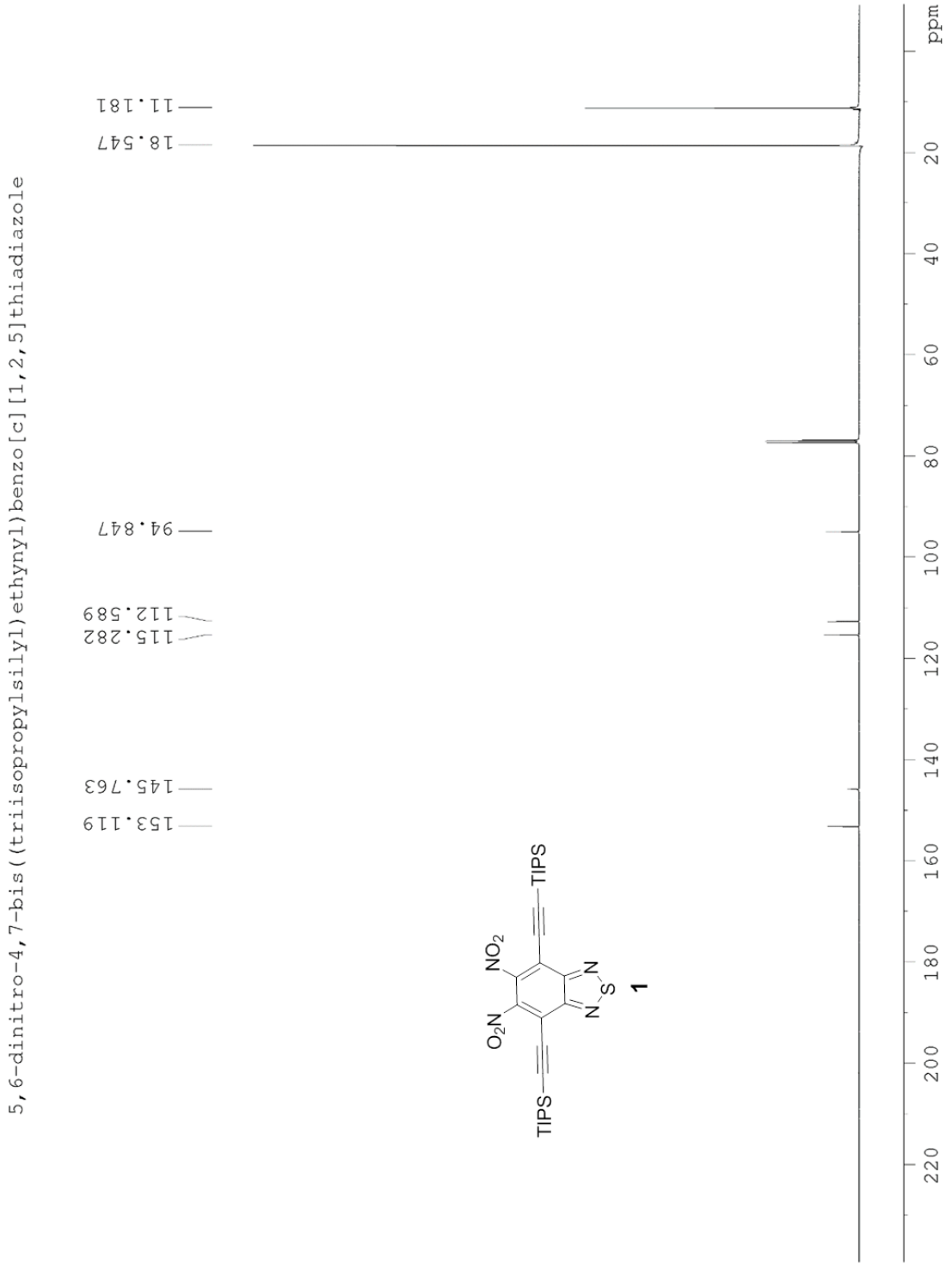

Figure 4.18. ^{13}C NMR spectrum of **1.**

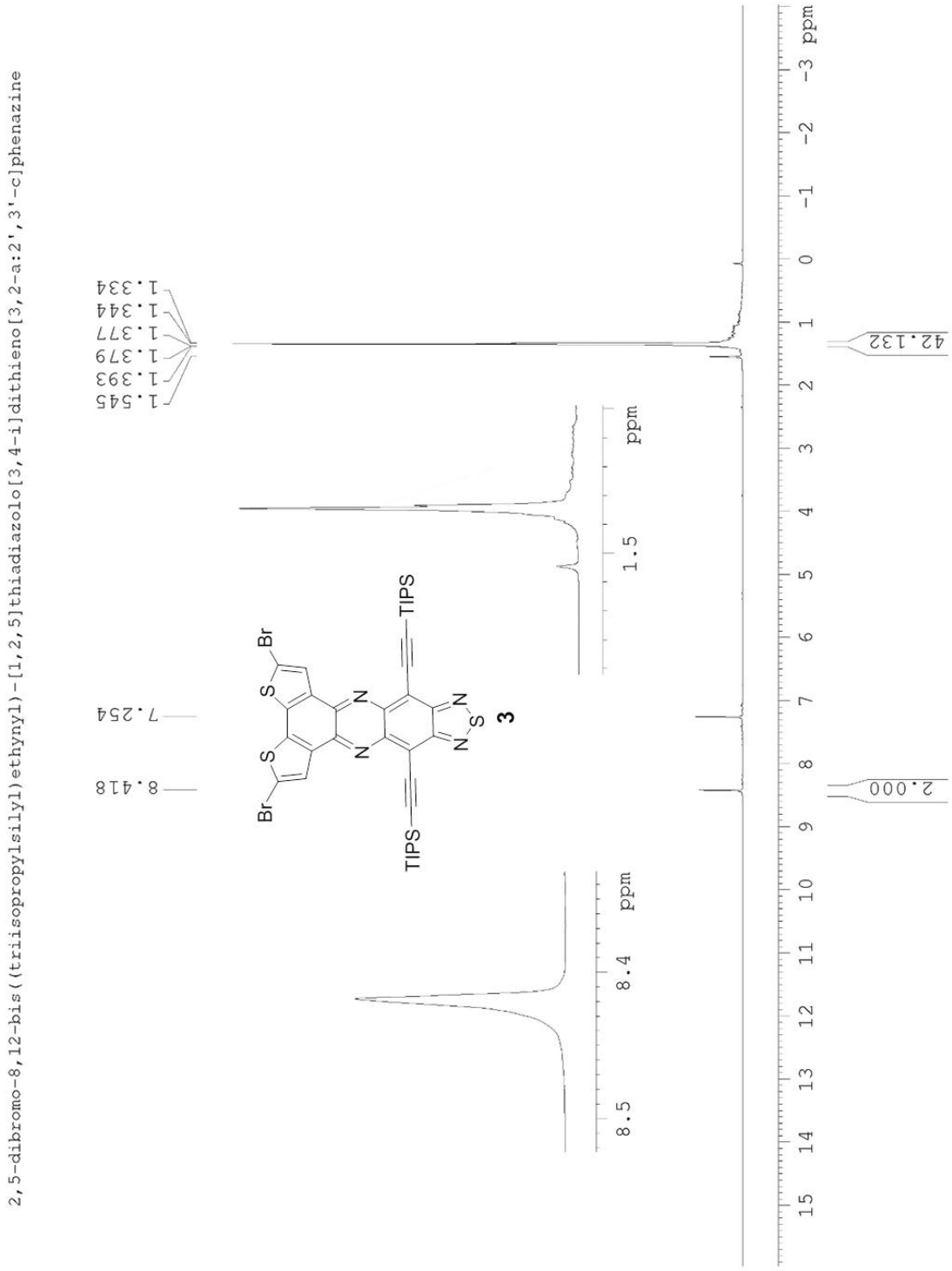

Figure 4.19. ^{1}H NMR spectrum of **3.**

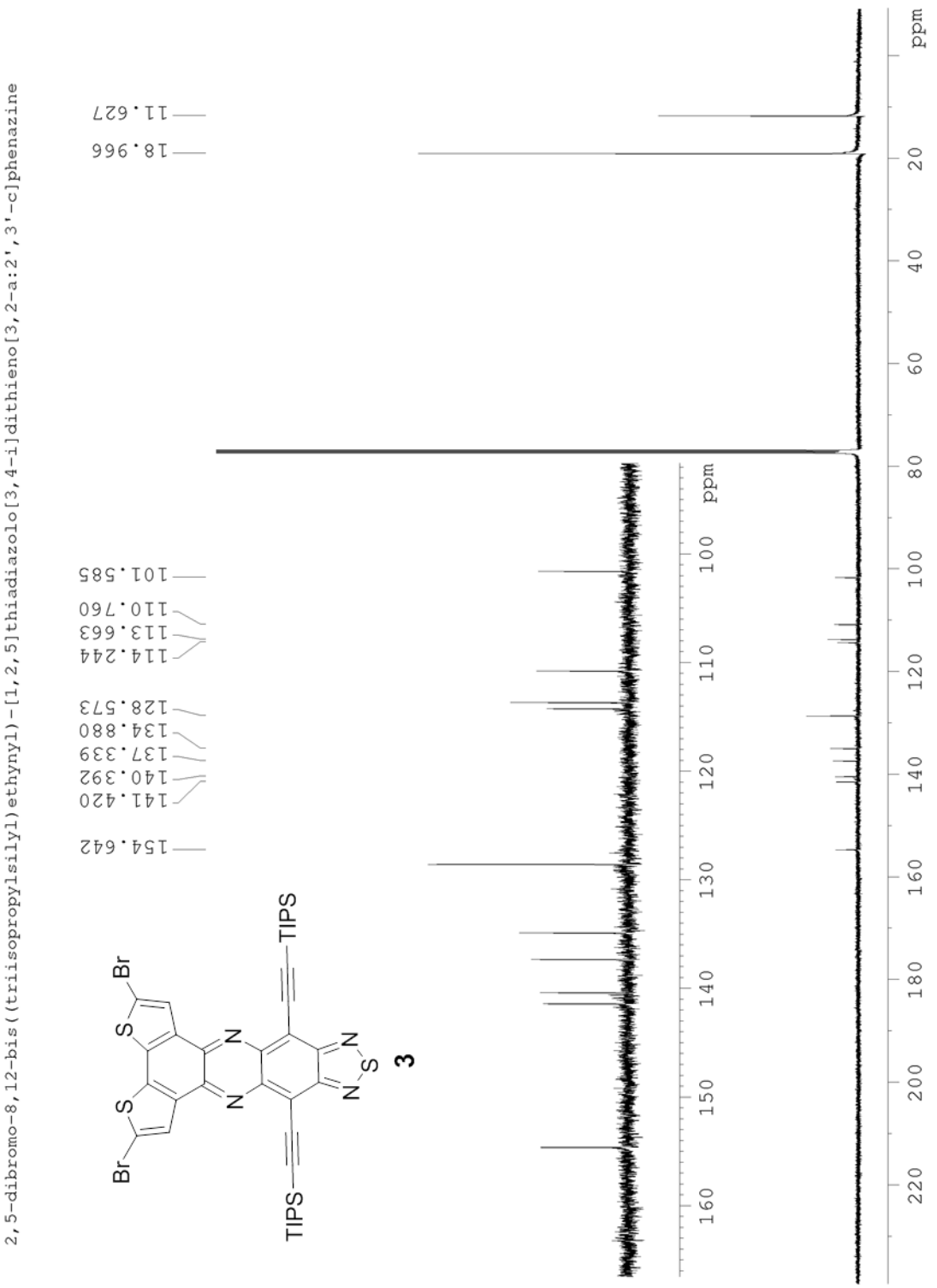

Figure 4.20. ^{13}C NMR spectrum of **3.**

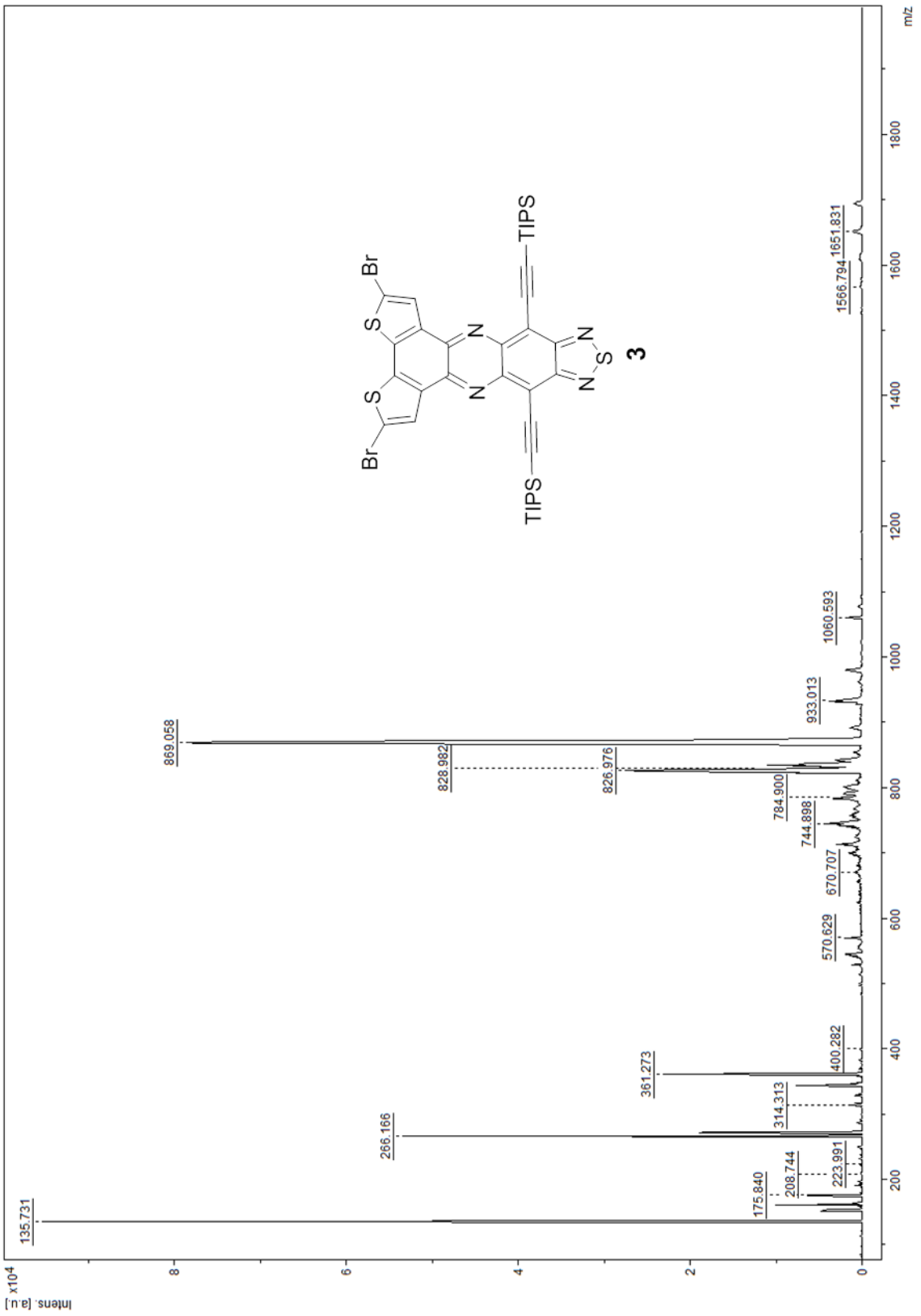

Figure 4.21. MALDI-TOF spectrum of **3.**

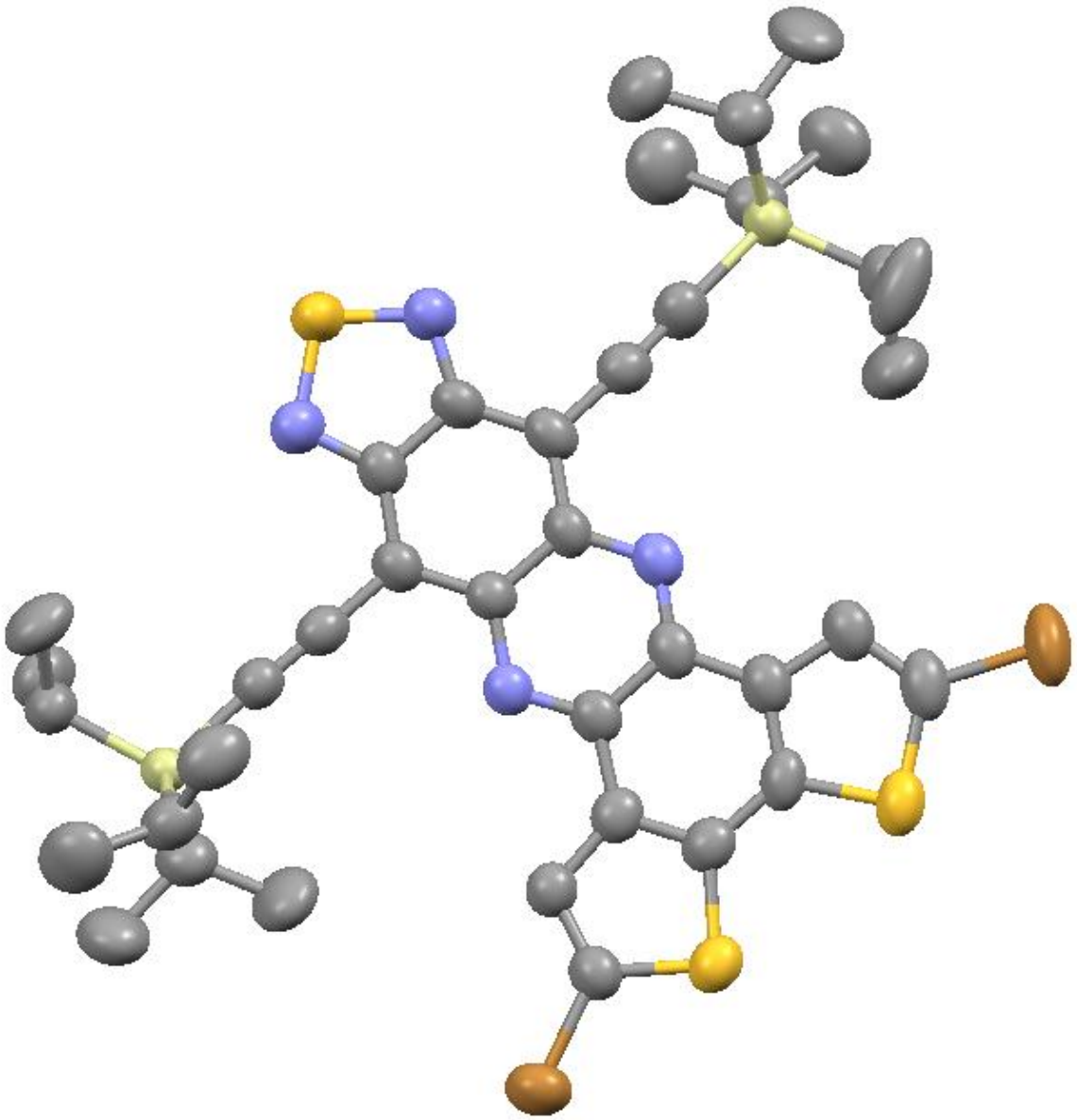

Figure 4.22. Crystal structure of **3** displaying 50% probability ellipsoids.

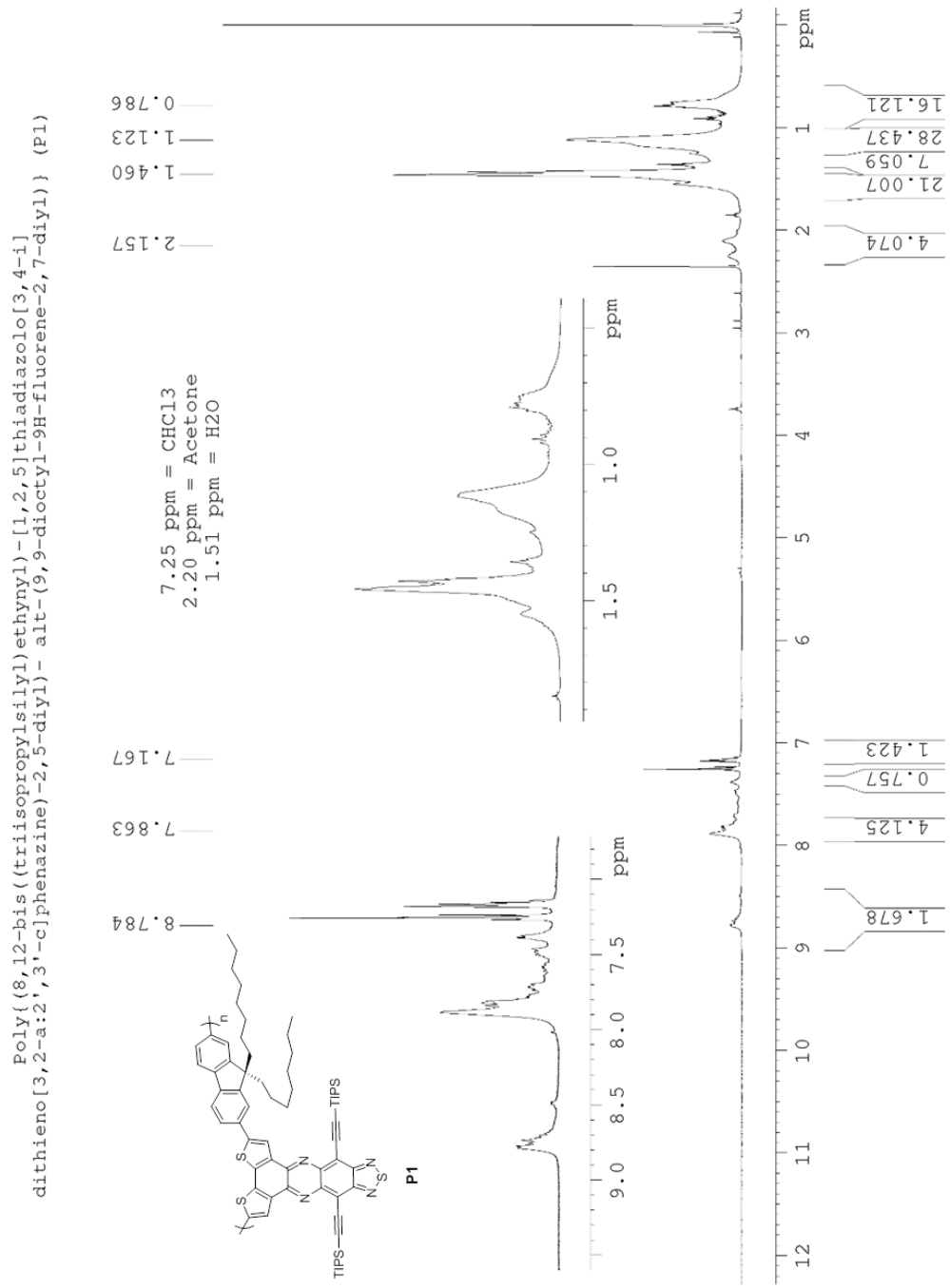

Figure 4.23. ^{1}H NMR spectrum of **P1.**

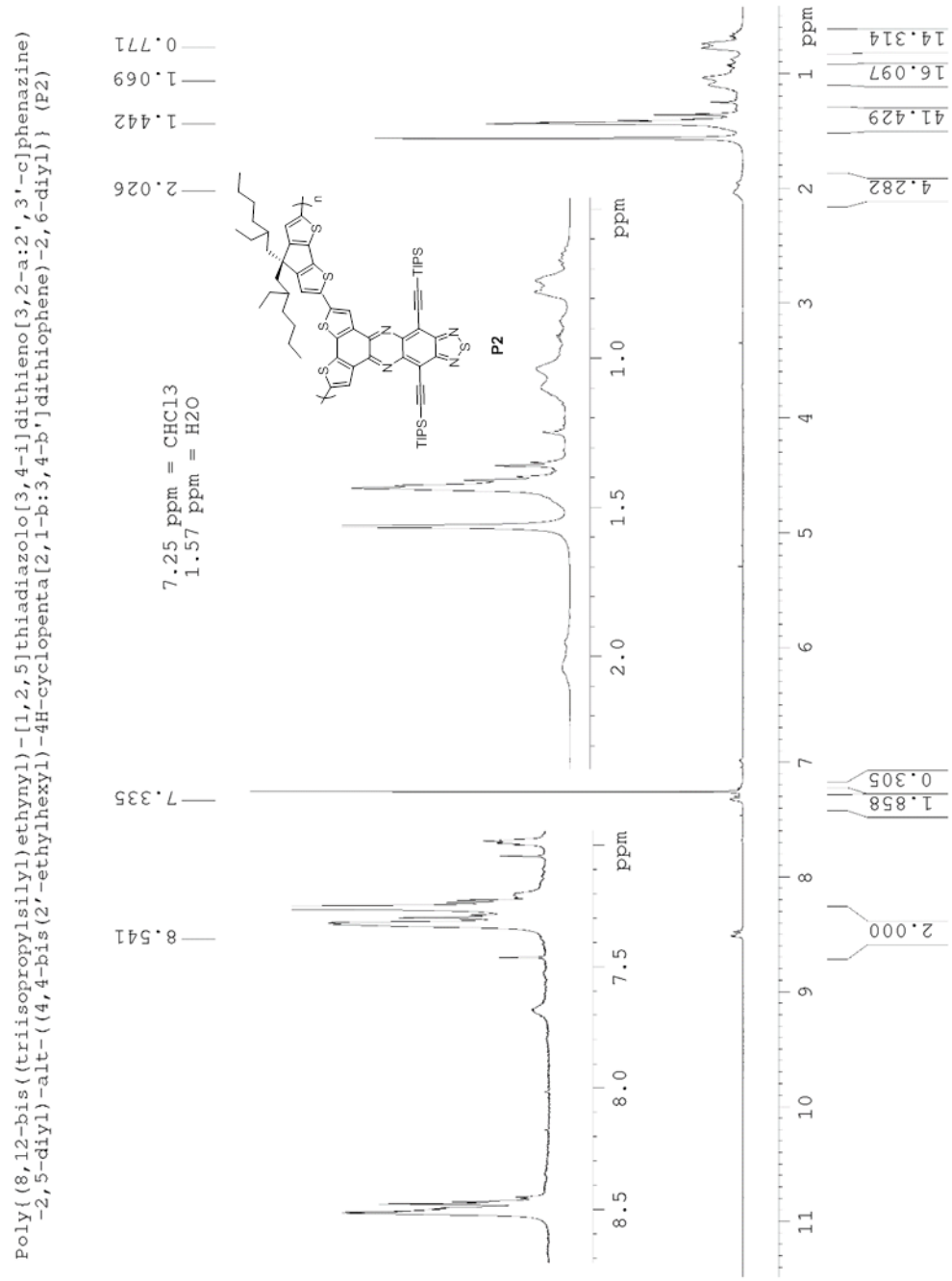

Figure 4.24. ^{1}H NMR spectrum of **P2.**

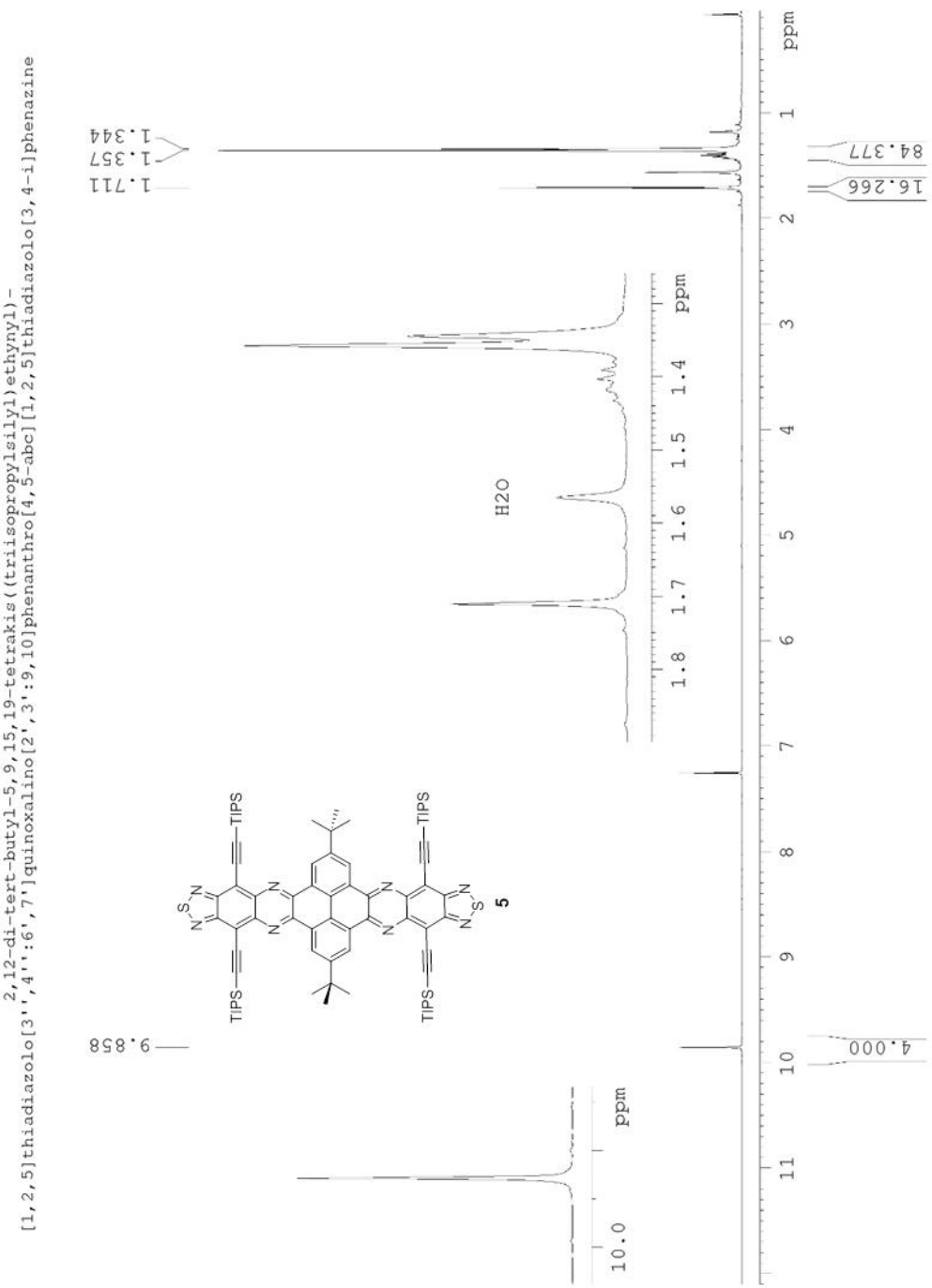

Figure 4.25. ^{1}H NMR spectrum of **5.**

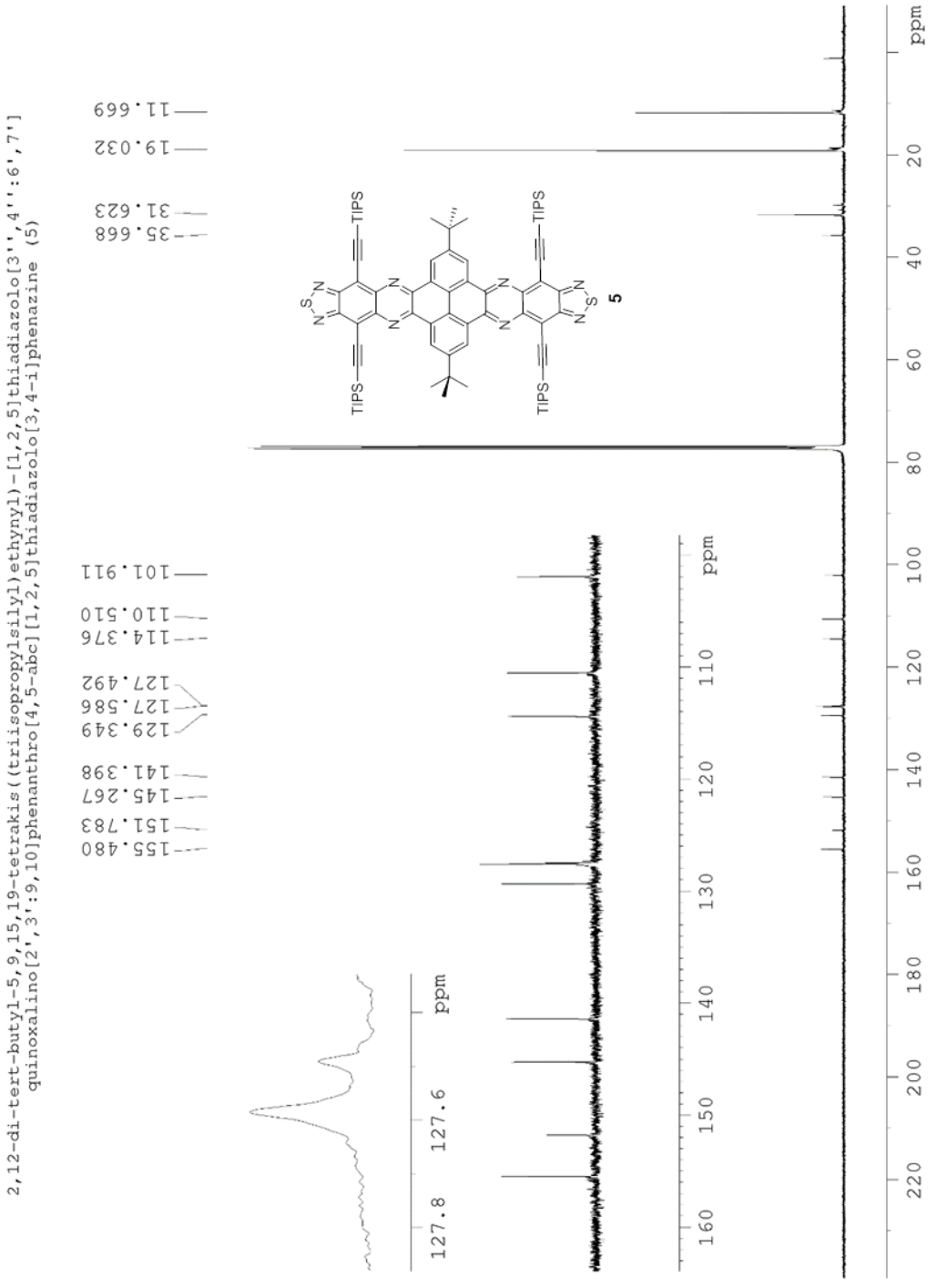

Figure 4.26. ^{13}C NMR spectrum of **5.**

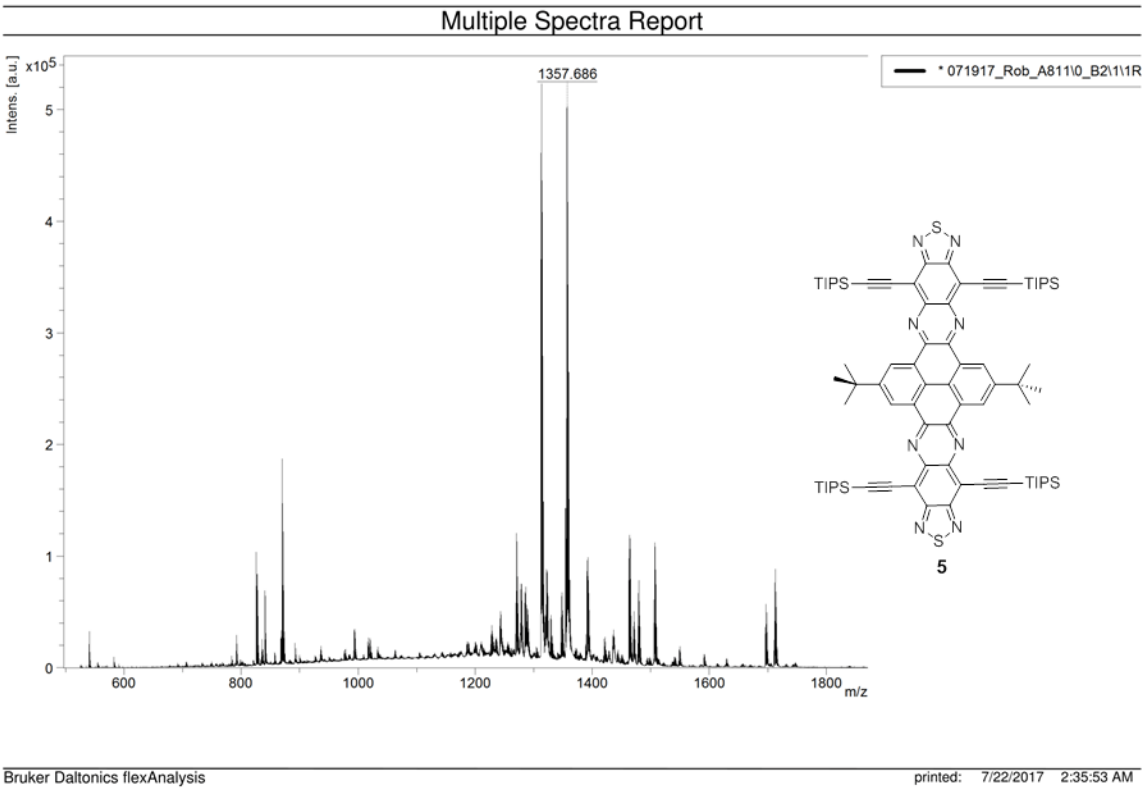

Figure 4.27. MALDI-TOF of **5.**

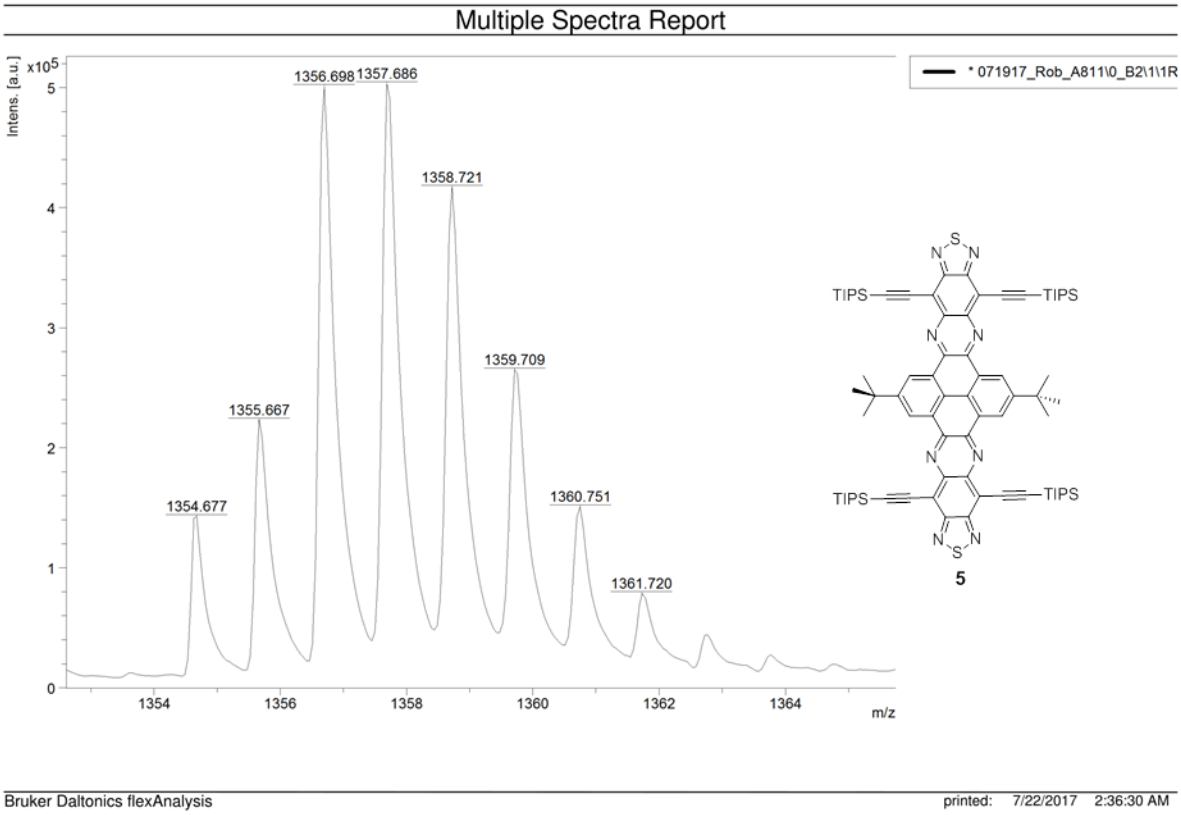

Figure 4.28. MALDI-TOF of **5** parent ion.

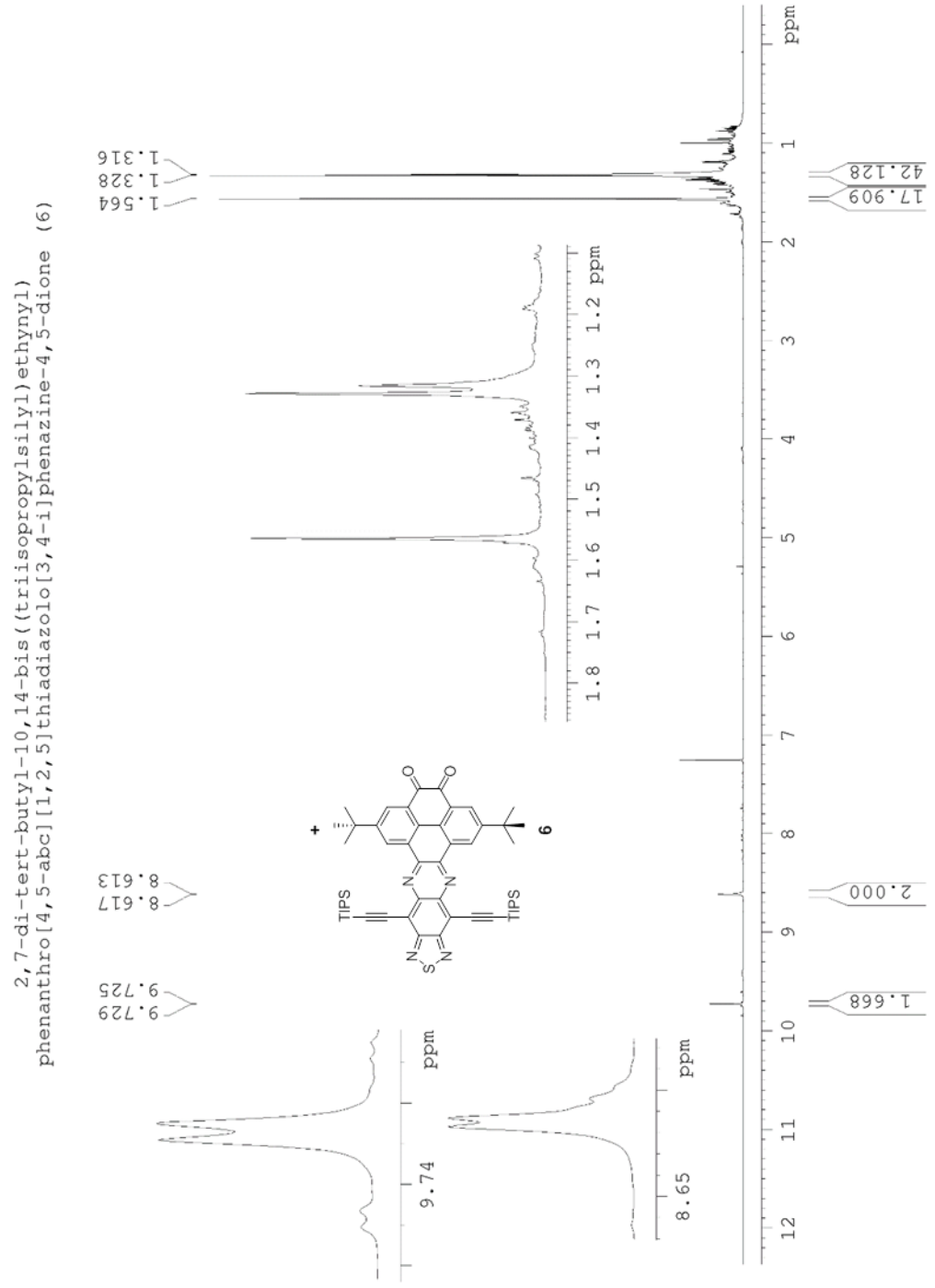

Figure 4.29. ^{1}H NMR of **6.**

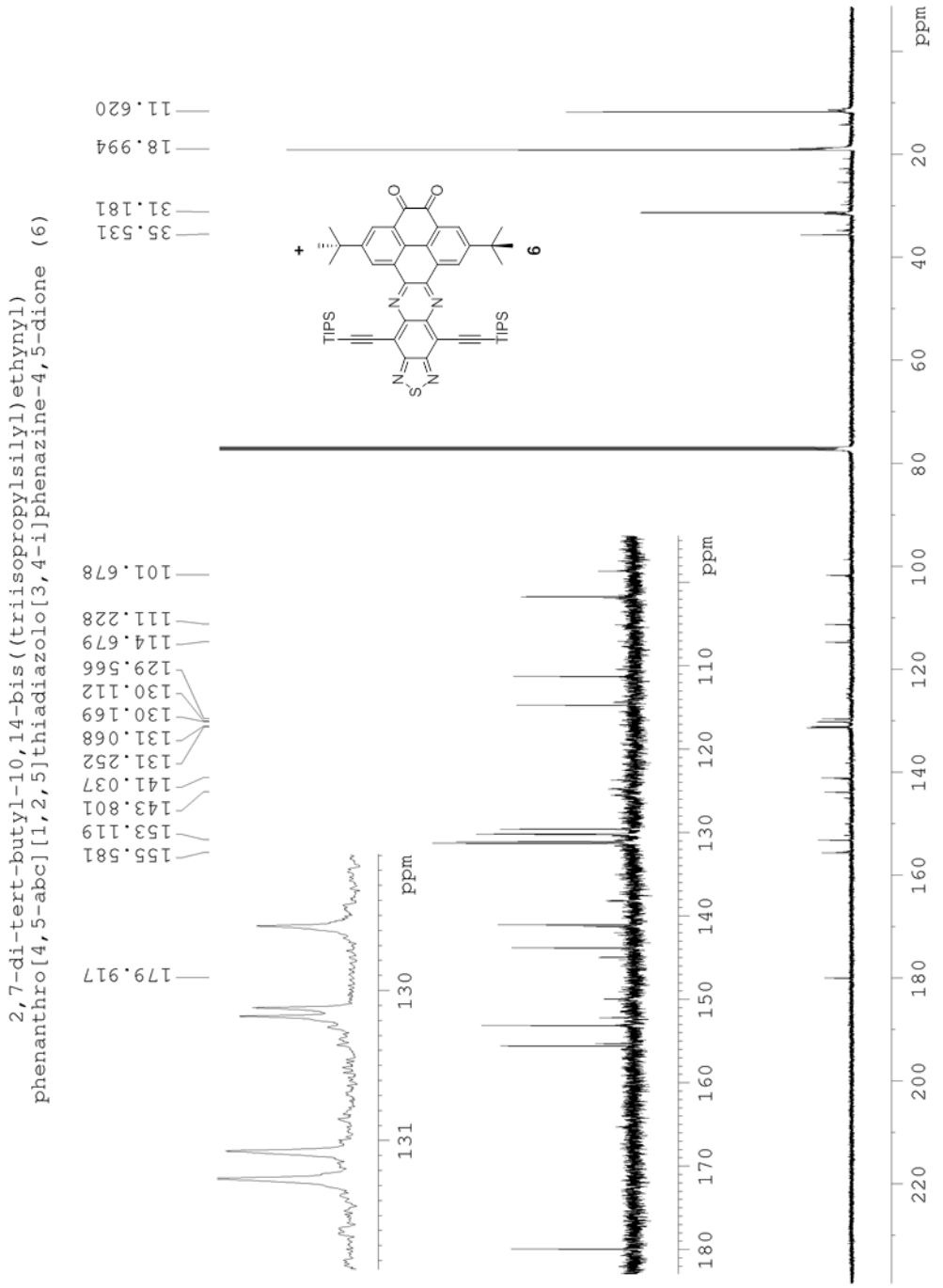

Figure 4.30. ^{13}C NMR spectrum of **6.**

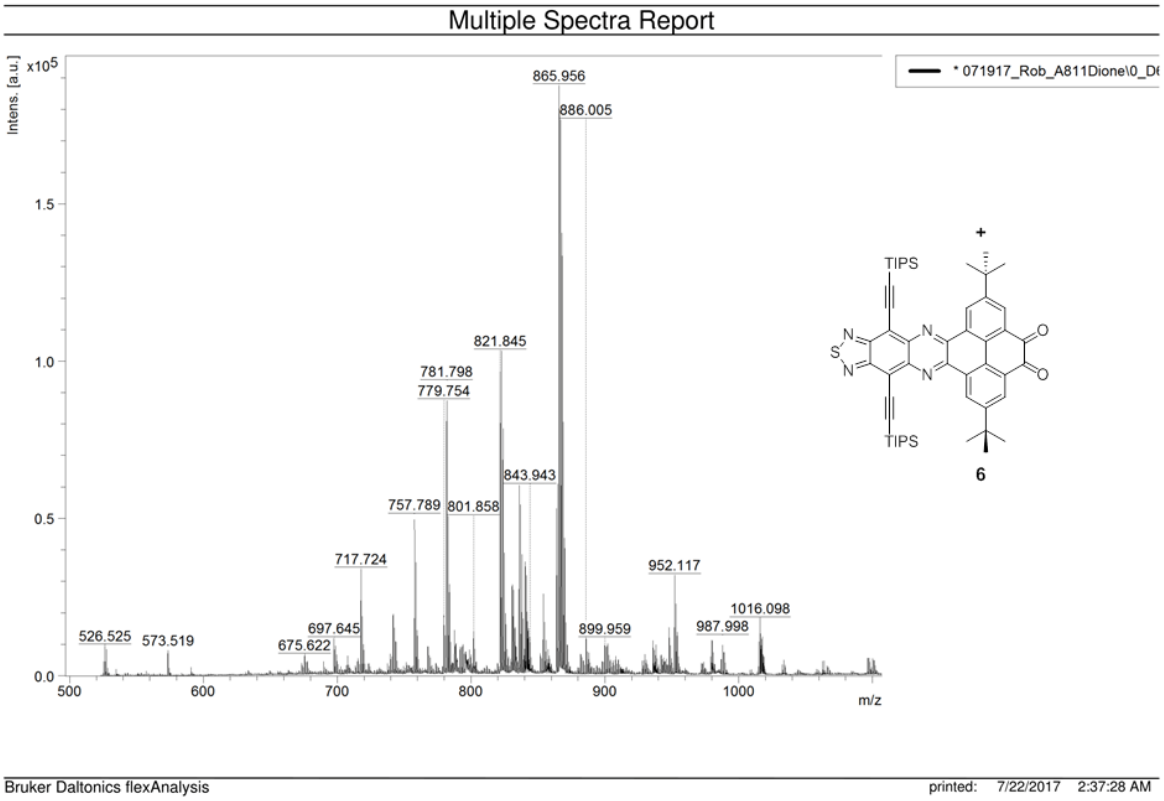

Figure 4.31. MALDI-TOF spectrum of **6.**

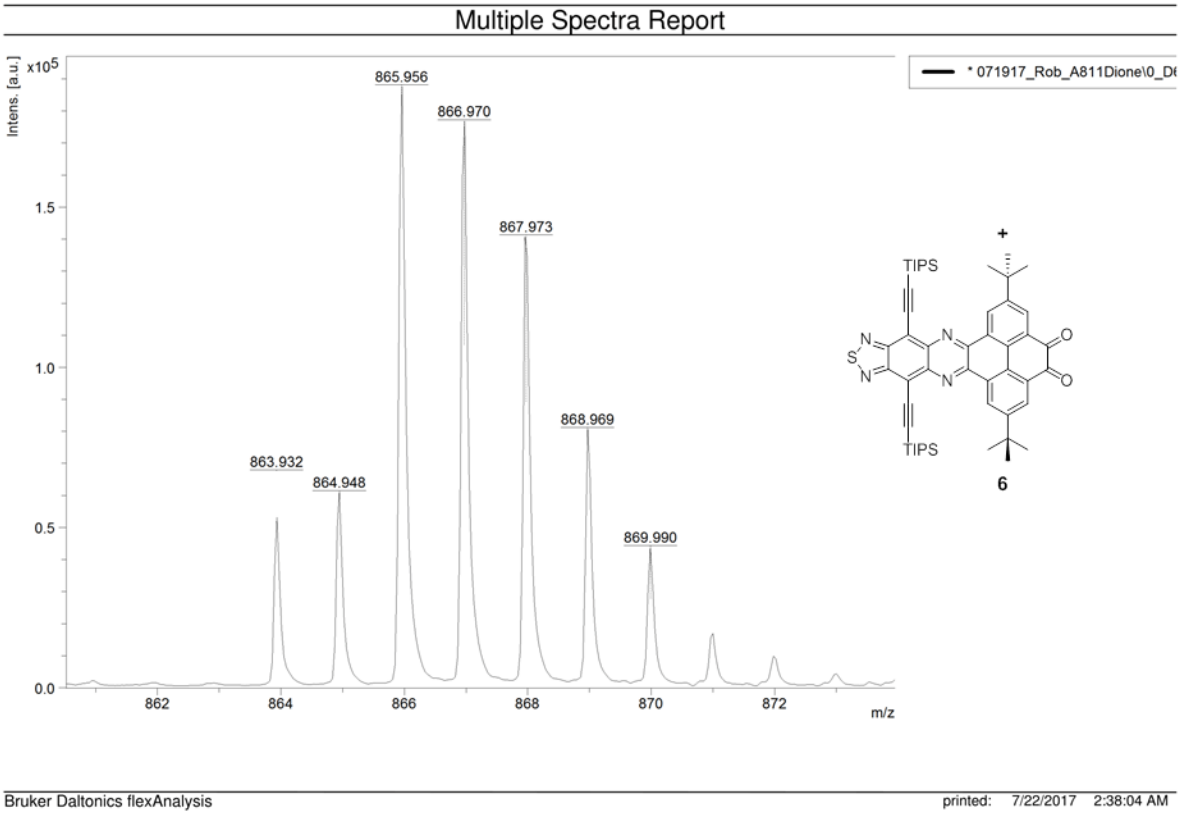

Figure 4.32. MALDI-TOF spectrum of **6** parent ion.

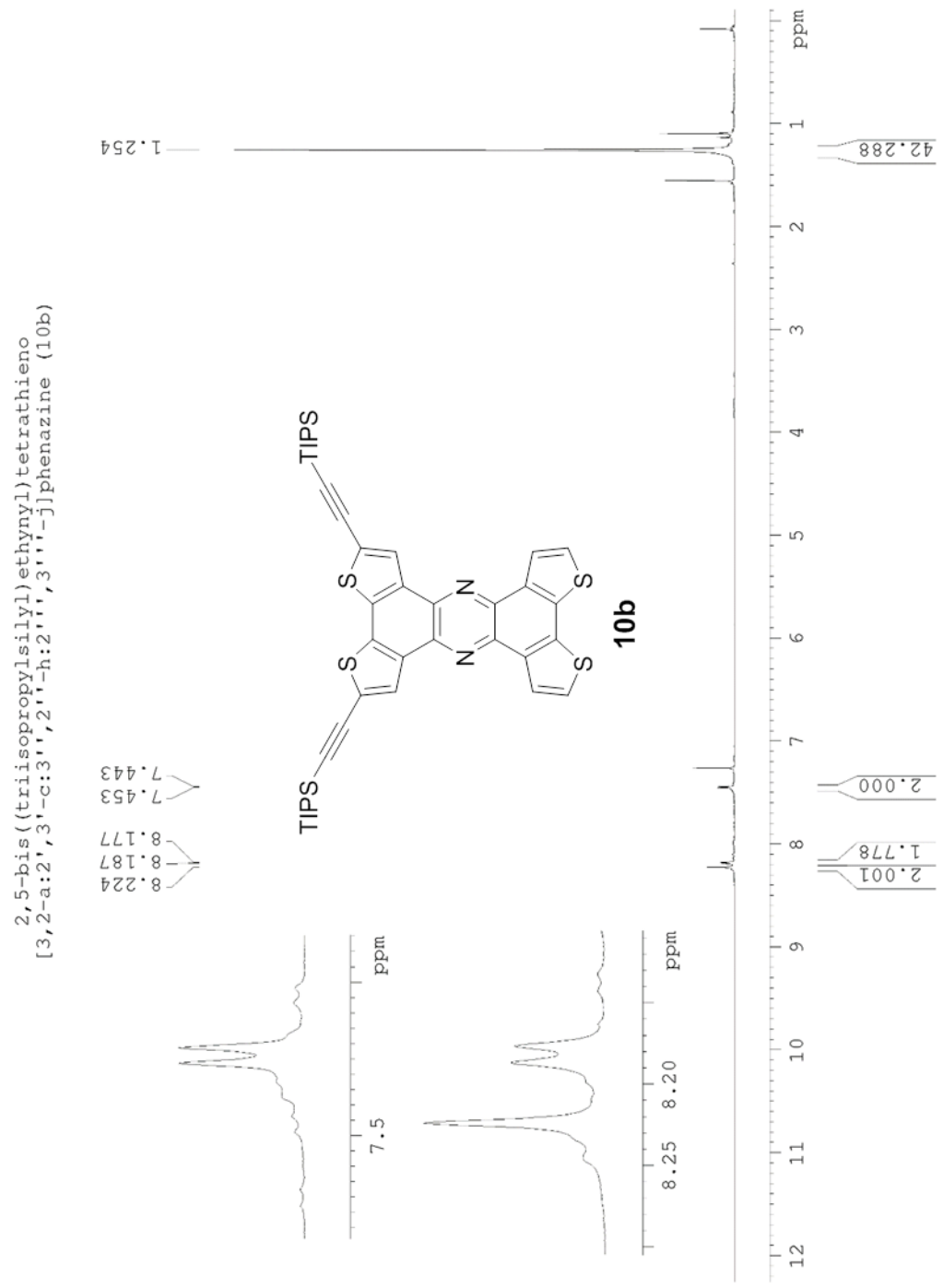

Figure 4.33. ^{1}H NMR spectrum of **10b.**

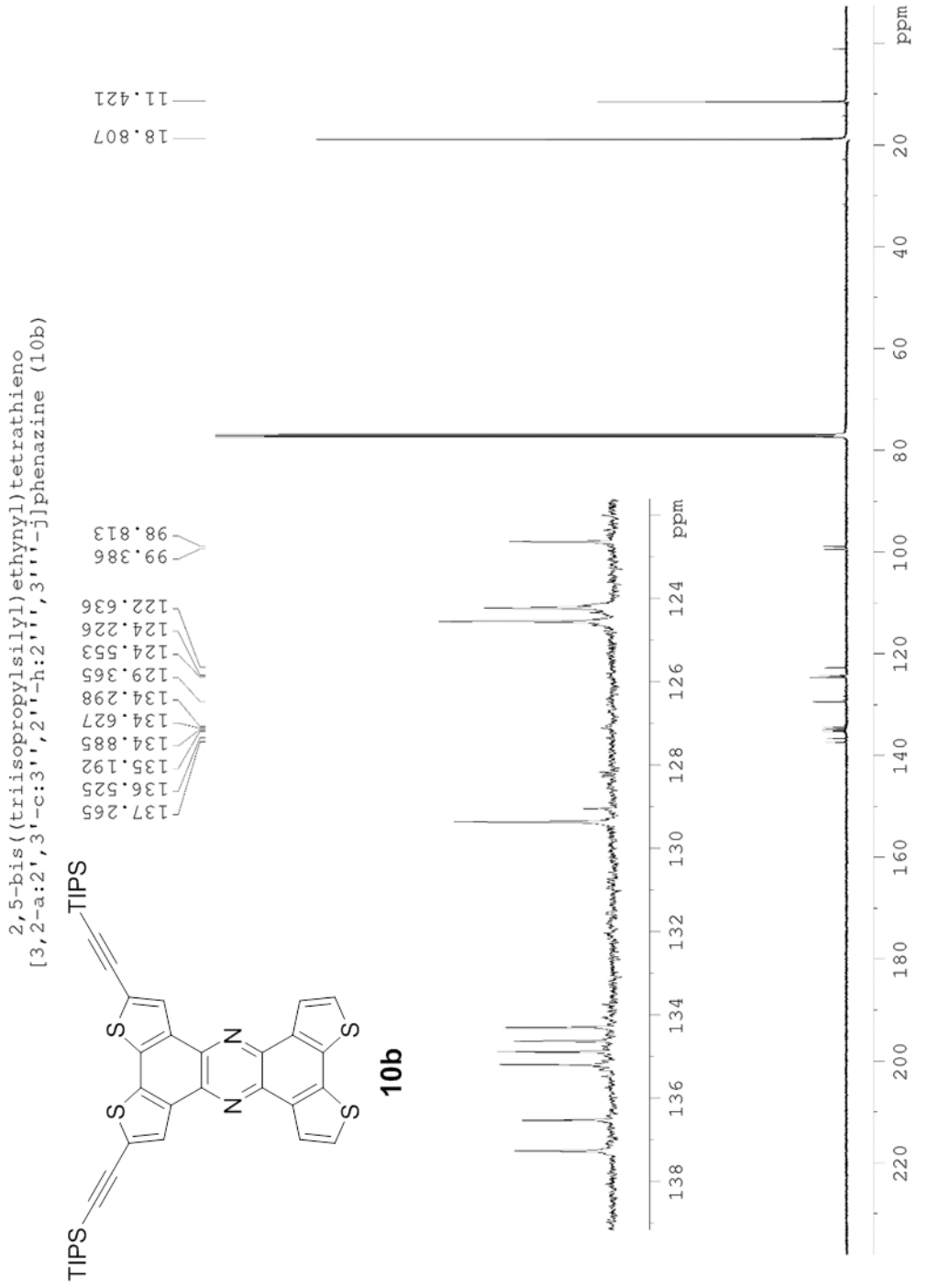

Figure 4.34. ^{13}C NMR of **10b.**

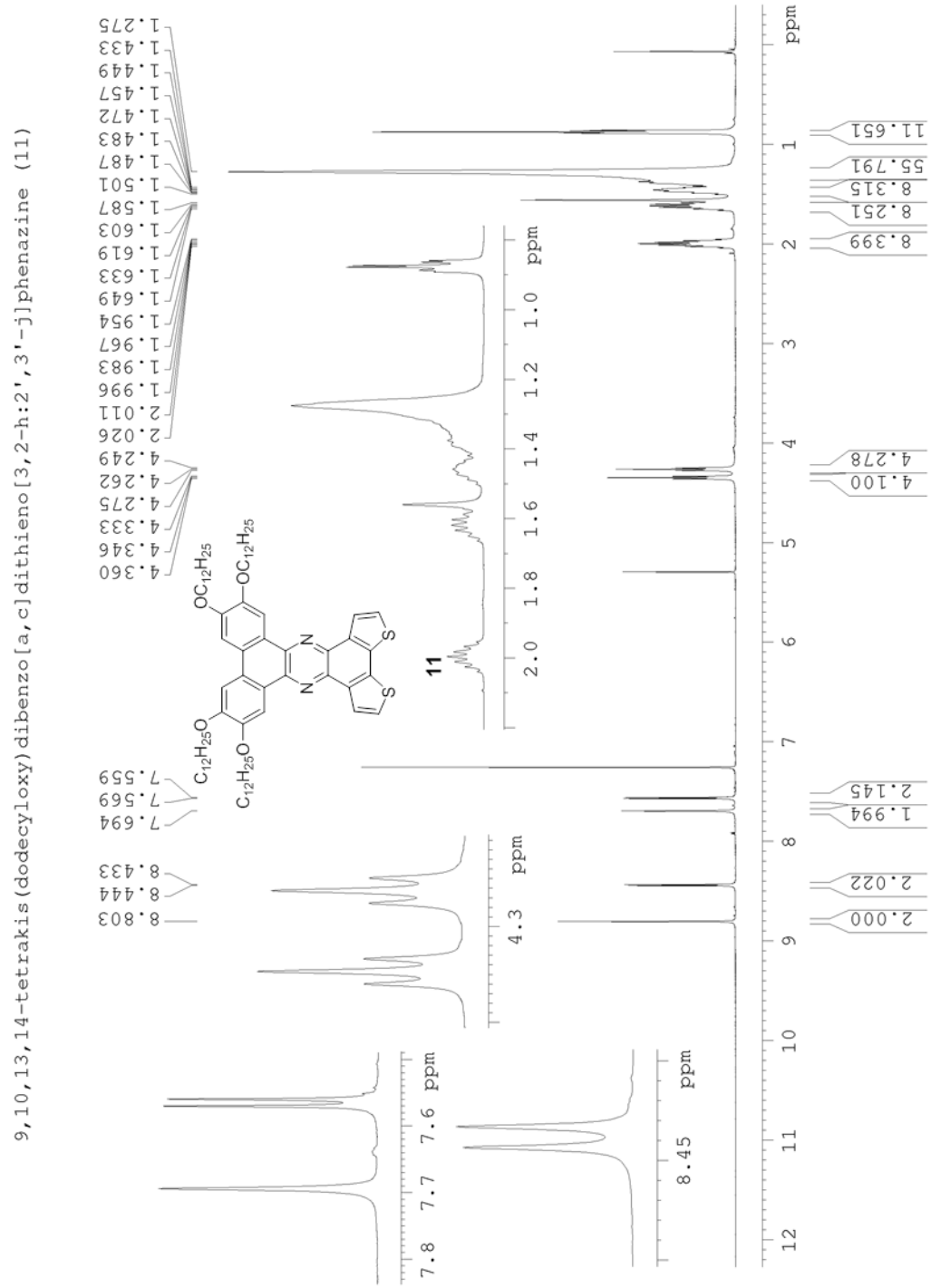

Figure 4.35. ^{1}H NMR spectrum of **11.**

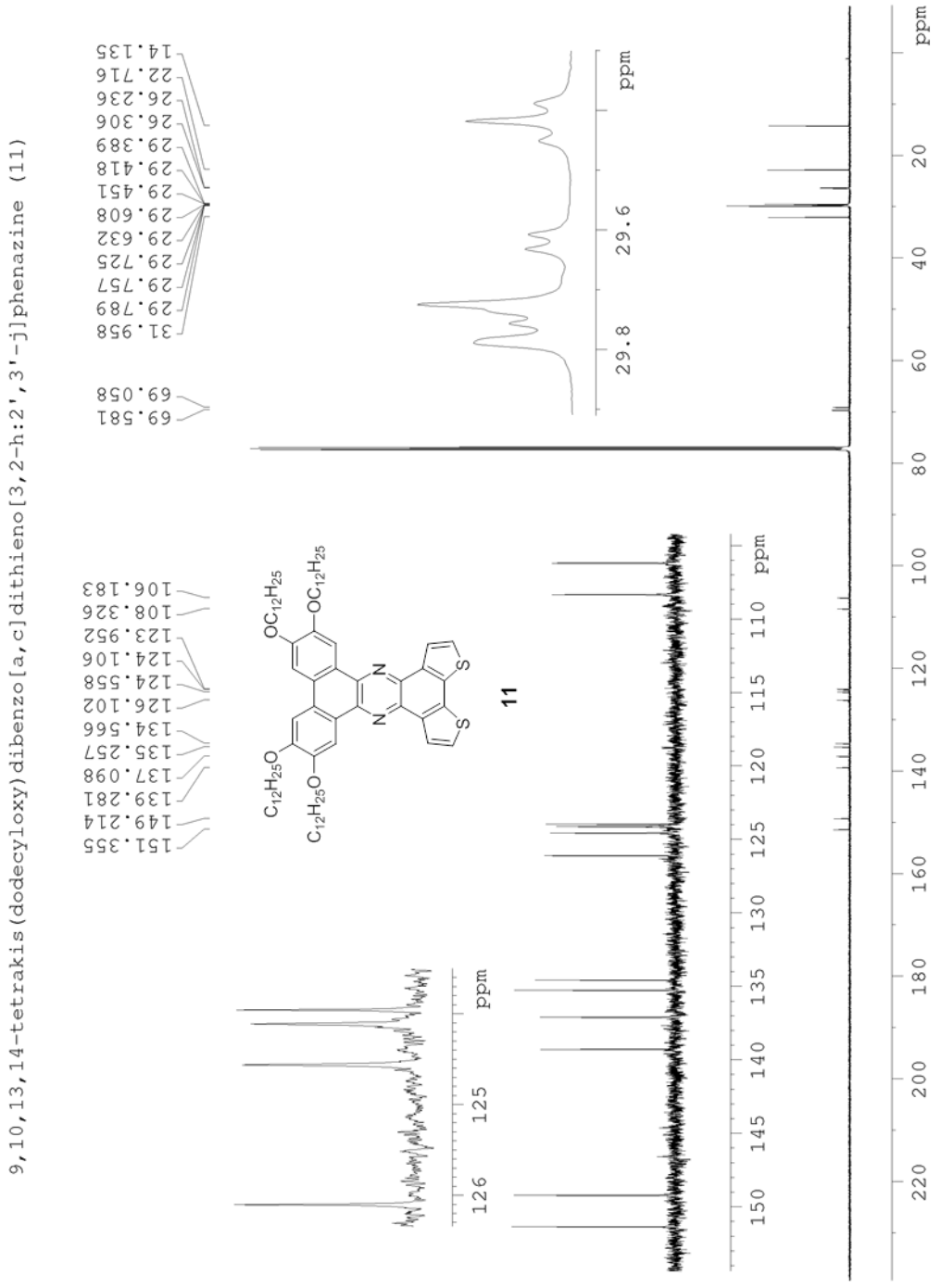

Figure 4.36. ^{13}C NMR spectrum of **11.**

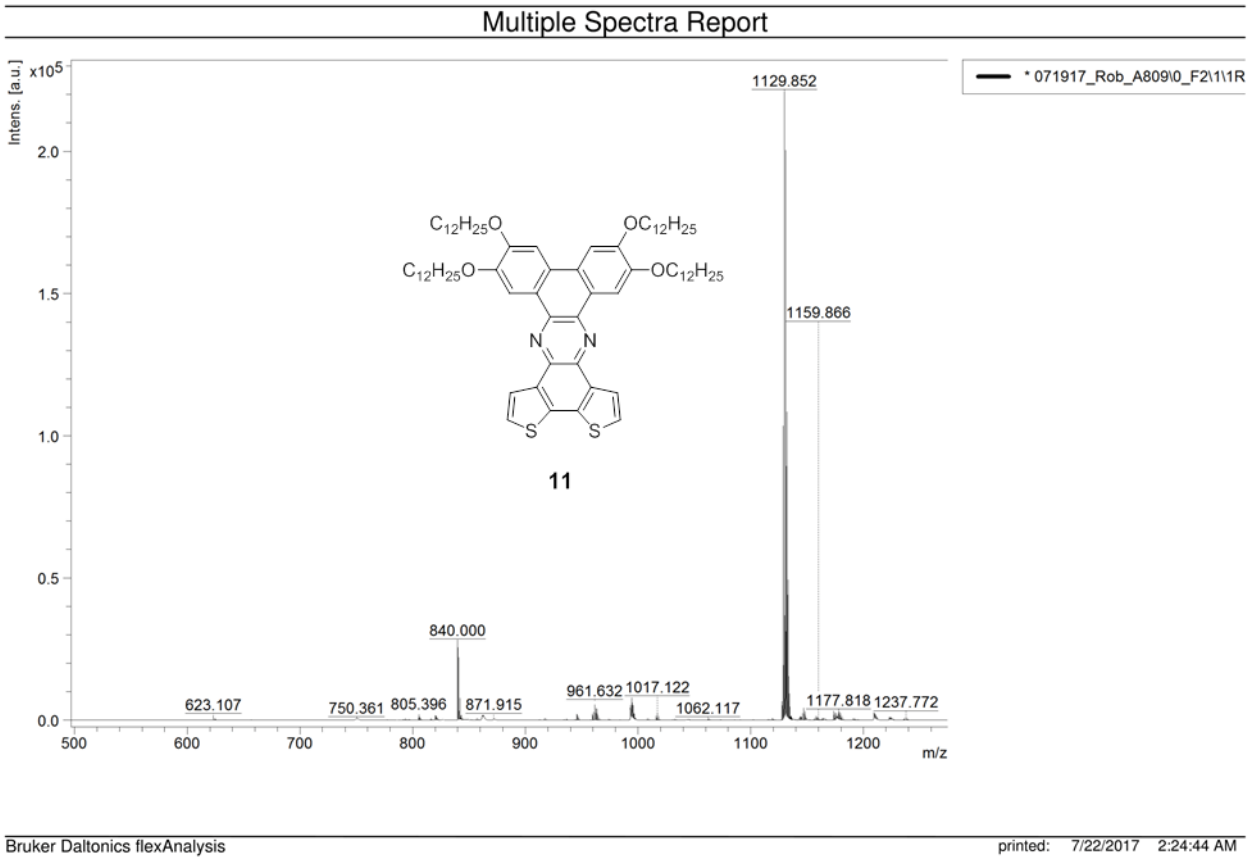

Figure 4.37. MALDI-TOF spectrum of **11.**

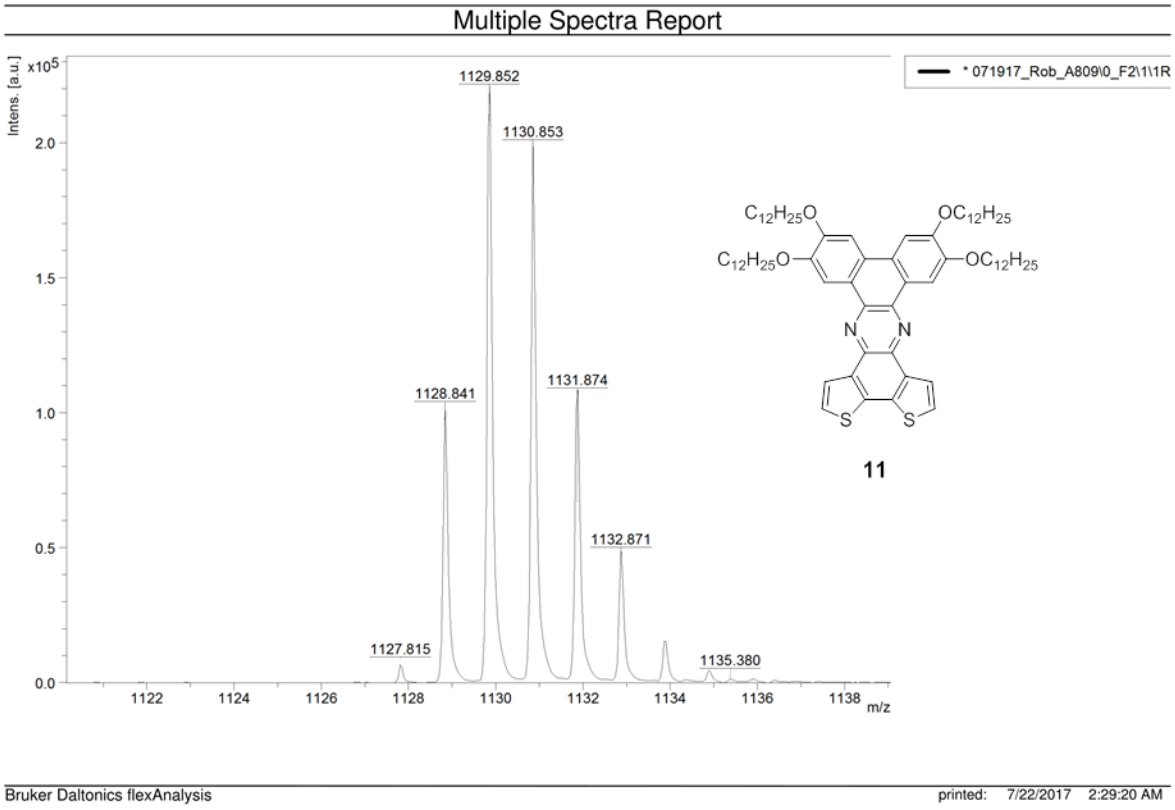

Figure 4.38. MALDI-TOF spectrum of **11** parent ion.

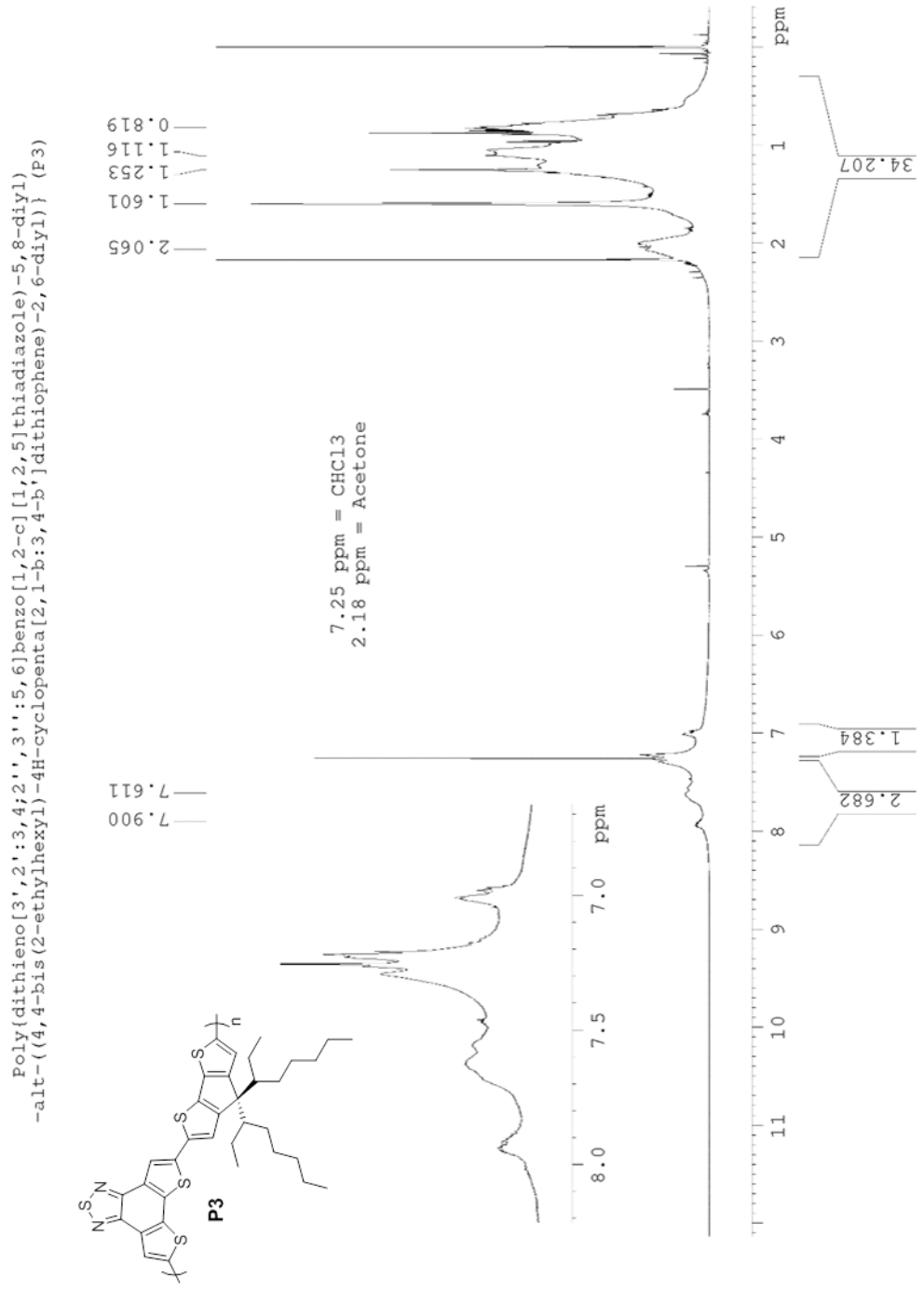

Figure 4.39. ^{1}H NMR spectrum of **P3**

References

(1) Van Mullekom, H. A. M.; Vekemans, J. A. J. M.; Havinga, E. E.; Meijer, E. W. Developments in the chemistry and band gap engineering of donor-acceptor substituted conjugated polymers. *Materials Science and Engineering R: Reports* **2001**, *32, 1-40*.

(2) Lu, L.; Zheng, T.; Wu, Q.; Schneider, A. M.; Zhao, D.; Yu, L. Recent Advances in Bulk Heterojunction Polymer Solar Cells. *Chem. Rev.* **2015**, *115*, 12666–12731. DOI: 10.1021/acs.chemrev.5b00098.

(3) Son, H. J.; Carsten, B.; Jung, I. H.; Yu, L. Overcoming efficiency challenges in organic solar cells: rational development of conjugated polymers. *Energy Environ. Sci.* **2012**, *5*, 8158. DOI: 10.1039/c2ee21608f.

(4) Li, Y. Molecular design of photovoltaic materials for polymer solar cells: Toward suitable electronic energy levels and broad absorption. *Acc. Chem. Res.* **2012**, *45*, 723–733. DOI: 10.1021/ar2002446.

(5) Salzner, U.; Karalti, O.; Durdağı, S. Does the donor-acceptor concept work for designing synthetic metals? III. Theoretical investigation of copolymers between quinoid acceptors and aromatic donors. *J. Mol. Model.* **2006**, *12*, 687–701. DOI: 10.1007/s00894-005-0046-2.

(6) Kitamura, C.; Tanaka, S.; Yamashitau, Y. Synthesis of New Narrow Bandgap Polymers Based on 5,7-Di(2-thienyl)thieno[3,4-b]pyrazine and its Derivatives. *J. Chem. Soc. Chem. Commun.* **1994**, *12*, 1585–1586. DOI: 10.1039/B813328J/Analyst.

(7) Kitamura, C.; Tanaka, S.; Yamashita, Y. Design of Narrow-Bandgap Polymers. Syntheses

and Properties of Monomers and Polymers Containing Aromatic-Donor and o-Quinoid-Acceptor Units. *Chem. Mater.* **1996**, *8*, 570–578. DOI: 10.1021/cm950467m.

(8) Rasmussen, S. C.; Schwiderski, R. L.; Mulholland, M. E. Thieno[3,4-b]pyrazines and their applications to low band gap organic materials. *Chem. Commun. (Camb).* **2011**, *47*, 11394–11410. DOI: 10.1039/c1cc12754c.

(9) Yao, H.; Ye, L.; Zhang, H.; Li, S.; Zhang, S.; Hou, J. Molecular design of benzodithiophene-based organic photovoltaic materials. *Chem. Rev.* **2016**, *116*, 7397–7457. DOI: 10.1021/acs.chemrev.6b00176.

(10) Pai, R. K.; Ahipa, T. N.; Hemavathi, B. Rational design of benzodithiophene based conjugated polymers for better solar cell performance. *Rsc Adv.* **2016**, *6*, 23760–23774. DOI: 10.1039/c6ra00651e.

(11) Zhang, S.; Ye, L.; Hou, J. Breaking the 10% Efficiency Barrier in Organic Photovoltaics: Morphology and Device Optimization of Well-Known PBDTTT Polymers. *Adv. Energy Mater.* **2016**, *6*, 1–20. DOI: 10.1002/aenm.201502529.

(12) Mei, C. Y.; Liang, L.; Zhao, F. G.; Wang, J. T.; Yu, L. F.; Li, Y. X.; Li, W. S. A family of donor-acceptor photovoltaic polymers with fused 4,7-dithienyl-2,1,3-benzothiadiazole units: Effect of structural fusion and side chains. *Macromolecules* **2013**, *46*, 7920–7931. DOI: 10.1021/ma401298g.

(13) Efrem, A.; Lei, Y.; Wu, B.; Wang, M.; Ng, S. C.; Ong, B. S. Dithienobenzochalcogenodiazole-based electron donor-acceptor polymers for organic electronics. *Dye. Pigment.* **2016**, *129*, 90–99. DOI: 10.1016/j.dyepig.2016.01.035.

(14) Planells, M.; Nikolka, M.; Hurhangee, M.; Tuladhar, P. S.; White, A. J. P.; Durrant, J. R.; Sirringhaus, H.; McCulloch, I. The effect of thiadiazole out-backbone displacement in indacenodithiophene semiconductor polymers. *J. Mater. Chem. C* **2014**, *2*, 8789–8795. DOI: 10.1039/C4TC01500B.

(15) Dallos, T.; Hamburger, M.; Baumgarten, M. Thiadiazoloquinoxalines: Tuning physical properties through smart synthesis. *Org. Lett.* **2011**, *13*, 1936–1939. DOI: 10.1021/ol200250e.

(16) An, C.; Puniredd, S. R.; Guo, X.; Stelzig, T.; Zhao, Y.; Pisula, W.; Baumgarten, M. Benzodithiophene-Thiadiazoloquinoxaline as an acceptor for ambipolar copolymers with deep LUMO level and distinct linkage pattern. *Macromolecules* **2014**, *47*, 979–986. DOI: 10.1021/ma401938m.

(17) Dallos, T.; Beckmann, D.; Brunklaus, G.; Baumgarten, M. Thiadiazoloquinoxaline-acetylene containing polymers as semiconductors in ambipolar field effect transistors. *J. Am. Chem. Soc.* **2011**, *133*, 13898–13901. DOI: 10.1021/ja2057709.

(18) An, C.; Zhou, S.; Baumgarten, M. Condensed derivatives of thiadiazoloquinoxaline as strong acceptors. *Cryst. Growth Des.* **2015**, *15*, 1934–1938. DOI: 10.1021/acs.cgd.5b00105.

(19) An, C.; Li, M.; Marszalek, T.; Li, D.; Berger, R.; Pisula, W.; Baumgarten, M. Thiadizoloquinoxaline-based low-bandgap conjugated polymers as ambipolar semiconductors for organic field effect transistors. *Chem. Mater.* **2014**, *26*, 5923–5929. DOI: 10.1021/cm502563t.

(20) Zhou, S.; Stelzig, T.; Puniredd, S. R.; Guo, X.; An, C. Strengthening the Acceptor Properties of Thiadiazoloquinoxalines via Planarization. *New J. Chem.* **2015**, *39*, 6765–6770. DOI: 10.1039/c5nj00517e.

(21) Luo, M.; Shadnia, H.; Qian, G.; Du, X.; Yu, D.; Dongge, M.; Wright, J. S.; Wang, Z. Y. Rational design, synthesis, and optical properties of film-forming, near-infrared absorbing, and fluorescent chromophores with multidonors and large heterocyclic acceptors. *Chem. - A Eur. J.* **2009**, *15*, 8902–8908. DOI: 10.1002/chem.200900891.

(22) Arroyave, F. A.; Richard, C. A.; Reynolds, J. R. Efficient Synthesis of Benzo[1,2-b:6,5-b']dithiophene-4,5-dione (BDTD) and Its Chemical Transformations into Precursors for π-Conjugated Materials. *Org. Lett.* **2012**, *14*, 6138–6141. DOI: 10.1021/ol302704v.

(23) Kato, S.; Watanabe, K.; Tamura, M.; Ueno, M.; Nitani, M.; Ie, Y.; Aso, Y.; Yamanobe, T.; Uehara, H.; Nakamura, Y. Tetraalkoxyphenanthrene-Fused Thiadiazoloquinoxalines: Synthesis, Electronic, Optical, and Electrochemical Properties, and Self-Assembly. *J. Org. Chem.* **2017**, *82*, 3132–3143. DOI: 10.1021/acs.joc.7b00084.

(24) Hu, S.; Bao, X.; Liu, Z.; Wang, T.; Du, Z.; Wen, S.; Wang, N.; Han, L.; Yang, R. Benzothiadiazole[1,2-b:4,3-b']dithiophene, a new ladder-type multifused block: Synthesis and photovoltaic application. *Org. Electron. physics, Mater. Appl.* **2014**, *15*, 3601–3606. DOI: 10.1016/j.orgel.2014.10.003.

(25) Aguirre, J. C.; Hawks, S. A.; Ferreira, A. S.; Yee, P.; Subramaniyan, S.; Jenekhe, S. A.; Tolbert, S. H.; Schwartz, B. J. Sequential processing for organic photovoltaics: Design rules for morphology control by tailored semi-orthogonal solvent blends. *Adv. Energy*

Mater. **2015**, *5*, 1–11. DOI: 10.1002/aenm.201402020.

(26) Li, H.; Hwang, Y. J.; Earmme, T.; Huber, R. C.; Courtright, B. A. E.; Obrien, C.; Tolbert, S. H.; Jenekhe, S. A. Polymer/polymer blend solar cells using tetraazabenzodifluoranthene diimide conjugated polymers as electron acceptors. *Macromolecules* **2015**, *48*, 1759–1766. DOI: 10.1021/ma502042k.

(27) Kim, C. H.; Hlaing, H.; Carta, F.; Bonnassieux, Y.; Horowitz, G.; Kymissis, I. Templating and charge injection from copper electrodes into solution-processed organic field-effect transistors. *ACS Appl. Mater. Interfaces* **2013**, *5*, 3716–3721. DOI: 10.1021/am400325k.

(28) Isse, A. A.; Gennaro, A. Absolute Potential of the Standard Hydrogen Electrode and the Problem of Interconversion of Potentials in Different Solvents. *J. Phys. Chem. B* **2010**, *114*, 7894–7899. DOI: 10.1021/jp100402x.

(29) Haynes W. M. *CRC Handbook of Chemistry and Physics, 97th Edition*; 2017.

(30) Larson, B. W.; Whitaker, J. B.; Wang, X. Bin; Popov, A. A.; Rumbles, G.; Kopidakis, N.; Strauss, S. H.; Boltalina, O. V. Electron affinity of Phenyl-C61-butyric acid methyl ester (PCBM). *J. Phys. Chem. C* **2013**, *117*, 14958–14964. DOI: 10.1021/jp403312g.

(31) Nielsen, C. B.; Holliday, S.; Chen, H.-Y.; Cryer, S. J.; McCulloch, I. Non-Fullerene Electron Acceptors for Use in Organic Solar Cells. *Acc. Chem. Res.* **2015**, *48*, 2803–2812. DOI: 10.1021/acs.accounts.5b00199.

(32) Zhang, Y.; Zou, J.; Yip, H.-L.; Sun, Y.; Davies, J. a.; Chen, K.-S.; Acton, O.; Jen, A. K.-Y. Conjugated polymers based on C, Si and N-bridged dithiophene and thienopyrroledione

units: synthesis, field-effect transistors and bulk heterojunction polymer solar cells. *J. Mater. Chem.* **2011**, *21*, 3895. DOI: 10.1039/c0jm03927f.

(33) Ribierre, J.-C.; Zhao, L.; Inoue, M.; Schwartz, P.-O.; Kim, J.-H.; Yoshida, K.; Sandanayaka, A. S. D.; Nakanotani, H.; Mager, L.; Méry, S.; et al. Low threshold amplified spontaneous emission and ambipolar charge transport in non-volatile liquid fluorene derivatives. *Chem. Commun.* **2016**, *52*, 3103–3106. DOI: 10.1039/C5CC08331A.

(34) Hu, J.; Zhang, D.; Harris, F. W. Ruthenium(III) chloride catalyzed oxidation of pyrene and 2,7-disubstitued pyrenes: An efficient, one-step synthesis of pyrene-4,5-diones and pyrene-4,5,9,10-tetraones. *J. Org. Chem.* **2005**, *70*, 707–708. DOI: 10.1021/jo048509q.

Acknowledgements

CV data was collected by Terri Lin, GIWAXs data was collected and reduced by KJ Winchell and Patrick Yee. Florescence spectra were collected by Mathew Voss, and single crystal diffractometry data was collected and analyzed by Saeed Khan. The author would also like to thank professor Barry Thompson and his student Betsy Melenbrink for help with gel permeation chromatography measurements and use of their laboratory.

Chapter 5 : Conclusion

Future work involving conjugated polymer electrolytes

This dissertation has covered the synthesis and characterization of several novel semiconducting polymers as well as a number of novel heteroacenes. The newly synthesized semiconducting polymer, **PCT**, has several attractive properties compared to the related polymer **PFT**[1] including a reduced band gap and a deeper HOMO level. Initial studies of this new polymer show that it forms hydrogels in aqueous solution much like **PFT**. Future work will focus on measuring the hole mobility of self-assembled micelles of **PCT** and comparing the measured mobility of **PCT** to the mobilities of the unquaternized, unassembled precursor polymer **4**. **PCT** will also be combined with fulleropyrrolidinium salts to see if they co-assemble and create long lived polaron species in a manner similar to the reports of Huber *et al*.[2]

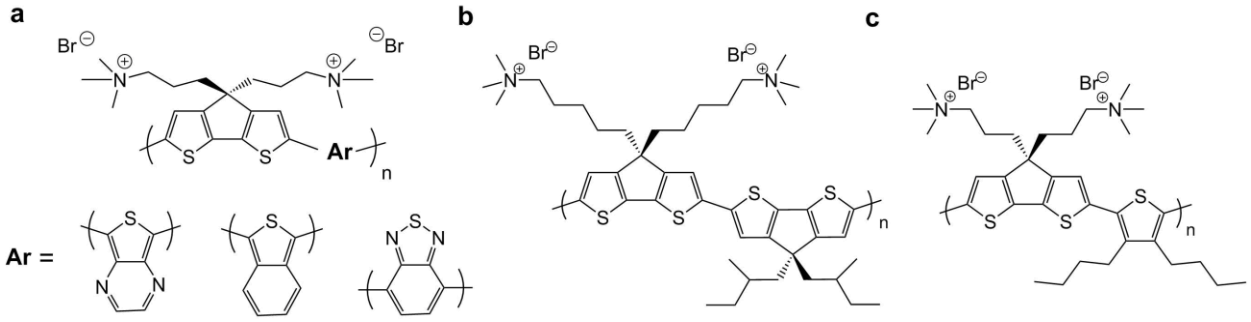

Figure 5.1. (a) Several copolymers synthesized using monomer **3** and strong electron withdrawing units such as thieno[3,4-b]pyrazine, isothianaphthene, and 2,1,3-benzothiadiazole. (b) copolymers consisting of alternating units of cyclopentadithiophene substituted with hydrophilic alkyl ammonium and hydrophobic alkyl side chains. (c) a copolymer similar to **PCT** but containing alkyl substituents substituted at the 3 and 4 positions of the thiophene ring.

There are many exciting new materials that can be synthesized using the synthetic procedures developed in chapter 2. There are several copolymers that can be synthesized from the 2,6-Dibromo-4,4-bis(3'-(*N*,*N*-dimethylamino)propyl) cyclopenta[2,1-b:3,4-b']dithiophene) monomer (**3**) which was synthesized in chapter 2 (see Figure 5.1). Substitution of the weakly electron accepting thiophene unit with more electron deficient units such as thieno[3,4-b]pyrazine, isothianaphthene, and 2,1,3-benzothiadiazole, should result in polymers with significantly reduced band gaps and deeper HOMO levels. Attempts were made to synthesize stannylated thieno[3,4-b]pyrazine units for the express purpose of creating copolymers, but it will be noted that unsubstituted thieno[3,4-b]pyrazines rapidly autopolymerize due to the rapid formation of singlet diradicals at room temperature.[3] Recently, Qin *et* al. outlined a high yielding synthesis of distannylated isothianapthene reagents which could be used in a Stille cross—coupling with **3**.[4] It will be noted that these reagents are much more stable compared to regents based on thieno[3,4-b]pyrazine, thus it may be more productive to synthesis polymers from distannylated isothianaphthene instead of distannylated thieno[3,4-b]pyrazine. Copolymers can also be created using a Suzuki coupling between **3** and the commercially available 2,1,3-Benzothiadiazole-4,7-diboronic acid, pinacol ester. The resulting polymer should possess the same properties as the polymer PCPDTBT which has a band gap of 1.7 eV and a HOMO level of -5.3 eV *vs*. vacuum level.[5]

More work can also be done on exploring the effects that chemical composition of these polymers has on the size and structure of the resulting micelle. For instance, it would be very interesting to see whether the strength of hydrogels would increase if hydrophilic substituents were added to **PCT** or **PFT** (see Figure 5.1c). Presumably the introduction of hydrophobic

substituents to the interior of the polymer micelle would both increase the size of the micelle and increase the strength of the interaction between hydrophobic units in the amphiphilic polymer. Introduction of hydrophobic substituents could be accomplished through use of alkyl substituted thiophene reagents during polymerization. It would also be interesting to explore the self—assembly properties of copolymers consisting of alternating hydrophilic and hydrophobic units as seen in Figure 5.1b. These polymers would still be driven to form micellular structures in aqueous solution due to the hydrophobic interactions between the alkyl side chains and the solvent, but the geometric constraints of the alkyl side chains would presumably alter the structure of these micellular assemblies.

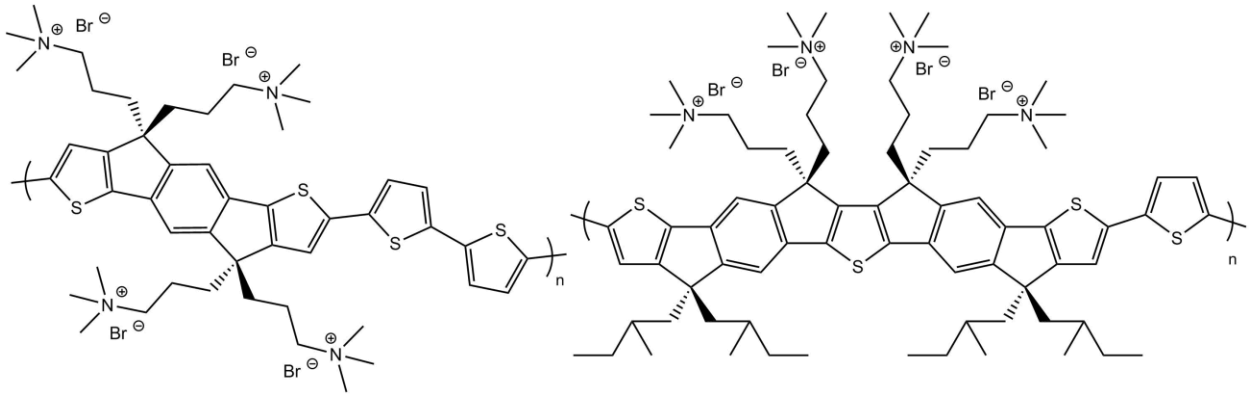

Figure 5.2. Examples of conjugated polyelectrolytes based on alkylammonium substituted indacenodithiophene units (left) and π extended indacenodithiophene units with both alkylammonium and alkyl substituents (right).

This last idea, using alkyl substitution patterns that drastically alter the geometric constraints of micelle formation lends itself to some interesting questions that can be answered with new materials. For instance, what if polymers were created using alkyl ammonium substituted indacenodithiophene[6] units instead of cyclopenta[2,1-b:3,4-b']dithiophene units?

The resulting polymers would have alkyl ammonium chains sitting on both sides of the conjugated polymer backbone (see Figure 5.2), and the self-assembly behavior of the resulting polymers would be drastically altered in aqueous solution, and the effects this change would have on the electronic and photophysical properties of the resulting polymer would be fascinating. Further extending the fused units of the indacenodithiophene[7] would lead to further opportunities to drastically alter the self—assembly properties of these conjugated polyelectrolytes because a modular synthesis of a π extended indacenodithiophene would allow for the placement of both alkyl ammonium and alkyl side chains on the π extended indacenodithiophene unit (see Figure 5.2).

Future work involving Dithieno[3,2-a:2',3'-c]phenazine based polymers

Chapter three covered the synthesis of twelve novel πD—πA copolymers containing the Dithieno[3,2-a:2',3'-c]phenazine (DTP) πA moiety and various πD moieties. Polymer solar cells were fabricated using many of the polymers synthesized in chapter 3, but most of the polymers proved too insoluble for use in solar cells. **P1**, however, was sufficiently soluble to fabricate solar cells, and optimized solar cells reached a power conversion efficiency of 1.27% when combined with PCBM. Several more polymers in the series, namely, **P9—P12** have yet to be explored as donors in polymer solar cells, but the solubilities of **P10—P12** are significantly higher than the rest of the polymers in the homologous series, allowing for thicker active layers and higher short-circuit currents compared to **P1**. Solubility of these DTP based polymers could also drastically be increased by substituting branched ethylhexyl chains for the straight alkyl chains attached to the oxygen atoms at the 9 and 10 positions of the DTP ring (see Figure 5.3a).

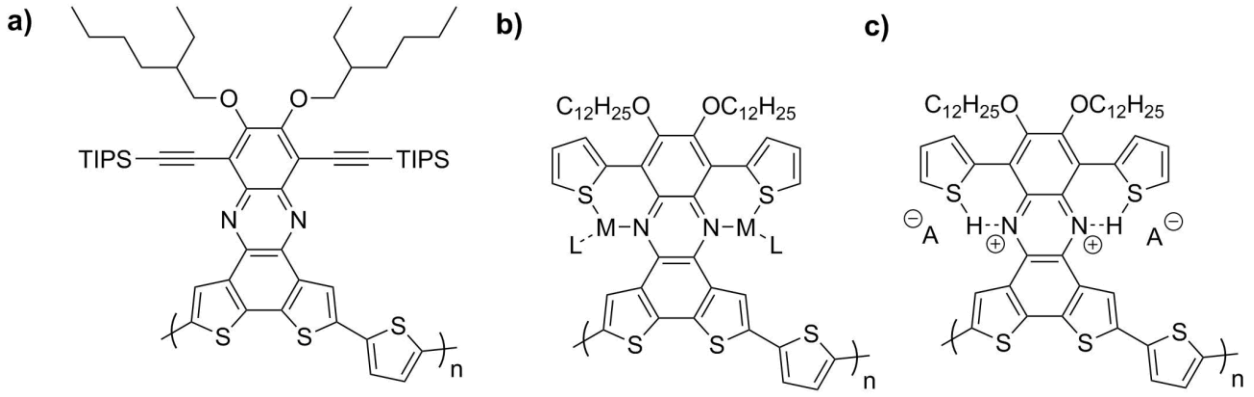

Figure 5.3. Substituting linear octyloxy chains for branched octyloxychains as seen in (a) should lead to polymers with greater solubility. DTP polymers such as **P9** and **P12** may possibly be able to ligate metal centers as seen in (b) and DTP polymers may exhibit an increase in conductivity upon protination of the nitrogens contained in the DTP units of the polymer.

There are several properties of **P1—P12** that are yet to be explored. For instance, the nitrogen atoms in the Dithieno[3,2-a:2',3'-c]phenazine (DTP) unit can be protinated with mineral acids, and it would be worthwhile to see whether **P1—P12** exhibited changes in conductivity after being doped with acids. The conductivity of polyaniline is drastically increased upon doping of polymer films with strong acids,[8] and it would be important to test whether these polymers also show a similarly drastic increase in conductivity after being doped with acids. The nitrogen atoms of **P1—P12** can also possibly chelate metal atoms, and chelation would be expected to change the optical absorption and photoluminescence behavior of the polymer. If such changes do occur upon chelation of metals, **P1—P12** could possibly be used as sensors which can qualitatively and quantitatively identify metal ions in aqueous solution.[9,10] It will also be noted that fluoride ions can deprotect the TIPS acetylene groups in **P1—P12**, therefore these polymers could also act as chemical sensors for fluoride ions.[11]

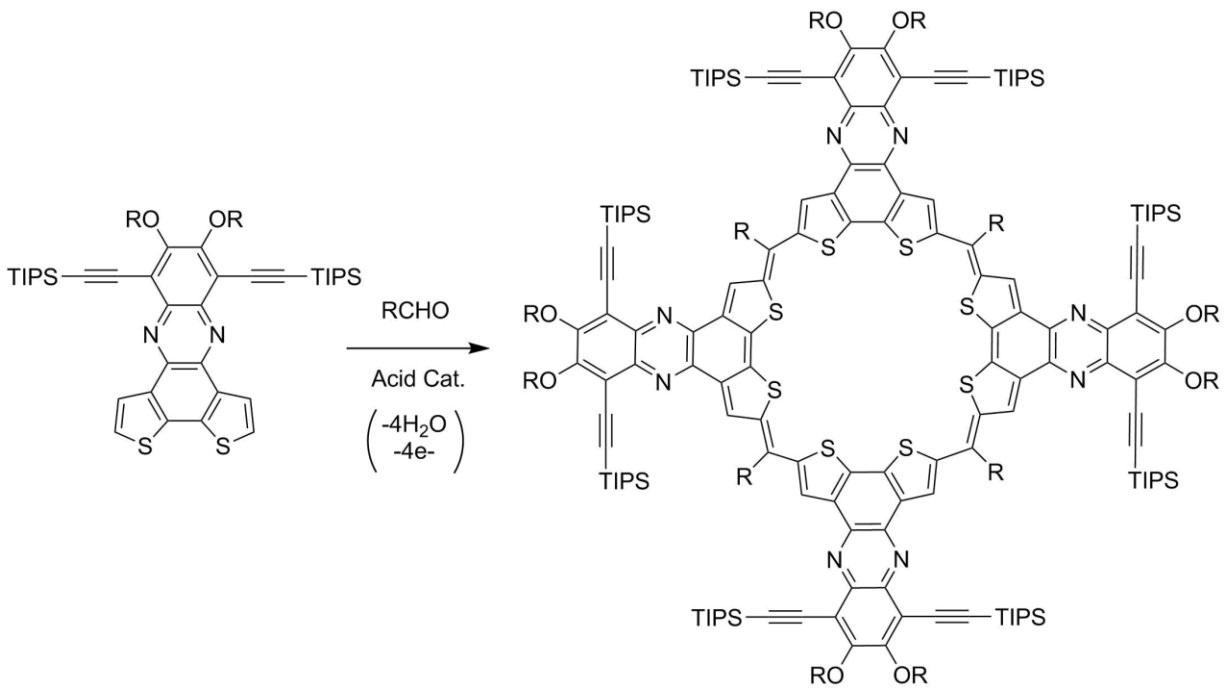

Figure 5.4. Possible synthetic route to macrocycles containing DTP units.

One final set of reactions that might merit an attempt would be a macrocyclization/condensation reaction between DTP units and aldehydes. This cyclization reaction would be somewhat reminiscent of the macrocyclization/condensation reactions employed for the synthesis of porphyrins.[12] The reaction is chemically feasible because the DTP unit readily adopts the quinoidal structure that is required for half the rings in the resulting macrocycle. The reaction conditions would have to be carefully chosen so that the Lewis acid catalyst used in the reaction would not ligate the nitrogen atoms of the DTP unit, thus making the DTP unit electron deficient.

Future work on the extended fused N-heteroacene small molecules and polymers

Several novel semiconducting polymers and heteroacenes were synthesized in chapter 3. **P1—P3** in chapter 4 have very attractive properties as donor polymers for solar cell devices, and small molecule **5** is very attractive as a small molecule acceptor for solar cell applications. The alkynyl substituted N-heteroacene **10b**, crystallizes quite easily and its resemblance to many of the high mobility *N*-heteroacenes reported by Bunz *et al*.[13] make it an attractive new material for OFET applications. Small molecule **11** forms organogels, and the structure of these gels should be explored using SEM and SAXs measurements. **11** should also possess a high enough LUMO orbital to facilitate electron transfer to amphiphilic fullerene derivatives as well.

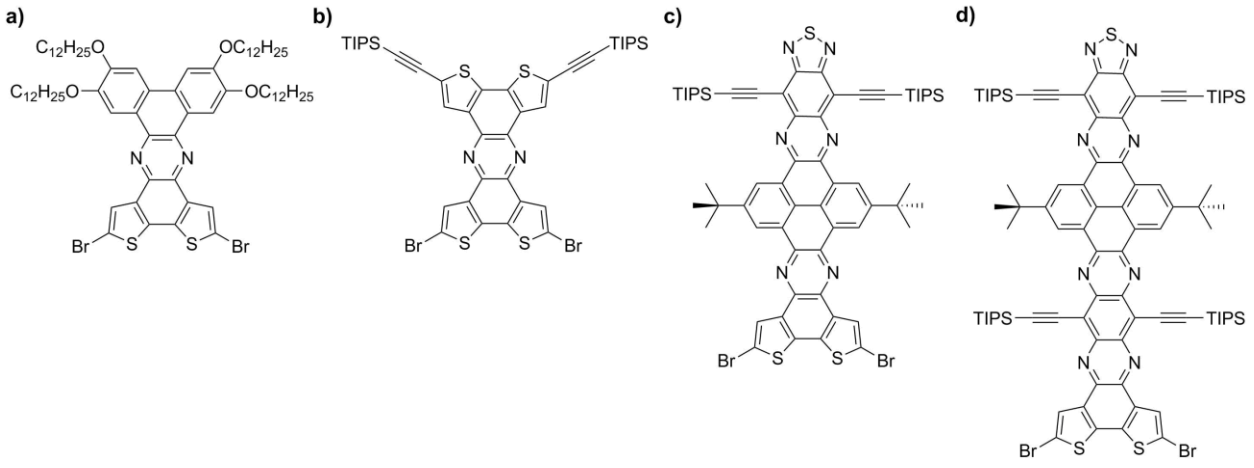

Figure 5.5. Several monomer units which can be copolymerized with Stille coupling reagents to create D-A copolymers. (a) monomer unit which can be created from **10b** (b) monomer unit which can be created from **11** (c) and (d) monomer units which can be created from condensation reactions outlined in chapter 4.

Future work with these systems should explore electrophysical changes that occur in **P1—P3** upon doping with mineral acids and chelation of transition metals. The synthetic

procedures used to create monomer **3** and small molecule **5** could also be utilized to create polymers containing monomer units containing 8 and 10 consecutive aromatic rings (see **Error! Reference source not found.**). Polymers can also be synthesized using monomers based on **10b** and **11**, and it would be of interest to see how the photoluminescence and absorptive behavior of these polymers compares to **P1**—**P3**.

References

(1) Clark, A. P.; Shi, C.; Ng, B. C.; Wilking, J. N.; Ayzner, A. L.; Stieg, A. Z.; Schwartz, B. J.; Mason, T. G.; Rubin, Y.; Tolbert, S. H.; et al. Self-Assembling Semiconducting Electronic Materials. *ACS Nano* **2013**, *7*, 962–977.

(2) Huber, R. C.; Ferreira, A. S.; Thompson, R.; Kilbride, D.; Knutson, N. S.; Devi, L. S.; Toso, D. B.; Challa, J. R.; Zhou, Z. H.; Rubin, Y.; et al. Long-lived photoinduced polaron formation in conjugated polyelectrolyte-fullerene assemblies. *Science 80.* **2015**, *348*, 1340–1343. DOI: 10.1126/science.aaa6850.

(3) Kenning, D. D.; Mitchell, K. A.; Calhoun, T. R.; Funfar, M. R.; Sattler, D. J.; Rasmussen, S. C. Thieno[3,4-b]pyrazines:, Synthesis, Structure, and Reactivity. *J. Org. Chem.* **2002**, *67*, 9073–9076. DOI: 10.1021/jo0262255.

(4) Qin, Y.; Kim, J. Y.; Frisbie, C. D.; Hillmyer, M. A. Distannylated Isothianaphthene : A Versatile Building Block for Low Bandgap Conjugated Polymers Distannylated Isothianaphthene : A Versatile Building Block for Low Bandgap Conjugated Polymers. *Macromolecules* **2008**, *41,* 5563–5570. DOI: 10.1021/ma8011575.

(5) Kettle, J.; Horie, M.; Majewski, L. A.; Saunders, B. R.; Tuladhar, S.; Nelson, J.; Turner, M. L. Optimisation of PCPDTBT solar cells using polymer synthesis with Suzuki coupling. *Sol. Energy Mater. Sol. Cells* **2011**, *95*, 2186–2193. DOI: 10.1016/j.solmat.2011.03.022.

(6) Zhang, W.; Smith, J.; Watkins, S. E.; Gysel, R.; McGehee, M.; Salleo, A.; Kirkpatrick, J.; Ashraf, S.; Anthopoulos, T.; Heeney, M.; et al. Indacenodithiophene semiconducting

polymers for high-performance, air-stable transistors. *J. Am. Chem. Soc.* **2010**, *132*, 11437–11439. DOI: 10.1021/ja1049324.

(7) Xu, X.; Cai, P.; Lu, Y.; Choon, N. S.; Chen, J.; Ong, S.; Hu, X. Synthesis of a Novel Low-Bandgap Polymer Based on a Ladder-Type Heptacyclic Arene Consisting of Outer Thieno [3 , 2-b] thiophene Units for Efficient Photovoltaic Application. *Macromolecular Rapid Communications* **2014**, *35*, 681–688.

(8) Hatchett, D. W.; Josowicz, M.; Janata, J. Acid Doping of Polyaniline : Spectroscopic and Electrochemical Studies. *J. Phys. Chem. B* **1999**, *103*, 10992–10998. DOI: 10.1021/jp991110z.

(9) Fan, L. J.; Zhang, Y.; Murphy, C. B.; Angell, S. E.; Parker, M. F. L.; Flynn, B. R.; Jones, W. E. Fluorescent conjugated polymer molecular wire chemosensors for transition metal ion recognition and signaling. *Coord. Chem. Rev.* **2009**, *253*, 410–422. DOI: 10.1016/j.ccr.2008.03.008.

(10) Mabeck, J. T.; Malliaras, G. G. Chemical and biological sensors based on organic thin-film transistors. *Anal. Bioanal. Chem.* **2006**, *384*, 343–353. DOI: 10.1007/s00216-005-3390-2.

(11) Kim, T. H.; Swager, T. M. A Fluorescent Self-Amplifying Wavelength-Responsive Sensory Polymer for Fluoride Ions. *Angew. Chemie - Int. Ed.* **2003**, *42*, 4803–4806. DOI: 10.1002/anie.200352075.

(12) Saito, S.; Osuka, A. Expanded porphyrins: Intriguing structures, electronic properties, and reactivities. *Angew. Chemie - Int. Ed.* **2011**, *50*, 4342–4373. DOI:

10.1002/anie.201003909.

(13) Bunz, U. H. F. The Larger Linear N-Heteroacenes. *Acc. Chem. Res.* **2015**, *48*, 1676–1686. DOI: 10.1021/acs.accounts.5b00118.